Optimal design and control of electrified powertrains

Optimal design and control of electrified powertrains

Caiyang Wei

Department of Mechanical Engineering

EINDHOVEN UNIVERSITY OF TECHNOLOGY

Eindhoven, The Netherlands 2020

The research leading to this dissertation is part of the "Thermicles" project, which is a common project of M2i, Bosch Transmission Technology, and TU/e. This research was carried out under project number T18001 in the framework of the Research Program of the Materials innovation institute (M2i) (www.m2i.nl) supported by the Dutch government.

A catalogue record is available from the Eindhoven University of Technology Library

ISBN: 978-90-386-5183-5

Typeset using LaTeX.
Cover design: Gildeprint
Reproduction: Gildeprint

Optimal design and control of electrified powertrains

PROEFSCHRIFT

ter verkrijging van de graad van doctor aan de Technische Universiteit Eindhoven, op gezag van de rector magnificus prof.dr.ir. F.P.T. Baaijens, voor een commissie aangewezen door het College voor Promoties, in het openbaar te verdedigen op donderdag 3 december 2020 om 16:00 uur

door

Caiyang Wei

geboren te Hubei, China

Dit proefschrift is goedgekeurd door de promotoren en de samenstelling van de promotiecommissie is als volgt:

voorzitter:	prof.dr. H. Nijmeijer
1^e promotor:	dr.ir. T. Hofman
2^e promotor:	prof.dr.ir. M. Steinbuch
leden:	prof.dr.habil. S. Delprat (Université Polytechnique Hauts-de-France)
	prof.dr. J. van Mierlo (Vrije Universiteit Brussel)
	dr. M. Lazar
adviseur(s):	dr. E. Ilhan Caarls (Bosch Transmission Technology)
	dr. S. Wilkins (TNO)

Het onderzoek dat in dit proefschrift wordt beschreven is uitgevoerd in overeenstemming met de TU/e Gedragscode Wetenschapsbeoefening.

Summary

Optimal design and control of electrified powertrains

Electrified powertrains, which provide opportunities for the improvement of energy efficiency, are emerging to meet unprecedented emissions regulations and energy shortages. The energy management system (EMS) and thermal management system (TMS) of an electrified vehicle are often treated independently in previous studies, and an optimal solution may not be guaranteed. Moreover, energy and thermal management systems are usually developed for a fixed powertrain. An optimal active dynamical system, however, demands concurrent plant (e.g., the topology and size) and controller optimization, considering the coupling between the physical system and the control strategy. In view of the drawbacks in the current literature, this study originally provides a comprehensive analysis of powertrain design and control optimization of electrified vehicles considering both the energy and thermal domains. The general problems of combined topology, component size and control optimization of electrified powertrains from energy and thermal perspectives are introduced. Energy and thermal management systems for electrified vehicles, which only started to appear recently, are then classified to highlight the importance of integration. The state-of-the-art combined energy and thermal management systems (CETMSs) are also surveyed in terms of optimality and causality. Moreover, it aims to identify potential research directions of combined design and control optimization of electrified powertrains with respect to energy saving and cost reduction. Based on the opportunities found, two case studies are conducted to demonstrate the effectiveness of integrated design approach, as electrified vehicles comprise hybrid electric vehicles (HEVs) and electric vehicles (EVs). For the second case study, extensive experiments have been conducted for model development and validation of the energy consumption.

In the first case study, for a plug-in HEV (PHEV) with a continuously variable transmission (CVT), an integrated energy and thermal management system (IETMS) is proposed. The IETMS aims to quantify the benefit of adopting a dual-source waste heat recovery (DSWHR) system on the ultimate fuel savings of the CVT-based PHEV, which is subject to a cold-start. A cold-start implies a low engine temperature, which increases the frictional power dissipation in the engine, leading to excess fuel usage. The DSWHR system recuperates waste heat from exhaust gases. The energy harvested is stored in a battery and can be retrieved when needed. Moreover, it recovers waste heat from an electric machine (EM) and a CVT, to boost the heating

performance of a heat pump for cabin heating. This results in a decrease in the load on the battery. The IETMS aims at maximizing the fuel efficiency. Based on validated component models, by using dynamic programming (DP), simulation results show that cold-start conditions have a significant impact on the fuel usage, up to around 7.1%. The DSWHR system has a significant improvement on the fuel economy, up to around 13.1%, from which the design of WHR technologies and dimensioning of powertrain components can be derived. The recovered power from the DSWHR system can potentially downsize the battery pack.

In the second case study, for an EV with a CVT, a combined design and control optimization (co-design) method on the basis of convex programming (CP) is proposed to minimize the total-cost-of-ownership (TCO), focusing on the integration of the EM and the CVT. Moreover, the co-design approach is extended by an integrated energy and thermal management design. A single-speed transmission (SST)-based EV model with reference to a series production vehicle is firstly created, which is experimentally validated. A CVT-based EV model is subsequently developed based on the SST-based EV model, where only the SST is replaced by a CVT (on the basis of an off-the-shelf component, which is not optimized). The CVT-based EV model is then convexified and optimized with the co-design optimization method. The strong coupling between the EM and CVT from design and control perspectives is presented. It is shown that the optimized system with the co-design approach decreases the TCO by around 2% compared with the SST-based EV and by around 5.9% compared with the non-optimized CVT-based EV (based on off-the-shelf component). The optimal design parameters: the battery, EM and CVT sizes; and control inputs: the CVT speed ratio and air-flow rate of the cooling system, are found simultaneously, by taking advantage of the control and design freedom provided by the CVT. Thereby, the drive train component models for the vehicle load, EM, CVT and SST (including thermal models) are developed based on experiments with sufficient accuracy and used for verification and validation of the developed integrated design methodology. Moreover, the advantages of the co-design method are highlighted by comparing to a sequential design, where the EM size is fixed. Insights into the design of a low-power EV that is energy-efficient and cost-effective for urban driving are also provided. The result shows that even though the current EV market is dominated by SSTs, multi-speed transmissions, for instance, CVTs, can be considered as competitive alternatives. For future EV applications, a highly and thermally integrated EM-CVT system, which is efficient, low-cost, and lightweight, through joint forces of automotive suppliers can be expected.

Acknowledgments

I would like to take this opportunity to express my gratitude to everyone who has supported me during this journey.

First of all, special thanks go to my supervisors Theo Hofman and Maarten Steinbuch. Theo, thank you for your guidance through each stage of the project. You encouraged and motivated me to pursue independent and innovative research. You insightful feedback has brought this dissertation to a higher level. Maarten, thank you for making this position possible. I appreciate your advice on my work. I am grateful for your support during this project.

I would like to extend my gratitude to my advisor Esin Ilhan Caarls at Bosch Transmission Technology. Esin, I am grateful for all your help and guidance. Thank you for all the fruitful discussions and I appreciate your valuable suggestions and insights from industry. Thank you for always reminding me of the importance of setting priorities. I wish to thank Rokus van Iperen at Bosch Transmission Technology for his feedback and support, who also played an important role in initiating the project. I would like to thank Jan-Dirk Kamminga at M2i for his support during this project.

I am also grateful to the many other colleagues at Bosch Transmission Technology, TU/e, and M2i for their help, feedback, and suggestions. I wish to thank the master students who have completed their internship and graduation projects with me.

The constructive feedback from the committee members, Prof. Delprat, Prof. Van Mierlo, Dr. Lazar and Dr. Wilkins, has enriched this thesis. I would like to thank them for reviewing the dissertation and taking part in the committee.

In addition, I wish to thank my roommates for creating a fun work environment. I would like to extend my sincere thanks to my friends for listening, encouraging, and supporting. I am grateful for the friendships.

Finally, I would like to extend my deepest gratitude to my family for their endless love.

Nomenclature

Acronyms

Acronym		Description
AC	–	alternating current
AMT	–	automated manual transmission
AOD	–	actuation on demand
AT	–	automatic transmission
BA	–	battery
BER	–	brake energy recuperation
CAB	–	cabin
CAC	–	charge air cooler
CADC	–	common artemis driving cycle
CAN	–	controller area network
CECMS	–	complete energy consumption minimization strategy
CETMS	–	combined energy and thermal management system
CH	–	charging
CP	–	convex programming
COP	–	coefficient of performance
CVT	–	continuously variable transmission
DC	–	direct current
DCT	–	dual clutch transmission
DDP	–	deterministic dynamic programming
DHT	–	dedicated hybrid transmission
DIRECT	–	dividing rectangles
DNR	–	drive, neutral and reverse
DO	–	distributed optimization
DP	–	dynamic programming
DSWHR	–	dual source waste heat recovery
ECMS	–	equivalent consumption minimization strategy
EGWHR	–	exhaust gas waste heat recovery
ELOP	–	electric oil pump
EM	–	electric machine

EMS	–	energy management system
EPWHR	–	electric path waste heat recovery
EV	–	electric vehicle
FCEV	–	fuel cell electric vehicle
FD	–	final drive
FHEV	–	full hybrid electric vehicle
FL	–	fuzzy logic
FT	–	fuel tank
FTP	–	federal test procedure
GA	–	genetic algorithm
GEN	–	generator
HEV	–	hybrid electric vehicle
HP	–	heat pump
HVAC	–	heating, ventilation, and air conditioning
ICDC	–	intercity drive cycle
ICE	–	internal combustion engine
ICEV	–	internal combustion engine vehicle
IETMS	–	integrated energy and thermal management system
JC08	–	japanese cycle '08
KPI	–	key performance indicator
MA	–	motor assist
MDSDO	–	multidisciplinary dynamic system design optimization
MHEV	–	mild hybrid electric vehicle
MINP	–	mixed integer nonlinear programming
MPC	–	model predictive control
NEDC	–	new european driving cycle
OB	–	optimization-based
OEM	–	original equipment manufacturer
OOL	–	optimal operating line
ORC	–	organic rankine cycle
PF	–	power follower
PHEV	–	plug-in hybrid electric vehicle
PID	–	proportional-integral-derivative
PMP	–	pontryagin's minimum principle
PMSM	–	permanent magnet synchronous machine
PSO	–	particle swarm optimization
RB	–	rule-based
SA	–	simulated annealing
SDP	–	stochastic dynamic programming
SETMS	–	separate energy and thermal management system
SOC	–	state of charge
SOD	–	start of development
SOE	–	state of energy
SOP	–	start of production
SQP	–	sequential quadratic programming

SS	–	standstill
SST	–	single speed transmission
TC	–	thermostat control
TCO	–	total cost of ownership
TEG	–	thermoelectric generator
TMS	–	thermal management system
TR	–	transmission
VA	–	variator
VCU	–	vehicle control unit
WH	–	wheel
WHR	–	waste heat recovery
WLTC	–	worldwide harmonized light vehicles test cycles

Greek

Symbol	Description	Unit
α	road grade, or pulley angle	$^\circ$
β	unit interval	-
γ	speed ratio	-
ϵ	effectiveness	-
ζ	fitting accuracy	-
η	efficiency	-
θ	temperature	$^\circ$C
ι	a small positive number	-
λ	co-state	-
μ	coefficient	-
ξ	state	-
Π	control policy	-
ρ	price, or density	€/kWh, or kg/m^3
σ	torque split	-
τ	torque	Nm
ϕ	air-flow rate	kg/s
ω	rotational speed	rpm

Roman uppercase

Symbol	Description	Unit
A	area	m^2
C	cost, or heat capacity	€, or J/K
D	diameter	m

E	energy	J
F	force	N
G	terminal cost	-
H	hamiltonian	-
I	current	A
J	cost function, or inertia	-, or kgm^2
N	countable number	-
P	power	W
Q	capacity	Ah
R	resistance, or radius	Ω, or m
S	distance	m
T	topology	-
U	control space	-
V	voltage, or volume	V, or m^3
X	state space	-
Z	surface	-

Roman lowercase

Symbol	Description	Unit
a	coefficient, or specific cost	-, or €/kg
b	specific cost	€
c	coefficient, or specific heat capacity	-, or J/kgK
f	function, or safety factor	-, or -
g	inequality constraint	-
h	equality constraint, or coefficient	-, or W/m^2K
k	stiffness coefficient, or heat transfer coefficient	N/m, or W/K
m	mass	kg
p	pressure	bar
q	flow rate	lpm
r	radius	m
s	design variable	-
t	time	s
u	control variable	-
w	external variable	-
x	state variable	-

Subscripts

Symbol	Description
a	ambient
b	battery, or pushbelt
c	cvt, or center
d	aerodynamic drag, or power demand
e	energy, or engine
f	fuel, or final drive
g	exhaust gas
h	electric path, or heating
i	inlet, or index
j	index
m	electric machine
o	outlet
p	primary pulley
r	rolling resistance, or pushbelt element rocking edge-saddle
s	secondary pulley, or single-speed transmission
t	thermal
v	vehicle, or variator
w	wheel
x	cabin

Superscripts

Symbol	Description
ad	admissible
fe	feasible
p	possible
s	small

Accents and operators

Symbol	Description
$\overline{y}$	upper bound of y
$\underline{y}$	lower bound of y
$\dot{y}$	derivative of y
y^{o}	optimum of y

Contents

Chapter 1

Introduction

Electrified powertrains are emerging to meet stringent emissions regulations and energy shortages. The continuously variable transmission (CVT) is gaining popularity, which improves energy efficiency and driving comfort of an electrified vehicle, due to the continuous ratio adjustment functionality. An optimal electrified powertrain design demands integrated design (e.g., the topology and component sizes) and control optimization considering both energy and thermal domains to minimize the energy consumption and system cost. This thesis aims to investigate the effectiveness of using this integrated design approach for electrified vehicles with the CVT technology. As electrified powertrains mainly comprise hybrid electric vehicles (HEVs) and electric vehicles (EVs), two case studies are conducted. From optimal control perspective, integrated energy and thermal management of a CVT-based plug-in hybrid electric vehicle (PHEV) with cabin heating, which is subject to a cold-start, is explored to identify the ultimate fuel savings of utilizing a dual-source waste heat recovery (DSWHR) system. From optimal design and control perspective, simultaneous powertrain design and control optimization of a CVT-based EV is investigated to minimize the total-cost-of-ownership (TCO) consisting of the energy consumption and system cost, which is extended by an integrated energy and thermal management design. Research questions related to the integrated design approach and these two case studies are formulated, which motivates the research objectives and scientific contributions, as will be discussed in this chapter.

1.1 Future of sustainable mobility

Faced with stringent emissions regulations and unprecedented energy shortages, various original equipment manufacturers (OEMs) have mapped out their electrification plans to reduce energy consumption and CO_2 emissions [2–4]. A recent forecast of new sales of passenger cars worldwide by 2030 is shown in Figure 1.1. It can be seen from Figure 1.1 that there are generally six types of passenger cars, namely internal

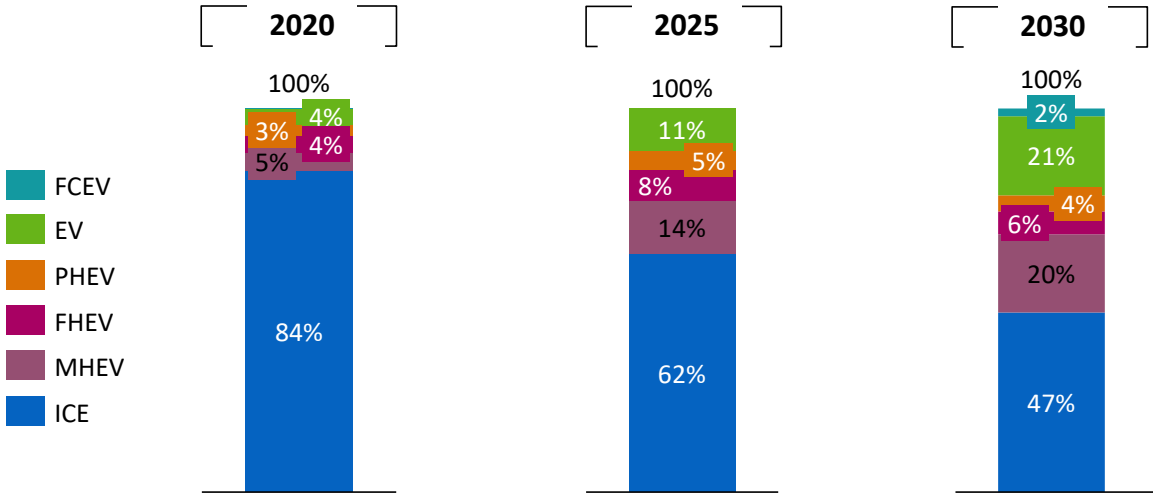

Figure 1.1: Market share of electrified vehicles in 2030 [1], where FCEV represents fuel cell electric vehicle, FHEV full hybrid electric vehicle, MHEV mild hybrid electric vehicle, and PHEV plug-in hybrid electric vehicle.

combustion engine vehicle (ICEV), mild hybrid electric vehicle (MHEV), full hybrid electric vehicle (FHEV), plug-in hybrid electric vehicle (PHEV), electric vehicle (EV), and fuel cell electric vehicle (FCEV). Furthermore, electrified powertrains will grow rapidly. Around half of the new passenger cars will have some form of electrification, and around one fifth of that will be an EV in 2030.

Automated transmissions, which let the electric machine (EM) and/or engine (e.g., hybrid system) operate at efficient regions by changing gear ratios, have the potential to increase the energy efficiency further [6]. Among them, owing to the continuous ratio adjustment functionality, increased energy efficiency, and improved driving comfort,

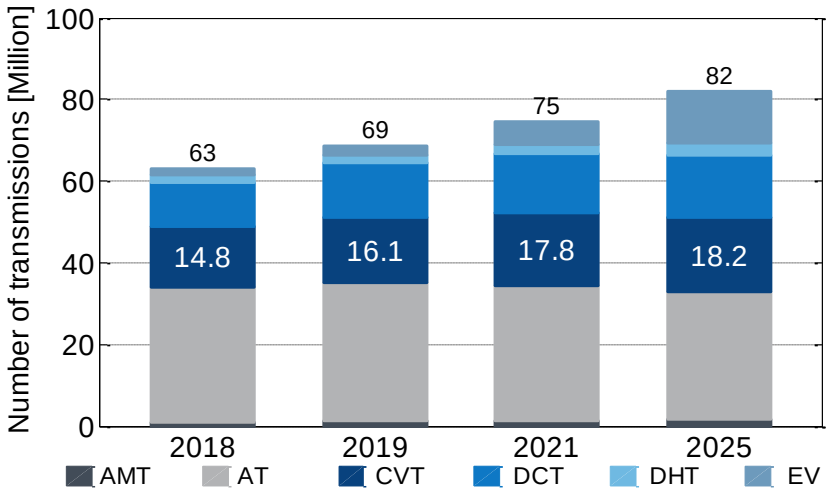

Figure 1.2: Forecast of worldwide produced automated transmissions with share of CVT [5], where AMT represents automated manual transmission, AT automatic transmission, DCT dual clutch transmission, DHT dedicated hybrid transmission, and EV single-speed transmission (SST).

the continuously variable transmission (CVT), as an advanced automated transmission, is gaining popularity [7], as demonstrated in Figure 1.2.

One of the most commonly developed CVT technologies is based on a pushbelt. The key component of the CVT is the variator, where two pulleys are connected by a pushbelt, as shown in Figure 1.3. Each pulley has a fixed sheave and a moveable sheave. The size of the pulleys can alter, resulting in infinite ratios within its ratio coverage. This allows the power source(s), e.g., internal combustion engine (ICE) and/or EM, to be independent of the power demand of the driver to optimize the operating point of the ICE and/or EM. Therefore, CVT-based electrified vehicles are considered as solutions for the future of sustainable mobility.

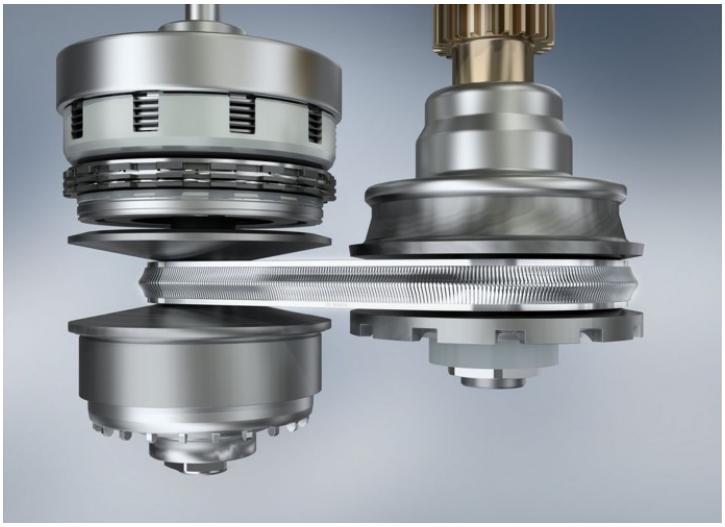

Figure 1.3: Pushbelt variator for CVT [8].

1.2 Integrated design approach

In order to obtain an optimal electrified vehicle design in the early design stage, in principle, three optimization layers should be considered, including topology, component size, and control optimization [9, 10], as illustrated in Figure 1.4. For example, control optimization refers to optimizing control performance using optimization (energy and thermal management). A topology that represents the connections between powertrain components influences the power flow (control). To realize a specific hybrid functionality, certain connections between components are needed [11]. Furthermore, the powertrain component size, e.g., the battery size, affects the control strategy, e.g., the power split between the engine and the battery, and vice versa [12]. Earlier studies have been mainly concerned with the energy domain, which only takes into consideration mechanical and electrical energy flows [13–16], and may not yield the optimal solution. Recent research has shown that the thermal domain, e.g., thermal management system (TMS), should also be taken into account, as it is an integral part of an electrified

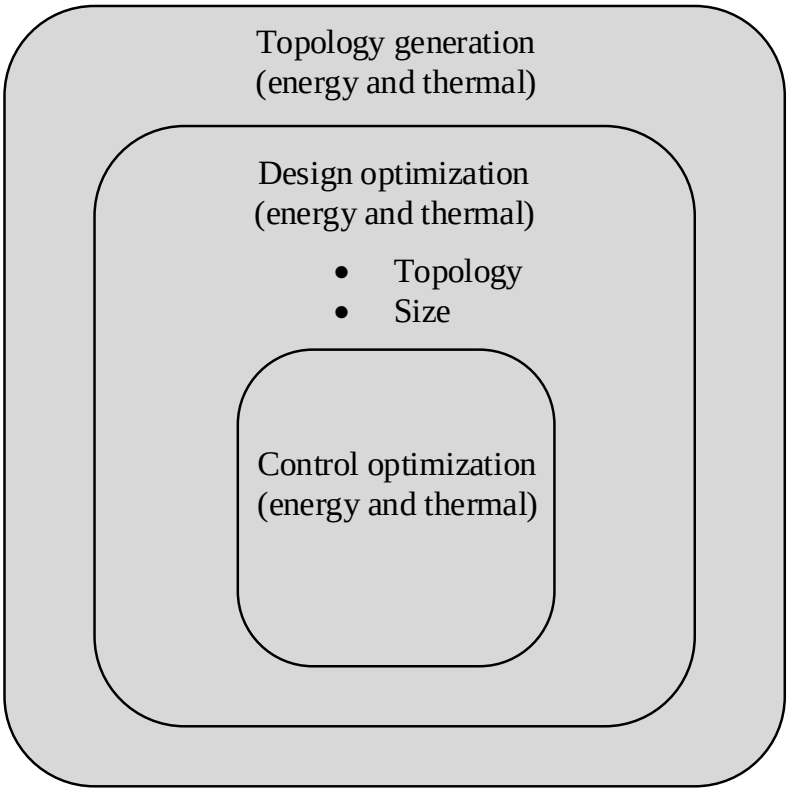

Figure 1.4: Design and control of electrified vehicles including both energy and thermal domains (Chapter 2). (**Outer** to **Inner**) Topology generation, plant, and controller.

powertrain (e.g., heat generation due to component power losses) and influences the overall energy consumption [7, 17, 18]. Hence, to arrive at an optimal active dynamical system design, these optimization layers should apply to both the energy and thermal domains. For instance, different powertrain topologies would require distinct thermal management architectures. This integrated design approach aims at optimizing the total-cost-of-ownership (TCO) comprising the energy consumption and system cost of an electrified vehicle. To minimize the energy consumption of an EV, the optimal power sharing between the powertrain and the cabin heating system is investigated in [19]; however, component sizing is not taken into account. For a double planetary gear hybrid powertrain, a combined topology and size optimization problem to minimize the fuel consumption is solved iteratively in [20], but the powertrain cost and the thermal domain are not considered. The thermal response and power consumption of the cooling system of a series HEV are investigated in [21]; however, the energy management system (EMS) is not optimized. Based on the current literature [12, 17, 20–26], a generic and systematic way to analyze and link those optimization layers for electrified vehicles has yet to be established, in consideration of both the energy and thermal domains. Therefore, the first set of research questions of this thesis regarding the integrated design approach for electrified vehicles ($\boldsymbol{R}_{1a}$ and $\boldsymbol{R}_{1b}$) is the following:

- $\boldsymbol{R}_{1a}$: *What are the interconnections between the various optimization layers (i.e., topology, component size, and control), considering both the energy and thermal domains; and,*

- $\boldsymbol{R}_{1b}$: *How do they influence the optimality of an electrified vehicle design?*

Identifying the interconnections between the optimization layers can provide insights into the selection of optimization strategies for different layers and opportunities for reducing the TCO of an electrified vehicle considering both the energy and thermal domains. Electrified vehicles, in this case, mainly comprise (P)HEVs and EVs.

1.3 Integrated energy and thermal management

For an HEV with a chosen powertrain topology, which means that the design layer is fixed, of particular importance is to develop an EMS to fulfill its potential in reducing the fuel consumption. The EMS represents the controller design at supervisory level. The primary goal of the EMS is to determine the power flow of the HEV (e.g., the torque split between the ICE and EM) in an optimal manner so that the fuel efficiency (CO_2 and/or other pollutant emission reductions) is maximized. To solve this control problem, a vast amount of literature exists, including both rule-based (RB) and optimization-based (OB) strategies, such as dynamic programming (DP), Pontryagin's minimum principle (PMP), and equivalent consumption minimization strategy (ECMS) [14, 16, 26, 27]. Note that a RB strategy provides a feasible solution but not the optimal one. Among OB strategies, DP is widely chosen, as it finds a globally optimal solution, while handling nonliear and non-convex constraints [13, 15, 16, 24]. However, one of the hidden assumptions of developing EMSs in these studies is that the engine is already at its operating temperature at the beginning of the driving mission (a warm-start), which is not realistic. The impact of cold-start conditions should be taken into consideration [7]. A cold-start implies a low engine temperature, which increases frictional losses in the engine, leading to excess fuel consumption due to high-viscosity effects. Due to efficient and intermittent engine operation, this effect holds for a longer time in an HEV than for its traditional equivalent. The difference in fuel consumption between a warm-start and a cold-start is regarded as the fuel-saving potential. Few attempts can be found to close this gap [28]; that is, to improve fuel efficiency with cold-start conditions and thereby quantify the ultimate fuel savings that could be realized in reality.

In order to gain qualitative insights into areas where most of the fuel economy improvements could be obtained, a numerical simulation was carried out to analyze the energy losses of a PHEV, as illustrated in Figure 1.5. The vehicle is subject to a cold-start. It can be observed that the engine accounts for most of the energy losses. A large part of the fuel energy is wasted into the surroundings, in the form of exhaust gases. Hence, recuperating a certain amount of that energy, which would otherwise be dissipated into the environment, is a promising way to improve powertrain efficiency

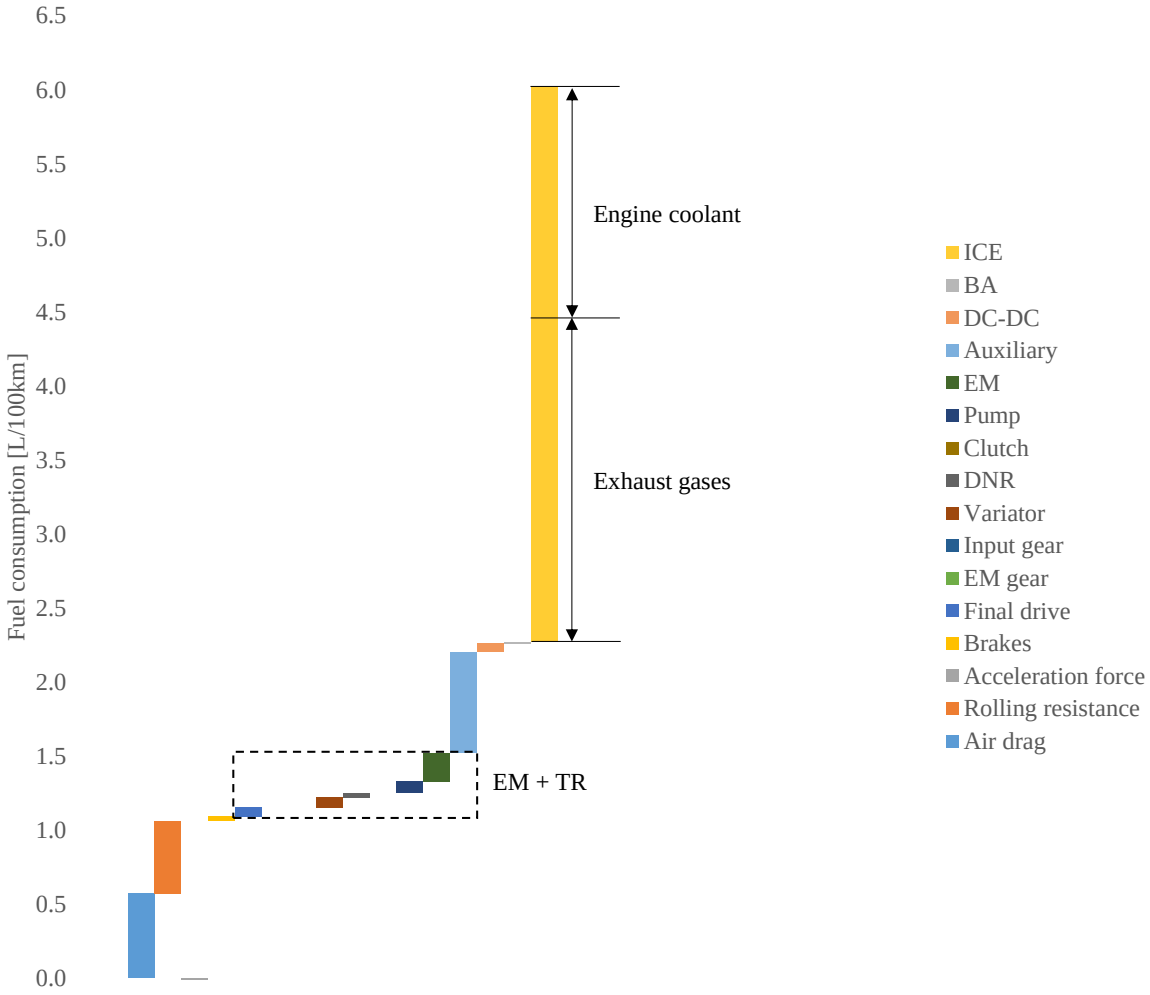

Figure 1.5: Typical energy balance of a PHEV in charge-sustaining mode, where BA represents the battery, DC-DC the DC (direct current) to DC converter, DNR the drive, neutral, and reverse set, EM the electric machine including inverter, and TR the transmission [29].

[30–33]. Harvesting waste heat from exhaust gases is termed exhaust gas waste heat recovery (EGWHR). It has been reported that EGWHR systems have an efficiency of up to 15% [31, 34–36]. This technology is mainly adopted for ICEVs [33, 37], even though a few applications can be found in HEVs. It can also be seen from Figure 1.5 that auxiliary power demand (cabin heating, in this case) consumes a significant amount of energy from the battery, which eventually leads to fuel consumption with charge sustenance. Obviously, using electricity from the battery directly, conventional electric heaters are not able to provide an economic solution. To reduce energy consumption, a heat pump (HP), owing to higher coefficient-of-performance (COP), has proved to be a promising alternative [38–40]. Traditionally, an HP only extracts heat from the outside air to heat the cabin. As is made evident by Figure 1.5, the amount of waste heat from EM (including inverter) and TR is significant as well. Recuperating a certain percentage of that power, which would otherwise be wasted ambiently, rather than using additional power from the battery, is a promising way

to promote energy efficiency. Recuperating waste heat from EM and TR is termed electric path waste heat recovery (EPWHR). It has been shown that, the heating capacity and COP increase by around 31.5% and 9.3% [41], respectively, by employing an EPWHR system. HPs are mostly used in EVs [41, 42].

An HEV, especially a PHEV, can be identified as a mixture of an ICEV and an EV, which benefits from the technological advancements on both sides. Yet, a combination of selected technologies—an EGWHR system and an EPWHR system—have hardly been investigated in the (P)HEV context. Thus, the second research question of this thesis with respect to integrated energy and thermal management of HEVs ($\boldsymbol{R}_2$) is formulated as follows:

- $\boldsymbol{R}_2$: *What is the fuel efficiency improvement of using a DSWHR system comprising an EGWHR sub-system and an EPWHR sub-system in a CVT-based PHEV with cabin heating and cold-start conditions?*

Figure 1.6 shows a schematic representation of the considered CVT-based parallel PHEV with an EGWHR sub-system and an EPWHR sub-system. There are three main types of HEVs, namely series, parallel, and series-parallel hybrids. Compared to a series hybrid, a parallel hybrid eliminates the need for conversion of engine mechanical power to electrical power. A parallel hybrid is also simpler than a series-parallel hybrid. The considered PHEV has five different driving modes: engine (ICE), charging (CH), electric vehicle (EV), motor assist (MA), and brake energy recuperation (BER). The ICE mode represents when only the engine is used to propel the vehicle. The CH mode indicates that the engine not only drives the wheels, but also charges the battery. The EV mode means that the EM is the only power source and the engine is off. The MA mode reflects when the EM is utilized to assist the engine to meet the driving demand. The BER mode is a mode where the braking energy is recuperated and stored into the battery. It is important to determine the driving mode to reduce the fuel consumption, by controlling the torque split between the ICE and EM. A cold-start is considered, which represents the thermodynamics heating of the engine, as indicated by the dashed block. The EGWHR sub-system represented by HX_1 recovers waste heat from exhaust gases, which is converted into electricity and stored in the battery as the energy storage system of the PHEV. It is advantageous to store that energy in the energy buffer from a control point of view. The EPWHR sub-system represented by HX_2 recuperates waste heat from the EM (including inverter) and a CVT, to boost the heating performance of an HP for cabin heating. The underlying fuel consumption (J_I) minimization problem for a known drive cycle starting at t_0 and ending at t_f is mathematically formulated by

$$J_I(\boldsymbol{x}_I(t), \boldsymbol{u}_I(t), t) = \int_{t_0}^{t_\mathrm{f}} P_I(\boldsymbol{x}_I(t), \boldsymbol{u}_I(t), t)\ \mathrm{d}t, \tag{1.1}$$

$$\text{s.t.} \quad \dot{\boldsymbol{x}}_I(t) = \boldsymbol{f}(\boldsymbol{x}_I(t), \boldsymbol{u}_I(t), t), \tag{1.1a}$$

$$h_I(\boldsymbol{x}_I(t), \boldsymbol{u}_I(t), t) = 0, \tag{1.1b}$$

$$g_I(\boldsymbol{x}_I(t), \boldsymbol{u}_I(t), t) \leq 0, \tag{1.1c}$$

$$\boldsymbol{x}_I(t_\mathrm{f}) = \boldsymbol{x}_I(t_0), \tag{1.1d}$$

where I represents the first case study regarding integrated energy and thermal management. P_I denotes the fuel power. The state vector $\boldsymbol{x}_I$ denotes the dynamics of the system (1.1a), for instance, the state-of-charge (SOC) of the battery that changes over time and the engine temperature. Equation (1.1d) constrains the dynamic states, such as charge-sustaining. This means the SOC of the battery at the beginning of a driving mission is equal to the SOC at the end of the trip. It is feasible, as there are multiple power sources in an HEV and the engine can be used to charge the battery. The battery is utilized as an energy buffer, and the energy is ultimately from the fuel tank. Charge-sustaining is a common way to evaluate the performance of the control strategy. $\boldsymbol{u}_I$ denotes the control inputs, e.g., the torque split between the ICE and EM. The remaining equality constraint $h_I(\cdot)$ denotes the power balance of the vehicle (1.1b). $g_I(\cdot)$ denotes the inequality constraints (1.1c), such as the torque limits of the EM,

$$\tau_{\mathrm{m},0}(t) \in [\underline{\tau}_{\mathrm{m},0}(\omega_{\mathrm{m}}(t)), \overline{\tau}_{\mathrm{m},0}(\omega_{\mathrm{m}}(t))], \tag{1.2}$$

where ω_{m} is the EM speed.

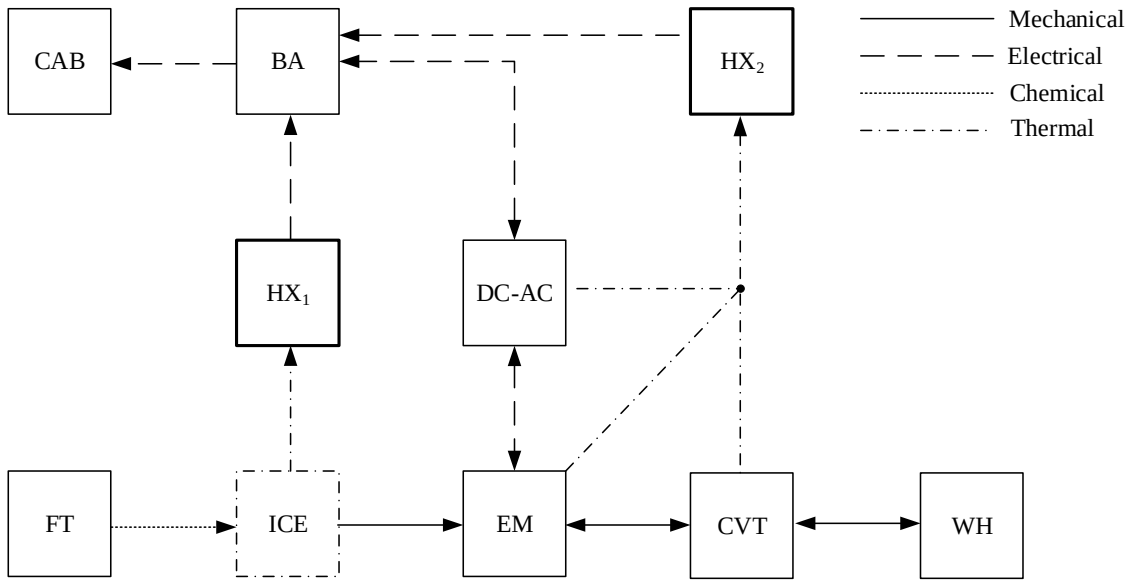

Figure 1.6: Schematic representation of the considered CVT-based plug-in hybrid electric vehicle with a dual-source waste heat recovery system (Chapter 3), where CAB represents the cabin, DC-AC the DC to AC (alternating current) inverter, FT the fuel tank, WH the wheel, HX_1 the exhaust gas waste heat recovery sub-system, and HX_2 the electric path waste heat recovery sub-system.

1.4 Integrated design and control

Section 1.3 focuses on the controller layer for a fixed powertrain. However, in addition to integrated energy and thermal management, an optimal active dynamical system demands combined design (e.g., powertrain topology and component size) and control

optimization, taking into account the coupling between the physical system and the control strategy [11, 43]. For a given vehicle configuration, the component size, e.g., the EM size in power, affects the control decision, and vice versa. Moreover, the component size influences the system cost. The combined design and control optimization aims to optimize the TCO. This is especially the case for EVs. In order to increase the market penetration of EVs, it is important to reduce both energy consumption and system cost [44, 45].

Currently, the emerging EV market is mainly dominated by the single-speed transmission (SST) due to its system simplicity. Despite its simplicity, an SST poses conflicting requirements for an EM. At low speeds, the EM has to offer a good drive-off performance, resulting in large dimensions and magnetic forces, which have a negative impact on their ability, at high speeds, to achieve the vehicle top speed. This leads to a relatively large and heavy design, which influences power density, energy consumption, driving range, and cost [45]. To address this issue, studies on multi-speed transmissions, such as two-speed transmissions and CVTs, are emerging, focusing on energy efficiency, system cost, and performance [45–51]. Porsche Taycan features a two-speed transmission [50]. Automotive supplier ZF presents a two-speed transmission for EVs, which promises increasing either the driving range by up to 5% or the vehicle top speed, compared to its single-speed counterpart [51]. Compared with an EV equipped with an SST, a CVT can improve the EM cycle efficiency by more than 3% [52]. Figure 1.7 shows the historical and future trends of the maximum number of speeds for ICEVs and EVs. It can be observed that, for EVs, the number of speeds is expected to increase, by analogy with ICEVs. A CVT can be used to solve the problem as mentioned above, due to ratio variation between the underdrive (UD) and overdrive (OD) ratio, as shown in Figure 1.8. At low vehicle speeds, the UD ratio can be used to increase the torque, and at high vehicle speeds, the OD ratio can be utilized to reduce the EM speed [53]. A CVT can reduce the nominal torque, maximum speed, and active materials of the EM, and because of a large speed range,

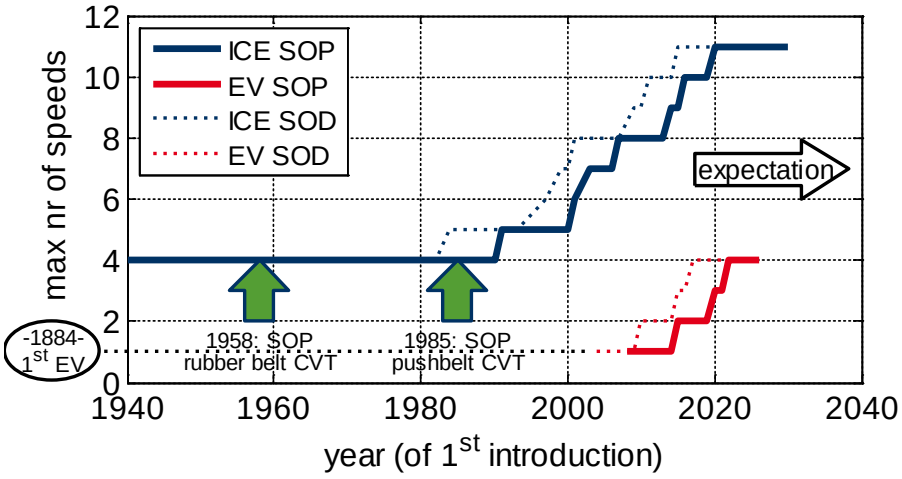

Figure 1.7: Historical and future trends of the maximum number of speeds for ICEVs and EVs, where SOD represents start-of-development and SOP start-of-production [45].

the EM can reduce the required ratio coverage of the CVT, leading to a compact design [52, 54]. A CVT can thus partly compensate the additional actuation losses.

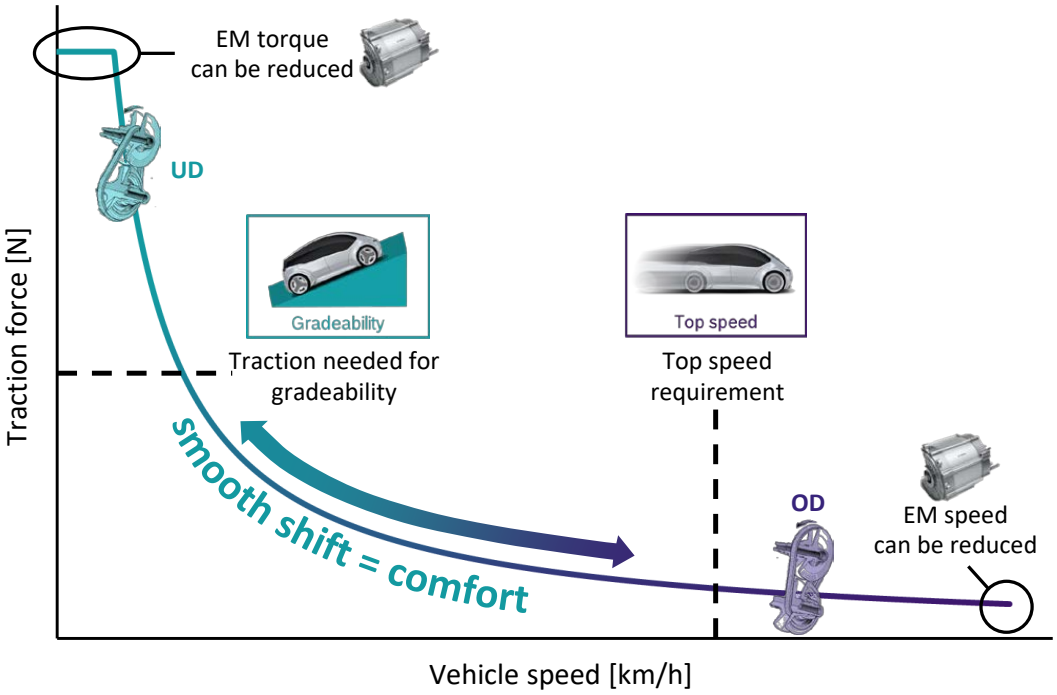

Figure 1.8: The continuously variable transmission technology for an electric vehicle, where UD represents the underdrive ratio of the CVT and OD the overdrive ratio [53].

To date, design of EVs (including CVT-based) is largely based on off-the-shelf components due to cost, and powertrain components are typically not optimized [44]. The component size, e.g., the EM size in kW and battery size in kWh, is associated with the component cost. Finding optimal component sizes would contribute to cost reduction. Moreover, EV energy consumption is largely influenced by the driveline efficiency. In this respect, the integration of the EM and the CVT, plays a key role [45]. The CVT could provide opportunities of optimizing the EM, thanks to the continuous ratio adjustment functionality, and the wider power availability of the EM, in turn, could offer opportunities of optimizing the CVT. In literature, however, the EM and the CVT are often treated independently and standard CVT controllers developed for conventional ICEVs are used, where the speed ratio of the CVT is controlled to reduce the EM power losses. The influence of the EM size, CVT size, and the CVT efficiency are not always considered simultaneously [44]. In order to maximize system (combined EM and CVT) efficiency and minimize system cost, the coupling between the EM and the CVT from design and control perspectives has yet to be investigated. In order to address these issues, design and control frameworks are required.

This type of design problem can be tackled by different approaches. For instance, the optimal component sizes can be found iteratively, by using RB control [55, 56]. However, these methods do not guarantee a globally optimal solution. To overcome this limitation, DP, as an OB strategy, can be used to find the optimal control inputs

[57]. DP can also be utilized in combination with an evolutionary algorithm to find component sizes [24]. However, the computation time increases rapidly with complexity and the number of state variables, which may not be tractable [10, 58]. An alternative is to use convex programming (CP), which finds optimal component sizes and control trajectories simultaneously without the need of checking optimality, and it is computationally efficient [59]. It enables optimization of problems with many dynamic states (e.g., thermal states), extensive parameter variation studies, and evaluation of diverse design aspects. CP requires the problem and models to be convex. Additionally, employing a CVT for an EV is a novel concept. Applying advanced optimization methods to optimize CVT-based EVs and providing design considerations for EVs including the thermal domain have hardly been found. Hence, the third set of research questions of this thesis regarding integrated design and control of CVT-based EVs ($\boldsymbol{R}_{3\mathrm{a}}$ and $\boldsymbol{R}_{3\mathrm{b}}$) is the following:

- $\boldsymbol{R}_{3\mathrm{a}}$: *What are the interconnections between the CVT and EM in an EV including the thermal domain; and,*
- $\boldsymbol{R}_{3\mathrm{b}}$: *How can they be efficiently and optimally designed and controlled in order to minimize the TCO?*

Identifying the interconnections between the CVT and EM can provide insights into the design of a CVT controller that controls the CVT speed ratio to reduce the powertrain losses. They can also provide insights into determining the CVT, EM and battery sizes to reduce the system cost. Figure 1.9 illustrates a schematic representation of the considered CVT-based EV. The CVT speed ratio over time (control) influences the EM and CVT operation and their sizes (design). The EM size has an effect on the CVT speed ratio and its size (e.g., ratio coverage). The EM size also influences the battery size. The CVT size affects its speed ratio and the EM size. There is a trade-off between the EM size, EM operation, CVT size, and CVT operation. Component sizes are associated with component costs. Moreover, a TMS is designed to remove heat (power losses) generated by the EM and CVT, maintain their temperatures below prescribed thermal limits, and reduce cooling power consumption. Finding the desired air-flow rate (control) of the cooling system is essential. Therefore, it is important to find the optimal design and control variables to reduce the TCO. The underlying design and control optimization problem to minimize the TCO (J_{II}) for a given drive cycle starting at t_0 and ending at t_f is mathematically formulated by

$$J_{II}(\boldsymbol{s}_{II}, \boldsymbol{x}_{II}(t), \boldsymbol{u}_{II}(t), t) = \int_{t_0}^{t_\mathrm{f}} (\rho_\mathrm{e}\ P_{II}(\boldsymbol{s}_{II}, \boldsymbol{x}_{II}(t), \boldsymbol{u}_{II}(t), t))\ \mathrm{d}t + C_{II}(\boldsymbol{s}_{II}), \tag{1.3}$$

$$\text{s.t.} \quad \dot{\boldsymbol{x}}_{II}(t) = \boldsymbol{f}(\boldsymbol{s}_{II}, \boldsymbol{x}_{II}(t), \boldsymbol{u}_{II}(t), t), \tag{1.3a}$$

$$h_{II}(\boldsymbol{s}_{II}, \boldsymbol{x}_{II}(t), \boldsymbol{u}_{II}(t), t) = 0, \tag{1.3b}$$

$$g_{II}(\boldsymbol{s}_{II}, \boldsymbol{x}_{II}(t), \boldsymbol{u}_{II}(t), t) \leq 0, \tag{1.3c}$$

$$\boldsymbol{s}_{II} \in [\underline{\boldsymbol{s}}_{II}, \overline{\boldsymbol{s}}_{II}], \tag{1.3d}$$

where II represents the second case study regarding integrated design and control.

$\boldsymbol{s}_{II}$ denotes the design variables, e.g., the EM size, ρ_{e} the price of electricity, P_{II} the battery power, and C_{II} the powertrain cost, e.g., the EM price C_{m}, which depends on the EM size represented by a scaling factor s_τ, i.e.,

$$C_{\mathrm{m}} = s_\tau \, C_{\mathrm{m},0}, \tag{1.4}$$

where $C_{\mathrm{m},0}$ is the initial EM cost. As an example, referring to (1.2), the component size influences the control strategy as follows:

$$\tau_{\mathrm{m}}(t) \in s_\tau \, [\underline{\tau}_{\mathrm{m},0}(\omega_{\mathrm{m}}(t)), \overline{\tau}_{\mathrm{m},0}(\omega_{\mathrm{m}}(t))]. \tag{1.5}$$

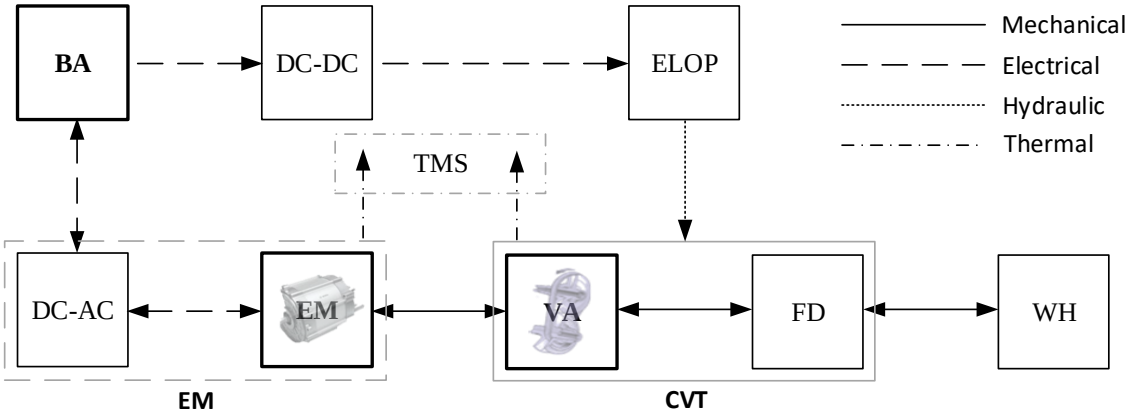

Figure 1.9: Schematic representation of the considered CVT-based electric vehicle (Chapter 4), where ELOP represents the electric oil pump, FD the final drive, and VA the variator. The EM and DC-AC inverter are combined together. The VA and FD are combined together.

1.5 Research objectives and contributions

In order to answer the first set of research questions of the thesis with respect to the integrated design approach for electrified powertrains ($\boldsymbol{R}_{1\mathrm{a}}$ and $\boldsymbol{R}_{1\mathrm{b}}$), the following objectives are defined:

- $\boldsymbol{O}_1$: Introduce the general problem of design (topology and component size) and control optimization of electrified powertrains taking into account both the energy and thermal domains.
- $\boldsymbol{O}_2$: Identify the challenges and opportunities in obtaining an optimal electrified vehicle design with respect to TCO.

The following objectives are defined to find a solution to the second research question of the thesis regarding integrated energy and thermal management of HEVs ($\boldsymbol{R}_2$):

- $\boldsymbol{O}_3$: Quantify the benefit of adopting a DSWHR system on the ultimate fuel savings of a CVT-based PHEV with cabin heating, which is subject to a cold-start.

- $\boldsymbol{O}_4$: Analyze the effects of engine temperature, driving conditions, and DSWHR efficiency on the fuel consumption of the CVT-based PHEV.

To tackle the third set of research questions of the thesis with respect to integrated design and control of CVT-based EVs ($\boldsymbol{R}_{3a}$ and $\boldsymbol{R}_{3b}$) leads to the following objectives:

- $\boldsymbol{O}_5$: Develop a computationally efficient and optimal design and control optimization strategy for a CVT-based EV to minimize its TCO.

- $\boldsymbol{O}_6$: Analyse the optimized CVT-based EV and provide design considerations for EVs including the thermal domain.

In order to realize these objectives, this study originally investigates design and control optimization methods for electrified powertrains taking into account both energy and thermal domains to reduce the energy consumption and TCO, resulting in the following contributions ($\boldsymbol{C}_1$ - $\boldsymbol{C}_5$).

- $\boldsymbol{C}_1$: The general problem of combined topology, size and control optimization of electrified powertrains is introduced from both energy and thermal perspectives and how they can be connected mathematically is revealed. Current energy and thermal management systems are also surveyed and classified in terms of optimality and causality. Potential research directions of design and control of electrified vehicles are identified to further reduce the energy consumption and system cost, considering both the energy and thermal domains (Chapter 2).

- $\boldsymbol{C}_2$: In order to investigate the effect of a WHR system on a CVT-based PHEV with a cold-start, a set of nonlinear and non-convex models is built, including energy dynamics and thermodynamics based on measurements. An integrated energy and thermal management system (IETMS) is proposed to identify the gain of employing a DSWHR system on the ultimate fuel savings of the CVT-based PHEV, by using DP. The DSWHR system is constituted of an EGWHR sub-system and an EPWHR sub-system (Chapter 3).

- $\boldsymbol{C}_3$: For the CVT-based PHEV with cabin heating and cold-start conditions, insights into reducing the impact of a cold-start, design of a DSWHR system, and dimensioning of powertrain components are provided (Chapter 3).

- $\boldsymbol{C}_4$: For an SST-based EV[1], an experimentally[2] validated driveline model including energy dynamics and thermodynamics is created to replicate the vehicle behavior. A CVT-based EV model is then developed on the basis of the SST-

[1]The SST-based EV model is with reference to a series production vehicle.
[2]Measurement data are obtained from a real-world drive cycle within Netherlands.

based EV model[3]. Based on measurements, a set of convex models of the CVT-based EV including component cost models is subsequently developed, especially the coupling between the EM and the CVT from design and control perspectives (Chapter 4).

- $\boldsymbol{C}_5$: On the basis of the developed convex models, a combined optimal design and control (co-design) optimization method based on convex programming (CP) is originally proposed to find the optimal CVT speed ratio and air-flow rate of the cooling system reducing the TCO. It also simultaneously identifies the optimal component sizes of the battery (kWh), EM (kW) and CVT (ratio coverage). The optimized CVT-based EV is then analyzed to provide design considerations for EVs including the thermal domain (Chapter 4).

1.6 Outline of the thesis

This thesis consists of an introductory chapter (Chapter 1), three research chapters (i.e., Chapters 2-4), and a final chapter (Chapter 5) that summarizes research findings and presents future work, as shown in Figure 1.10.

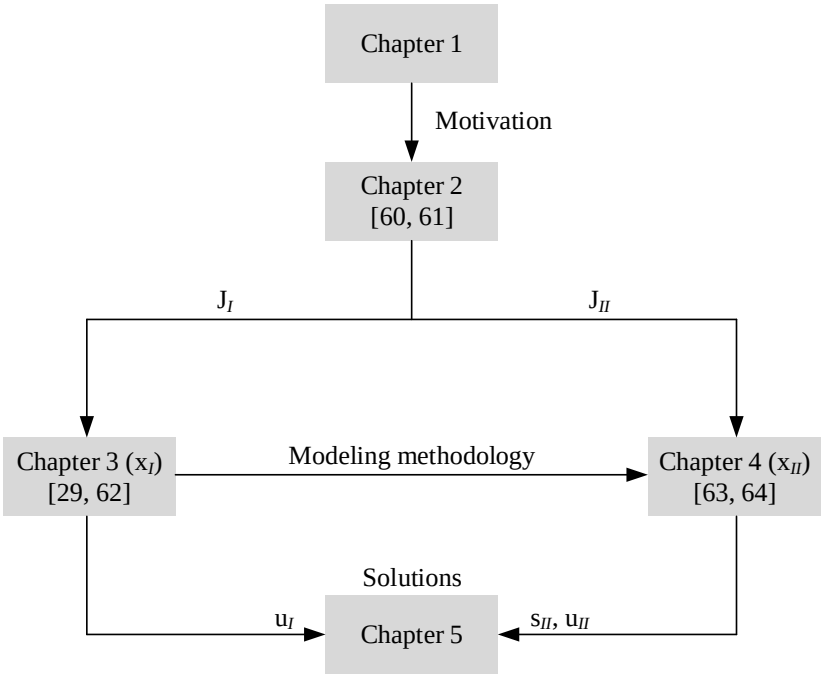

Figure 1.10: Outline of the thesis.

[3]Only the SST is replaced by the CVT (based on off-the-shelf component, which is not optimized) and other components remain the same. The CVT model is developed based on experiment data from a test rig.

Motivated by the above discussion, a review of the integrated design and control of electrified powertrains considering both energy and thermal domains is presented in Chapter 2. The content of Chapter 2 is based on [60, 61]. Specifically, from energy perspective, the problem definition of combined topology, size and control optimization of electrified vehicles is given mathematically, which is then introduced to the thermal domain. The connections between the optimization layers, coordination methods, energy domain, and the thermal domain are provided. Afterwards, energy and thermal management systems, which only started to appear recently, are surveyed and classified into separate energy and thermal management systems (SETMSs) and combined energy and thermal management systems (CETMSs). The importance of integration is highlighted. In order to reduce TCO further, potential research directions in this field are identified.

Based on the opportunities found in Chapter 2, as electrified powertrains comprise (P)HEVs and EVs, two case studies are conducted so as to demonstrate the effectiveness of integrated design approach, which are given as follows:

- *Integrated energy and thermal management*: From optimal control perspective (J_I in (1.1)), an IETMS is presented to quantify the benefit of using a DSWHR system in a CVT-based PHEV (Figure 1.6) with cold-start conditions (Chapter 3).

- *Integrated design and control*: From optimal design and control perspective (J_{II} in (1.3)), a simultaneous powertrain (e.g., component size) and control design optimization method is proposed to optimize a CVT-based EV (Figure 1.9), which is extended by integrated energy and thermal management (Chapter 4).

The content of Chapter 3 is based on [29, 62]. Specifically, in Chapter 3, for a CVT-based PHEV with cabin heating, a set of nonlinear and non-convex models including the coupling between energy dynamics and thermodynamics (x_I) is firstly developed to investigate cold-start and WHR. Based on the models created, an IETMS is designed to identify the influence of cold-start conditions on the fuel-saving potential and the gain of utilizing the DSWHR system. The optimal control input (u_I) to minimize the fuel consumption is obtained by using DP. The effects of parameter variation on the fuel consumption are also explored. Insights into reducing the impact of cold-start conditions, design of WHR technologies, and dimensioning of powertrain components are provided as well.

The content of Chapter 4 is based on [63, 64]. Specifically, in Chapter 4, an SST-based EV model comprising energy dynamics and thermodynamics (x_{II}) is firstly created (Appendix C), which follows the same modeling methodology as Chapter 3. This model is validated against measurement data obtained from a series production vehicle. A CVT-based EV model is then developed based on the SST-based EV model, where only the SST is replaced by a CVT (based on off-the-shelf component), which is presented in Appendix D. The CVT-based EV model is subsequently convexified, where the coupling between the CVT and the EM from design and control perspectives

is given in detail. Convex cost models are also developed. On the basis of these convex models, a co-design optimization method based on CP is developed. It simultaneously finds the optimal design and control variables (s_{II},u_{II}) to minimize the TCO. The optimized CVT-based EV with co-design is also analyzed in detail to provide design considerations for EVs including the thermal domain.

The research findings are summarized in Chapter 5, which also gives recommendations for future research.

1.7 List of publications

This thesis results in the following publications.

Refereed journal publications

[1] Wei, C.; Hofman, T.; Ilhan Caarls, E.; van Iperen, R. Integrated Energy and Thermal Management for Electrified Powertrains. Energies 2019, 12, 2058. https://doi.org/10.3390/en12112058

[2] Wei, C.; Hofman, T.; Ilhan Caarls, E.; van Iperen, R. A Review of the Integrated Design and Control of Electrified Vehicles. Energies 2020, 13, 5454. https://doi.org/10.3390/en13205454

[3] Wei, C.; Hofman, T.; Ilhan Caarls, E.; van Iperen, R. Co-design of CVT-based Electric Vehicles, submitted as journal article, currently under review.

[4] Wei, C.; Hofman, T.; Ilhan Caarls, E.; van Iperen, R. Design and Analysis of CVT-based Electric Vehicles, submitted as journal article, currently under review.

Refereed conference publications

[5] Wei, C.; Hofman, T.; Ilhan Caarls, E.; van Iperen, R. Progress in Maximizing Electrified Powertrain Efficiency. In Proceedings of the 32nd International Electric Vehicle Symposium, Lyon, France, 19-22 May 2019.

[6] Wei, C.; Hofman, T.; Ilhan Caarls, E.; van Iperen, R. Zone Model Predictive Control for Battery Thermal Management Including Battery Aging and Brake Energy Recovery in Electrified Powertrains. In Proceedings of the 9th IFAC International Symposium on Advances in Automotive Control, Orléans, France, 24-27 June 2019. https://doi.org/10.1016/j.ifacol.2019.09.049

[7] Wei, C.; Hofman, T.; Ilhan Caarls, E.; van Iperen, R. Optimal Control of an Integrated Energy and Thermal Management System for Electrified Powertrains. In Proceedings of the 2019 American Control Conference, Philadelphia, PA, USA, 10-12

July 2019. https://doi.org/10.23919/ACC.2019.8815244

[8] Wei, C.; Hofman, T.; Ilhan Caarls, E.; van Iperen, R. Energy-Efficiency Improvement Potential of Electric Vehicles Considering Transmission Temperature. In Proceedings of the 8th IFAC Symposium on Mechatronic Systems, Vienna, Austria, 4-6 September 2019. https://doi.org/10.1016/j.ifacol.2019.11.676

[9] Wei, C.; Hofman, T.; Ilhan Caarls, E.; van Iperen, R. Evolution and Classification of Energy and Thermal Management Systems in Electrified Powertrains. In Proceedings of the 2019 IEEE Vehicle Power and Propulsion Conference, Hanoi, Vietnam, 14-17 October 2019. https://doi.org/10.1109/VPPC46532.2019.8952261

[10] Wei, C.; Hofman, T.; Ilhan Caarls, E.; van Iperen, R. Combined Design and Control Optimization of CVT-based Electric Vehicles, submitted as conference paper, currently under review.

Non-refereed publications

[11] Wei, C.; Hofman, T.; Ilhan Caarls, E.; van Iperen, R. Integrated Energy and Thermal Management Systems for CVT-based Electrified Powertrains. International VDI Workshop – System design for advanced CVTs, Baden-Baden, Germany, 18 March 2019.

[12] Wei, C.; Hofman, T.; Ilhan Caarls, E.; van Iperen, R. Integrated Energy and Thermal Management of Electrified Powertrains - A Material Perspective, M2i Conference 2019, Noordwijkerhout, The Netherlands, 9-10 December 2019.

Chapter 2

A review of the integrated design and control of electrified vehicles

This chapter[1] gives an overview of design and control optimization of electrified vehicles including energy and thermal domains. An introduction to the topic is given in Section 2.1. Section 2.2 analyzes the optimization layers and coordination schemes from energy perspective, which are investigated from thermal viewpoint in Section 2.3. Recent combined energy and thermal management systems (CETMSs) proposed in literature are discussed in detail in Section 2.4. Section 2.5 presents opportunities found for future developments. Finally, conclusions are drawn in Section 2.6.

2.1 Introduction

Powertrain electrification plays a crucial role in reducing the unsustainable consumption of natural resources to tackle energy and environmental issues. To fulfill the potential of an electrified vehicle, it is important to develop an energy management system (EMS). The main goal of the EMS is to maximize powertrain efficiency, by optimizing the power flow, such as the power split between the internal combustion engine (ICE) and the battery in a parallel hybrid electric vehicle (HEV). While electrified powertrains bring opportunities of improving energy efficiency, due to added heat source components and distinct driving modes, they introduce complexities to the associated thermal management systems (TMSs) [65–67]. A TMS is essential to maintain powertrain components at predefined temperatures to guarantee efficiency,

[1]The content of this chapter is based on the following publications:
Wei, C.; Hofman, T.; Ilhan Caarls, E.; van Iperen, R. Evolution and Classification of Energy and Thermal Management Systems in Electrified Powertrains. In Proceedings of the 2019 IEEE Vehicle Power and Propulsion Conference, Hanoi, Vietnam, 14-17 October 2019.
Wei, C.; Hofman, T.; Ilhan Caarls, E.; van Iperen, R. A Review of the Integrated Design and Control of Electrified Vehicles. Energies 2020, 13, 5454.

comfort, safe operation, and reliability. Earlier works have shown that a TMS has a significant impact on the energy consumption of an electrified vehicle, e.g., heating, ventilation, and air conditioning (HVAC) [68, 69]. The EMS and the TMS of an electrified powertrain were often treated independently in previous studies, as shown in Figure 2.1. In this scheme, the TMS requests a certain amount of power from the EMS, but whether the control decision of the TMS is energy beneficial is not verified by the EMS. It may not yield the optimal solution [66]. Therefore, it is imperative to integrate these two systems.

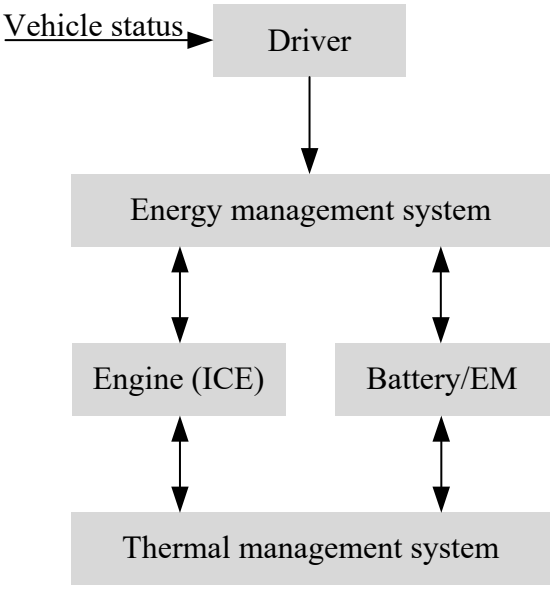

Figure 2.1: Separate energy and thermal management.

The EMS and the TMS are referred as control algorithms, which are often developed for fixed configurations and parameters [70, 71]. However, concurrent design and control optimization is required to arrive at an optimal system, considering the coupling between the physical system and the control algorithm [11, 43]. In principle, there are three optimization layers for designing an electrified vehicle, including topology, size and control optimization [9, 10], as illustrated in Figure 1.4. Hence, these optimization layers should apply to both energy and thermal domains. In this respect, the thermal domain was usually not considered in previous research, which may not arrive at an optimal solution [72]. For instance, different powertrain configurations would require distinct thermal management topologies.

As far as the coupling between the plant (topology and size) and the controller is concerned, there are generally four coordination schemes, including sequential, iterative, nested, and simultaneous [11, 43], as demonstrated in Figure 2.2. *Sequential* indicates that the dependency between the plant and the controller is not taken into consideration, and the controller is developed for a fixed plant, where only the operational cost (e.g., fuel consumption) is considered. *Iterative* means that the plant that determines the component cost (e.g., battery price) is first designed, and the controller that determines the operational cost is built based on the given plant. The

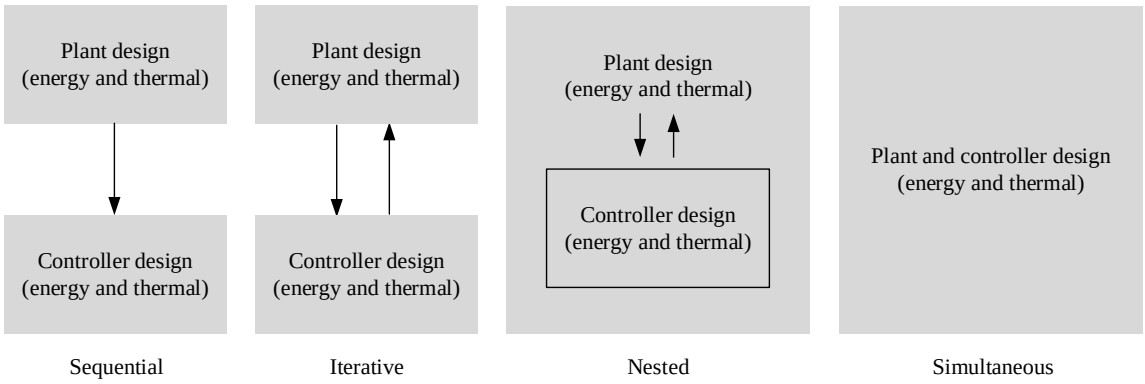

Figure 2.2: Coordination schemes between the plant and the controller.

loop repeats until the coupled variables converge. *Nested* implies that the controller is optimized for each evaluation of the plant. *Simultaneous* represents that the plant and the controller are optimized simultaneously. Based on the current literature [12, 17, 20–26], a systematic way to analyze and to link those optimization layers for electrified powertrains has yet to be established, in consideration of both energy and thermal aspects. For example, from energy perspective, an iterative coordination scheme to solve a combined topology and size optimization problem is proposed for double planetary gear hybrid powertrains in [20], but the thermal domain is not taken into consideration. The thermal response and power consumption of the cooling system and its sizing of a series HEV are investigated in [21] with a sequential approach; however, the energy aspect has yet to be considered.

Energy-efficient and cost-effective electrified powertrains, however, demand a holistic and integrated approach to synthesize design and control aspects in consideration of both energy and thermal domains. Motivated by the above discussion, this study originally provides a comprehensive overview of those optimization layers and coordination methods for electrified vehicles considering both energy and thermal aspects.

2.2 Energy-aware design and control optimization

If a system is optimized from energy point of view, e.g., identifying an optimal powertrain configuration with optimized component sizes and power flow, neglecting the thermal domain, it is termed energy-aware design and control optimization.

As illustrated in Figure 1.4, normally, a design process starts with choosing an architecture to focus on. A configuration that defines the connections between components influences efficiency, cost, comfort, performance, complexity, and durability. The best topology can be identified with the lowest total-cost-of-ownership (TCO), consisting of operational cost, e.g., the battery energy consumption, and component cost, such as the engine price, subject to various constraints, for example, performance requirements. The operational cost is related to the control algorithm, for instance,

how the battery is used, and the component cost is associated with the component size, e.g., the electric machine size in kW. Topology optimization is therefore often coupled with the control and size layers [22]. Additionally, for a given vehicle architecture, there is a strong dependency between the size and control layers [12]. For example, the battery would be used differently depending on the battery size of an electrified powertrain.

2.2.1 Topology generation

Common electrified powertrain architectures are depicted in Figure 2.3, including series, parallel, and series-parallel hybrids. Eliminating the engine path, an electric vehicle (EV) configuration is built. Descriptions of the driving modes are defined in Section 1.3. Each topology has its advantages and disadvantages [73–75]. Selecting a suitable architecture is essential, as it influences efficiency and cost. Topology generation, essentially a feasibility search problem, can be formulated as follows [76]:

$$\text{Find} \quad \boldsymbol{T}_{\mathrm{e}}^{\mathrm{f}} \subseteq \boldsymbol{T}_{\mathrm{e}}^{\mathrm{p}}, \tag{2.1}$$

$$\text{s.t.} \quad g_e(\boldsymbol{T}_{\mathrm{e}}^{\mathrm{f}}) \leq 0, \tag{2.1a}$$

where subscript e represents the energy domain, $\boldsymbol{T}_{\mathrm{e}}^{\mathrm{f}}$ the feasible architectures, and $\boldsymbol{T}_{\mathrm{e}}^{\mathrm{p}}$ the possible configurations. It should be noted that if a minimal cost is considered, (2.1) becomes an optimization problem.

In reality, an HEV configuration is typically chosen based on expert knowledge, taking into account, for example, application, component availability, and market trend. The chosen configuration is likely not optimal. As reported in [77], for power-split hybrids with one planetary gear, a thorough analysis of all possible architectures shows that small design changes can bring significant cost and energy benefits, where Toyota Prius and Chevy Volt are modified into $Prius^{+}$ and $Volt^{-}$. It should be noted that in this study, the design space is still small, i.e., there are only 12 possible configurations for power-split hybrid powertrains with a single planetary gear, which make enumeration of topologies possible. When the design space is large, however, it is intractable, as exploring feasible architectures is combinatorial in nature. Therefore, a systematic and efficient way is required to evaluate all possible topologies. In this context, automatic topology generation that aims to find feasible architectures is emerging [22, 76, 78–82]. For power-split hybrids with multiple planetary gears, clutches and brakes, automated modeling techniques are developed, which capture the fundamental dynamics of the vehicle based on physics to represent modes and configurations [22, 79–82] . Subsequently, various constraints, such as kinematics, complexity and redundancy constraints, are utilized to eliminate infeasible topologies. In [78], a bond graph is used to represent an architecture and constraints are employed to arrive at feasible configurations. But these studies are limited to power-split hybrids with multiple planetary gears. For a predefined set of 16 components, feasible series, parallel, and series-parallel hybrid topologies are found in [76], by using constraint

logic programming, which automatically generates all possible HEV architectures efficiently and in a structured way. Specially, each component is a node of an undirected connected finite graph that represents an architecture. Afterwards, functionality and cost constraints are applied, essentially a screening process, to filter out infeasible configurations. Functionality constraints mean that, for instance, to realize hybrid functions, certain connections between components are required. Cost constraints indicate that component redundancy is restricted. Finally, the initial search space of $5.7 \cdot 10^{45}$ possible topologies is reduced to 4779 feasible topologies in less than 5 min. However, the generated feasible configurations have yet to be assessed based on TCO and vehicle performance, by integrating with control and size layers.

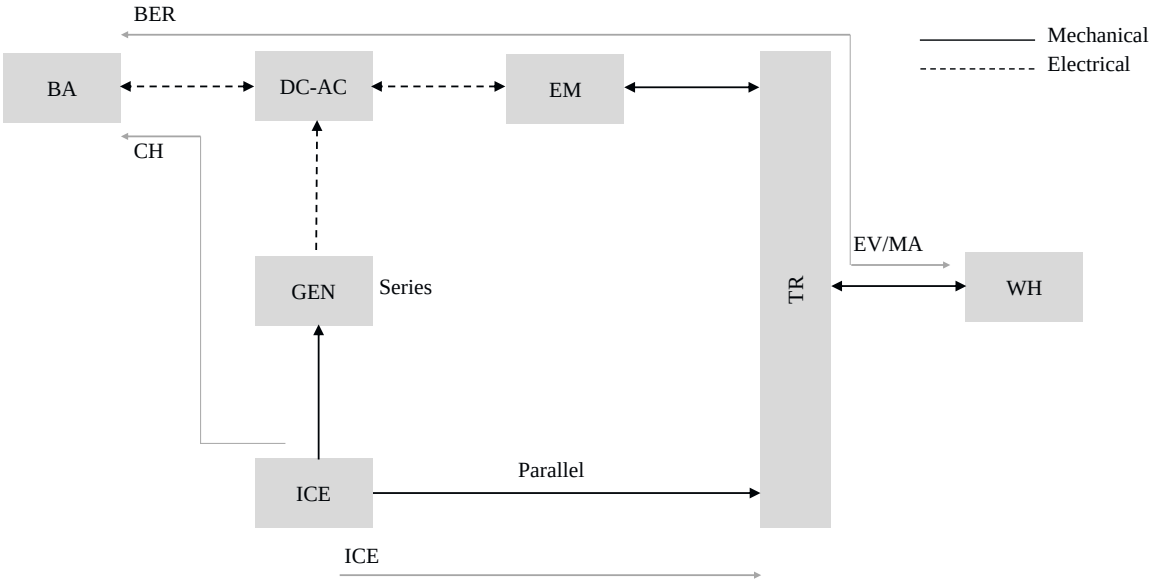

Figure 2.3: Common electrified powertrain architectures, where BA represents the battery, DC-AC the DC (direct current) to AC (alternating current) inverter, GEN the generator, TR the transmission, WH the wheel, ICE the engine only mode, CH the charging mode, EV the electric vehicle mode, MA the motor assist mode, and BER the brake energy recuperation mode. The series and parallel HEVs are indicated with "series" and "parallel". The main powertrain components are shown as blocks connected via bi-directional mechanical (solid) and electrical (dashed) energy flows.

2.2.2 Control optimization

In this respect, earlier works mainly focused on the control layer for a given architecture $\boldsymbol{T}_{\mathrm{e}}^{\mathrm{f}}$ generated by (2.1) and fixed powertrain parameters represented by $\boldsymbol{s}_{\mathrm{e}}$. The main objective of the controller (EMS) is to determine the power flow of the electrified powertrain in an optimal manner so that the energy efficiency is maximized, such as the torque split between the engine and the EM in a parallel HEV. For a known drive cycle starting at t_0 and ending at t_{f}, the EMS aims to find the optimal control variables to minimize a cost function J_{e}, for example, fuel consumption of an HEV or electricity of an EV, given by

$$\min \; J_{\mathrm{e}}(\boldsymbol{x}_{\mathrm{e}}(t), \boldsymbol{u}_{\mathrm{e}}(t), t \mid (\boldsymbol{T}_{\mathrm{e}}^{\mathrm{f}}, \boldsymbol{s}_{\mathrm{e}})) = \int_{t_0}^{t_{\mathrm{f}}} P_{\mathrm{e}}(\boldsymbol{x}_{\mathrm{e}}(t), \boldsymbol{u}_{\mathrm{e}}(t), t) \, \mathrm{d}t, \tag{2.2}$$

$$\text{s.t.} \quad \dot{\boldsymbol{x}}_{\mathrm{e}}(t) = \boldsymbol{f}(\boldsymbol{x}_{\mathrm{e}}(t), \boldsymbol{u}_{\mathrm{e}}(t), t), \tag{2.2a}$$

$$h_{\mathrm{e}}(\boldsymbol{x}_{\mathrm{e}}(t), \boldsymbol{u}_{\mathrm{e}}(t), t) = 0, \tag{2.2b}$$

$$g_{\mathrm{e}}(\boldsymbol{x}_{\mathrm{e}}(t), \boldsymbol{u}_{\mathrm{e}}(t), t) \leq 0, \tag{2.2c}$$

$$\boldsymbol{x}_{\mathrm{e}}(t_{\mathrm{f}}) = \boldsymbol{x}_{\mathrm{e}}(t_0), \tag{2.2d}$$

where $\boldsymbol{x}_{\mathrm{e}}$ denotes the energy dynamics of the system, for instance, the state-of-charge of the battery, which is defined as the available capacity (in Ah) relative to its rated capacity. $\boldsymbol{u}_{\mathrm{e}}$ denotes the control inputs, e.g., the power sharing between the engine and the battery. For a given control input at each time instance, the battery power, current and efficiency can be obtained. With the rated capacity of the battery, the state-of-charge can thus be calculated. $h_{\mathrm{e}}(\cdot)$ denotes the equality constraints, for example, the power balance of the vehicle, and $g_{\mathrm{e}}(\cdot)$ the inequality constraints, such as the torque limits of the electric machine,

$$\tau_{\mathrm{m},0}(t) \in [\underline{\tau}_{\mathrm{m},0}(w_{\mathrm{m}}(t)), \overline{\tau}_{\mathrm{m},0}(w_{\mathrm{m}}(t))]. \tag{2.3}$$

Equation (2.2d) constrains the dynamic states, such as charge-sustaining for HEVs, which would be different for plug-in HEVs (PHEVs) and EVs. Charge-sustaining implies that the initial and final values of the state-of-charge of the battery are the same. The initial value of the state-of-charge is typically known. Therefore, the optimization problem (2.2) has a fixed final state. In this case, the final time is also fixed, as the drive cycle is known a priori.

This problem can be solved by two main categories of methods: Rule-based and optimization-based (OB), as illustrated in Figure 2.4. Rule-based approaches use a set of rules, e.g., if-then conditions, derived from engineering intuition, to make decisions, e.g., let power sources operate at their efficient regions [83–85]. These strategies are easy to implement and computationally efficient. However, the rules are configuration-dependent. In addition, they require tuning of many parameters and cannot obtain the optimal solution [86, 87]. These drawbacks necessitate the development of optimal controllers. Optimization-based methods can be categorized into offline [13, 18, 59, 88, 89] and online [27, 90, 91] algorithms. For example, dynamic programming is widely adopted for handling non-linear constraints and finding a global optimal solution [13]. But it is not implementable. This disadvantage motivates the development of online controllers, such as equivalent consumption minimization strategy (ECMS). It translates the battery electricity into its equivalent fuel cost using an equivalence factor, which can be used in real-time control [27]. However, it may lose optimality, since ECMS is derived using Pontryagin's minimum principle conditions. More analyses of EMSs can be found in [92, 93].

It should be noted that all these energy management strategies are developed for given design parameters. For a fixed vehicle configuration, however, the powertrain

component size, e.g., the battery size, affects the control decision, e.g., the torque split between the engine and the electric machine, and vice versa. Previous studies have reported that energy efficiency can be improved remarkably by integrating the control and size layers [15, 57, 59, 94]. Moreover, the component size influences the system cost and performance. To obtain better designs, the size layer should be included.

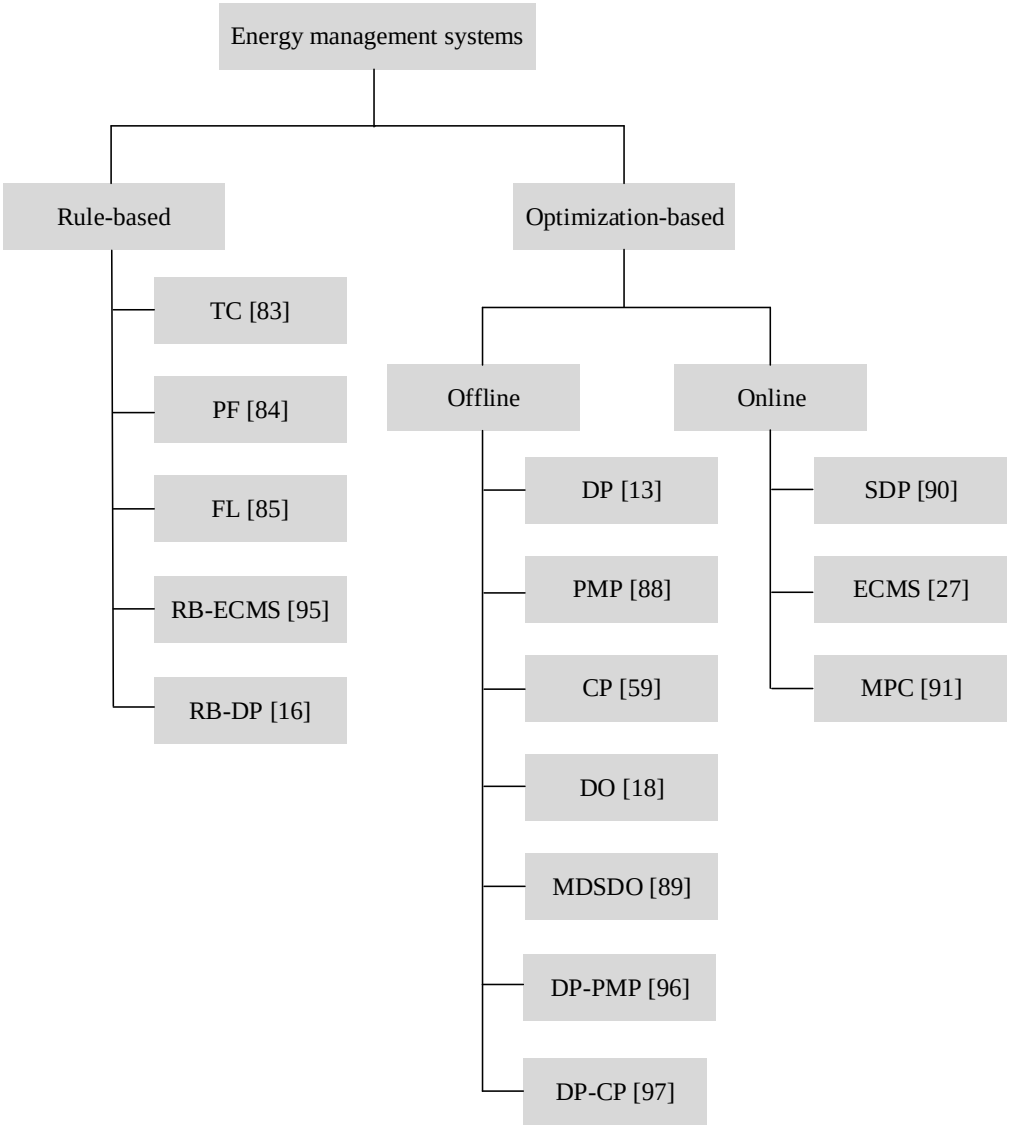

Figure 2.4: Energy management systems [95–97], where TC represents thermostat control, PF power follower, FL fuzzy logic, DO distributed optimization, MDSDO multidisciplinary dynamic system design optimization, and MPC model predictive control.

2.2.3 Combined size and control optimization

Generally, there are two ways to size the components, i.e., rule-based and optimization-based strategies. Rule-based approaches based on experience and simple calcula-

tions often fail in view of optimality and large numbers of plant variables [98–101]. Optimization-based algorithms in this regard can be classified into derivative-free and gradient-based methods, as demonstrated in Figure 2.5. Derivative-free strategies [24, 102–104] can generally deal with nonlinear cost functions and constraints, but require more function evaluations and parameter tuning, compared to gradient-based ones [59, 89, 105].

For generality, assuming a PHEV context, the main goal of a combined size and control method is to find the optimal set-point of the power source to increase the energy efficiency and the optimal component sizes to reduce the powertrain cost, by minimizing

$$\begin{aligned}
&\min\ J_{\mathrm{e}}(\boldsymbol{s}_{\mathrm{e}}, \boldsymbol{x}_{\mathrm{e}}(t), \boldsymbol{u}_{\mathrm{e}}^{\mathrm{s}}(t), t \mid \boldsymbol{T}_{\mathrm{e}}^{\mathrm{f}}) \\
&= \int_{t_0}^{t_{\mathrm{f}}} [\rho_{\mathrm{f}}\ P_{\mathrm{f}}(\boldsymbol{s}_{\mathrm{e}}, \boldsymbol{x}_{\mathrm{e}}(t), \boldsymbol{u}_{\mathrm{e}}^{\mathrm{s}}(t), t) + \rho_{\mathrm{e}}\ P_{\mathrm{b}}(\boldsymbol{s}_{\mathrm{e}}, \boldsymbol{x}_{\mathrm{e}}(t), \boldsymbol{u}_{\mathrm{e}}^{\mathrm{s}}(t), t)]\ \mathrm{d}t + C_{\mathrm{e}}(\boldsymbol{s}_{\mathrm{e}}), \qquad (2.4)\\
\text{s.t.}\quad &\dot{\boldsymbol{x}}_{\mathrm{e}}(t) = \boldsymbol{f}(\boldsymbol{s}_{\mathrm{e}}, \boldsymbol{x}_{\mathrm{e}}(t), \boldsymbol{u}_{\mathrm{e}}^{\mathrm{s}}(t), t), \qquad (2.4a)\\
&h_{\mathrm{e}}(\boldsymbol{s}_{\mathrm{e}}, \boldsymbol{x}_{\mathrm{e}}(t), \boldsymbol{u}_{\mathrm{e}}^{\mathrm{s}}(t), t) = 0, \qquad (2.4b)\\
&g_{\mathrm{e}}(\boldsymbol{s}_{\mathrm{e}}, \boldsymbol{x}_{\mathrm{e}}(t), \boldsymbol{u}_{\mathrm{e}}^{\mathrm{s}}(t), t) \leq 0, \qquad (2.4c)\\
&\boldsymbol{s}_{\mathrm{e}} \in [\underline{\boldsymbol{s}}_{\mathrm{e}}, \overline{\boldsymbol{s}}_{\mathrm{e}}], \qquad (2.4d)\\
&x_{\mathrm{e}}(t_{\mathrm{f}}) = x_{\mathrm{e}}(t_0), \qquad (2.4e)
\end{aligned}$$

where $\boldsymbol{s}_{\mathrm{e}}$ represents the design parameters, e.g., the electric machine size, ρ_{f} the price of gasoline, P_{f} the fuel power, ρ_{e} the price of electricity, P_{b} the battery power, and C_{e} the powertrain cost, e.g., the battery price C_{b}, which depends on the battery size represented by a scaling factor s_{b} [106], i.e.,

$$C_{\mathrm{b}} = C_{\mathrm{b},0} + s_{\mathrm{b}}\ C_1, \qquad (2.5)$$

where $C_{\mathrm{b},0}$ is the initial battery cost and C_1 the linear cost coefficient. As an example, referring to (2.3), the component size influences the control strategy in the sense that

$$\tau_{\mathrm{m}}(t) \in s_{\mathrm{m}}\ [\underline{\tau}_{\mathrm{m},0}(w_{\mathrm{m}}(t)), \overline{\tau}_{\mathrm{m},0}(w_{\mathrm{m}}(t))], \qquad (2.6)$$

where s_{m} is the scaling factor for the electric machine. Therefore, the control input $\boldsymbol{u}_{\mathrm{e}}$ in (2.2) is changed to $\boldsymbol{u}_{\mathrm{e}}^{\mathrm{s}}$ in (2.4) due to the influence of design parameters $\boldsymbol{s}_{\mathrm{e}}$ introduced, which is reflected by the superscript s.

Theoretically, the combination of the size layer from Figure 2.5 and the control layer from Figure 2.4 yield different solution methods to (2.4), which are connected with the four coordination schemes as shown in Figure 2.2, sequential [14, 107], iterative [106], nested [24, 102–105], and simultaneous [59, 89]. For given component sizes, a real-time power split control strategy based on ECMS for an HEV is developed in [14], which uses a sequential approach. Obviously, the coupling between the component sizes and the controller is ignored in this case, which finds a sub-optimal solution. To consider this dependency, for a parallel PHEV, the energy management problem is solved by using dynamic programming and the battery, engine and electric machine sizes are

optimized by utilizing convex programming with an iterative scheme, which is one step forward from the sequential method, resulting in a near-optimal solution [106]. In order to obtain an optimal solution, a nested approach is used in [24] for a parallel HEV, where particle swarm optimization is employed in the outer loop to optimize the component sizes and the optimal control input for each candidate is selected by adopting dynamic programming to minimize the fuel consumption. Furthermore, the authors report that compared to a rule-based strategy, particle swarm optimization using optimal control improves energy efficiency by around 11% and reduces cost by around 14% [24]. However, the computation time is high. To overcome this limitation, simultaneous optimization of torque split, charging, and component sizes is solved via convex programming [59], which achieves the optimal solution. Yet, both the optimal control problem and the quasi-static models are required to be convex.

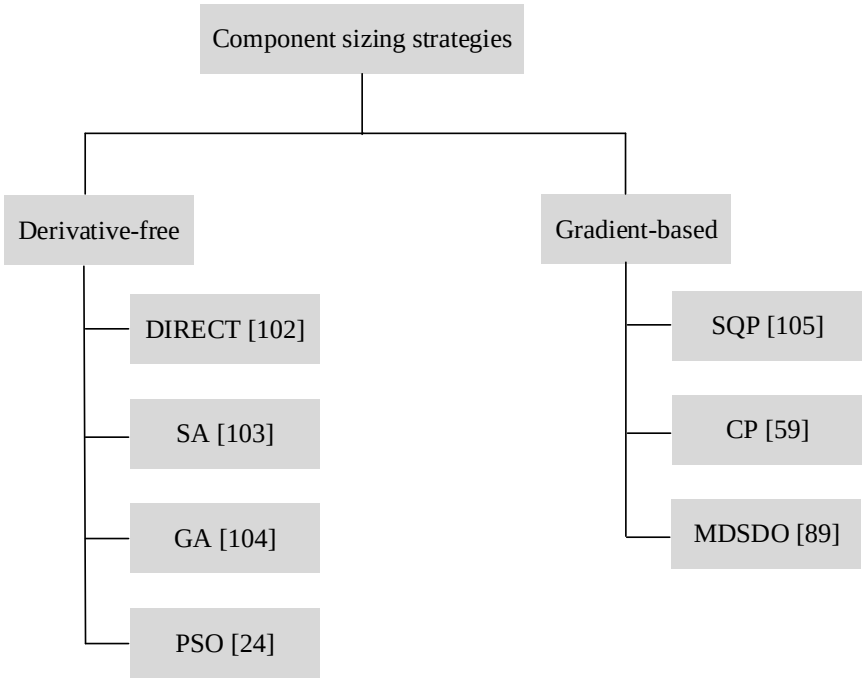

Figure 2.5: Component sizing strategies, where DIRECT represents dividing rectangles, PSO particle swarm optimization, GA genetic algorithm, SA simulated annealing, and SQP sequential quadratic programming.

Notice that all these combined size and control methods are developed for a given vehicle configuration. Topology layer will influence design parameters and control variables. For example, as described in [11], the design and control variables of a parallel HEV are very different from that of a series or a series-parallel topology. Each configuration results in a TCO. Therefore, the generated powertrain architectures $\boldsymbol{T}_{\mathrm{e}}^{f}$ from (2.1) should be compared based on TCO.

2.2.4 Combined topology, size and control optimization

To fully consider the design aspect and to obtain an optimal system, topology optimization should also be taken into consideration. Integrated topology, size, and control optimization can be formulated by combing (2.1), (2.2), and (2.4). The goal is to find the best design that has the lowest TCO, while satisfying performance requirements, e.g.,

$$\min \; J_{\mathrm{e}}(\boldsymbol{T}_{\mathrm{e}}^{f}, \boldsymbol{s}_{\mathrm{e}}^{\mathrm{T}}, \boldsymbol{x}_{\mathrm{e}}(t), \boldsymbol{u}_{\mathrm{e}}^{\mathrm{T}}(t)), \tag{2.7}$$

$$\text{s.t.} \quad \overline{v}(\boldsymbol{T}_{\mathrm{e}}^{f}, \boldsymbol{s}_{\mathrm{e}}^{\mathrm{T}}, \boldsymbol{x}_{\mathrm{e}}(t), \boldsymbol{u}_{\mathrm{e}}^{\mathrm{T}}(t)) \geq \overline{v}_{\mathrm{d}}, \tag{2.7a}$$

$$t_{\mathrm{a}}(\boldsymbol{T}_{\mathrm{e}}^{f}, \boldsymbol{s}_{\mathrm{e}}^{\mathrm{T}}, \boldsymbol{x}_{\mathrm{e}}(t), \boldsymbol{u}_{\mathrm{e}}^{\mathrm{T}}(t)) \leq t_{\mathrm{a,d}}, \tag{2.7b}$$

$$\overline{\alpha}(\boldsymbol{T}_{\mathrm{e}}^{f}, \boldsymbol{s}_{\mathrm{e}}^{\mathrm{T}}, \boldsymbol{x}_{\mathrm{e}}(t), \boldsymbol{u}_{\mathrm{e}}^{\mathrm{T}}(t)) \geq \overline{\alpha}_{\mathrm{d}}. \tag{2.7c}$$

$J_{\mathrm{e}}(\boldsymbol{T}_{\mathrm{e}}^{f}, \boldsymbol{s}_{\mathrm{e}}^{\mathrm{T}}, \boldsymbol{x}_{\mathrm{e}}(t), \boldsymbol{u}_{\mathrm{e}}^{\mathrm{T}}(t))$ represents the effect of topology on (2.4). Specifically, the design parameters $\boldsymbol{s}_{\mathrm{e}}$ and control vector $\boldsymbol{u}_{\mathrm{e}}^{\mathrm{s}}$ in (2.4) are updated to $\boldsymbol{s}_{\mathrm{e}}^{\mathrm{T}}$ and $\boldsymbol{u}_{\mathrm{e}}^{\mathrm{T}}$ in (2.7), respectively. Performance requirements are in this example the top speed, acceleration time, and gradability, which are enforced by (2.7a), (2.7b), and (2.7c), respectively. Other constraints on control and size optimization are associated with (2.2) and (2.4).

Recent studies have attempted to investigate the influence of architecture layer [20, 108–110]. Note that the four coordination schemes introduced before are also applicable here to solve the combined optimization problem. A layered control strategy is proposed in [108], where a supervisory controller is used to determine the powertrain configuration, including series and parallel types, and an EMS is utilized to determine the power split. Optimal topologies are designed for HEVs with different transmission technologies in [109], which include precoupled, postcoupled, and switching topologies, by using dynamic programming. A reduction of up to around 8% in CO_2 emission is shown, by finding the optimal fixed topology. For a torque-assist and a full-parallel topology, [110] presents a method to identify the best configuration based on minimization of fuel usage and powertrain cost by using dynamic programming and particle swarm optimization with a nested approach. Constraints on top speed and acceleration time are taken into account. However, all those studies only consider a small number of configurations, which may not be optimal. For double planetary gear hybrid powertrains, [20] generates and evaluates $3.4 \cdot 10^9$ possible configurations. The integrated optimization problem is solved with two methods, namely nested optimization and iterative optimization. The nested approach based on exhaustive search finds the optimal solution, but it is computationally heavy. The iterative method can converge to the optimal design found by the nested one much faster, as shown in Figure 2.6. It starts from an initial design (T_{e}^{0}, s_{e}^{0}), and topology optimization and component sizing are executed alternately. The best design is determined based on the minimum fuel consumption. This study shows that integrated configuration, size and control optimization can improve energy efficiency by around 16.6%, compared to only combined size and control optimization. However, this research does not consider the influence of topology on design and control variables. In addition, only few powertrain parameters are optimized and powertrain cost is not taken into account.

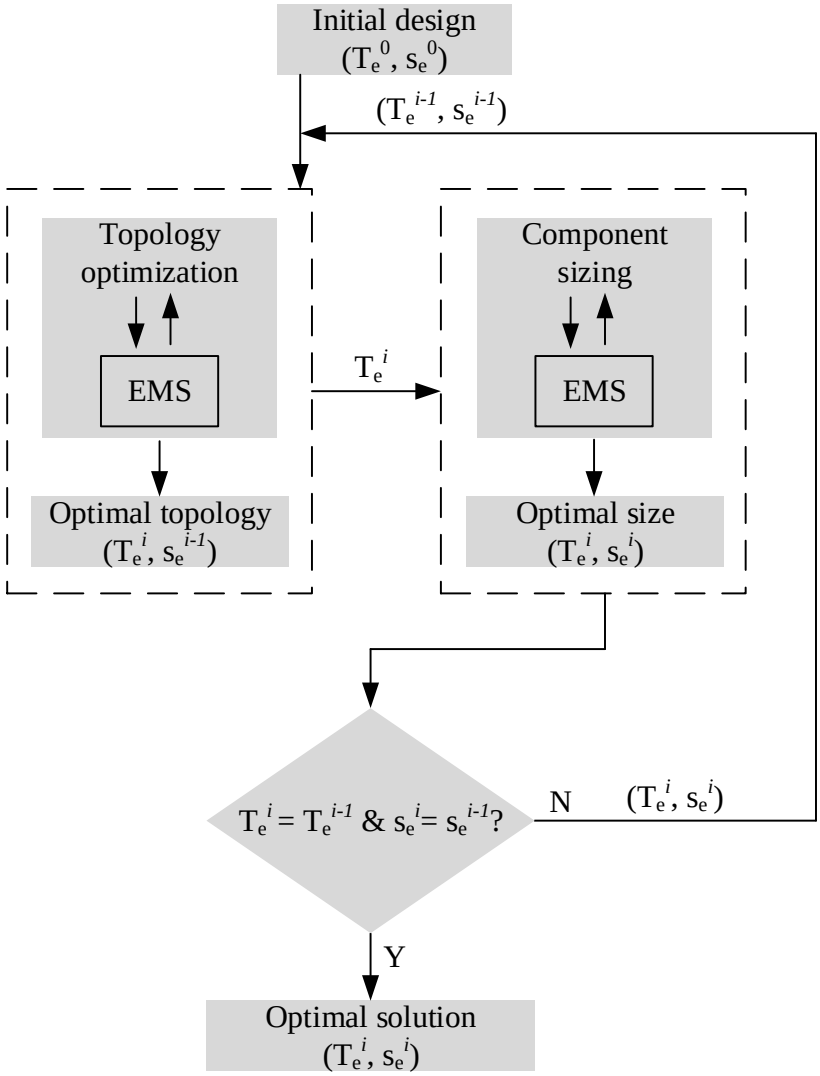

Figure 2.6: Flowchart of integrated topology, size, and control optimization via an iterative approach, where T_e represents the topology and s_e the component size.

It should be noted that a similar analysis of integrated optimization applies to EVs, see [63, 78, 111, 112]. Current studies mainly focus on the energy domain. The thermal domain is also important as it influences vehicle energy efficiency and cost, but it is often not considered in optimization problems.

2.3 Thermal-aware design and control optimization

If a system is only optimized from thermal viewpoint for a given EMS, for example, finding an optimal thermal management architecture with optimized thermal system size and heating/cooling power flow, it is termed thermal-aware design and control optimization.

A thermal management system may be defined as a system, which is capable of maintaining specified component temperatures for efficiency and comfort with minimum power consumption, recovering waste heat energy, and exchanging heat between components efficiently. As far as the thermal domain is concerned, combined control, size and configuration optimization is generally not available in the literature. Therefore, these design layers are analyzed separately.

2.3.1 Topology generation

Typical temperature levels of electrified powertrain components, also termed heat source components, can be seen in Figure 2.7. It can be observed that there are relatively three temperature levels in an electrified vehicle and three cooling circuits can thus be created. A common thermal management configuration for an electrified powertrain is shown in Figure 2.8, including both transient and steady-state behaviors. Here, the battery is cooled with an air conditioning (AC) system onboard [67]. The transmission is cooled with the electric drive circuit [65]. For example, the engine is not only a power source but also a heat source. When $\theta_\mathrm{e} < \overline{\theta}_\mathrm{e}$, indicating the transient behavior, the engine heats up itself and the radiator as the heat sink is bypassed. When $\theta_\mathrm{e} \geq \overline{\theta}_\mathrm{e}$, representing the steady-state phase, the fluid circulated by the pump as the fluid delivery device flows through the radiator to remove heat from the engine. This process is controlled by the thermostat as the control device. The same analysis can be applied to other powertrain components.

From thermal perspective, automatic topology generation is not available in the literature. If automatic generation of thermal management architectures is considered, similar to the energy domain in Section 2.2.1, feasible thermal management topologies can be found by

$$\text{Find} \quad \boldsymbol{T}_\mathrm{t}^\mathrm{f} \subseteq \boldsymbol{T}_\mathrm{t}^\mathrm{p}, \tag{2.8}$$

$$\text{s.t.} \quad g_\mathrm{t}(\boldsymbol{T}_\mathrm{t}^\mathrm{f}) \leq 0, \tag{2.8a}$$

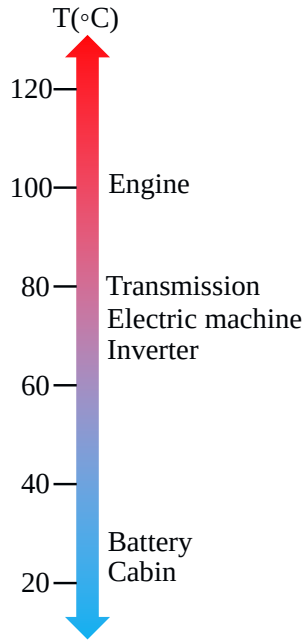

Figure 2.7: Typical temperature levels of electrified vehicle components.

where subscript t represents the thermal domain, $\boldsymbol{T}_{\mathrm{t}}^{\mathrm{p}}$ the possible thermal management architectures, and $\boldsymbol{T}_{\mathrm{t}}^{\mathrm{f}}$ the feasible thermal management configurations. Equation (2.8a) represents constraints, for example, each cooling circuit should have at least a heat source component, a heat sink, and a fluid delivery device, to filter out infeasible topologies. The generated feasible architectures have yet to be evaluated based on TCO and packaging constraints, by combining with control and size layers.

2.3.2 Control optimization

In this regard, previous studies mostly concentrated on the control layer for a given thermal management configuration T_{t}^{f} generated from (2.8) and fixed thermal system parameters (e.g., heating/cooling capacity in kW) denoted by $\boldsymbol{s}_{\mathrm{t}}$. The main goals of the controller (TMS) are to improve temperature tracking with respect to a prescribed threshold of the component and to reduce heating/cooling power consumption J_{t} [113], i.e.,

$$\min \; J_{\mathrm{t}}(\boldsymbol{x}_{\mathrm{t}}(t), \boldsymbol{u}_{\mathrm{t}}(t), t \mid (\boldsymbol{T}_{\mathrm{t}}^{\mathrm{f}}, \boldsymbol{s}_{\mathrm{t}})) = \int_{t_0}^{t_{\mathrm{f}}} [(\boldsymbol{x}_{\mathrm{t}} - \boldsymbol{x}_{\mathrm{t,d}})^T \; R_{\boldsymbol{x}} \; (\boldsymbol{x}_{\mathrm{t}} - \boldsymbol{x}_{\mathrm{t,d}}) +$$
$$(\boldsymbol{u}_{\mathrm{t}} - \boldsymbol{u}_{\mathrm{t,d}})^T \; R_{\boldsymbol{u}} \; (\boldsymbol{u}_{\mathrm{t}} - \boldsymbol{u}_{\mathrm{t,d}})] \; \mathrm{d}t, \tag{2.9}$$
$$\text{s.t.} \quad \dot{\boldsymbol{x}}_{\mathrm{t}}(t) = \boldsymbol{f}(\boldsymbol{x}_{\mathrm{t}}(t), \boldsymbol{u}_{\mathrm{t}}(t), t), \tag{2.9a}$$
$$\boldsymbol{x}_{\mathrm{t}} \in [\underline{\boldsymbol{x}}_{\mathrm{t}}, \overline{\boldsymbol{x}}_{\mathrm{t}}], \tag{2.9b}$$
$$\boldsymbol{u}_{\mathrm{t}} \in [\underline{\boldsymbol{u}}_{\mathrm{t}}, \overline{\boldsymbol{u}}_{\mathrm{t}}], \tag{2.9c}$$

where $\boldsymbol{x}_{\mathrm{t}}$ represents the thermodynamics of the system, e.g., the electric machine temperature, which depends on how the electric machine is used from the EMS (u_{e}), see

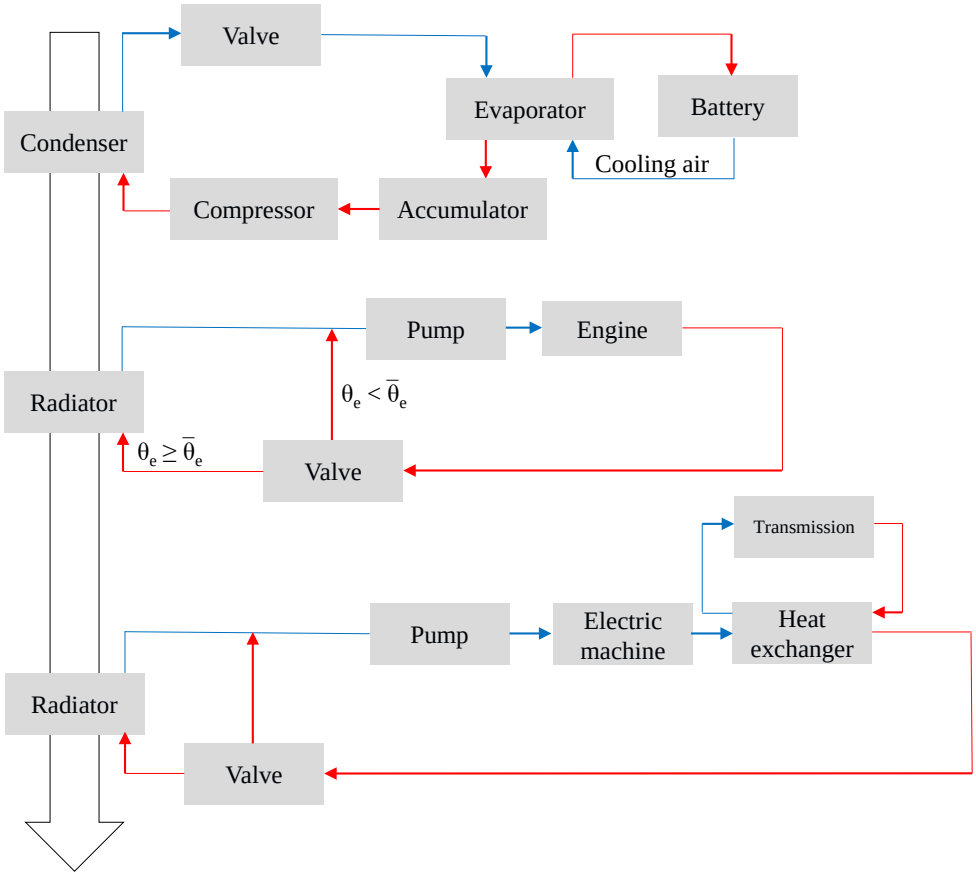

Figure 2.8: A common thermal management configuration for electrified vehicles, where the blue line represents the cold cooling medium, the red line the hot cooling medium, which can be gaseous and liquid (water and oil), θ_e the engine temperature, and $\bar{\theta}_e$ the desired engine temperature.

(2.2), resulting in different power losses (heat generation) and temperatures. However, the electric machine temperature is constrained by (2.9b). Therefore, cooling power is required to keep the electric machine temperature below its thermal limit. $\boldsymbol{u}_t$ denotes the control variables, for example, the cabin heating power P_c,

$$P_c(t) \in [\underline{P}_c, \overline{P}_c]. \tag{2.10}$$

$\boldsymbol{x}_{t,d}$ and $\boldsymbol{u}_{t,d}$ are the references of the state vector and control vector, respectively. $\boldsymbol{x}_{t,d}$ can be determined based on the component specification (optimal temperature for efficiency or comfort), for instance, maintaining the battery temperature at around 25 °C (temperature tracking) for improved efficiency or the cabin temperature at around 22 °C for improved passenger thermal comfort. $\boldsymbol{u}_{t,d}$ can be determined depending on the use case. For example, it can be set to zero when minimizing the cooling power for the electric machine. $R_{\boldsymbol{x}}$ and $R_{\boldsymbol{u}}$ are the weighting matrices.

This control problem can be tackled by two major groups of strategies: Rule-based and optimization-based, as shown in Figure 2.9. Rule-based approaches utilize a set of rules to compute the control signals on the basis of predefined thresholds. These thresholds

are often determined based on expert knowledge. An On/Off control method is utilized in [114] for battery cooling. The cooling system is triggered On with maximum speed, when the battery temperature is greater than the prescribed upper threshold. The cooling system is switched Off when the battery temperature is lower than the predefined lower limit. Rule-based methods are easy to understand and implement. But they generally require tuning effort [115] and yield non-optimal solution. Moreover, the On/Off control strategy is typically related to mechanical actuators, such as mechanical fans and pumps that are coupled with the engine through clutches, which have only two states, open and closed. Because of engine speed-dependent actuation, this kind of system often provides more than necessary, leading to parasitic losses and excess energy usage. To reduce energy consumption, of particular importance is to adopt electrified actuators, e.g., electronic thermostats, electric fans, electric water pumps, and electric compressors, instead of their mechanical counterparts. Continuous adjustment of thermal actuators is now possible, for example, with motors. Costs of electrified actuators are higher, which depend on their sizes [116]. Note that the price difference is decreasing. In this context, optimization-based controllers can be used to provide heating/cooling on demand, depending on driving conditions. An electric radiator fan matrix of an engine cooling system is controlled to minimize the cooling power consumption by using mixed integer nonlinear programming in [117]. It should be noted that, however, the control action of the TMS is not checked by the EMS, which may not be optimal. The TMS has yet to be integrated into the EMS, where the control signal of the TMS is generated from the EMS, considering overall energy consumption from both energy and thermal aspects.

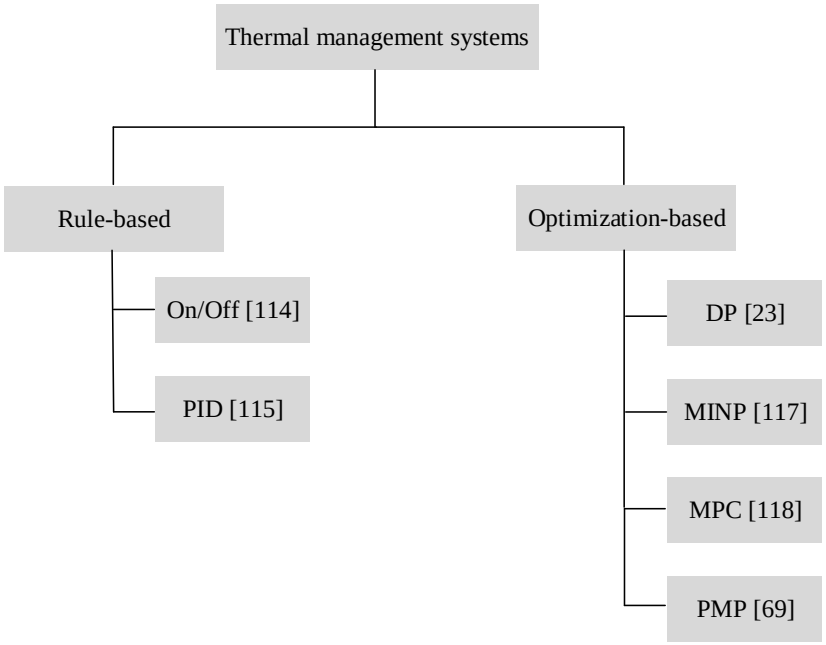

Figure 2.9: Thermal management systems [118], where PID represents proportional-integral-derivative and MINP mixed integer nonlinear programming.

Additionally, all these thermal management strategies are developed for a given thermal system size. However, the thermal system size influences the control strategy and vice versa. For example, a large radiator would reduce the need of providing more cooling power. The control algorithm helps optimize the thermal system size [119]. Furthermore, the thermal system size affects the system cost. From thermal perspective, the control layer has yet to be integrated with the size layer.

2.3.3 Size optimization

All powertrains have tight packaging constraints. It is desirable to reduce cooling system size, resulting in reduced volume, weight, air drag, parasitic losses, and cost, while meeting cooling requirements. The main sizing methods can be categorized into rule-based and optimization-based strategies.

As described in [120], the cooling capacity of a radiator is proportional to the temperature difference between the component coolant temperature and the cooling air temperature. Moreover, [120] shows that for the engine cooling system of a minivan, increasing the temperature difference by around 20°C can reduce the radiator size by around 30%. This can be achieved by increasing the component coolant temperature through technology advancements [121], where powertrain components can work at elevated temperatures but lower than their allowable limits to avoid failure. For the engine cooling system of a class 3 pickup truck, [122] demonstrates that the pump power can be reduced significantly by around 87% and the radiator can be downsized by around 27% under a grade load condition on Federal Test Procedure (FTP) 74 driving cycle. This is realized by upgrading the mechanical water pump to an electric one. However, solution optimality in terms of radiator size cannot be guaranteed in these studies, which motivates the development of optimization-based strategies.

For a series hybrid heavy duty vehicle under a grade load condition, [123] takes a reference to a similar class conventional vehicle to obtain initial cooling system parameters. The optimal pump and radiator sizes are found by using sequential quadratic programming to minimize power consumption, subject to temperature and packaging constraints. Taking into account cooling power consumption and heat removal capability, a search-based optimization algorithm is implemented in [124] to minimize the heat exchanger size of the engine cooling system of a heavy duty military truck, subject to a power constraint. However, the size layer and the control layer have yet to be coupled to obtain better thermal system designs.

For a fixed thermal management topology, if the control and size loops are integrated, the optimal control problem may be formulated as follows:

$$\min \; J_{\mathrm{t}}(\boldsymbol{s}_{\mathrm{t}}, \boldsymbol{x}_{\mathrm{t}}(t), \boldsymbol{u}_{\mathrm{t}}^{\mathrm{s}}(t), t \mid \boldsymbol{T}_{\mathrm{t}}^{\mathrm{f}}) = \int_{t_0}^{t_{\mathrm{f}}} (\rho_{\mathrm{e}} \; P_{\mathrm{t}}(\boldsymbol{s}_{\mathrm{t}}, \boldsymbol{x}_{\mathrm{t}}(t), \boldsymbol{u}_{\mathrm{t}}^{\mathrm{s}}(t), t)) \; \mathrm{d}t + C_{\mathrm{t}}(\boldsymbol{s}_{\mathrm{t}}), \tag{2.11}$$

$$\text{s.t.} \quad \dot{\boldsymbol{x}}_{\mathrm{t}}(t) = \boldsymbol{f}(\boldsymbol{s}_{\mathrm{t}}, \boldsymbol{x}_{\mathrm{t}}(t), \boldsymbol{u}_{\mathrm{t}}^{\mathrm{s}}(t), t), \tag{2.11a}$$

$$\boldsymbol{x}_{\mathrm{t}} \in [\underline{\boldsymbol{x}}_{\mathrm{t}}, \overline{\boldsymbol{x}}_{\mathrm{t}}], \tag{2.11b}$$
$$\boldsymbol{u}_{\mathrm{t}}^{\mathrm{s}} \in [\underline{\boldsymbol{u}}_{\mathrm{t}}^{\mathrm{s}}, \overline{\boldsymbol{u}}_{\mathrm{t}}^{\mathrm{s}}], \tag{2.11c}$$
$$\boldsymbol{s}_{\mathrm{t}} \in [\underline{\boldsymbol{s}}_{\mathrm{t}}, \overline{\boldsymbol{s}}_{\mathrm{t}}], \tag{2.11d}$$

The thermal power P_{t} is converted to cost using ρ_{e}. s_{t} denotes the thermal design parameters, e.g., the pump scaling factor, and C_{t} the thermal system cost. Because of the effect of $\boldsymbol{s}_{\mathrm{t}}$, the control variable $\boldsymbol{u}_{\mathrm{t}}$ in (2.9) is updated to $\boldsymbol{u}_{\mathrm{t}}^{\mathrm{s}}$ in (2.11), which reveals the strong coupling between them.

Note that the component sizing strategies (Figure 2.5) from the energy domain can theoretically also be employed here. Hence, the combination of the size layer from Figure 2.5 and the control layer from Figure 2.9 yield different solution methods to (2.11), which are connected with the four coordination schemes as introduced in Figure 2.2. Furthermore, the size of the powertrain component influences its cooling system size. For example, a downsized and more efficient engine would imply a compact and smaller cooling system, i.e., $\boldsymbol{s}_{\mathrm{t}} \propto \boldsymbol{s}_{\mathrm{e}}$. It indicates that the thermal system size is proportional to the powertrain component size. Moreover, similar to (2.6), the thermal system size affects the control decision of the thermal management system. Additionally, topology optimization needs to be considered, as thermal management configurations are important for efficiency, comfort, cost, and reliability.

2.3.4 Topology optimization

In general, design of thermal management architectures for electrified vehicles is less available, compared to design of powertrain configurations. Compared with conventional vehicles, thermal management of power electronics and electric machine adds a new challenge to electrified ones. Normally, power electronics (inverter) and electric machine are combined together with a dedicated water or oil cooling circuit because the coolant temperature is in a similar range, as illustrated in Figure 2.7. In order to reduce size, weight and cost, two ways of integration of cooling circuits for a parallel HEV are proposed in [65]. The first method is to incorporate the power electronics and electric machine cooling loop into the engine cooling circuit and the second approach is to combine it with the AC circuit. The criteria to combine systems are having similar temperature levels and exhibiting misalignment of peak heat loads after integration. For the first strategy, even though it seems possible to combine them with respect to misalignment of peak heat loads, the issue remains on the different temperature specifications of engine and power electronics and electric machine as mentioned before. It is reported that future technologies may be possible to increase the temperature of electronic modules [121]. However, currently it is still an obstacle. Regarding the second approach, it appears that this integration meets the requirements as stated above, for instance, with a low temperature liquid coolant, but a thorough analysis is required to verify such concepts.

A comprehensive thermal modeling and architecture design guidelines are given in [66]

for a heavy-duty series HEV, where two induction motors are used to drive the wheels. Two main design guidelines derived can be summarized as follows. Heat sources with different temperature specifications should not share the same cooling loop. Moreover, powertrain components working in different operation groups should not share the same cooling circuit. Based on these guidelines and simulation results in terms of power consumption of the cooling system, the authors propose the following topology [125], as demonstrated in Figure 2.10. Obviously, this system is modular because almost all the components have their own cooling loops. However, in consideration of cost, weight and size, this configuration is hardly appealing. The authors report that in this case, parasitic losses can be reduced significantly, resulting in a fuel saving of up to around 6.1%, because of the separate loops compared with combined circuits. In combined loops, powertrain components are cooled in a single circuit, where the coolant temperature is limited by the component that has the lowest temperature specification, resulting in over-cooled components and unnecessary power consumption. However, one of the reasons may be that not all the components in this system are electronically controlled, leading to this conclusion. Here, the simulation results are dependent on the simulation conditions, assumptions and the vehicle type.

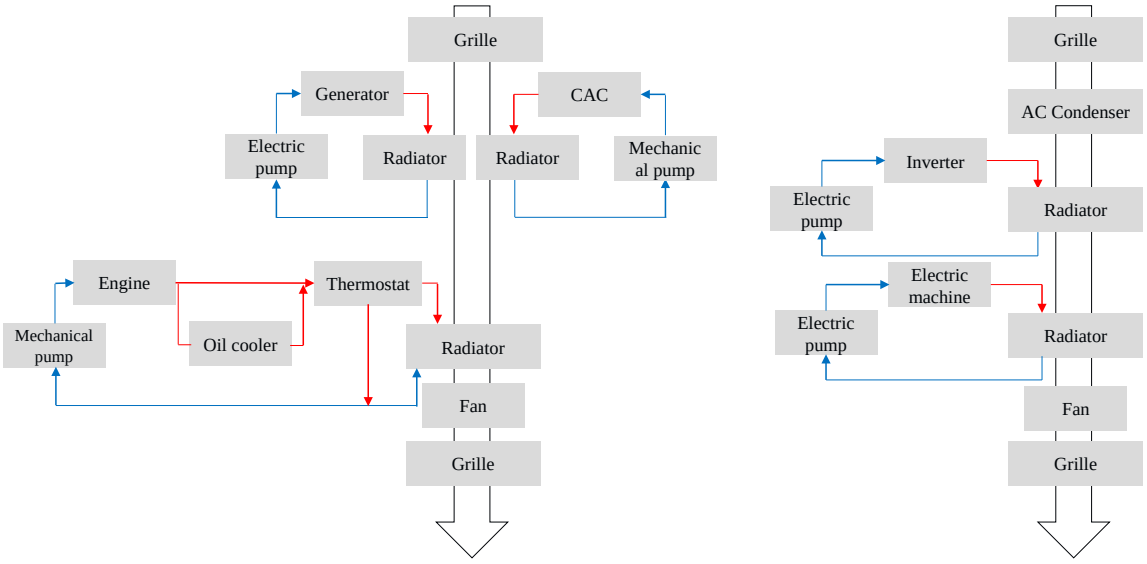

Figure 2.10: Thermal management topology for a series hybrid electric vehicle, where CAC represents the charge air cooler.

In [126], a variable thermal management topology is proposed for EVs to optimize driving range and minimize power derating, which switches between different architectures by utilizing one or more 4-way valves during operation. Here, a chiller activated by the compressor of an AC system is used to assist radiators and fans in cooling the battery pack and powertrain. It is more efficient than a fixed configuration, as it continuously switches to the most efficient cooling circuit, depending on the driving conditions and cooling requirements. For example, when the heat generation from the battery and powertrain is low, they are cooled in a single loop, while they are cooled separately in two circuits when the heat generation is high. But there are only three

configurations to switch.

Overall, current thermal management topologies for electrified vehicles are designed based on expert knowledge, and the identified architecture is likely sub-optimal because of limited choices. Moreover, in order to obtain an optimal thermal management configuration, topology optimization has to be coupled with the size and control layers. If these layers are integrated, e.g., by combining (2.8), (2.9), and (2.11), for simplicity, the optimization problem may be described as

$$\min \ J_{\mathrm{t}}(\boldsymbol{T}_{\mathrm{t}}^{f}, \boldsymbol{s}_{\mathrm{t}}^{\mathrm{T}}, \boldsymbol{x}_{\mathrm{t}}(t), \boldsymbol{u}_{\mathrm{t}}^{\mathrm{T}}(t)), \tag{2.12}$$

$$\text{s.t.} \quad \theta_{\mathrm{i}}(\boldsymbol{T}_{\mathrm{t}}^{f}, \boldsymbol{s}_{\mathrm{t}}^{\mathrm{T}}, \boldsymbol{x}_{\mathrm{t}}(t), \boldsymbol{u}_{\mathrm{t}}^{\mathrm{T}}(t)) \leq \theta_{\mathrm{i,d}}, \tag{2.12a}$$

$$V(\boldsymbol{T}_{\mathrm{t}}^{f}, \boldsymbol{s}_{\mathrm{t}}^{\mathrm{T}}, \boldsymbol{x}_{\mathrm{t}}(t), \boldsymbol{u}_{\mathrm{t}}^{\mathrm{T}}(t)) \leq V_0, \tag{2.12b}$$

where $J_{\mathrm{t}}(\boldsymbol{T}_{\mathrm{t}}^{f}, \boldsymbol{s}_{\mathrm{t}}^{\mathrm{T}}, \boldsymbol{x}_{\mathrm{t}}(t), \boldsymbol{u}_{\mathrm{t}}^{\mathrm{T}}(t))$ represents the influence of topology on (2.11). To be more specific, the design parameters $\boldsymbol{s}_{\mathrm{t}}$ and control vector $\boldsymbol{u}_{\mathrm{t}}^{\mathrm{s}}$ in (2.11) are changed to $\boldsymbol{s}_{\mathrm{t}}^{\mathrm{T}}$ and $\boldsymbol{u}_{\mathrm{t}}^{\mathrm{T}}$ in (2.12), respectively. Equation (2.12a) ensures that the component temperature is always maintained below its thermal limit and (2.12b) means that the thermal system should respect the packaging constraint. Other constraints are related to (2.9) and (2.11). This optimization problem can be solved in a similar fashion as (2.7).

This study mainly focuses on system-level thermal management. For overview of thermal management of individual powertrain components, interested readers are referred to [62, 113, 127–135]. Additionally, given the strong coupling between energy and thermal domains, a suitable thermal management topology should be determined in combination with energy-aware design and control optimization.

2.4 Energy- and thermal-aware design and control optimization

Taking into account design and control aspects, if a system is optimized from both energy and thermal perspectives, it is termed energy- and thermal-aware design and control optimization.

2.4.1 Topology generation

Choosing a suitable powertrain and thermal management configuration is vital, since it affects vehicle energy efficiency, cost, performance, comfort and reliability. From both energy and thermal viewpoints, automatic topology generation is not available in the literature. If automatic generation of powertrain and thermal management architectures is taken into consideration, feasible powertrain and thermal management

configurations can be identified by combing (2.1) and (2.8), given by

$$\text{Find} \quad \boldsymbol{T}^{\mathrm{f}}_{\mathrm{e,t}} \subseteq \boldsymbol{T}^{\mathrm{p}}_{\mathrm{e,t}}, \tag{2.13}$$

$$\text{s.t.} \quad g_{\mathrm{e,t}}(\boldsymbol{T}^{\mathrm{f}}_{\mathrm{e,t}}) \leq 0, \tag{2.13a}$$

where $\boldsymbol{T}^{\mathrm{f}}_{\mathrm{e,t}}$ represents the feasible powertrain and thermal management topologies and $\boldsymbol{T}^{\mathrm{p}}_{\mathrm{e,t}}$ the possible powertrain and thermal management configurations. Equation (2.13a) includes the constraints from (2.1) and (2.8). The generated feasible architectures have yet to be compared based on TCO, by integrating with control and size layers.

2.4.2 Control optimization

In this respect, earlier works mainly focused on the control layer for a given topology $\boldsymbol{T}^{\mathrm{f}}_{\mathrm{e,t}}$ generated by (2.13) and fixed powertrain and thermal parameters represented by $\boldsymbol{s}_{\mathrm{e}}$ and $\boldsymbol{s}_{\mathrm{t}}$. The aim of an integrated energy and thermal controller is to optimally decide the power flow of the electrified powertrain considering the energy and thermal aspects to minimize the overall energy consumption, while satisfying the driver demand and heating/cooling requirements. By combing (2.2) and (2.9), this control problem can be expressed as

$$\begin{aligned}
&\min \; J_{\mathrm{e,t}}(\boldsymbol{x}_{\mathrm{e}}(t), \boldsymbol{x}_{\mathrm{t}}(t), \boldsymbol{u}_{\mathrm{e}}(t), \boldsymbol{u}_{\mathrm{t}}(t), t \mid (\boldsymbol{T}^{\mathrm{f}}_{\mathrm{e,t}}, \boldsymbol{s}_{\mathrm{e}}, \boldsymbol{s}_{\mathrm{t}})) = && (2.14a)\\
&\int_{t_0}^{t_{\mathrm{f}}} [w_{\mathrm{p}} \; (P_{\mathrm{e}}(\boldsymbol{x}_{\mathrm{e}}(t), \boldsymbol{x}_{\mathrm{t}}(t), \boldsymbol{u}_{\mathrm{e}}(t), \boldsymbol{u}_{\mathrm{t}}(t), t)) + \\
&w_{\mathrm{t}} \; (P_{\mathrm{t}}(\boldsymbol{x}_{\mathrm{e}}(t), \boldsymbol{x}_{\mathrm{t}}(t), \boldsymbol{u}_{\mathrm{e}}(t), \boldsymbol{u}_{\mathrm{t}}(t), t))] \; \mathrm{d}t, && (2.14)\\
\text{s.t.} \quad &\dot{\boldsymbol{x}}_{\mathrm{e}}(t) = \boldsymbol{f}(\boldsymbol{x}_{\mathrm{e}}(t), \boldsymbol{x}_{\mathrm{t}}(t), \boldsymbol{u}_{\mathrm{e}}(t), \boldsymbol{u}_{\mathrm{t}}(t), t), && (2.14b)\\
&\dot{\boldsymbol{x}}_{\mathrm{t}}(t) = \boldsymbol{f}(\boldsymbol{x}_{\mathrm{e}}(t), \boldsymbol{x}_{\mathrm{t}}(t), \boldsymbol{u}_{\mathrm{e}}(t), \boldsymbol{u}_{\mathrm{t}}(t), t), && (2.14c)\\
&h_{\mathrm{e,t}}(\boldsymbol{x}_{\mathrm{e}}(t), \boldsymbol{x}_{\mathrm{t}}(t), \boldsymbol{u}_{\mathrm{e}}(t), \boldsymbol{u}_{\mathrm{t}}(t), t) = 0, && (2.14d)\\
&g_{\mathrm{e,t}}(\boldsymbol{x}_{\mathrm{e}}(t), \boldsymbol{x}_{\mathrm{t}}(t), \boldsymbol{u}_{\mathrm{e}}(t), \boldsymbol{u}_{\mathrm{t}}(t), t) \leq 0, && (2.14e)
\end{aligned}$$

where w_{p} and w_{t} are the weights. The energy domain and the thermal domain are coupled, as can be seen in the constraints.

The associated algorithm to solve (2.14) is referred to as the energy and thermal management system. Recall that there are two categories for both EMSs and TMSs: rule-based and optimization-based algorithms. Hence, the combination of the EMS from Figure 2.4 represented by $\{RB, OB\}$ and the TMS from Figure 2.9 represented by $\{RB, OB\}$ yields different solution methods represented by $\{RB, OB\} \times \{RB, OB\}$ to (2.14). Consequently, energy and thermal management systems can be divided into two principle groups, separate energy and thermal management systems (SETMSs) and combined energy and thermal management systems (CETMSs), as shown in Table 2.1 with examples found in the literature [60]. The SETMS is denoted by EMS + TMS, while the CETMS is denoted by (EMS,TMS). The key difference is that the control variables are determined simultaneously at the supervisory level in a CETMS,

considering whether the control decision of the thermal management system is energy beneficial. The TMS receives the control signal from the EMS, which can be seen in Figure 2.11. In a SETMS, however, there are explicitly two layers, and the energy management system and the thermal management system are treated independently.

Table 2.1: Energy and thermal management strategies.

Control strategy	Composition	Optimality	Causality	Application
SETMS	PF + On/Off	Sub-optimal	Causal	Heavy-duty series HEV powertrain [66]
	TC + MPC	Sub-optimal	Causal	Battery pack of a series HEV [136]
	ECMS + On/Off	Sub-optimal	Causal	Battery of a hybrid electric truck [17]
	OB + MPC	Sub-optimal	Causal	HEV powertrain [67]
CETMS	(RB, RB)	Sub-optimal	Causal	Engine and electrical power equipment of an HEV [137]
	(RB, OB)	Sub-optimal	Causal	Engine and electrical power equipment of an HEV [137]
	(DO, On/Off)	Close-to-optimal	Acausal	Climate control system, refrigerated semitrailer, and air supply system [18]
	(DP, MPC)	Optimal	Acausal	Battery pack of a series HEV [23]

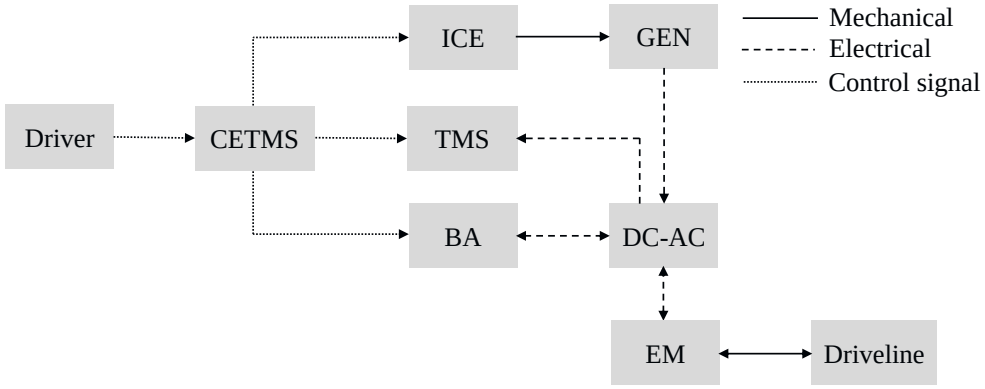

Figure 2.11: Combined energy and thermal management.

Previous research mostly focused on SETMSs. For a heavy-duty series HEV powertrain, a power follower control strategy is developed in [66] based on heuristics to decide the operation of a power generation unit to meet the power request from the driver. Powertrain components generate heat accordingly. A low-level On/Off controller is utilized to remove the heat to keep the component temperatures below their prescribed thermal limits. These controllers are easy to implement and can be used in real-time control. However, they cannot provide an economic solution in terms of energy consumption, because both control strategies are rule-based. An improved version is presented in [136], even though the EMS is similar, a rule-based thermostat control, the thermal management system is developed based on MPC, which reduces cooling power consumption. A clear drawback of this study is that the EMS is a rule-based method, which generates non-optimal set-point of the power source and has a negative impact on the MPC result. To overcome this limitation, for an HEV powertrain, both optimization-based algorithms are implemented for high-level energy management and low-level thermal management in [67] to improve energy efficiency. However, the EMS does not verify whether the control action of the thermal management system is energy beneficial, resulting in a sub-optimal solution. This disadvantage of SETMSs motivates the development of CETMSs, which started to appear recently and are proved to be superior to their separate counterparts [17].

In this respect, the EMS designed based on rules still cannot yield an optimal solution, regardless of the TMS used [137]. To overcome this issue, an online energy and battery thermal management system is presented in [138] to tackle multiple states with energy dynamics and thermodynamics. The battery pack can be cooled down with a radiator or chilled down with a chiller in association with an AC system, which maintains the battery temperature within its optimal range. The switch between the cooling mode and the chilling mode is decided by physics. The AC compressor can only be turned On or Off, as it is linked to the engine with a clutch. The propulsion and cooling requirements are eventually met by the engine. The main objective is to minimize the fuel consumption, while keeping the battery temperature within its optimal range, by finding the optimal control inputs. This problem is solved with ECMS (Figure 2.4). The optimal solution is found using necessary conditions and the initial values of the co-states are calculated offline. Proportional controllers are employed to update co-states in real-time. A fuel saving of around 1.8% is reported, compared to its separate counterpart, where the EMS makes decisions without considering the battery cooling power consumption, i.e., ECMS + On/Off [138]. Notice that, however, the solution can be sensitive to the initial values of the co-states [27]. It is also sensitive to the physics-based mode selection. Moreover, even though in this study only battery thermal management is taken into account, this method can be extended to consider other powertrain components. But as the number of states increases, many parameters need to be tuned and the optimal solution cannot be obtained, which necessitates the development of offline optimal control strategies.

In order to tackle these problems, a scalable distributed optimization (Figure 2.4) approach is proposed in [18], concentrating on convex approximation of auxiliaries. The auxiliaries consist of an air supply system, a refrigerated semitrailer, and a climate control system, which can only be turned On or Off, as they are connected to the engine with clutches. The complete problem can be seen as an energy network. Each auxiliary is a subsystem of the energy network, comprising energy storage systems, for example, the battery, and converters, for instance, the electric machine. The aim is to minimize the fuel consumption of the whole system, which is equivalent to minimizing the energy losses of the subsystems. The subsystems are connected to meet the power demand. To preserve convexity, quadratic equality constraints that describe the input and output power of the converter are relaxed to inequality constraints. It should be noted that the equality holds at the optimum [59]. In the presence of propulsion requirements, where power is aggregated in the energy network, the problem cannot be separated and solved easily. The original problem is then decomposed into several smaller optimization problems via dual decomposition, which augments the cost function with the power demand. Owing to the one-on-one mapping between the subsystem and the Lagrange dual function, the subsystems can be solved individually and efficiently, by utilizing Lagrangian method and alternating direction method of multipliers. Compared with its separate counterpart, where the energy management system and the thermal management system are treated independently, a fuel saving of around 1.08% is reported [18]. The presented method can be extended to include more thermal systems. However, in this study, the thermal management

system is limited to On/Off control, leading to a large number of switches and excess power consumption, which needs to be upgraded to optimal controllers.

To address this issue, [23] presents an integrated DP and MPC approach. The system architecture is similar to Figure 2.11, where the CETMS represented by DP consideres both propulsion and battery cooling requirements. The TMS represented by MPC receives the control signal from DP to regulate an AC system so as to maintain the battery temperature within its optimal range. Specifically, the cooling air circulated by an air pump, removes heat from the battery. The compressor that is attached to the electric machine provides the desired coolant flow rate continuously. In view of high computation time of DP, the battery cooling system is simplified as a static map, where the compressor power of the AC system is described as a function of heat rejection and cooling air temperature. The propulsion power and the cooling power are ultimately met by the battery power and engine-generator power. Overall, the system has two state variables, the state-of-charge of the battery and cooling air temperature, and two control variables, the engine-generator power and compressor power. Discretization of these variables is required, which entails a trade-off between accuracy and computation time [10, 58]. The objective is to evaluate system dynamics and find optimal control variables at each time instance to minimize the fuel consumption in charge-sustaining mode. Compared to a SETMS as the baseline, where the energy management and the thermal management are not integrated, up to around 5% fuel saving is achieved [23]. Note that, however, the result can be sensitive to the discretization of those state and control variables. In addition, simplified models are not representative in reality. Moreover, as the number of states grows, it can be expected that the computation time increases exponentially, which may not be tractable.

Although CETMSs are investigated mostly for HEVs, the same principles hold for EVs as well. For example, in [19], DP is applied to find the optimal power sharing between the powertrain and the cabin heating system, taking into account battery health. However, the foregoing studies only consider control optimization and the plant has yet to be incorporated to obtain an optimal system.

2.5 Observations and future trends

2.5.1 Controller design

From EMS point of view, optimization-based algorithms (Figure 2.4) are gaining popularity, such as using DP as an offline strategy to obtain a global optimal solution to benchmark online controllers [139]. Since DP is computationally heavy [58], to shorten the computation time and achieve the same accuracy, CP is a promising alternative [140]. Even though the online counterparts of the offline optimization-based methods facilitate real-time implementation, to simplify the problem, rules can be extracted from offline optimization-based algorithms to form control strategies, as

shown in Figure 2.4. Examples are RB-ECMS [95] and RB-DP [16], which strike a balance between optimality, computation time, and complexity. Moreover, taking into account discrete variables, for example, engine on-off and gear shift [96], which results in a mixed-integer optimization problem, necessitates the development of integrated algorithms [97] and hybrid optimal control techniques [141]. In [97], the engine on-off and gear shift are determined by DP in the outer loop, and the continuous variable, power split, is solved by using CP in the inner loop. Apart from energy consumption (fuel and electricity), the objective function to be minimized is also expected to consider more factors to find the trade-off, such as emissions for eco-driving [142], battery aging for cost reduction [143], and drivability for comfort [144, 145]. Additionally, to further increase powertrain efficiency, it is essential to include the thermal domain.

From TMS perspective, since conventional mechanical actuators with On/Off control method fail to provide an economic solution, current trend is to upgrade them to their electrified counterparts, enabling heating/cooling on demand with optimization-based algorithms [146–152]. For example, compared with a traditional control method, the overall power consumption of the cooling system with advanced electromechanical actuators and control strategies can be reduced by around 45% [152].

Regarding energy and thermal management systems, as CETMSs achieve better performance than their separate counterparts, they will get more and more attention. As is made evident by Table 2.1, there are eight ways of integrating energy and thermal management systems, but limited comparisons can be found in the literature. To identify energy saving in different scenarios, it is important to conduct more comparisons. Furthermore, in CETMSs, there is a trade-off between optimality, complexity, causality, and computation time. Such integrated systems can also communicate with other electronic control units onboard and provide guidelines for drivers via human machine interface to maximize efficiency.

Currently, however, only the control layer has been taken into consideration for energy and thermal management systems. To obtain an optimal system and reveal the real coupling between the energy and thermal domains, it is imperative to incorporate the design layer.

2.5.2 Waste heat recovery

As described in Section 1.3, recovering a certain percentage of the engine exhaust thermal energy is a promising way to improve energy efficiency. Two types of WHR technologies can be found: Thermoelectric generators (TEGs) [153–157] and Organic Rankine cycle (ORC)-based WHR systems [30–33]. A TEG consists of various P-type and N-type semiconductor materials, which convert heat into electricity directly, based on the Seebeck effect [158]. The Seebeck effect describes the voltage generated across the junctions of two dissimilar materials, owing to a temperature gradient. It has the advantages of no moving parts and no chemical reactions and, as long as there is a

temperature difference, it produces electricity. Nevertheless, considering conversion efficiency, technical readiness, and cost, Rankine cycle systems are preferable. It has been shown that ORC systems have an efficiency of up to 15% [31, 34–36]. A PMP-based EMS for controlling Rankine cycle systems is presented in [34]. Maximizing the power output of a Rankine cycle system on board a diesel-electric railcar is reported in [36], by using DP and dynamic real-time optimization. Furthermore, [159] demonstrates a recovery efficiency of 10% for an electrified powertrain on the NEDC. Additionally, the turbine in a Rankine cycle system can be coupled with a generator, which constitutes a Rankine cycle-based electrical WHR system. From a control point of view, it is advantageous to store the recovered waste heat energy in the energy buffer. A Rankine cycle-based electrical WHR system is comprised of five main components: Evaporator, expander, generator, condenser, and pump, as shown in Figure 2.12. The working fluid is pumped from low pressure to high pressure, which then absorbs heat from exhaust gases through the evaporator and undergoes a phase change, from liquid to vapor. Expansion of the vaporized fluid subsequently produces mechanical energy by the expander, which is converted into an electrical form by the generator. The generated electricity is eventually stored in the energy buffer, which can be retrieved when needed. Consequently, the working fluid dissipates heat to the surroundings at the condenser and undergoes another phase change, from vapor to liquid. This technology is mainly used in ICEVs [37].

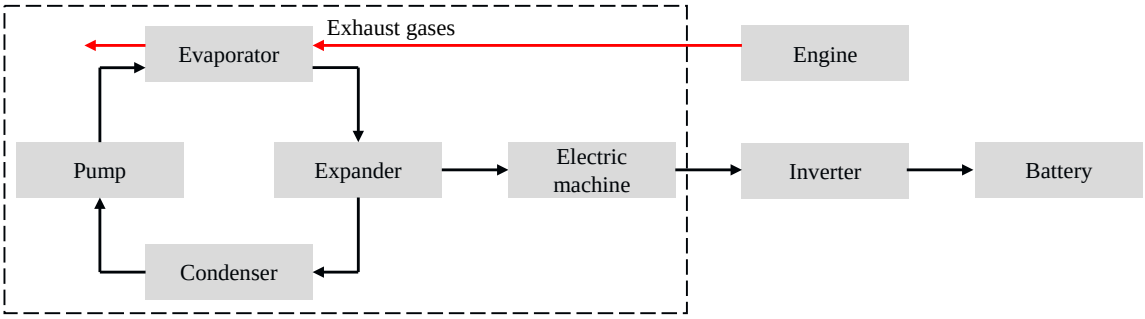

Figure 2.12: A Rankine cycle-based electrical WHR system.

Furthermore, as presented in Section 1.3, recuperating a certain amount of the waste heat from an electric drive by using an HP is a promising way to improve energy efficiency of an electrified vehicle with cabin heating. It exchanges the heat with the refrigerant circuit and cabin heating system to boost heating performance, resulting in a decrease in battery load, as demonstrated in Figure 2.13. This, ultimately, contributes to energy efficiency improvement. It has been reported that, by utilizing the waste heat from ambient and electric devices, the coefficient-of-performance (COP) and heating capacity increase by 9.3% and 31.5% [41], respectively. HPs are mostly adopted for EVs [42]. Furthermore, observing the temperature levels of the major components of an electrified powertrain, as shown in Figure 2.7, the EM can be integrated into the same housing as the transmission. They can be combined into a single heat source, by sharing the same cooling loop (e.g., with oil cooling) [160–162] and contributing together to the heat which can be harvested by the HP, resulting in

improved heating performance.

Note that design and control of ORC system and HP system have yet to be integrated at system level to identify the energy saving. A detailed cost-benefit analysis would also be required before mass production of these systems.

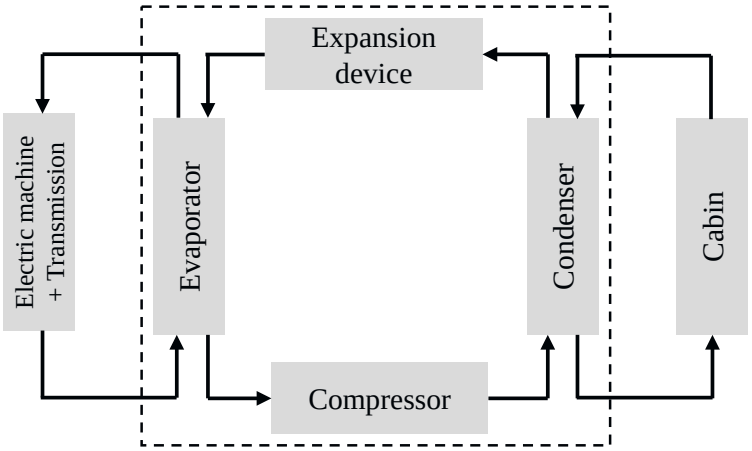

Figure 2.13: Heat pump system utilizing waste heat from transmission and electric drive.

2.5.3 Heat exchange

At low temperatures, the engine has higher frictional losses because of increased hydrodynamic effects and poor combustion. The difference in fuel consumption between a warm engine and a cold one is around 12% [163]. The battery performance deteriorates remarkably at low temperatures, which has a negative impact on reliability, safety, and efficiency. Because of cabin heating, the driving range of an EV can be reduced by up to around 68% [164]. It can be observed from Figure 1.5 that the heat energy transferred to the engine coolant is significant, which can be utilized to heat up lubrication oils, cabin, battery and so on [165–169]. As shown in Figure 2.15, where electrified actuators are used, engine coolant is utilized to warm up engine oil, transmission oil, and cabin heater core using a three-way valve. It is reported that powertrain efficiency can be improved by around 4% due to fast warm-up [169].

Additionally, as illustrated in Figure 2.14, in EV mode, the electric drive and transmission coolant can be utilized to heat up the engine and battery during cold-start conditions to reduce power dissipation. Overall, the heat exchange between powertrain components can be summarized in Figure 2.16. Assume each cooling circuit is self-contained, consisting of heat source, fluid delivery device, and heat sink. However, optimal control strategies are needed to allocate and remove heat effectively, which would increase efficiency and reduce the thermal system size and cost.

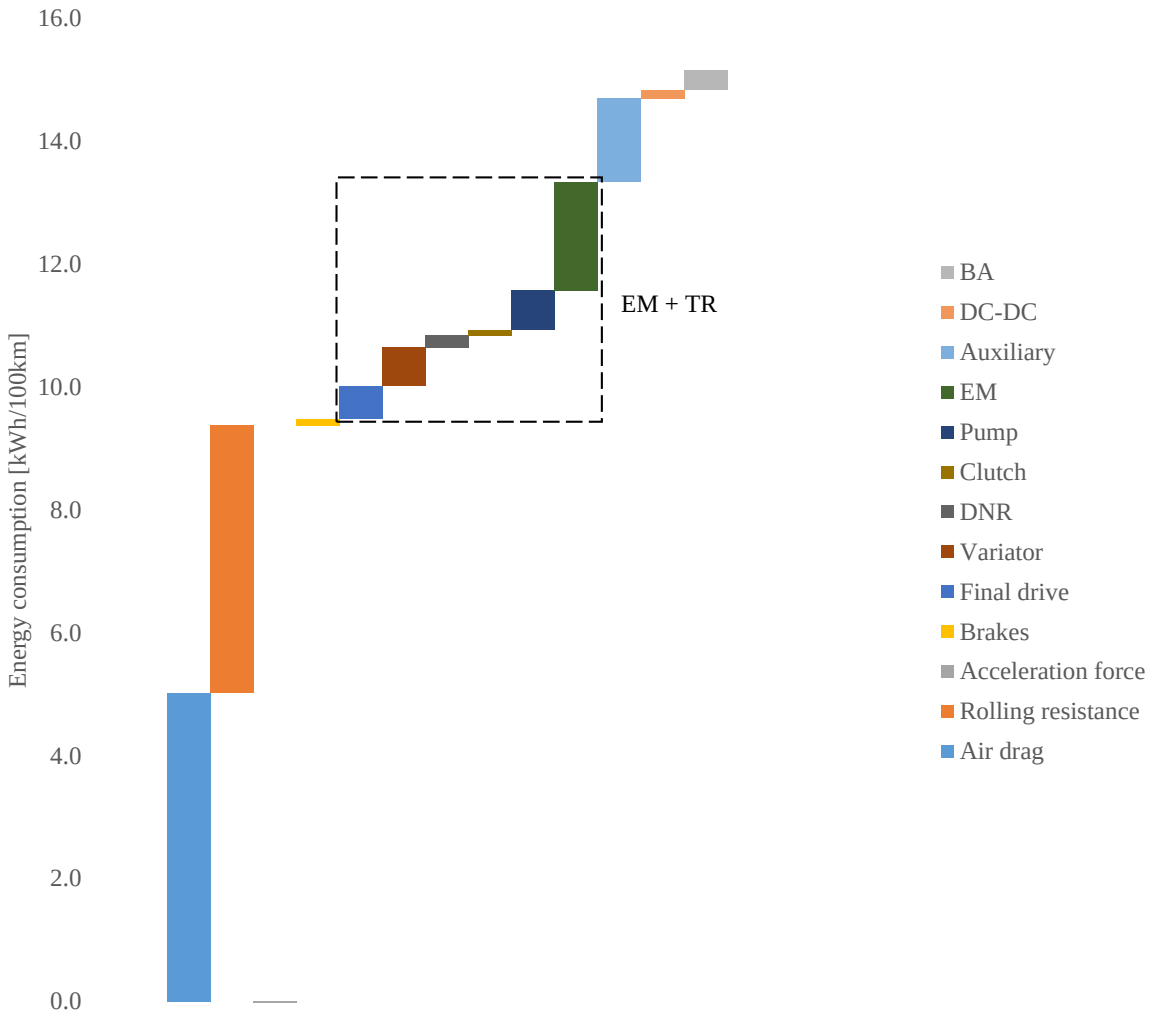

Figure 2.14: Typical energy balance of a PHEV in charge-depleting mode [170].

2.5.4 Transition to electric vehicles

In the electrification of vehicles, the first front is HEVs. They have played a pivotal role in reducing energy consumption in the past decades. Nowadays, EVs have an increased positive impact on the environment, compared to HEVs, which accelerates EV's resurgence. There exists a variety of EV architectures, depending on the transmission type, the number of EMs, and their locations [171, 172]. Even though single-speed transmissions currently dominate the EV market, research on multi-speed transmissions, such as two-speed and continuously variable transmission (CVT), are emerging, focusing on cost function optimization, energy efficiency, and vehicle performance [48, 173–176]. For example, depending on loading conditions, e.g., hill climbing, EVs would benefit from various operational states provided by a CVT without torque interruption. In this respect, the integration of such as the EM and the transmission, plays an important role [64]. As shown in [45], a CVT could provide opportunities of optimizing the EM due to continuous ratio adjustment. In turn, the wider constant power region of the EM could help in the optimization of the

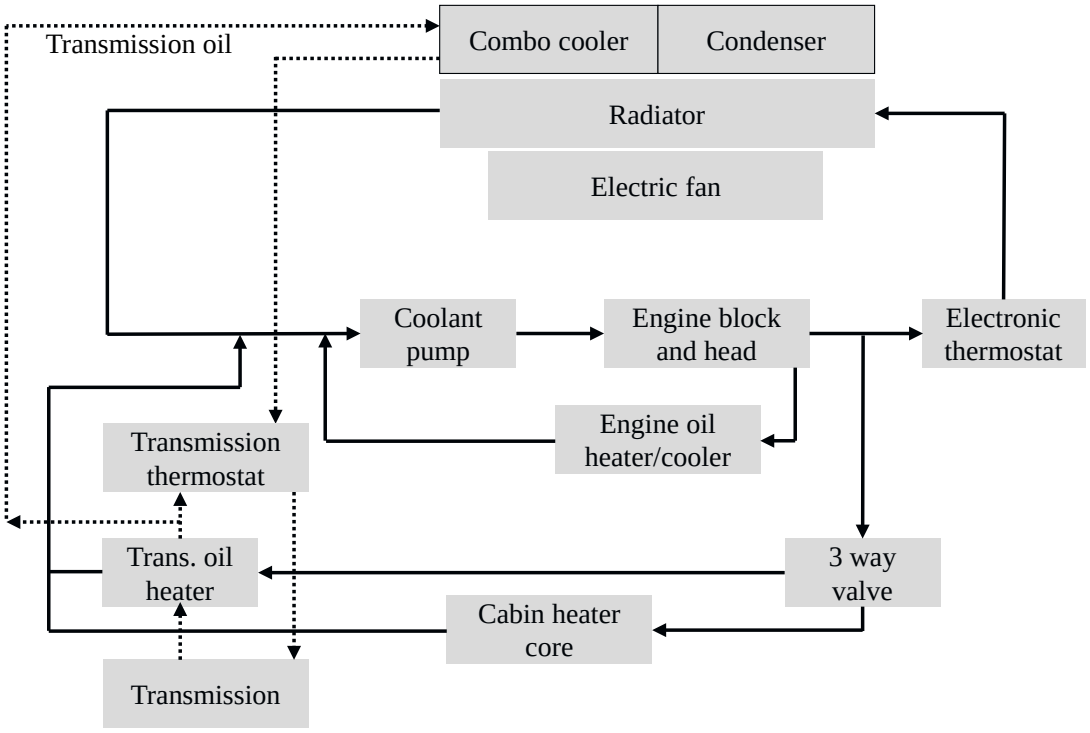

Figure 2.15: Heat energy distribution between powertrain components [169].

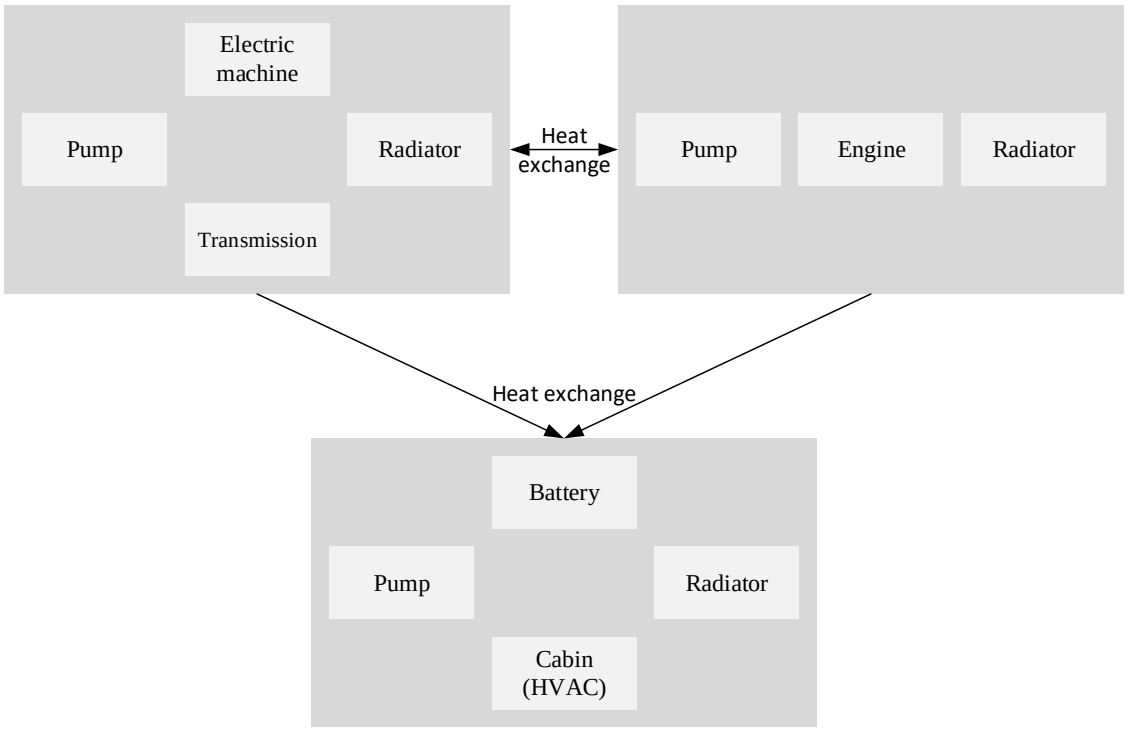

Figure 2.16: Heat exchange between powertrain components.

CVT. These would result in an optimized battery and thermal system. Finding optimal component sizes and letting the system operate at high efficiency regions would contribute to cost function reduction. An optimal thermal management with electrified actuators also contributes to reducing the size and cost of the thermal system. Additionally, if waste heat from electric drive and transmission is used in an EV, the sizes of the heat pump and the battery pack would be reduced.

2.5.5 Plant design

For sizing of powertrain components, current studies mainly focus on optimization-based methods (Figure 2.5), such as widely used GA and PSO [177, 178]. Limited research can be found in terms of applying optimization-based algorithms to determine the thermal system size. Moreover, to arrive at an optimal system design, component sizing needs to be coupled with the control layer. Generally, in terms of optimality, nested and simultaneous approaches outperform sequential and iterative ones. Simultaneous methods that require convex features of a system are computationally more efficient than nested schemes relying on exhaustive search. Recent studies mostly concentrate on nested and simultaneous schemes because of optimality. Each method has its own strengths and limitations. For example, to find optimal energy management and component sizes of a series PHEV, two methods are employed in [179], where CP represents the simultaneous coordination scheme and PSO/DP represents the nested approach. In [179], the same optimal solution is obtained, which achieves a fuel efficiency improvement of around 10.4% compared to the initial powertrain design. CP delivers superior performance to PSO by a factor of 20 in terms of computation time. Tuning effort for PSO is also required. Nevertheless, heuristics or DP is needed in CP to handle integer variables, e.g., engine on-off. Moreover, CP requires the problem to be solved in a convex form. To strike a balance between computation time and solution optimality, an iterative coordination method can be utilized, such as DP/CP [106]. The (close-to) optimal solution is then obtained in a considerably short time. Furthermore, topology dictates vehicle energy efficiency and cost. In order to choose a suitable configuration with large design space, topology generation has proven beneficial for design. However, current methods do not take into account the thermal management architecture, which may not yield an optimal system. Topology optimization needs to be integrated with size and control optimization so as to select the best configuration based on minimum TCO. Additionally, integrated design and control of a complete electrified vehicle considering both energy and thermal domains to reduce the TCO has yet to be addressed, while satisfying performance, driving comfort, passenger thermal comfort, and reliability requirements.

2.6 Conclusions

A comprehensive analysis of design and control optimization layers and coordination approaches for electrified powertrains including energy and thermal domains is presented in this chapter. By combing these optimization layers, energy consumption reduction and cost saving can be obtained. Although depending on the coupling and how sensitive the solution is to uncertainties in the design parameters, nested and simultaneous schemes outperform sequential and iterative ones in terms of optimality. Nested approaches are usually relying on exhaustive search, which is computationally heavy, whereas simultaneous coordination schemes often demand the original problem to be convex. Moreover, recent energy and thermal management systems are thoroughly surveyed and divided into two principle groups, SETMSs and CETMSs. With respect to energy efficiency improvement, CETMSs deliver superior performance to SETMSs, as control decisions are made only once at the supervisory level in CETMSs. It is shown that a trade-off exists between optimality, causality, computation time, and complexity. Additionally, an analysis of future trends in terms of improving energy efficiency and reducing system cost is presented.

Based on the findings from this chapter, as electrified vehicles comprise HEVs and EVs, two case studies are carried out to show the effectiveness of integral design approach in Chapter 3 and Chapter 4, respectively. In Chapter 3, from optimal control perspective, integrated energy and thermal management of a CVT-based PHEV is investigated, where design considerations are also derived. In Chapter 4, from optimal design and control viewpoint, simultaneous design and control optimization of a CVT-based EV is explored, which is extended by integrated energy and thermal management.

Chapter 3

Integrated energy and thermal management of CVT-based hybrid electric vehicles

In this chapter[1], for a continuously variable transmission (CVT)-based plug-in hybrid electric vehicle (PHEV) with cabin heating, which is subject to a cold-start, an integrated energy and thermal management system (IETMS) is proposed to identify the gain of using waste heat recovery (WHR) technologies on the ultimate fuel savings. Dynamic programming (DP) is used to maximize the fuel efficiency for a pre-defined drive cycle. It is found that a cold-start has a significant impact on the fuel consumption, up to around 7.1%, and a dual-source waste heat recovery (DSWHR) system has a significant improvement on the fuel saving, up to around 13.1%. Optimization results also provide insights into design of the DSWHR system and sizing of powertrain components. Additionally, taking into account WHR, transient, and steady-state thermal behavior, a complete energy consumption minimization strategy (CECMS) framework is proposed to minimize the overall energy consumption, which enables online implementation. An introduction to the topic is given in Section 3.1. Optimization problem is then formulated in Section 3.2. Section 3.3 describes the PHEV model required for solving the optimization problem. Based on the developed PHEV model, numerical optimization is given in Section 3.4, by using DP. Optimization results are subsequently presented in Section 3.5. On the basis of the optimal solution found offline, the CECMS framework is presented in Appendix B. Finally, conclusions are given in Section 3.6.

[1]The content of this chapter is based on the following publications:
Wei, C.; Hofman, T.; Ilhan Caarls, E.; van Iperen, R. Optimal Control of an Integrated Energy and Thermal Management System for Electrified Powertrains. In Proceedings of the 2019 American Control Conference, Philadelphia, PA, USA, 10-12 July 2019.
Wei, C.; Hofman, T.; Ilhan Caarls, E.; van Iperen, R. Integrated Energy and Thermal Management for Electrified Powertrains. Energies 2019, 12, 2058.

3.1 Introduction

Hybrid electric vehicles (HEVs) play a pivotal role in improving fuel economy, which take advantage of advanced control freedom provided by hybridization, very different from their traditional counterparts. As HEVs use multiple power sources, of particular importance is the development of energy management systems (EMSs) for HEVs so as to maximize their fuel economy [10, 61]. An EMS aims at controlling the power-flow of the hybrid powertrain in an optimal way; for example, the torque split between the internal combustion engine (ICE) and the electric machine (EM). As illustrated in Figure 2.4, various energy management strategies have been proposed. Among these control strategies, dynamic programming (DP) is widely chosen, thanks to its advantages in obtaining a global optimal solution, handling nonlinear constraints, and assessing online controllers, as discussed in [108]. However, the thermal domain is often not taken into account.

A majority of researchers currently devise EMSs under the assumption that the engine is already at its operating temperature at the outset; namely, a warm-start [13]. This may not be realistic, and we may have the case where the vehicle has been parked for a few hours, resulting in a cold-start; which is common in the real world. Cold-start conditions imply a low engine temperature, which increases frictional losses in the engine, leading to excess fuel consumption due to high-viscosity effects. Furthermore, some drive cycles—for instance, the New European Driving Cycle (NEDC) and the Worldwide Harmonized Light Vehicles Test Cycles (WLTC)—require cold-start conditions to measure fuel consumption [180]. The required starting temperature is far below the engine operating temperature. The impact is particularly high in the first few minutes of driving. The fuel-saving potential can be obtained by extending the design space of conventional EMSs with an extra continuous dynamic state, the engine temperature. The fuel-saving potential has been reported to be large (12% [163]) for the NEDC. It has also been shown, in [181], that cold-start conditions increase fuel consumption by up to 14.6% in the urban part of the NEDC, which well-represents the warm-up phase. This is particularly true for a plug-in HEV (PHEV) due to intermittent operation. Furthermore, little attention has been paid to improve the fuel economy with a cold-start and thereby quantify the ultimate fuel savings. Due to such effects, original equipment manufacturers (OEMs) are also in the process of defining and implementing more realistic drive cycles in their development processes.

As introduced in Section 1.3, a large portion of the fuel energy is wasted as exhaust gases, and recovering a certain percentage of the exhaust thermal energy is a promising way to promote fuel efficiency. Furthermore, the amount of waste heat from continuously variable transmission (CVT) and EM (including inverter) is significant, and recovering a certain amount of that heat is a promising way to improve energy efficiency. As presented in Section 2.5.2, an exhaust gas waste heat recovery (EGWHR) system, namely a Rankine cycle-based electrical waste heat recovery (WHR) system, can be utilized to recuperate the exhaust thermal energy. It convert that into an electrical form, which is eventually stored in the battery and can be retrieved when

needed. It increases the energy content of the battery. Moreover, an electric path waste heat recovery (EPWHR) system can be used to recuperate the waste heat from the CVT and EM to boost the heating performance of a heat pump (HP) for cabin heating. It reduces the load on the battery. EGWHR systems are mostly used in internal combustion engine vehicles (ICEVs) and EPWHR systems are mainly adopted for electric vehicles (EVs) to improve vehicle energy efficiency. Since a PHEV benefits from the features of an ICEV and an EV, a dual-source WHR (DSWHR) system consisting of an EGWHR sub-system and an EPWHR sub-system can be employed. It bridges the gap between a cold-start and a warm-start and improves fuel efficiency.

It has been widely acknowledged that the optimal solution obtained from DP is not implementable. Earlier studies mainly focused on the transient behavior of powertrain components, when it comes to thermal aspects (e.g., heating up the component from a cold-start to its operating temperature) [7, 182]. After the cold-start, the operating temperature is assumed to be well maintained, which is actually the main goal of the corresponding thermal management system (TMS) in practice. It is obvious that in this case, the cooling system is not integrated and the cooling power consumption is neglected, which would influence the control strategy and the fuel consumption measurement. A systematic approach, based on optimal control theory, to facilitate an online implementation of complete energy and thermal management for PHEVs, including WHR, transient, and steady-state behavior, has not yet been developed.

In view of the above discussion, this study proposes an integrated energy and thermal management system (IETMS) for a CVT-based parallel PHEV to quantify the impact of a cold-start on the fuel consumption. In addition, it identifies the benefit of employing a DSWHR system on the ultimate fuel savings. The approach is as follows:

- A CVT-based PHEV model including the coupling between energy dynamics and thermodynamics based on a concept vehicle is firstly created, by using experimentally-based lookup tables.

- The thermodynamics models comprise a thermal ICE model and a DSWHR model. The thermal ICE model obtains the engine temperature and cold factor so as to adjust the nominal fuel consumption with a warm-start. The engine cold factor represents the excess frictional power dissipation due to high-viscosity effects at low engine temperatures. As the goal of this study is to gain qualitative insights of fuel savings, a simplified DSWHR model is used. The DSWHR model obtains the power recovered from the engine exhaust gases, and hence increasing the energy content of the battery, and from the electric path (EM and CVT), and thus decreasing the battery load for cabin heating.

- There is a trade-off between the ICE heating, and hence reducing the cold impact, and the utilization of the DSWHR system, and thus increasing the recovered power. DP is then applied to minimize the overall fuel consumption for a pre-defined drive cycle. It controls the torque split between the ICE and EM and the CVT speed ratio that aims at optimizing the operation of the power

source.

- As the optimal solution is found by DP, which is an offline optimization strategy, a complete energy consumption minimization strategy (CECMS) framework that is online implementable is presented in Appendix B. It aims to minimize the complete energy flow, taking into account WHR, transient, and steady-state thermal behavior, by establishing relationships between DP, Pontryagin's minimum principle (PMP), and equivalent consumption minimization strategy.

3.2 Problem definition

The proposed IETMS for a CVT-based PHEV is shown in Figure 3.1. The engine can be disengaged from the powertrain via a clutch, which is not depicted. PHEVs are best characterized by their charge-sustaining and charge-depleting modes. In this study, a charge-sustaining mode is assumed, as it is a common way to assess the performance of the control strategy [159, 183]. The major components of the considered PHEV are the engine, battery, DC-AC inverter, EM, CVT, and vehicle. The DC (direct current)-AC (alternating current) inverter and EM are combined together. As can be seen from Figure 3.1, apart from traditional chemical, mechanical, and electrical energy flows, thermal energy (dash-dot lines) is added. In this system, the waste heat from the engine is recovered by the EGWHR sub-system, and the recovered power is stored into the battery. Further, the EM and CVT are combined, and the resulting waste heat is recuperated by the EPWHR sub-system, which reduces the load on the battery due to cabin heating demand.

The PHEV model is backward-facing (i.e., the drive cycle has to be known a priori), and includes both energy dynamics and thermodynamics. As far as the energy dynamics are concerned, the most relevant inertias are taken into account: The inertias of the engine, EM, variator in the CVT, and the vehicle. CVT, ICE, and EM efficiency models are represented by experimentally-based lookup tables, due to their non-linear behavior. In terms of thermodynamics, it is assumed that, except for the engine, the heat source components are in thermal equilibrium with the ambient conditions. The engine thermodynamics model, utilizing first principles [138], is developed on the basis of [7], in which the experiments are performed, and parameters are used where applicable. Once the engine temperature reaches its operating temperature, after which the cold effect on fuel consumption becomes negligible, the engine temperature is assumed to be kept at this reference. Therefore, the effect of the radiator and the cooling power consumption are neglected for now, but it will be taken into account in Appendix B to design a CECMS. Kinematics, dynamics, and constraints are modeled with a discrete time-step of one second, which is sufficient for the design of the integrated energy and thermal controller. The key model parameters are listed in Table 3.1 [7, 184]. The battery considered is a lithium-ion type battery with specific energy density of 113 Wh/kg.

Table 3.1: Main parameters of PHEV model[7, 184].

Parameter	**Value**	**Unit**	**Description**
m_{v}	1600	kg	Vehicle mass
$\overline{\gamma}_{\mathrm{v}}/\underline{\gamma}_{\mathrm{v}}$	7	-	Ratio coverage of CVT
$\overline{\tau}_{\mathrm{e}}$	239	Nm	Maximum engine torque
$\overline{\omega}_{\mathrm{e}}$	4500	rpm	Maximum engine speed
$\overline{P}_{\mathrm{e}}$	99	kW	Maximum engine power
$\overline{\tau}_{\mathrm{m}}$	350	Nm	Maximum EM torque
τ_{m}	210	Nm	Continuous EM torque
$\overline{\omega}_{\mathrm{m}}$	7800	rpm	Maximum EM speed
$\overline{P}_{\mathrm{m}}$	74	kW	Maximum EM power
P_{m}	50	kW	Continuous EM power
Q_{b}	40	Ah	Battery capacity
V_{n}	3.75	V	Cell voltage
c_{e}	630	J/kgK	Engine specific heat
c_{h}	0.62	-	Engine heating coefficient
$\overline{\theta}_{\mathrm{e}}$	80	°C	Engine operating temperature
$c_{\mathrm{e},1}$	0.0034	1/K	Engine cold factor coefficient
$c_{\mathrm{e},2}$	0.016	1/K	Engine cold factor coefficient
$c_{\mathrm{g},1}$	0.42	-	Exhaust gas fraction coefficient
$c_{\mathrm{g},2}$	0.0002	s/rad	Exhaust gas fraction coefficient

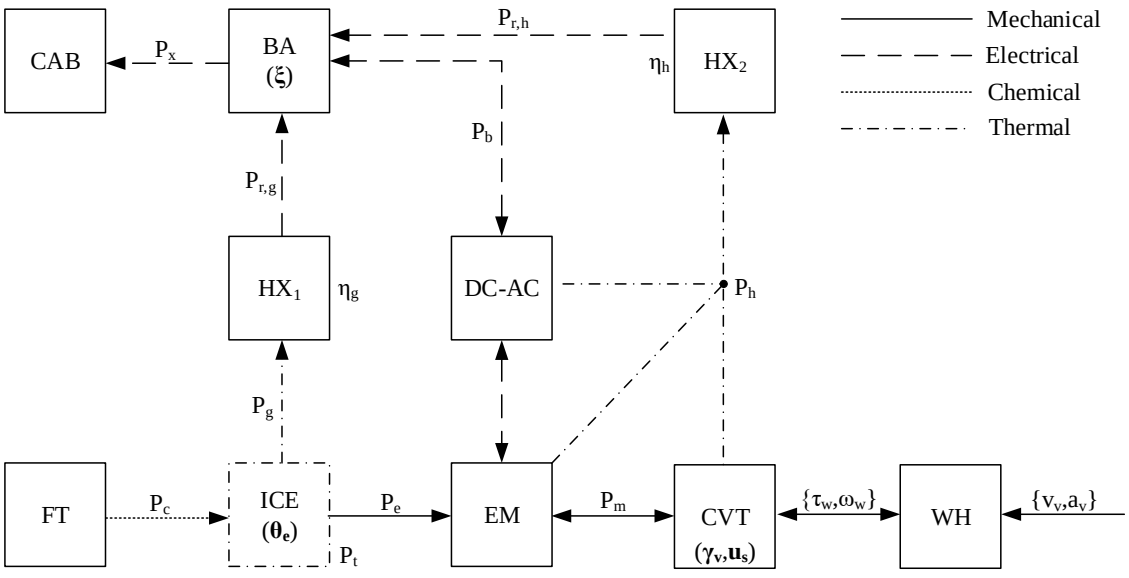

Figure 3.1: Integrated energy and thermal management system for a CVT-based plug-in hybrid electric vehicle, where BA represents the battery, CAB the cabin, DC-AC the DC (direct current) to AC (alternating current) inverter, FT the fuel tank, HX_1 the exhaust gas waste heat recovery sub-system, HX_2 the electric path waste heat recovery sub-system, and WH the wheel. Control and state variables are highlighted in bold.

The main design criterion to identify the optimal control variables is the minimization of the overall fuel consumption:

$$\text{Minimize fuel consumption}$$

$$\text{with respect to } \begin{cases} \text{energy management} \\ \text{thermal management} \end{cases}$$

$$\text{subject to } \begin{cases} \text{drive cycle} \\ \text{powertrain model} \\ \text{thermal model} \\ \text{component limits} \end{cases}$$

The overall fuel consumption is given in a discrete time format, using time index k, by

$$\min_{\boldsymbol{x}(k),\boldsymbol{u}(k)} \; J_{\mathrm{f}}(\boldsymbol{x}(k), \boldsymbol{u}(k) \mid w(k)), \tag{3.1}$$

$$\text{s.t.} \quad \boldsymbol{x}(k+1) = \boldsymbol{x}(k) + \boldsymbol{f}(\boldsymbol{x}(k), \boldsymbol{u}(k), w(k))\ \Delta t, \tag{3.1a}$$

$$\boldsymbol{h}(\boldsymbol{x}(k), \boldsymbol{u}(k)) = 0, \tag{3.1b}$$

$$\boldsymbol{g}(\boldsymbol{x}(k), \boldsymbol{u}(k)) \leq 0, \tag{3.1c}$$

where Δt is the time step. The state variables $\boldsymbol{x}(k)$ consist of the state-of-charge (SOC) of the battery, which represents the energy dynamics, and the engine temperature, which reflects the thermodynamics; that is,

$$\boldsymbol{x}(k) = [\xi(k), \theta_{\mathrm{e}}(k)]^T. \tag{3.2}$$

The control variables $\boldsymbol{u}(k)$ comprise the speed ratio of the CVT and the torque split factor describing the torque split between the EM and the engine, i.e.,

$$\boldsymbol{u}(k) = [\gamma_{\mathrm{v}}(k), \sigma_{\mathrm{s}}(k)]^T. \tag{3.3}$$

Equation (3.1b) represents the power balance of the vehicle and (3.1c) represents the feasible design space, where the state and control variables are bounded, and the component limits. The disturbance vector $w(k)$ consists of vehicle speed and acceleration, which are provided by the drive cycle, i.e.,

$$w(k) = [v_{\mathrm{v}}(k), a_{\mathrm{v}}(k)]^T. \tag{3.4}$$

Note that the control variables $\boldsymbol{u}(k)$ are selected depending on the disturbance vector $w(k)$, which influence the state variables $\boldsymbol{x}(k)$. The consumed fuel C_{f} over the drive cycle represented by $w(k)$ starting at index value $k = 1$ and ending at $k = N$ is calculated by

$$J_{\mathrm{f}}(\boldsymbol{x}(k), \boldsymbol{u}(k)) = \sum_{k=1}^{N} H_{\mathrm{l}}\ \Delta m_{\mathrm{f}}(\boldsymbol{x}(k), \boldsymbol{u}(k))\ \Delta t, \tag{3.5}$$

where H_{l} is the lower heating value of gasoline in (J/g). The term $\Delta m_{\mathrm{f}}(\boldsymbol{x}(k), \boldsymbol{u}(k))$ represents the fuel mass flow in (g/s).

This section formulates the fuel consumption minimization problem of a CVT-based PHEV with cold-start and WHR. To solve this optimal control problem, the required PHEV model based on measurements, especially the mathematical coupling between energy dynamics and thermodynamics, is described in the next section.

3.3 System modeling

This section presents the nonlinear and non-convex PHEV model needed for solving the optimization problem defined in (3.1). Given the drive cycle in Section 3.3.1, the vehicle longitudinal dynamics are described in Section 3.3.2, which is an input to the CVT model (Section 3.3.3). Based on the total torque demand calculated, the torque split strategy between the ICE and EM is formulated in Section 3.3.4. Given the torque split, the ICE efficiency and thermal models are presented in Section 3.3.5 to calculate the required fuel power, and the EGWHR sub-system is described in Section 3.3.6 to obtain the recovered power that can be stored into the battery. Similarly, based on the torque split factor, the EM efficiency model including inverter is presented in Section 3.3.7 to compute the demanded electric power. The EPWHR sub-system is then provided in Section 3.3.8 to calculate the recovered power that can be used to reduce the battery load for cabin heating. Eventually, the demanded electric power including the cabin (Section 3.3.9) is supplied by the battery, which is described in Section 3.3.10.

3.3.1 Drive cycle

As reported in [185], the average European driving distance is 10 km. The NEDC, which is commonly used to measure fuel consumption, has a duration of 1180 s and a length of 11 km. It describes the speed of a vehicle versus time. Moreover, it well-captures the transient behavior of the engine, which is the main focus of this chapter. Therefore, the NEDC is selected as the input for the control problem in this study. For purposes of comparison, the WLTC is also used (Section 3.5.1). Notice that, for other drive cycles, although the quantity (fuel consumption) might vary, the methodology presented also applies.

3.3.2 Longitudinal dynamics

Taking into account the forces acting on the vehicle and assuming no variations in wind, altitude and road surface, the required traction force to follow the drive cycle, which is represented by vehicle velocity v_{v} and acceleration a_{v}, is given by

$$F_{\mathrm{t}}(k) = F_{\mathrm{a}}(k) + F_{\mathrm{r}}(k) + F_{\mathrm{i}}(k), \tag{3.6}$$

where the aerodynamic drag force F_{a} is calculated by

$$F_{\mathrm{a}}(k) = \frac{1}{2}\ \rho_{\mathrm{a}}\ c_{\mathrm{d}}\ A_{\mathrm{f}}\ v_{\mathrm{v}}^2(k), \tag{3.7}$$

where ρ_{a} represents the density of air, c_{d} the aerodynamic drag coefficient, and A_{f} the frontal area. The rolling resistance is obtained by

$$F_{\mathrm{r}}(k) = c_{\mathrm{r}}\ m_{\mathrm{v}}\ g\ \mathrm{sign}(v_{\mathrm{v}}(k)), \tag{3.8}$$

where c_{r} represents the rolling resistance coefficient, m_{v} the vehicle mass, and g the gravitational acceleration. The inertia force is given by

$$F_{\mathrm{i}}(k) = \left(m_{\mathrm{v}} + 4\ \frac{J_{\mathrm{w}}}{r_{\mathrm{w}}^2}\right)\ a_{\mathrm{v}}(k), \tag{3.9}$$

where J_{w} represents the wheel inertia and r_{w} the wheel radius.

Therefore, the demanded wheel torque τ_{w} and speed ω_{w} can be expressed as follows:

$$\tau_{\mathrm{w}}(k) = F_{\mathrm{t}}(k)\ r_{\mathrm{w}}, \tag{3.10}$$

$$\omega_{\mathrm{w}}(k) = \frac{v_{\mathrm{v}}(k)}{r_{\mathrm{w}}}. \tag{3.11}$$

3.3.3 Continuously variable transmission

The considered vehicle has a pushbelt CVT consisting of four main parts: Variator, pump, DNR (drive, neutral, and reverse), and final drive. It provides a continuous variable speed ratio γ_{v} between the primary pulley and the secondary pulley. This allows the speed of the power source (e.g., engine) to be decoupled from the wheel speed, in order to optimize the operating point of the power source. The required minimum pump speed is 1000 rpm. Given the required torque and speed at the wheels, the torque and speed of the final drive are obtained by

$$\tau_{\mathrm{f}}(k) = \begin{cases} \frac{\tau_{\mathrm{w}}(k)}{\eta_{\mathrm{f}}\ \gamma_{\mathrm{f}}}, & \text{if } \tau_{\mathrm{w}}(k) > 0, \\ \frac{\eta_{\mathrm{f}}\ \tau_{\mathrm{w}}(k)}{\gamma_{\mathrm{f}}}, & \text{if } \tau_{\mathrm{w}}(k) \leq 0, \end{cases} \tag{3.12}$$

$$\omega_{\mathrm{f}}(k) = \omega_{\mathrm{w}}(k)\ \gamma_{\mathrm{f}}, \tag{3.13}$$

where γ_{f} is a constant ratio between the secondary pulley and the wheel (i.e., final drive) and η_{f} is the efficiency of the final drive. Taking into consideration the inertia effects ($J_{\mathrm{v,i}}$ and $J_{\mathrm{v,o}}$), the torque and speed of the primary pulley are calculated by

$$\tau_{\mathrm{p}}(k) = J_{\mathrm{v,i}}\ \Delta\omega_{\mathrm{p}}(k) + \frac{J_{\mathrm{v,o}}\ \Delta\omega_{\mathrm{f}}(k) + \tau_{\mathrm{f}}(k)}{\gamma_{\mathrm{v}}(k)}, \tag{3.14}$$

$$\omega_{\mathrm{p}}(k) = \omega_{\mathrm{w}}(k)\ \gamma_{\mathrm{f}}\ \gamma_{\mathrm{v}}(k), \tag{3.15}$$

where $\Delta\omega_{\mathrm{f}}$ and $\Delta\omega_{\mathrm{p}}$ are the rotational acceleration of the final drive and the primary pulley, respectively. The total torque demand is thus given by

$$\tau_{\mathrm{d}}(k) = \tau_{\mathrm{loss}}(\omega_{\mathrm{p}}(k), \tau_{\mathrm{p}}(k), \gamma_{\mathrm{v}}(k)) + \tau_{\mathrm{p}}(k), \tag{3.16}$$

where $\tau_{\mathrm{loss}}(\omega_{\mathrm{p}}, \tau_{\mathrm{p}}, \gamma_{\mathrm{v}})$ represents the torque loss in the CVT, consisting of the torque loss in the DNR, pump, and variator, which are computed using detailed loss-maps based on measurement data.

Bounds on the CVT speed ratio and the primary pulley torque are

$$\gamma_{\mathrm{v}}(k) \in [\underline{\gamma}_{\mathrm{v}}, \overline{\gamma}_{\mathrm{v}}], \tag{3.17}$$

$$\tau_{\mathrm{p}}(k) \in [\underline{\tau}_{\mathrm{p}}, \overline{\tau}_{\mathrm{p}}]. \tag{3.18}$$

Constraints on the primary pulley speed will be implicitly constrained by the engine speed.

3.3.4 Torque split

The total torque demand (3.16) is met by the EM and the engine. The torque split between them is determined by the torque split factor σ_{s}. Given the total torque request, the torque provided by the engine and EM are expressed as

$$\tau_{\mathrm{e,t}}(k) = (1 - \sigma_{\mathrm{s}}(k))\ \tau_{\mathrm{d}}(k), \quad \text{if } \tau_{\mathrm{d}}(k) > 0, \tag{3.19}$$

$$\tau_{\mathrm{m,t}}(k) = \sigma_{\mathrm{s}}(k)\ \tau_{\mathrm{d}}(k), \quad \text{if } \tau_{\mathrm{d}}(k) > 0 \vee \tau_{\mathrm{d}}(k) \leq 0 \wedge \omega_{\mathrm{p}}(k) \geq \frac{1000\ \pi}{30}. \tag{3.20}$$

Taking into account the constraints on the EM, battery, and charge sustenance, the additional torque supplied by mechanical braking is written as

$$\tau_{\mathrm{b}}(k) = \tau_{\mathrm{d}}(k) - \tau_{\mathrm{m,t}}(k), \quad \text{if } \tau_{\mathrm{d}}(k) < 0. \tag{3.21}$$

The torque split factor is limited by

$$\sigma_{\mathrm{s}}(k) \in [\underline{\sigma}_{\mathrm{s}}, \overline{\sigma}_{\mathrm{s}}], \tag{3.22}$$

where $\overline{\sigma}_{\mathrm{s}} = 1$ and $\underline{\sigma}_{\mathrm{s}} < 0$, depending on the engine size. The relationship between the driving modes and the torque split factor can be summarized as follows: When $\sigma_{\mathrm{s}} = 1$, it indicates that the engine is shut off and either the EV or brake energy recuperation (BER) mode is activated (depending on the torque demand). The car is in the motor assist (MA) mode if $0 < \sigma_{\mathrm{s}} < 1$, and $\sigma_{\mathrm{s}} = 0$ represents that the engine (ICE) mode is active. The vehicle is in the charging (CH) mode if $\sigma_{\mathrm{s}} < 0$, with $\sigma_{\mathrm{s}} = \underline{\sigma}_{\mathrm{s}}$ representing full recharge. Detailed descriptions of the driving modes can be found in Section 1.3.

3.3.5 Internal combustion engine

In the considered PHEV, the crankshaft of the engine is coupled to the primary pulley (CVT) shaft directly, which implies that the engine speed is equal to the primary pulley speed. Moreover, engine speeds below 1000 rpm are prevented to avoid high engine losses. In consideration of the engine inertia, the torque and speed of the engine are given by

$$\tau_{\mathrm{e}}(k) = J_{\mathrm{e}}\ \Delta\omega_{\mathrm{p}}(k) + \tau_{\mathrm{e,t}}(k), \tag{3.23}$$

$$\omega_{\mathrm{e}}(k) = \omega_{\mathrm{p}}(k), \quad \text{if } \tau_{\mathrm{e}}(k) > 0. \tag{3.24}$$

With warm-start conditions, a lookup table is utilized to obtain the fuel consumption represented by the injected fuel mass flow $\Delta m_{\mathrm{f}}(k)$, i.e.,

$$\Delta m_{\mathrm{f}}(k) = \Delta m_{\mathrm{f}}(\omega_{\mathrm{e}}(k), \tau_{\mathrm{e}}(k)). \tag{3.25}$$

The engine torque and speed are subject to the lower and upper limits

$$\tau_{\mathrm{e}}(k) \in [\underline{\tau}_{\mathrm{e}}(\omega_{\mathrm{e}}(k)), \overline{\tau}_{\mathrm{e}}(\omega_{\mathrm{e}}(k))], \tag{3.26}$$

$$\omega_{\mathrm{e}}(k) \in [\underline{\omega}_{\mathrm{e}}, \overline{\omega}_{\mathrm{e}}]. \tag{3.27}$$

Subsequently, the consumed fuel power is calculated by

$$P_{\mathrm{f}}(k) = \Delta m_{\mathrm{f}}(k)\ H_{\mathrm{l}}. \tag{3.28}$$

With cold-start conditions, however, because of higher frictional losses, the fuel consumption is higher than that of a warm-start. In order to mimic the real situation, an engine cold factor is introduced to adjust the nominal fuel power P_{f}, which is a function of the engine temperature that is always greater than or equal to one, as illustrated in Figure 3.2. The engine cold factor is defined as

$$c(\theta_{\mathrm{e}}(k)) = \begin{cases} 1 + c_{\mathrm{e,1}}\ (\overline{\theta}_{\mathrm{e}} - \theta_{\mathrm{e}}(k))\ e^{c_{\mathrm{e,2}}\ (\overline{\theta}_{\mathrm{e}} - \theta_{\mathrm{e}}(k))}, & \text{if } \theta_{\mathrm{e}}(k) < \overline{\theta}_{\mathrm{e}}, \\ 1, & \text{if } \theta_{\mathrm{e}}(k) = \overline{\theta}_{\mathrm{e}}, \end{cases} \tag{3.29}$$

where $c_{\mathrm{e,1}}$ and $c_{\mathrm{e,2}}$ are the cold factor coefficients to correct the nominal fuel consumption, which are fitted parameters that are experimentally identified; and $\overline{\theta}_{\mathrm{e}}$ is the operating temperature [7]. Figure 3.2 is representative for ICEs. Therefore, the temperature-dependent fuel power is calculated by

$$P_{\mathrm{c}}(k) = c(\theta_{\mathrm{e}}(k))\ P_{\mathrm{f}}(k). \tag{3.30}$$

A significant portion (e.g., 36%) of the fuel power is converted into mechanical power P_{e} to propel the vehicle, whereas another large part (e.g., 33%) is wasted as the exhaust gases P_{g}, followed by a relatively small power dissipation; that is, thermal

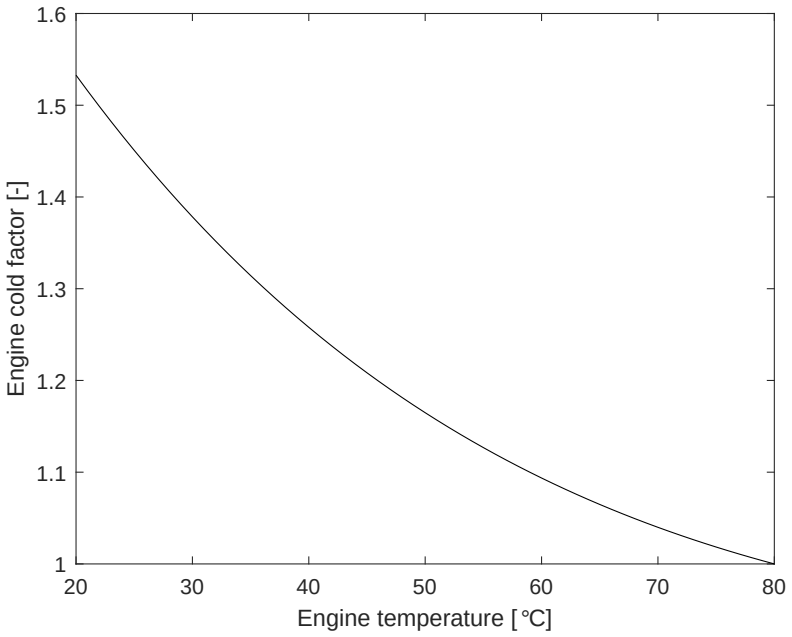

Figure 3.2: Engine cold factor as a function of its temperature [7].

convection to the ambient air P_{a}. The remainder of the power is converted into heat, given by

$$P_{\mathrm{t}}(k) = P_{\mathrm{c}}(k) - P_{\mathrm{e}}(k) - P_{\mathrm{g}}(k) - P_{\mathrm{a}}(k). \tag{3.31}$$

The mechanical power produced is obtained by

$$P_{\mathrm{e}}(k) = \omega_{\mathrm{e}}(k)\ \tau_{\mathrm{e}}(k). \tag{3.32}$$

The exhaust gas heat is approximated as a function of the injected chemical power and the engine speed; that is,

$$P_{\mathrm{g}}(k) = (c_{\mathrm{g},1} - c_{\mathrm{g},2}\ \omega_{\mathrm{e}}(k))\ P_{\mathrm{c}}(k), \tag{3.33}$$

where $c_{\mathrm{g},1}$ and $c_{\mathrm{g},2}$ are the exhaust gas fraction coefficients to estimate the engine speed-dependent exhaust gas power, as described in [186]; and P_{g} decreases with ω_e linearly. The convection to the ambient air is given by

$$P_{\mathrm{a}}(k) = h_{\mathrm{e}}\ A_{\mathrm{e}}\ (\theta_{\mathrm{e}}(k) - \theta_{\mathrm{a}}), \tag{3.34}$$

where h_{e} is the heat transfer coefficient to the ambient air, A_{e} the heat exchange area, and θ_{a} the ambient temperature. Therefore, the engine temperature can be calculated by

$$\theta_{\mathrm{e}}(k+1) = \begin{cases} \theta_{\mathrm{e}}(k) + \frac{P_{\mathrm{t}}(k)}{C_{\mathrm{p}}}\ \Delta t, & \text{if } \theta_{\mathrm{e}}(k) < \overline{\theta}_{\mathrm{e}}, \\ \theta_{\mathrm{e}}(k), & \text{if } \theta_{\mathrm{e}}(k) = \overline{\theta}_{\mathrm{e}}, \end{cases} \tag{3.35}$$

where C_{p} is the engine heat capacity, given by

$$C_{\mathrm{p}} = c_{\mathrm{h}}\ c_{\mathrm{e}}\ m_{\mathrm{e}}, \tag{3.36}$$

where c_{h} is a heating coefficient, which compensates for the slower heating of the metal parts than that of lubrication oil; c_{e} is the engine specific heat; and m_{e} is its mass.

3.3.6 Exhaust gas waste heat recovery

As discussed in Section 3.1, by using a EGWHR system, the fuel consumption of a PHEV could be reduced. As shown in Figure 2.12, the EGWHR sub-system is utilized to recuperate a certain amount (up to 10%) of the exhaust gas power P_{g} with recovery efficiency η_{g}, and the recuperated power $P_{\mathrm{r,g}}$ is eventually stored in the battery. As the objective of this study is to gain qualitative insights of fuel savings, a detailed EGWHR model is not developed. Instead, a black-box approach is adopted [187], where a lumped efficiency [188] taking into account the efficiencies of all the components of the EGWHR sub-system [189] is used. Here, the maximum efficiency is 10% [159]. The EGWHR model is described as

$$P_{\mathrm{r,g}}(k) = \eta_{\mathrm{g}}\ P_{\mathrm{g}}(k), \tag{3.37}$$

where $\eta_{\mathrm{r,g}} \in [\underline{\eta}_{\mathrm{r,g}}, \overline{\eta}_{\mathrm{r,g}}]$.

3.3.7 Electric machine

The EM employed is a permanent magnet synchronous machine (PMSM), which is an integrated motor-generator. These machines tend to have a large stator diameter to axial length ratio to optimize the overall packaging. It is linked to the input shaft of the CVT directly. Taking the EM inertia into account, the torque and speed of the EM are obtained by

$$\tau_{\mathrm{m}}(k) = J_{\mathrm{m}}\ \Delta\omega_{\mathrm{m}}(k) + \tau_{\mathrm{m,t}}(k), \tag{3.38}$$

$$\omega_{\mathrm{m}}(k) = \max\left(\omega_{\mathrm{p}}(k), \frac{1000\ \pi}{30}\right), \quad \text{if } \omega_{\mathrm{p}}(k) > 0. \tag{3.39}$$

The mechanical power generated by the EM is, then, calculated by

$$P_{\mathrm{m}}(k) = \omega_m(k)\ \tau_m(k). \tag{3.40}$$

A lookup table is used to describe the power loss of the EM, including inverter:

$$P_{\mathrm{m,loss}}(k) = P_{\mathrm{m,loss}}(\omega_{\mathrm{m}}(k), \tau_{\mathrm{m}}(k)). \tag{3.41}$$

Consequently, the electrical power supplied to/by the EM is given by

$$P_{\mathrm{m,el}}(k) = P_{\mathrm{m}}(k) + P_{\mathrm{m,loss}}(k). \tag{3.42}$$

The constraints on the EM are

$$\tau_{\mathrm{m}}(k) \in [\underline{\tau}_{\mathrm{m}}(\omega_{\mathrm{m}}(k)), \overline{\tau}_{\mathrm{m}}(\omega_{\mathrm{m}}(k))], \tag{3.43}$$

$$\omega_{\mathrm{m}}(k) \in [\underline{\omega}_{\mathrm{m}}, \overline{\omega}_{\mathrm{m}}]. \tag{3.44}$$

3.3.8 Electric path waste heat recovery

The total heat production from the CVT and the EM—namely, the electric path—can be computed by

$$P_{\mathrm{h}}(k) = P_{\mathrm{m,loss}}(k) + P_{\mathrm{c,loss}}(k), \tag{3.45}$$

where $P_{\mathrm{c,loss}}(k)$ is derived as follows:

$$P_{\mathrm{c,loss}}(k) = P_{\mathrm{loss}}(\omega_{\mathrm{p}}(k), \tau_{\mathrm{p}}(k), \gamma_{\mathrm{v}}(k)) + P_{\mathrm{f,loss}}(k), \tag{3.46}$$

where $P_{\mathrm{loss}}(\omega_{\mathrm{p}}, \tau_{\mathrm{p}}, \gamma_{\mathrm{v}})$ consists of the power loss in the DNR, pump, and variator, similar to (3.16). $P_{\mathrm{f,loss}}$ is the power loss of the final drive. Similar to EGWHR (Figure 2.12), Figure 2.13 shows how the EPWHR sub-system is employed to recover a certain percentage of the waste heat P_{h} with recuperation efficiency η_{h}, and the waste heat harvested $P_{\mathrm{r,h}}$ ultimately reduces the load on the battery. For the sake of simplicity and to obtain qualitative insights, this work assumes a lumped efficiency [188] considering heat exchange between the electric path cooling circuit, HP, and the cabin heater system, where the maximum efficiency is 20% [41, 164, 190]. The reason for this is that, first of all, liquid-to-liquid heat exchange is relatively efficient (e.g., when using a liquid to liquid counter-flow plate fin heat exchanger) [169]. Furthermore, with proper arrangement of the heat exchangers in the systems as mentioned above, the heat exchange can be efficient [190]. The EPWHR model is given by

$$P_{\mathrm{r,h}}(k) = \eta_{\mathrm{h}}\ P_{\mathrm{h}}(k), \tag{3.47}$$

where $\eta_{\mathrm{h}} \in [\underline{\eta}_{\mathrm{h}}, \overline{\eta}_{\mathrm{h}}]$.

3.3.9 Cabin

For the purpose of this study, identifying the cost of cold-start conditions on the fuel usage and the benefits of adopting a DSWHR system, a detailed cabin model is not considered. Instead, the auxiliary power demand, represented by the cabin heating request, is assumed to take a constant value [40]; that is,

$$P_{\mathrm{x}} = 1 \quad [\mathrm{kW}]. \tag{3.48}$$

The cabin heating power is provided by the high-voltage battery.

3.3.10 Battery

The high-voltage battery is modeled by using an equivalent circuit approach; that is, a voltage source in series with an internal resistance, as demonstrated in Figure 3.3. The electric power supplied by the battery is obtained by

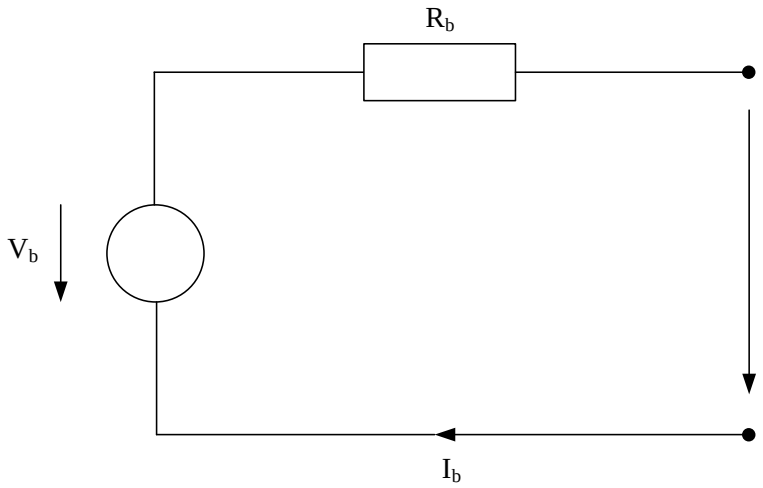

Figure 3.3: Equivalent circuit of the battery.

$$P_{\mathrm{b}}(k) = P_{\mathrm{m,el}}(k) + P_{\mathrm{x}}. \tag{3.49}$$

The battery current is, then, calculated by

$$I_{\mathrm{b}}(k) = \frac{V_{\mathrm{b}}(k) - \sqrt{V_{\mathrm{b}}^2(k) - 4\ P_{\mathrm{b}}(k)\ R_{\mathrm{b}}(k)}}{2R_{\mathrm{b}}(k)}, \tag{3.50}$$

where V_{b} is the open circuit voltage of the battery and R_{b} is its internal resistance. Both V_{b} and R_{b} are described by lookup tables, which are functions of the SOC. Consequently, the battery SOC is given by

$$\xi(k+1) = -\frac{\eta_{\mathrm{b}}(I_{\mathrm{b}}(k))\ I_{\mathrm{b}}(k)}{3600\ Q_{\mathrm{b}}}\ \Delta t + \xi(k), \tag{3.51}$$

where η_{b} is the battery charging efficiency and Q_{b} is the battery capacity. The battery current is bounded by

$$I_{\mathrm{b}}(k) \in [\underline{I}_{\mathrm{b}}, \overline{I}_{\mathrm{b}}]. \tag{3.52}$$

This section presents a PHEV model for the fuel optimization problem considering cold-start and WHR. The CVT speed ratio that aims to optimize the operating point of the power source and the torque split factor between the ICE and EM are the decision variables. The modular component models are represented by experimentally-based lookup tables (efficiency maps). In particular, the coupling between the energy dynamics and thermodynamics is described in detail. A cold-start indicates a low engine temperature, which increases the frictional losses in the engine, resulting in excess fuel consumption because of high-viscosity effects. To compute the fuel consumption with a cold-start, an engine cold factor is introduced to adjust the nominal fuel consumption with a warm-start, which decreases with increasing engine temperature. A significant part of the fuel power is wasted as exhaust gases. A EGWHR model is developed to recover a certain amount of the exhaust gas power, and the recovered power is stored in the battery, which increases the energy content of

the battery. The waste heat from the EM (including inverter) and CVT is significant as well. A EPWHR model is created to recuperate a certain percentage of the waste heat from the EM and CVT, and the recuperated waste heat eventually reduces the load on the battery for cabin heating. The developed PHEV model is highly nonlinear and non-convex. By applying DP as an offline optimization algorithm, not only will it find an optimal solution but also it will provide insights into design of an online optimization strategy taking into account energy and thermal aspects, which will be discussed in the next section.

3.4 Numerical optimization

In this study, the engine is not only a power source to propel the wheels, but also a thermal accumulator. It accumulates thermal energy to bring its temperature to the required operating temperature as fast as possible, so as to reduce the cold penalty, as reflected by (3.30). Moreover, the battery is regarded as an energy storage system (energy buffer), which stores energy from other sources and exchanges energy with the driven load. In addition to the five driving modes described in Section 3.2, this section introduces two additional thermal-related modes: ICE-Heating (ICEH) and waste heat recovery (WHR). These modes can be described as follows. In ICEH, the engine temperature is lower than its efficient operating temperature, which implies a cold-start. The engine thermal energy level is lower than the desired level, and thermal energy is accumulated by the thermal accumulator. In WHR, the recuperated energy from the exhaust gases is stored in the battery, which increases the energy content of the battery and can be retrieved for propulsion when needed. The recovered power from the electric path results in a decrease in battery load to heat the cabin.

Due to the cold-start, the engine has to generate heat to warm up itself during the ICEH mode to reduce the cold effect, leading to an additional fuel cost. The additional fuel cost represents the fuel-saving potential, which shows the difference between a cold-start and a warm-start; essentially, the cost of the ICEH mode. In Section 3.2, with charge sustenance, the energy used in the MA and EV modes eventually came from the CH and BER modes. Now, the energy harvested from the WHR mode reduces the battery load directly, and can also be utilized for the MA and EV modes, resulting in extra fuel savings. The extra fuel savings indicate the ultimate fuel savings in reality, which demonstrates the discrepancy between a cold-start and a cold-start with DSWHR; essentially, the benefit of the WHR mode. It is clear that there is a trade-off between the ICE heating, and hence the cost on the fuel usage, and the utilization of the DSWHR system, and thus the gain on the fuel economy. To be more specific, in the presence of cold-start conditions, the IETMS attempts to generate not only an optimal SOC profile but also an ideal warm-up trajectory of the engine. This is achieved by controlling the driving modes and the ICEH mode. The fuel-saving potential can then be identified. Featuring the DSWHR, the IETMS aims to minimize the overall fuel consumption by optimally determining the driving modes and the

thermal-related modes; namely, the ICEH and WHR modes. The ultimate fuel savings can thus be quantified. Given a drive cycle (vehicle velocity and acceleration) starting at time $k = 0$ and ending at $k = N$, the optimal control objective is to minimize the following function

$$\min \; J_{\mathrm{f}} = \sum_{k=0}^{k=N} \left[1 + c_{\mathrm{e},1} \; (\overline{\theta}_{\mathrm{e}} - \theta_{\mathrm{e}}(k)) \; e^{c_{\mathrm{e},2} \; (\overline{\theta}_{\mathrm{e}} - \theta_{\mathrm{e}}(k))} \right] \Delta m_{\mathrm{f}}(k). \tag{3.53}$$

Apart from the constraints described in Section 3.3, additional constraints on the system dynamic states are

$$\xi(0) = \xi(N), \tag{3.54}$$

$$\xi(k) \in [\underline{\xi}, \overline{\xi}], \tag{3.55}$$

$$\theta_{\mathrm{e}}(k) \in [\underline{\theta}_{\mathrm{e}}, \overline{\theta}_{\mathrm{e}}]. \tag{3.56}$$

Equation (3.54) ensures charge-sustaining. Overall, the optimization problem has two dynamics state, namely the SOC of the battery (ξ) and the engine temperature (θ_{e}), and two control inputs, namely the CVT speed ratio (γ_{v}) and the torque split factor σ_{s}. The initial value of the SOC ($\xi(0)$) is chosen as the average of the lower ($\underline{\xi}$) and upper ($\overline{\xi}$) limits of the SOC, which is equal to the final value of the SOC (3.54). Other values are determined based on (3.56), (3.17) and (3.22). These state and control variables are discretized, which entails a trade-off between accuracy and computation time [10, 58]. Infeasible states are penalized by using a high cost, which is selected based on the maximum value that can occur in the cost-to-go. The control inputs represented by the CVT speed ratio γ_{v} ((3.15) and (3.16)) and the torque split factor σ_{s} (3.19) influence the engine speed, torque and eventually the fuel mass flow (3.25). DP [58, 191] (based on Bellman's principle of optimality) is applied to obtain optimal control inputs, by minimizing the objective function 3.53. An introduction to DP is given in Appendix A. In this case, with backward iterations, DP finds the optimal control inputs (γ_{v},σ_{s}) that minimizes 3.53 by evaluating $(\xi, \theta_{\mathrm{e}})$ at each time instant. The global optimal solution is found in approximately one hour. Although DP is an offline optimization method, it provides insights into the design of online implementable strategies. The optimal control inputs, decided by the optimization algorithm, determine the driving mode (as defined in Section 3.3.4) and the thermal-related mode (as introduced above).

Recall that the aim of this study is to quantify the fuel-saving potential caused by cold-start conditions and the ultimate fuel savings contributed by the DSWHR system as introduced in Section 3.1. Therefore, the numerical optimization problem given by (3.53) is solved for three simulation settings, which are described as follows:

S_0 : The engine is already at its efficient operating temperature at the outset, which indicates that there is no cold impact. This is the ideal scenario, which is usually implemented in powertrain efficiency simulations based on drive cycles, such as NEDC and WLTC. The system has only one continuous dynamic state, the SOC of the battery, and the energy controller aims at finding an optimal SOC trajectory;

S_1 : The engine is subject to a cold-start, which is a common case in real driving conditions. The optimization problem contains two continuous dynamic states, i.e., the SOC of the battery and the engine temperature. The optimization strategy attempts to generate an optimal SOC profile and an ideal warm-up trajectory of the engine simultaneously, by taking into account the ICEH mode;

S_2 : On the basis of S_1, the DSWHR system with $\overline{\eta}_{\mathrm{r,g}}$ (Section 3.3.6) and $\overline{\eta}_{\mathrm{h}}$ (Section 3.3.8) is included. The IETMS aims to maximize the overall fuel efficiency by striking a balance between the driving modes, ICEH mode and the WHR mode.

It should be noted that S_1 does not include the DSWHR system, which is the main difference from S_2. The fuel-saving potential can be obtained by comparing the results between S_0 and S_1. With the aid of the WHR technologies, S_2 attempts to bridge the gap between S_0 and S_1. By comparing the outputs from S_1 and S_2, the ultimate fuel savings can be quantified, which shows the upper bound of what can be achieved in practice.

3.5 Optimization results and discussion

The results for the proposed integrated energy and thermal management in the PHEV introduced in Section 3.2 for the NEDC are shown in Figure 3.4. The NEDC consists of an urban portion ([0, 780] s), where the driving load is low, and a highway part ([780, 1180] s), which features a high power demand. All the strategies (S_0, S_1, and S_2) use the BER mode as much as possible to charge the battery, because braking energy is considered to be free energy. Generally, inefficient engine operation in low driving conditions restricts the driving mode in the urban region to the EV mode, especially the first 160 s. The battery propels the wheels, leading to a decrease in the SOC. This also reveals the fact that the battery (40 Ah) of the PHEV alone is able to satisfy the driving demand. Less frequent engine operation results in a slow rise of the engine temperature, which increases the cold impact on the fuel consumption. The highway section, in contrast, is mainly dominated by the CH mode, where engine driving is preferred. The engine drives the vehicle and charges the battery, which increases the SOC to meet the final constraint, due to charge-sustaining. This results in a rapid rise of engine temperature, which decreases the cold effect on the fuel usage. Overall, however, intermittent and efficient engine operation prevents the engine from heating up fast. It is clear that the engine operating temperature is reached almost at the end of the drive cycle, around 994 s, which confirms the significance of considering the cold impact. It is, therefore, imperative to alleviate this situation. Surprisingly, the heating time of the engine in S_2 is longer than that in both S_0 and S_1. This is because the recuperated power from the EPWHR sub-system reduces the load on the battery, thus reducing the power needed for charging, as made evident by Figure 3.5.

Note that, because of the resolution in Figure 3.5, the SOC (ξ) trajectory appears to be a straight line. Moreover, the power recovered from the EGWHR sub-system is stored

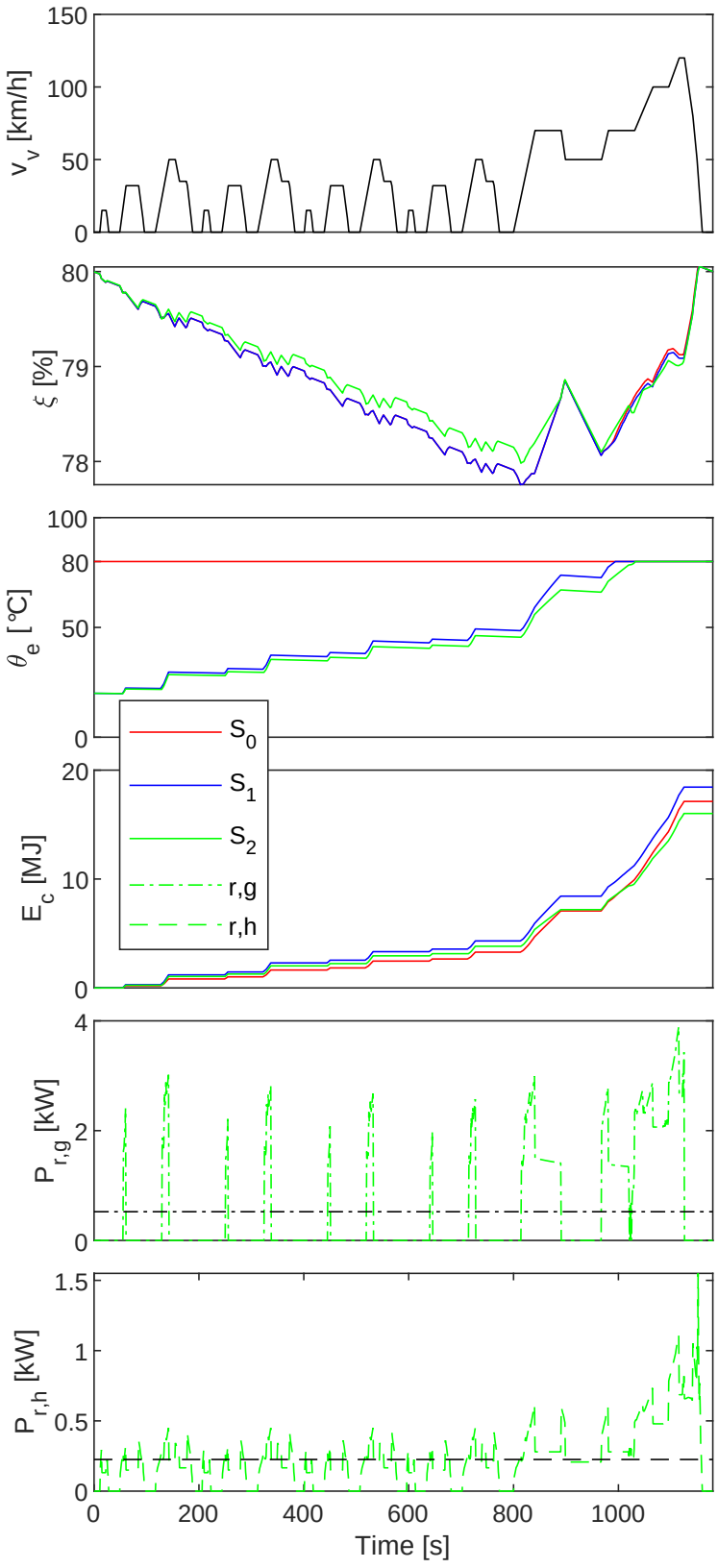

Figure 3.4: Integrated energy and thermal management for the NEDC using three simulation settings. (**Top** to **bottom**) Vehicle velocity (v_v), SOC of the battery (ξ), engine temperature (θ_e), chemical energy (E_c), recovered power from the exhaust gases ($P_\mathrm{r,g}$), and recovered power from the electric path ($P_\mathrm{r,h}$).

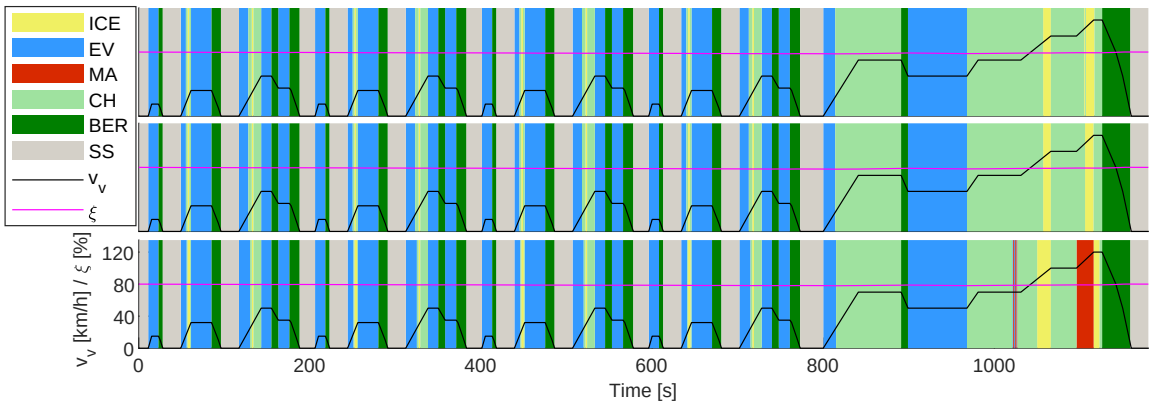

Figure 3.5: Hybrid mode visualization for three simulation settings on the NEDC, where SS represents standstill. (**Top** to **bottom**) S_0, S_1, and S_2.

into the battery temporarily and utilized efficiently at high driving load, resulting in significant fuel consumption reduction. However, the impact of the cold-start on the integrated energy and thermal controller is small. The reason for this is that the optimal strategy aims at minimizing the energy loss of the engine, which is found to be similar in all of the cases (S_0, S_1, and S_2). This is in accordance with the observation as above, where the engine accounts for most of the losses of a PHEV and maintaining a high engine efficiency plays an important role. It also explains the similarities between S_0 and S_1 in Figure 3.5, in terms of hybrid mode visualization. As a result, a cold-start has a substantial influence on the fuel usage (up to around 7.1% on the NEDC, S_1 versus S_0) and the DSWHR system has a significant improvement on the fuel efficiency (up to around 13.1% on the NEDC, S_2 versus S_1). On average, the recovered power from the exhaust gases is 523 W and from the electric path is 225 W in S_2. Clearly, the gain of the WHR mode outperforms the pay of the ICEH mode, to a large extent. It should be noted that the heating time of the engine and the energy that can be recovered from the DSWHR system are dependent on driving conditions.

3.5.1 Influence of driving conditions

In order to investigate the effect of the driving scenario, the real-world WLTC is used for comparison purposes. In the WLTC, the engine temperature increases faster—in particular, in the beginning phase—which reduces the cold impact substantially, as shown in Figure 3.6. The heating time of the engine is 860 s. This is best explained by the fact that the WLTC is more aggressive than the NEDC. As this work primarily concentrates on the transient behavior of the engine, the first 780 s (the urban portion of the NEDC) is chosen for both driving cycles, for fair comparison. It can be seen that, first of all, the average speed of the WLTC is (slightly) higher than that of the NEDC. Moreover, the engine-on time is significantly longer in the WLTC. Additionally, the percentage of high driving power demand in the WLTC is significantly higher than that in the NEDC. The percentage of high driving power demand is defined as the

time instants in which the driving power demand $P_{\mathrm{d}} = \tau_{\mathrm{w}}\ \omega_{\mathrm{w}}$, referring to (3.10) and (3.11), is greater than 10 kW, with respect to the duration of the drive cycle.

Comparing WLTC results to NEDC results, it can be inferred that, as the cold effect is reduced, the fuel-saving potential on the WLTC is much less than that on the NEDC. Furthermore, the WLTC contains more opportunities for recovering waste heat, which results in larger fuel savings. However, the assumptions made in Section 3.2, where the heating period is taken into account and the effect of the radiator is neglected, do not hold for the WLTC. In the WLTC, the operating temperature is reached at 860 s with respect to the total duration of 1800 s and the radiator would have a significant influence on the energy consumption. For the purpose of this study—considering cold-start conditions and engine thermodynamics under transient operating conditions—the NEDC is used for further analysis.

For the NEDC, it can also be observed that the average speed of the urban part is much lower than that of the highway section. For the DSWHR system, the average recuperated power is 338 W for urban conditions, while it is 1550 W for the highway situations. As the optimal controller aims to maintain a high engine mechanical efficiency, it is expected that, as the average speed increases, the waste heat power that can be recovered increases. Notice that the fuel-saving potential obtained from the NEDC is representative for similar driving scenarios; for example, the Japanese Cycle '08 (JC08) and the urban part of the Common Artemis Driving Cycle (CADC). These drive cycles have similar durations and average speeds for the urban sections, where the engine transient behavior is well-captured. The ultimate fuel savings from the NEDC is applicable to drive cycles that have similar speed trends. More importantly, the methodology introduced in this study works the same for other drive cycles.

3.5.2 Analysis of engine temperature

In Section 3.5, a fuel-saving potential of 7.1% was found for the PHEV on the NEDC by comparing S_1 and S_0. It should be noted that this fuel-saving potential on the NEDC is identified when the initial engine temperature is 20 °C, as shown in Figure 3.7. In practice, the fuel-saving potential varies; for example, depending on how long the car has been parked. The fuel economy improvement rate can be expressed as

$$\Delta FS_{\theta_{\mathrm{e}}(\mathrm{k_0})} = \frac{FC\Big|_{\theta_{\mathrm{e}}(k_0)=20°C} - FC_{\theta_{\mathrm{e}}(\mathrm{k_0})}}{FC\Big|_{\theta_{\mathrm{e}}(k_0)=20°C}}, \tag{3.57}$$

where $\theta_{\mathrm{e}}(k_0) \in [20°C, 80°C]$ represents the initial engine temperature. As illustrated in Figure 3.7, the relationship between the initial engine temperature and the fuel efficiency improvement rate can be approximated by a quadratic function as follows,

$$\Delta FS_{\theta_{\mathrm{e}}(\mathrm{k_0})} = c_1\ \theta_{\mathrm{e}}^2(k_0) + c_2\ \theta_{\mathrm{e}}(k_0) + c_3, \tag{3.58}$$

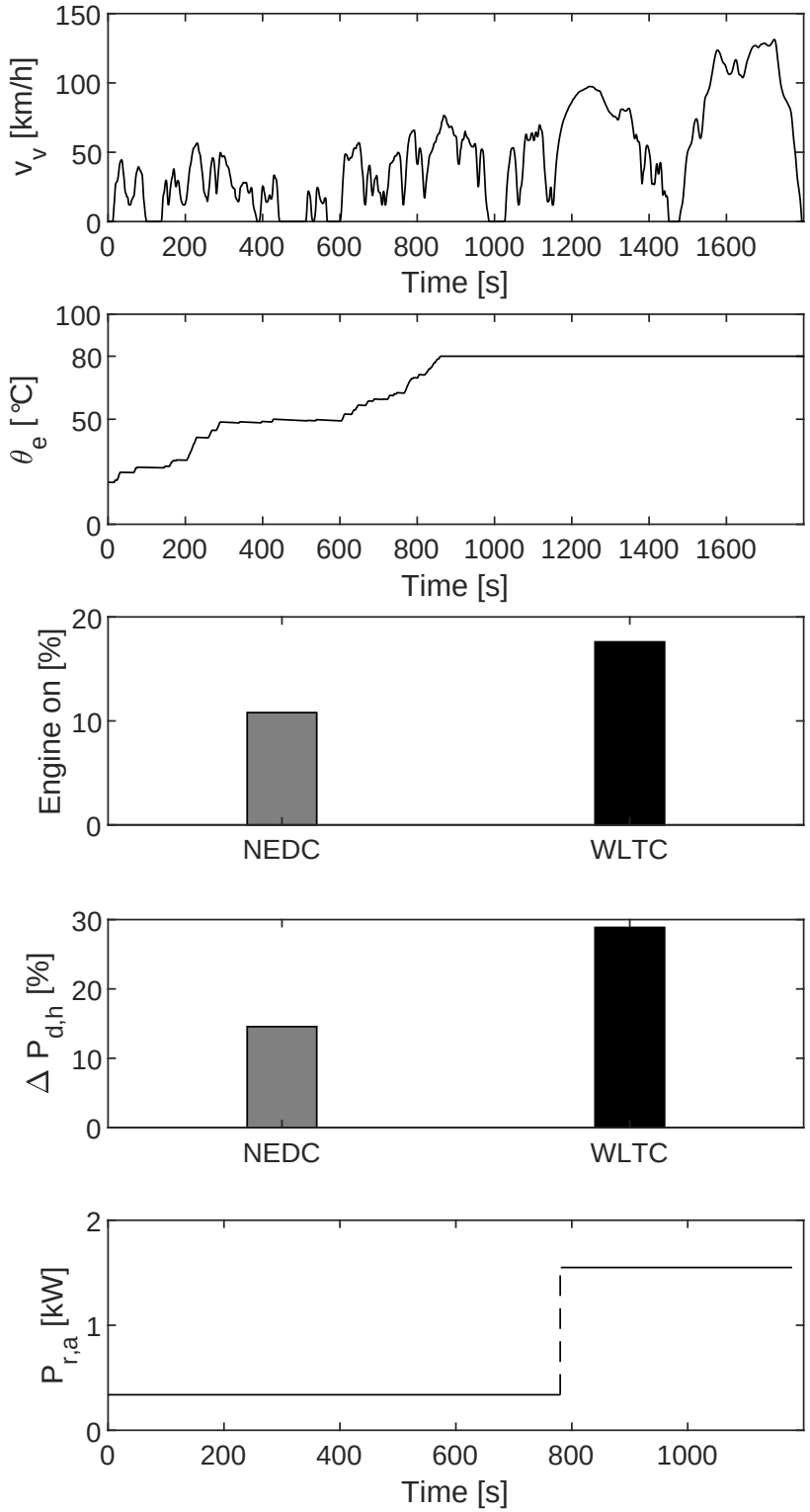

Figure 3.6: Influence of driving conditions on the fuel-saving potential and the waste heat recovery. (**Top** to **bottom**) Vehicle velocity of the WLTC (v_{v}), engine temperature on the WLTC (θ_{e}), comparison of the engine-on time between the NEDC and the WLTC for the first 780 s (Engine on), comparison of the high driving power demand between the NEDC and the WLTC for the first 780 s ($\Delta P_{\mathrm{d,h}}$), and the average recovered power during the urban and highway parts on the NEDC ($P_{\mathrm{r,a}}$).

with $c_1 = -0.0015$, $c_2 = 0.2739$, and $c_3 = -4.9$. It can be seen that the fuel economy increases while increasing the initial engine temperature, due to the cold factor (3.29). Given an initial engine temperature, the corresponding fuel-saving potential can be computed. The required thermal budget, that the system should provide to bring the engine from an initial thermal state to the desired thermal energy level, is estimated by

$$E_{\mathrm{t}} = C_{\mathrm{p}} \, (\overline{\theta}_{\mathrm{e}} - \theta_{\mathrm{e}}(k_0)), \tag{3.59}$$

where E_{t} is a constant value, independent of drive cycles. It is only related to a specific engine and its initial engine temperature. As long as the system can allocate the demanded thermal energy to heat the engine, the impact of a cold-start on the fuel consumption can be reduced. Using waste heat from the electric path to warm up the engine during electric driving is a case in point.

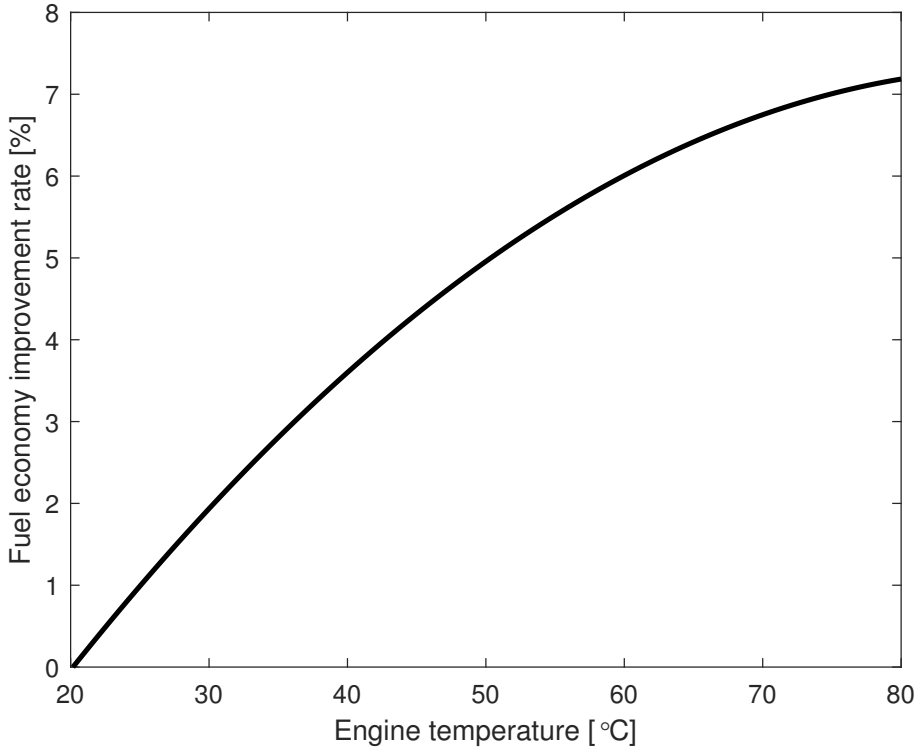

Figure 3.7: Effect of engine temperature on the fuel economy for the NEDC.

3.5.3 Effect of DSWHR efficiencies

In Section 3.5, a fuel efficiency improvement of 13.1% was identified for the PHEV on the NEDC by comparing S_2 and S_1. Notice that this fuel efficiency improvement represents the maximum recovering efficiencies, which may not be economically feasible in practice. The relative fuel savings, represented by the surface Z_2, with different efficiencies of the DSWHR system (i.e., $\eta_{\mathrm{g}} \times \eta_{\mathrm{h}}$), is shown in Figure 3.8. The relative

fuel saving is calculated by

$$\Delta FS = \frac{FC_{S_0} - FC_{S_2}}{FC_{S_1}}, \tag{3.60}$$

where FC_{S_0}, FC_{S_1}, and FC_{S_2} are the fuel consumptions of S_0, S_1, and S_2, respectively. The part of Z_2 above Z_0 implies that the recuperated energy is able to cover the heating energy required; namely, $WHR > ICEH$. The part of Z_2 below Z_0 indicates that the recovered benefit is not sufficient enough to pay for the heating cost; namely, $WHR < ICEH$. The surface $Z_0 = 0$ is determined by $\Delta FS = 0$. The intersection L_o represents the combinations of harvesting efficiencies that satisfy $\Delta FS = 0$—namely, $WHR = ICEH$—which means that the heating cost is compensated for by the energy harvested. It can be inferred, from $WHR = ICEH$, that, in reality, with a small EGWHR sub-system and a small EPWHR sub-system, the fuel efficiency can be improved remarkably. It achieves the same fuel economy as the ideal warm-start condition, which serves as the first step towards the design of WHR technologies. Furthermore, it provides insights into the sizing of electrified powertrain components. For example, the recovered power from the DSWHR system can downsize the battery pack.

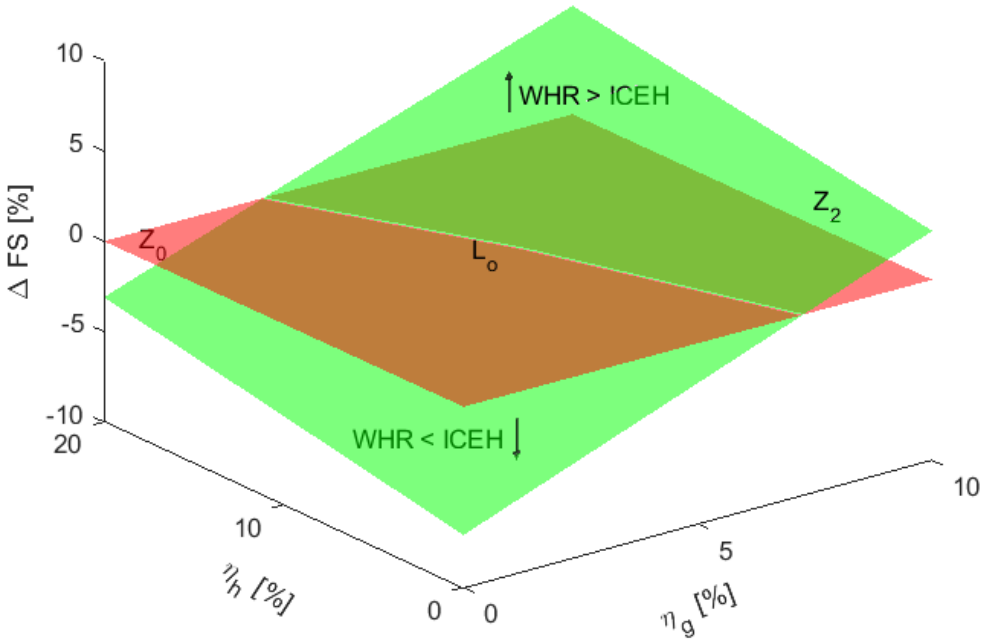

Figure 3.8: Relative fuel savings of the PHEV with different efficiencies of the DSWHR system on the NEDC.

3.6 Conclusions

An IETMS is presented to quantify the fuel-saving potential caused by cold-starting a CVT-based PHEV with cabin heating. It also identifies the benefit of utilizing

WHR technologies on the ultimate fuel savings. The engine has to bring its thermal energy to the desired thermal energy level in a cold-start, resulting in additional fuel usage. The DSWHR system recuperates waste heat from the engine exhaust gases, which increases the SOC of the battery. In addition, it recovers waste heat from the electric path (EM and transmission), which decreases the battery energy consumption for cabin heating. These contribute to extra fuel savings. Based on validated component models, optimization results, which are obtained by using DP, show that a cold-start significantly increases the fuel consumption, up to around 7.1%, depending on the initial engine temperature. The DSWHR system remarkably improves the fuel economy, up to around 13.1%, depending on the DSWHR efficiencies, and insights are gained in the design of WHR technologies and sizing of powertrain components. It is found that with a small EGWHR sub-system and a small EPWHR sub-system, the fuel efficiency can be remarkably improved and it achieves the same fuel economy as the ideal warm-start condition. The identified fuel-saving potential and ultimate fuel savings are also dependent on driving conditions. The fuel efficiency improvement of using the DSWHR system in the CVT-based PHEV is even higher on a more aggressive drive cycle. Detailed WHR and cabin models have yet to be developed and including the corresponding dynamics and constraints in the optimization problem may change the control decision, leading to different fuel savings. A cost-benefit analysis of the DSWHR system would also be required.

From optimal control perspective, integrated energy and thermal management of a CVT-based PHEV is investigated in this chapter, which also gives insights into design of WHR technologies and dimensioning of powertrain components. Combined optimal design and control is applied to optimize a CVT-based EV in the next chapter, which is extended by integrated energy and thermal management.

Chapter 4

Co-design of CVT-based electric vehicles

For the development of this chapter[1], an extensive analysis has been performed on vehicle level using a series production vehicle under real driving conditions to derive the essential powertrain models that are used here for design-in-simulation. For an electric vehicle (EV) with a continuously variable transmission (CVT), a novel and computationally efficient convex programming (CP)-based co-design method is proposed to minimize the total-cost-of-ownership (TCO), focusing on the integration of the electric machine (EM) and the CVT. The optimized system with co-design reduces the TCO by around 5.9% compared to a non-optimized CVT-based EV (based on off-the-shelf components) and by around 2% compared to the EV equipped with a single-speed transmission (SST). By taking advantage of the control and design freedom provided by the CVT, the optimal CVT, EM and battery sizes are found to reduce the system cost. It simultaneously finds the optimal CVT speed ratio and air-flow rate of the cooling system reducing the energy consumption. The strength of co-design is highlighted and insights into the design of a low-power EV for urban driving are provided. An introduction to the topic is presented in Section 4.1. Co-design optimization problem is then defined in Section 4.2. Section 4.3 describes the convex EV model needed for solving the co-design optimization problem. On the basis of the developed EV model, numerical optimization is presented in Section 4.4. Optimization results and discussion are subsequently given in Section 4.5. Finally, conclusions are drawn in Section 4.6.

[1]The content of this chapter is based on the following publications:
Wei, C.; Hofman, T.; Ilhan Caarls, E.; van Iperen, R. Co-design of CVT-based Electric Vehicles, submitted as journal article, currently under review.
Wei, C.; Hofman, T.; Ilhan Caarls, E.; van Iperen, R. Design and Analysis of CVT-based Electric Vehicles, submitted as journal article, currently under review.

4.1 Introduction

Growing concerns of environmental contamination and depletion of natural resources have led to the resurgence of electric vehicles (EVs). Even though single-speed transmissions (SSTs) currently dominate the EV market, research on multi-speed transmissions to optimize key performance indicators (KPIs), e.g., energy consumption, system cost, and performance, is gaining popularity, such as two-speed transmissions and continuously variable transmissions (CVTs) [46–49, 192, 193].

The first attempts to design today's EVs (including CVT-based) are largely based on off-the-shelf components, which are typically oversized for drive cycles [44]. The component size, for example, the electric machine (EM) size in kW and the battery size in kWh, relates to the component cost, and identifying the optimal component size would result in cost reduction. The component size also influences the vehicle performance, such as top speed and acceleration time. Furthermore, EV energy usage is largely affected by the driveline efficiency, such as the integration of the EM and the CVT [45]. However, the EM and the CVT are often considered separately in the literature, for example, using the CVT speed ratio (control) to reduce the EM power losses. The influence of the CVT efficiency, CVT and EM size (design) are not always taken into account simultaneously [44].

Moreover, employing multi-speed transmissions such as CVT for the next generation of EVs is relatively new. In the literature, limited research can be found regarding applying optimization algorithms to optimize KPIs of CVT-based EVs [45, 48]. Additionally, current research mainly concentrates on the energy domain, taking into account the mechanical and electrical energy flows, to increase the energy efficiency [194–197]. The thermal domain, however, for instance, evaluation of cooling power consumption and temperature profile, has yet to be explored. It is also an integral part of an EV and would affect the total energy consumption.

To address these issues, integrated design and control frameworks are needed. An overview of design and control optimization methodologies is given in [11]. As presented in Chapter 2, there are generally four approaches to solve the design (plant) and control (controller) problem. With respect to solution optimality, simultaneous and nested coordination schemes outperform iterative and sequential ones, although depending on the coupling and how sensitive the solution is to uncertainties in the design parameters. Among them, convex programming (CP) as a simultaneous approach, which is also a co-design optimization method, has gained popularity. It finds optimal design parameters and control trajectories simultaneously without the need of checking optimality, and it is computationally efficient [59]. Due to the low computation time, CP enables optimization of problems with many dynamic states, such as thermal states, which may not be tractable by using dynamic programming (DP) for example.

Considering the integration of the EM and CVT, as shown in Figure 4.1, the CVT speed ratio over time (γ_{v}) for a use case changes the EM and CVT operating points,

thus influencing the EM ($P_{\mathrm{m,loss}}$) and CVT ($P_{\mathrm{c,loss}}$) power losses. Furthermore, the desired CVT speed ratio affects the CVT size (s_γ), e.g., the ratio coverage of the CVT, and the EM size (s_τ) to meet the power demand for example. The CVT and EM sizes are related to their costs. The CVT size that determines the ratio range, in turn, affects the CVT speed ratio and the EM size. The EM size also has an effect on the CVT size and its speed ratio. In addition, the component size affects its own efficiency. Moreover, the battery size and losses are affected indirectly. Hence, the hypothesis is that there exists an optimal combination of the CVT speed ratio over time, battery size, EM size, and the CVT size for an application, which results in the lowest total-cost-of-ownership (TCO) consisting of energy consumption and system cost. The system cost comprises the CVT, EM (including inverter) and battery prices. Given the interactions between these variables, this optimal solution for a use case can best be found by means of a simultaneous approach in an efficient manner.

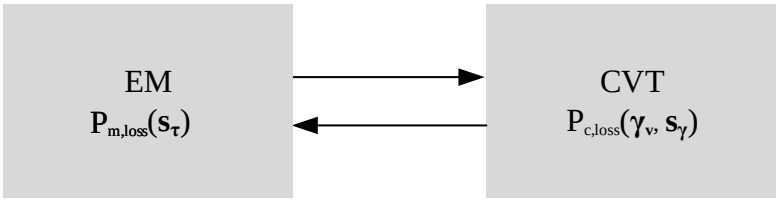

Figure 4.1: Schematic representation of the coupling between the CVT and EM, where γ_{v} represents the CVT speed ratio, s_γ the CVT size, s_τ the EM size, $P_{\mathrm{c,loss}}$ the CVT power losses, and $P_{\mathrm{m,loss}}$ the EM power losses.

Motivated by the above discussion, this study originally proposes a CP-based co-design optimization strategy for a CVT-based EV to reduce the TCO. It identifies the optimal CVT speed ratio over time and the desired air-flow rate of a thermal management system (TMS) to maintain the EM temperature below its thermal limit. Furthermore, it finds the optimal sizes of the CVT, EM and battery. The approach is as follows:

S_1 : An SST-based EV model including energy dynamic and thermodynamics with reference to a series production vehicle is firstly created. It is developed based on static efficiency maps represented by lookup tables, which is validated against measurement data from real-world driving and replicates the physical behavior of the vehicle in reality.

S_2 : A CVT-based EV model is then developed based on S_1, where only the SST is replaced by a CVT (an off-the-shelf component, which is not optimized). Other components, for example, the battery and EM, are the same. The CVT model is created based on experimental data from a test rig.

S_3 : Component models from S_2 are convexified to fit the measurement data from real-world driving and experimental data from the test rig. S_2 is subsequently optimized with the co-design optimization strategy.

All the systems (S_1, S_2 and S_3) have the same maximum EM power and similar vehicle

performance (i.e., 0-100 km/h acceleration time below 11 s, top speed above 165 km/h, gradability above 30%). Therefore, the goal of this study is to show the advantages of the co-design approach in optimizing a CVT-based EV (e.g, sizing) and to compare TCO between S_1, S_2 and S_3. System cost comprising the expenses of the battery, EM and CVT are solely given for the implementation of the co-design approach. Moreover, the strengths of the co-design method are highlighted, by comparing with a sequential approach, where the EM size is fixed to meet performance requirements. Additionally, for urban driving that does not require high performance, insights into the design of a low-power EV are provided.

4.2 Problem definition

The configuration of the considered EV is demonstrated in Figure 4.2. The integration of the EM and the CVT is the primary focus, which are highlighted in bold. The major components of the EV are the battery, DC (direct current)-DC converter, DC-AC (alternating current) inverter, EM, CVT, electric oil pump (ELOP), and vehicle. If not specified, the DC-AC inverter and EM are combined together in this study. The final drive (FD) that takes a constant value and a fixed efficiency is lumped into the variator (VA), which together is regarded as CVT. In order to change the CVT speed ratio, hydraulic actuation power is required from the ELOP. The ELOP power is supplied by the DC-DC converter onboard, which is assumed to be always charged. The EM is directly connected to the input shaft of the CVT without a pre-reduction gear. The heat generated by the EM and CVT is removed by a TMS, which is described in Section 4.3.7. The battery is assumed to provide the power requested by the EM. The EV model describes the longitudinal dynamics and is backward-facing, i.e., the drive cycle is given, with a discrete time-step of one second using time index k, which is sufficient for this study. The vehicle inertia is considered. The main model parameters are listed in Table G.1 (Appendix G). The main design criterion to find the optimal control and design variables is the minimization of the TCO:

$$\text{Minimize TCO}$$

$$\text{with respect to} \begin{cases} \text{component sizes} \\ \text{energy management} \\ \text{thermal management} \end{cases}$$

$$\text{subject to} \begin{cases} \text{drive cycle} \\ \text{powertrain model} \\ \text{thermal model} \\ \text{component limits} \\ \text{performance requirements} \end{cases}$$

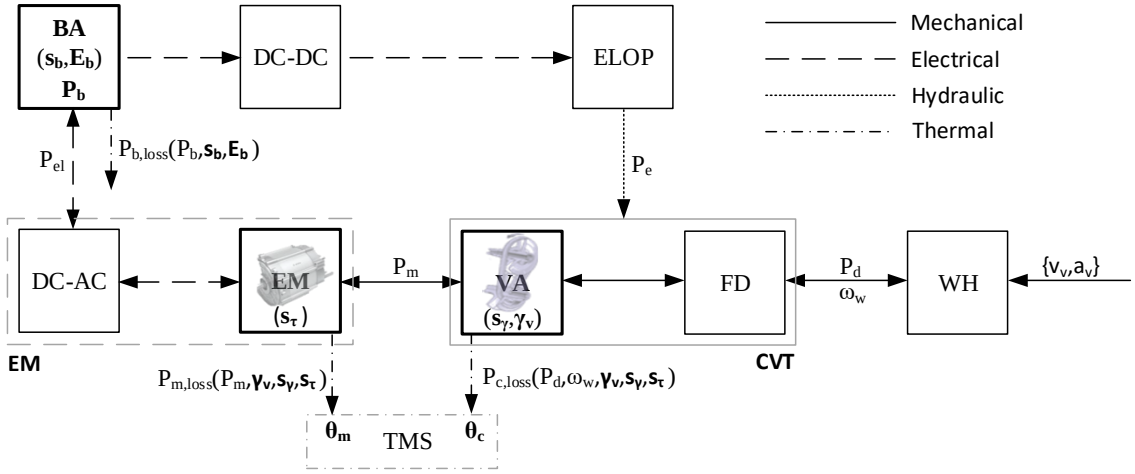

Figure 4.2: A CVT-based electric vehicle, where BA represents the battery, DC-AC the DC (direct current) to AC (alternating current) inverter, DC-DC the DC to DC converter, ELOP the electric oil pump, FD the final drive, VA the variator, and WH the wheel. Design, control, and state variables are highlighted in bold.

TCO consists of the consumed electricity J_e and system cost J_s, given by

$$\min_{\boldsymbol{s},\boldsymbol{x}(k),\boldsymbol{u}(k)} \quad J_\mathrm{e}(\boldsymbol{s},\boldsymbol{x}(k),\boldsymbol{u}(k) \mid w(k)) + J_\mathrm{s}(\boldsymbol{s} \mid w(k)), \tag{4.1}$$

$$\text{s.t.} \quad \boldsymbol{x}(k+1) = \boldsymbol{x}(k) + \boldsymbol{f}(\boldsymbol{s},\boldsymbol{x}(k),\boldsymbol{u}(k),w(k))\ \Delta t, \tag{4.1a}$$

$$\boldsymbol{h}(\boldsymbol{s},\boldsymbol{x}(k),\boldsymbol{u}(k)) = 0, \tag{4.1b}$$

$$\boldsymbol{g}(\boldsymbol{s},\boldsymbol{x}(k),\boldsymbol{u}(k)) \leq 0, \tag{4.1c}$$

where Δt is the time step. The design variables $\boldsymbol{s}$ consist of the ratio coverage of the CVT s_γ, the scaling factor s_τ for scaling the maximum EM torque and the scaling factor s_b for scaling the battery cells, i.e.,

$$\boldsymbol{s} = [s_\gamma, s_\tau, s_\mathrm{b}]^T. \tag{4.2}$$

The state variables $\boldsymbol{x}(k)$ are the state-of-energy (SOE) of the battery and temperature states of the TMS, which are described in Section 4.3.7, given by

$$\boldsymbol{x}(k) = [E_\mathrm{b}(k), \theta_\mathrm{m}(k), \theta_\mathrm{c}(k), \theta_\mathrm{o}(k), \theta_\mathrm{i}(k)]^T. \tag{4.3}$$

The control variables $\boldsymbol{u}(k)$ are the speed ratio of the CVT (γ_v) and the air-flow rate of the TMS (ϕ_a) to keep the EM temperature below its prescribed thermal limit, i.e.,

$$\boldsymbol{u}(k) = [\gamma_\mathrm{v}(k), \phi_\mathrm{a}(k)]^T. \tag{4.4}$$

The power balance of the vehicle is represented by (4.1b), and (4.1c) represents the feasible design space, where the design, state and control variables are bounded. Equation (4.1c) also represents the component limits. The disturbance vector $w(k)$ contains vehicle speed (v_v) and acceleration (a_v), which are prescribed by the drive cycle, given by

$$w(k) = [v_\mathrm{v}(k), a_\mathrm{v}(k)]^T. \tag{4.5}$$

The consumed electricity J_e over the drive cycle represented by $w(k)$ starting at $k = 1$ and ending at $k = N$ is obtained by

$$J_\mathrm{e}(\boldsymbol{s}, \boldsymbol{x}(k), \boldsymbol{u}(k)) = \sum_{k=1}^{N} \rho_\mathrm{e}\ P_\mathrm{b}(\boldsymbol{s}, \boldsymbol{x}(k), \boldsymbol{u}(k))\ \Delta t, \tag{4.6}$$

where ρ_e is the price of electricity (€/kWh). The term $P_\mathrm{b}(\boldsymbol{s}, \boldsymbol{x}, \boldsymbol{u})$ represents the battery output power. The system cost J_s over the drive cycle is calculated by

$$J_\mathrm{s}(\boldsymbol{s}) = \frac{S_\mathrm{d}}{S_\mathrm{v}}\ (C_\mathrm{c}(s_\gamma) + C_\mathrm{m}(s_\tau) + C_\mathrm{b}(s_\mathrm{b})), \tag{4.7}$$

where S_d is the length of the drive cycle (km) and S_v the traveled distance of the vehicle in its lifetime. The variable $C_\mathrm{c}(s_\gamma)$ represents the CVT cost, $C_\mathrm{m}(s_\tau)$ the EM cost (including inverter) and $C_\mathrm{b}(s_\mathrm{b})$ the battery cost.

Based on the configuration shown in Figure 4.2, three systems, namely S_1, S_2 and S_3, are developed and compared in terms of TCO as in (4.1). S_1 is developed with reference to the series production vehicle, which is described in Appendix C. S_2 is created based on S_1, where only the SST is replaced by the CVT, which is presented in Appendix D. In S_1 and S_2, the component models are represented by experimentally-based lookup tables (efficiency maps), which describe the power generation or power dissipation of each component. The design variables are fixed. In S_2, the CVT speed ratio is predetermined by a low-level CVT controller, which is developed based on [186]. The goal of the CVT controller is to reduce the EM power losses depending on the power demand, which is common in literature, such as [44]. The air-flow rate of the TMS is tuned to maintain the EM temperature below its thermal limit. In S_3, convex models are developed based on measurements. The design and control variables are to be determined by the co-design optimization strategy.

This section formulates the co-design optimization problem of a CVT-based EV. To solve this co-design optimization problem, the required convex EV model based on measurements, especially the mathematical coupling between the CVT and EM from design and control perspectives, is presented in more detail in the next section.

4.3 System modeling

This section presents the convex EV model and cost models needed for solving the co-design problem defined in (4.1). An introduction to CP is first given in Appendix E, which serves as a guideline for developing convex models. A data-driven approach used to derive the convex models is then provided in Section 4.3.1. Subsequently, given the drive cycle in Section 4.3.2, the vehicle longitudinal dynamics are described in Section 4.3.3, which is an input to the convex models in S_3. Given the input, however, the torque input to the CVT is not available. Because the CVT speed ratio is a control variable, which is not known in advance and will be determined

by the co-design optimization strategy. Dealing with torque information will lead to non-convexity (Appendix E), e.g., the speed ratio over time as a variable in the denominator. Therefore, to preserve convexity for the co-design optimization problem, all the relations are converted to power level. By utilizing the data-driven approach as mentioned above, three convex models are consequently developed, namely the CVT power loss model (Section 4.3.4), EM power loss model (Section 4.3.5), and the EM power limitation model (Section 4.3.6). Equality constraints are also relaxed with inequalities where applicable, and the equality holds at the optimum. Notice that, this study mainly focuses on the CVT, EM and battery sizing, and the ELOP sizing is not required at this level. Therefore, the ELOP is only considered in the calculation of energy consumption, and no convex representation is required. The ELOP power losses are computed offline using the equations in Section D.2, meaning the ELOP power losses are obtained based on the optimal CVT speed ratio found by the optimization algorithm and then added to the energy consumption. Furthermore, to remove the heat (power losses) generated by the EM and CVT, the TMS and its associated thermal model are presented in Section 4.3.7. Eventually, the required power is supplied by the battery, which is described in Section 4.3.8. The convex battery model is developed based on physics [198]. Additionally, in Section 4.3.9, convex mass and cost models related to CVT, EM and battery sizes are developed for the implementation of the co-design approach.

4.3.1 Derivation of convex models

As mentioned in Appendix E, the component models, for example, the power loss models, are required to be convex for the CP algorithm. The general idea to derive the convex models can be seen in Figure 4.3. This study adopts a data-driven approach, where measurements are used as inputs for the modeling. The measurement data (top) about the CVT and EM, e.g., power losses, torque, speed, and ratio over time, are first served as inputs. Based on these measurements, a set of convex expressions capturing input and output relationships with sufficient accuracy is created. With different combinations of those expressions, e.g., CVT and EM power loss models, are then developed. These parameterized models are subsequently fitted to capture the loss behaviors of components with sufficient accuracy ($\geq 95\%$), which have a small influence on the result. The comparison between the approximated convex model and the original model based on measurements is done by means of goodness of fit, which is defined by

$$\zeta = 1 - \frac{\sum_{i=1}^{n}(y_{\mathrm{o,i}} - y_{\mathrm{c,i}})^2}{\sum_{i=1}^{n}(y_{\mathrm{o,i}} - \frac{1}{n}\sum_{i=1}^{n} y_{\mathrm{o,i}})^2}, \tag{4.8}$$

where $y_{\mathrm{o,i}}$ represents the original model, $y_{\mathrm{c,i}}$ the convex model, and n the sample size. The higher the ζ, the better the fit. Fourth, the convex models are utilized by the co-design optimization method to find the optimal solution of the system.

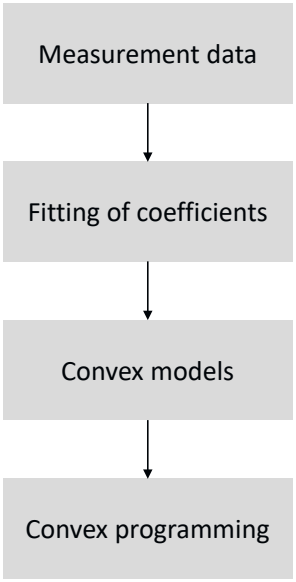

Figure 4.3: A data-driven approach to derive convex models. In order to apply convex programming, constraints and cost function are also required to be convex.

4.3.2 Drive cycle

In this work, a realistic and representative real-world drive cycle, Worldwide Harmonized Light Vehicles Test Cycles (WLTC), as shown in Figure 4.4, is chosen, because it is currently widely adopted in the automotive sector to certify energy consumption. It includes low, medium, high, and extra high speed scenarios, which can represent, for example, urban, rural, and highway driving conditions. The methodology presented applies to other drive cycles as well. In order to show the thermal effect, two repeated WLTC is used. The drive cycle contains the vehicle speed $v_{\mathrm{v}}(k)$ and acceleration $a_{\mathrm{v}}(k)$. Note that, although the quantity (e.g., energy consumption) might vary, the methodology presented also applies to other drive cycles.

4.3.3 Longitudinal dynamics

Note that, in this case the total vehicle mass is a variable because of the scaling factors for the CVT, EM and battery, which will be presented in the next sections. Considering all the forces acting on the vehicle, the power demand for the known WLTC can be obtained by

$$P_{\mathrm{d}}(k) = \left(\frac{1}{2}\,\rho_{\mathrm{a}}\,c_{\mathrm{d}}\,A_{\mathrm{f}}\,v_{\mathrm{v}}^2(k) + c_{\mathrm{r}}\,m_{\mathrm{v}}\,g\,\mathrm{sign}(v_{\mathrm{v}}(k)) + \left(m_{\mathrm{v}} + 4\,\frac{J_{\mathrm{w}}}{r_{\mathrm{w}}^2}\right)\,a_{\mathrm{v}}(k)\right)\,v_{\mathrm{v}}(k), \quad (4.9)$$

where the total vehicle mass m_{v} is given by

$$m_{\mathrm{v}} = m_{\mathrm{cw}} + m_{\mathrm{c}} + m_{\mathrm{m}} + m_{\mathrm{b}} + m_{\mathrm{d}}, \quad (4.10)$$

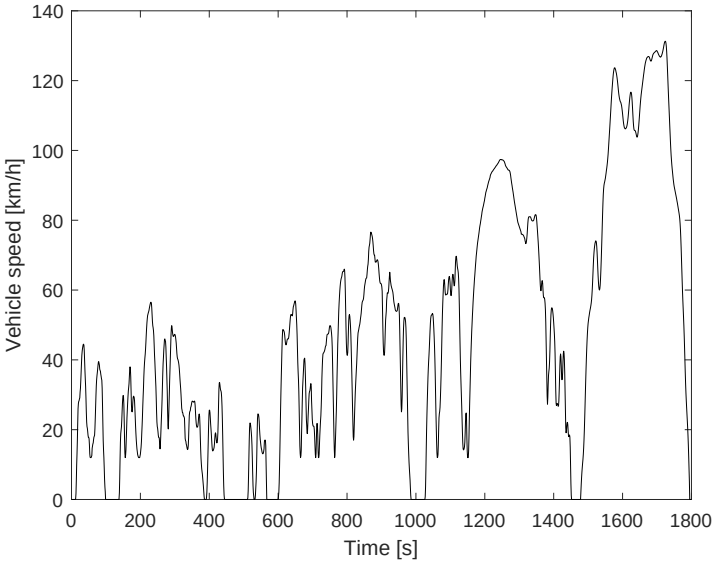

Figure 4.4: Worldwide Harmonized Light Vehicles Test Cycles.

where m_{cw} is the curb weight excluding the CVT (m_{c}), EM (m_{m}) and battery (m_{b}) mass. m_{d} is the driver mass.

4.3.4 Convex CVT model

Based on the measurement data, the CVT torque losses $\tau_{\mathrm{c,loss}}$ can be expressed as a function of its input torque τ_{c}, input speed ω_{p}, and ratio over time γ_{v}. As shown in Figure 4.2, the relationships in S_3 are converted to the power domain. At given input speeds to the CVT, the CVT torque losses $\tau_{\mathrm{c,loss}}$ are converted to their corresponding power losses $P_{\mathrm{c,loss}}$, i.e.,

$$P_{\mathrm{c,loss}}(k) = \tau_{\mathrm{c,loss}}(k)\ \omega_{\mathrm{p}}(k). \tag{4.11}$$

On the basis of these inputs (τ_{c}, ω_{p}, and γ_{v}) to the CVT, the outputs (P_{d} and w_{w}) of the CVT can be determined as

$$P_{\mathrm{d}}(k) = \tau_{\mathrm{c}}(k)\ \omega_{\mathrm{p}}(k) - P_{\mathrm{c,loss}}(k), \tag{4.12}$$

$$w_{\mathrm{w}}(k) = \frac{\omega_{\mathrm{p}}(k)}{\gamma_{\mathrm{v}}(k)}. \tag{4.13}$$

The input-output relationship of the CVT implies that the CVT power losses can also be formulated on system level as (Figure 4.5a):

$$P_{\mathrm{c,loss}}(k) = P_{\mathrm{c,loss}}(P_{\mathrm{d}}(k), w_{\mathrm{w}}(k), \gamma_{\mathrm{v}}(k)). \tag{4.14}$$

Clearly, the CVT power dissipation is influenced by the control variable γ_{v}. However, while P_{d} and w_{w} are known here, the CVT speed ratio γ_{v} will be decided by the optimization algorithm, and dealing with this speed ratio alone would lead to non-convexity, e.g., the speed ratio over time as a variable in the denominator (Appendix

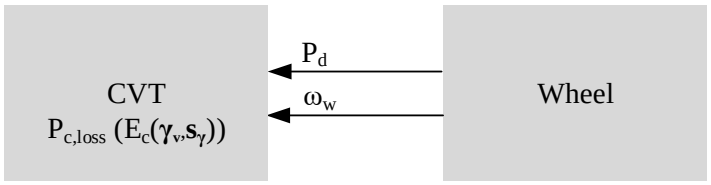

(a) Effect of design (s_γ) and control (γ_v) on the CVT power dissipation

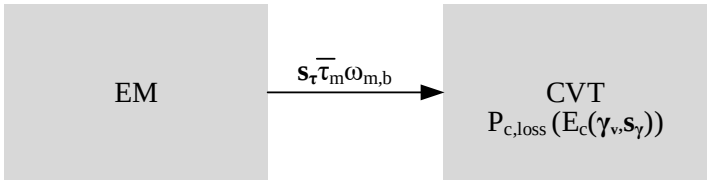

(b) Effect of EM design (s_τ) on the CVT power dissipation

Figure 4.5: Convex modeling of the CVT.

E). Hence, considering the co-design problem and in order to preserve convexity, the information of γ_v is embedded in another variable E_c, by applying a change of variables [199], given by

$$E_c(k) = \gamma_v^2(k)\ \omega_w^2(k). \tag{4.15}$$

Notice that there is no information loss and the optimization strategy will assess every possible combination of γ_v and ω_w. There are also two other reasons of selecting E_c.

- Firstly, the CVT is a rotating mechanical component, and this term is closely related to its kinetic energy.
- Secondly, in practice, the CVT speed ratio is often determined based on the EM speed $\gamma_v\ \omega_w$ and wheel speed ω_w, since there is always torque loss in between, but there is no speed loss.

Therefore, the CVT power dissipation is affected by $E_c(\gamma_v)$ (Figure 4.5a), as it contains the information of speed ratio. Furthermore, the variable $E_c(\gamma_v)$ is influenced by the ratio coverage of the CVT s_γ, the range that the CVT can actually shift, as illustrated in Figure 4.6, which is defined by

$$s_\gamma = \overline{\gamma}_v / \underline{\gamma}_v. \tag{4.16}$$

The CVT sizing is carried out on the basis of the design variable s_γ (Figure 4.5a), because it is one of the most influencing factors that affect cost, efficiency, drivability, and packaging of CVT and powertrain [45]. Note that there are other factors that affect the variator efficiency and hence the CVT loss, such as the center distance of the pulleys and variator asymmetry [200]. Since this study focuses on system-level representation and there is no pre-reduction between the EM and CVT, these factors are not considered. The underdrive ratio $\overline{\gamma}_v$ and the overdrive ratio $\underline{\gamma}_v$ are known. In

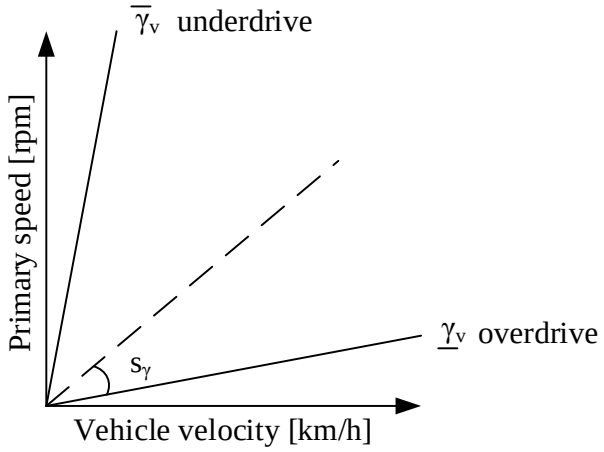

Figure 4.6: Ratio coverage of the CVT.

order to avoid non-convexity for the co-design problem, e.g., a product of two variables (Appendix E), the overdrive ratio $\underline{\gamma}_v$ is fixed in this study. Therefore, constraints on γ_v, E_c, and s_γ are

$$\gamma_v(k) \in [\underline{\gamma}_v, s_\gamma\ \underline{\gamma}_v], \tag{4.17}$$

$$E_c(k) \in [\underline{\gamma}_v^2\ \omega_w^2(k), s_\gamma^2\ \underline{\gamma}_v^2\ \omega_w^2(k)], \tag{4.18}$$

$$s_\gamma^2 \in [\underline{s}_\gamma^2, \overline{s}_\gamma^2]. \tag{4.19}$$

The CVT power dissipation in (4.11) is measured based on an original CVT product (sold on the current market) with a full ratio range of [0.38, 2.63] and hence large ratio coverage, which has a large torque capacity ($\overline{\tau}_c$) and power capacity ($\overline{P}_c$). In case of a CVT with reduced ratio coverage (s_γ), smaller ELOP and on-demand actuation, resulting in a compact and small CVT (superscript "s") with smaller power capacity (P_c^s), a higher CVT efficiency is expected [7, 45]. This higher efficiency potential means a lower power dissipation. Compared with the original CVT power losses $P_{c,loss}$ in (4.14), this lower power dissipation can be modeled by a multiplier μ_c, which is a function of the EM scaling factor, giving

$$P_{c,loss}^s(k) = \mu_c(s_\tau)\ P_{c,loss}(k). \tag{4.20}$$

This multiplier is sensitive to many parameters and technological advances. For example, as reported in [5], the maximum efficiency of the current variator could be above 98%. Notice that, the final drive does not benefit from this loss reduction. Additionally, the current CVT and EM are designed separately, which leads to a mismatch between the specifications. In this work, as shown in Figure 4.2, the EM is connected to the CVT without a pre-reduction gear. The required CVT torque capacity is determined by the output of the EM $s_\tau\ \overline{\tau}_m$, as demonstrated in Figure 4.5b. Here, s_τ, the scaling factor for the EM, is a design variable, which will be explained in

Section 4.3.5. Thus, the multiplier $\mu_{\mathrm{c}}(s_\tau)$ can be obtained by [7]

$$\begin{aligned}\mu_{\mathrm{c}}(s_\tau) =& 0.7 + 0.3\frac{\overline{P}^{s}_{\mathrm{c}}}{\overline{P}_{\mathrm{c}}} \\ =& 0.7 + 0.3\frac{s_\tau\ \overline{\tau}_{\mathrm{m}}\ \omega_{\mathrm{m,b}}}{\overline{\tau}_{\mathrm{c}}\ \omega_{\mathrm{m,b}}} \\ =& 0.7 + 0.3\frac{s_\tau\ \overline{\tau}_{\mathrm{m}}}{\overline{\tau}_{\mathrm{c}}},\end{aligned} \tag{4.21}$$

where $\overline{\tau}_{\mathrm{m}}$ is the maximum EM torque when $s_\tau = 1$ and $\omega_{\mathrm{m,b}}$ is the EM base speed. Similar to [7], this multiplier can be interpreted as a proportional improvement of the more efficient variator, which typically accounts for thirty percent of the total power losses in previous applications.

Consequently, the factors that influence the CVT power losses are P_{d}, w_{w}, $E_{\mathrm{c}}(\gamma_{\mathrm{v}}, s_\gamma)$, and s_τ (Figure 4.5a and Figure 4.5b). Taking into account convexity and possible combinations of expressions, various models are developed to represent the CVT power losses. The models are fitted to capture the loss behavior of the CVT. Based on the evaluated fitting accuracy, the convex CVT model is identified as follows:

$$P^{\mathrm{s}}_{\mathrm{c,loss}}(k) = c_{\mathrm{c},0}\ \left(\frac{P_{\mathrm{d}}(k)}{w_{\mathrm{w}}(k)}\right)^2 + c_{\mathrm{c},1}\ E_{\mathrm{c}}(k) + c_{\mathrm{c},2}\ |P_{\mathrm{d}}(k)| + c_{\mathrm{c},3}\ s_\tau\ w_{\mathrm{w}}(k) + c_{\mathrm{c},4}\ s_\tau + c_{\mathrm{c},5}, \tag{4.22}$$

where $c_{\mathrm{c},0}$, $c_{\mathrm{c},1}$, $c_{\mathrm{c},2}$, $c_{\mathrm{c},3}$, $c_{\mathrm{c},4}$, and $c_{\mathrm{c},5}$ are the coefficients found, which are shown in Table G.1. Notice that the power losses are always constrained to be equal to (i.e., vehicle velocity $v_v = 0$) or larger than zero. This model has a fitting accuracy of around 98% based on (4.8). It should be noted that, information is exchanged between the terms. For example, the information of s_τ is not only explicitly expressed in s_τ and $s_\tau\ w_{\mathrm{w}}$, but also implicitly embedded in other terms. The term $s_\tau\ w_{\mathrm{w}}$ is important for CVT applications, as generally CVT does not operate at very high speeds, yet would lead to lower friction losses of the EM. Another design variable (s_γ) and control variable (γ_{v}) are reflected in E_{c}. While the information of speed and torque are conveyed already by $|P_{\mathrm{d}}|$ and $s_\tau\ w_{\mathrm{w}}$, it is further reinforced by torque squared $(\frac{P_{\mathrm{d}}}{w_{\mathrm{w}}})^2$ and speed squared E_{c} to capture essential CVT dynamics. An example of $\gamma_{\mathrm{v}} = 0.7$ and $s_\tau = 1$ is shown in Figure 4.7. Such correlations in data analysis can be done by clustering the data sets for certain physical attributes. In this case, the CVT power dissipation is considered as the attribute.

4.3.5 Convex EM model

To obtain the convex EM model, the steps in Figure 4.3 are followed, as it is done for the CVT in Section 4.3.4. As shown in Figure 4.2, the EM is directly linked to the input shaft of the CVT and provides the power requested by the CVT, referring to (4.20), i.e.,

$$P_{\mathrm{m}}(k) = P_{\mathrm{d}}(k) + P^{\mathrm{s}}_{\mathrm{c,loss}}(k). \tag{4.23}$$

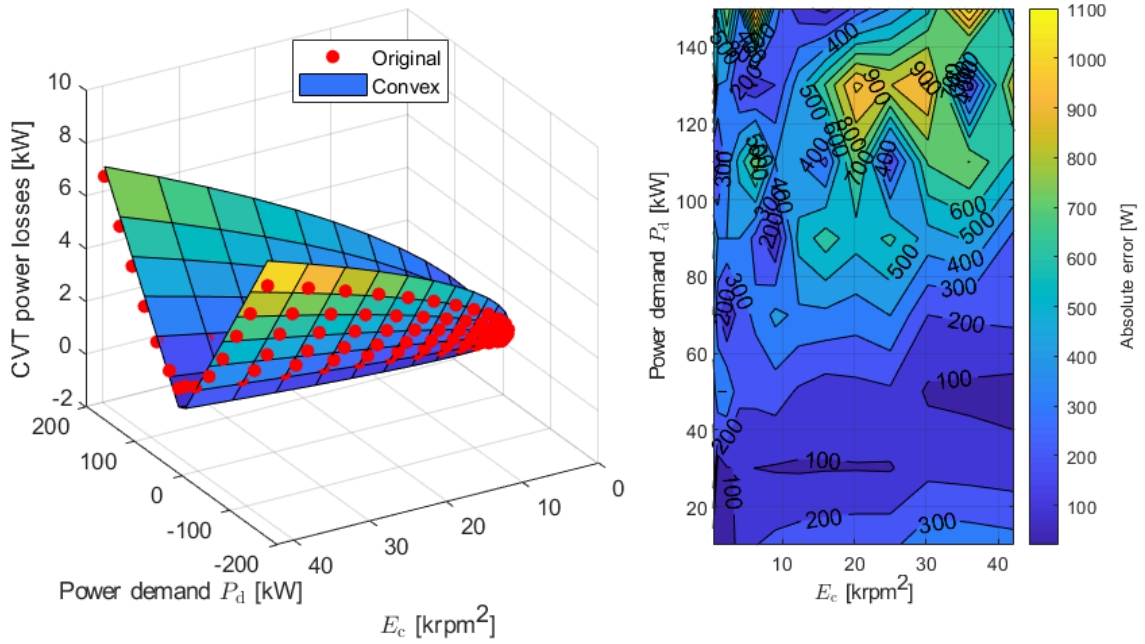

Figure 4.7: Convex CVT power loss model for $\gamma_v = 0.7$ and $s_\tau = 1$. The absolute error represents the difference in power loss between the convex model and the original model. This model has a fitting accuracy of around 98%, i.e., ζ=98% (4.8).

Based on the measurement data, the EM power losses can be expressed as a function of its output torque τ_m and speed ω_m. The EM power dissipation is given by

$$P_{m,loss}(k) = P_{m,loss}(\tau_m(k), \omega_m(k)). \tag{4.24}$$

On the basis of the output torque and speed of the EM, its output power can be calculated by

$$P_m(k) = \tau_m(k)\ \omega_m(k). \tag{4.25}$$

Combing (4.24) and (4.25), as depicted in Figure 4.8, leads to

$$P_{m,loss}(k) = P_{m,loss}(\tau_m(k), \omega_m(k), P_m(k)). \tag{4.26}$$

Moreover, the EM power dissipation $P_{m,loss}$ is influenced by its size (in torque and speed). In this work, the maximum EM torque ($\overline{\tau}_m$) is scaled down by using the scaling factor s_τ and the base speed is increased ($\omega^s_{m,b}$) such that the maximum output power is maintained, as shown in Figure 4.9, i.e.,

$$\overline{P}_m = \overline{\tau}_m\ \omega_{m,b} = s_\tau\ \overline{\tau}_m\ \omega^s_{m,b}. \tag{4.27}$$

The EM sizing is performed based on the design variable s_τ, because it affects the EM efficiency, weight and cost. For example, reducing the maximum EM torque decreases the usage of active materials of the EM. Note that because of physical limitations of the CVT, the EM speeds above 6500 rpm are not used for the CVT application, which has a negligible impact on the result. The EM scaling factor s_τ influences the EM torque, optimal operating line (OOL), and power losses, which is bounded by

$$s_\tau \in [\underline{s}_\tau, \overline{s}_\tau]. \tag{4.28}$$

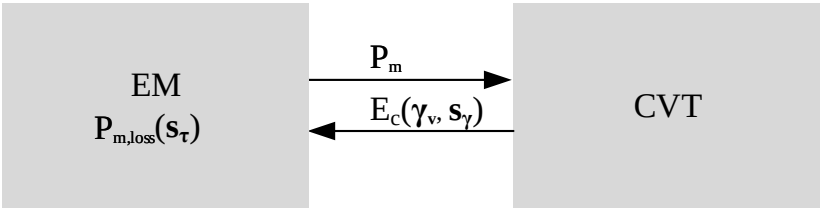

Figure 4.8: Convex modeling of the EM.

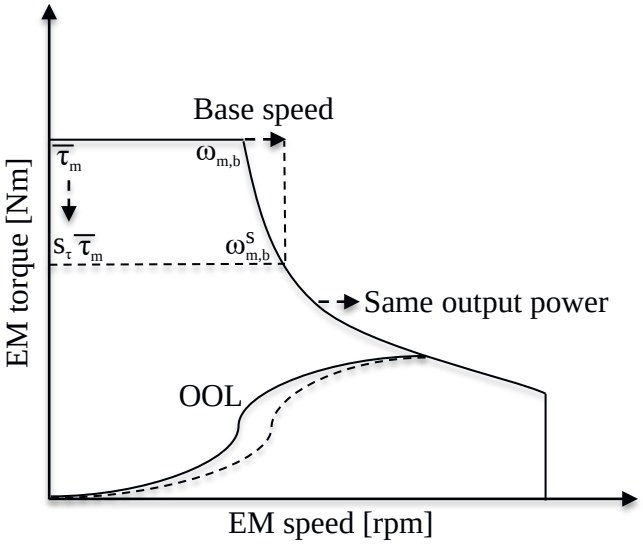

Figure 4.9: Scaling factor of the EM including the DC-AC inverter, where the solid lines represent the original EM, dashed lines the scaled EM while keeping the same output power, and OOL the optimal operating line minimizing the EM losses for every power demand.

As illustrated in Figure 4.5b, the scaling of EM has a direct effect on the CVT design requirements. Furthermore, as explained before, the EM power dissipation $P_{\mathrm{m,loss}}$ is influenced by another design variable s_γ and control variable γ_v, which change its operating point and hence the power losses. The information of s_γ and γ_v are represented by E_c.

To sum up, the identified parameters that affect the EM power losses are P_m, s_τ, and $E_\mathrm{c}(\gamma_\mathrm{v}, s_\gamma)$, which are shown in Figure 4.8. Models that contain these parameters and their combinations, which are also potentially convex, are built. In a similar fashion as with the convex CVT modeling (Section 4.3.4), the EM models are fitted to capture the loss behavior of the EM. On the basis of fitting accuracy, the convex EM model is found as follows:

$$P_{\mathrm{m,loss}}(k) = c_{\mathrm{m},0}\ \frac{P^2_\mathrm{m}(k)}{E_\mathrm{c}(k)} + c_{\mathrm{m},1}\ E_\mathrm{c}(k) + c_{\mathrm{m},2}\ |P_\mathrm{m}(k)| + c_{\mathrm{m},3}\ s_\tau + c_{\mathrm{m},4}, \tag{4.29}$$

where $c_{\mathrm{m},0}$, $c_{\mathrm{m},1}$, $c_{\mathrm{m},2}$, $c_{\mathrm{m},3}$, and $c_{\mathrm{m},4}$ are the coefficients found, which are provided in Table G.1. The information of speed and torque are conveyed already by $|P_\mathrm{m}|$, and it is further reinforced by torque squared $\frac{P^2_\mathrm{m}}{E_\mathrm{c}}$ and speed squared E_c to capture essential EM dynamics. An example of $s_\tau = 1$ is illustrated in Figure 4.10. This model has a fitting

accuracy of around 95% based on (4.8). Notice that all the EM torque and speed combinations are taken into consideration in constructing the model, and some of them result in higher losses, leading to a larger discrepancy in the upper part of Figure 4.10. The EM, in practice, however, will not operate at those points, because these points are outside the torque-speed envelope, which will be constrained by the EM power limitation model and will be described next. The relatively lower correlation accuracy in the lower part is due to the fact that both motoring and generating modes are considered. Taking into account limited operating points in this part for a long drive cycle in practice, the impact is small. Note that Figure 4.10 appears more dense than Figure 4.7, because there are more data in the EM data set.

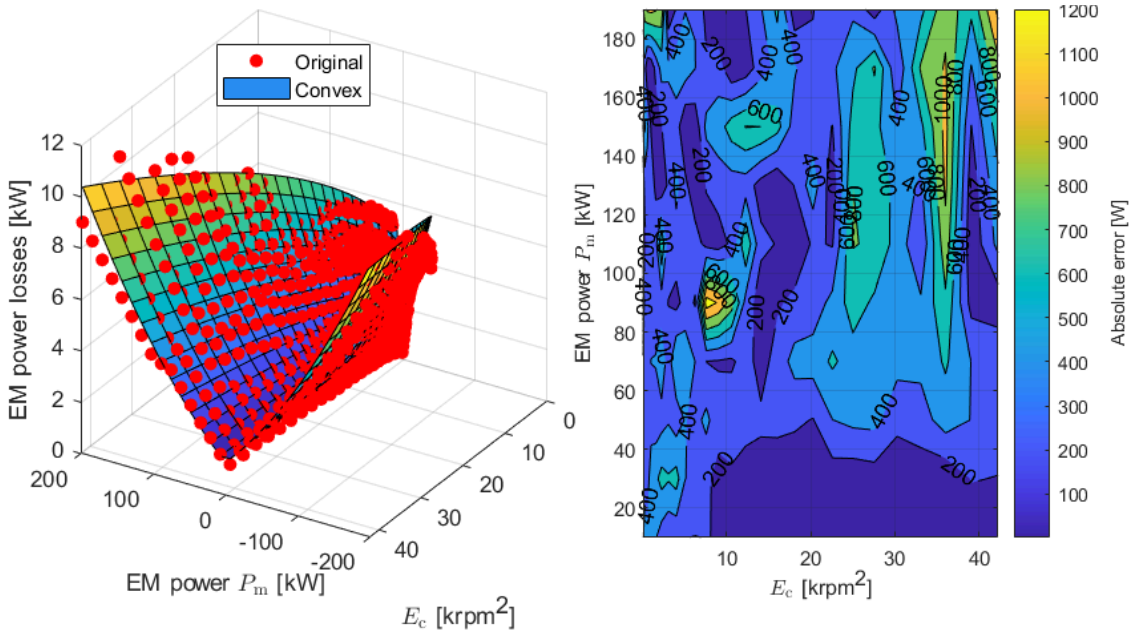

Figure 4.10: Convex EM power loss model for $s_\tau = 1$. The absolute error represents the difference in power loss between the convex model and the original model. This model has a fitting accuracy of around 95%, i.e., ζ=95% (4.8).

4.3.6 Convex EM power limitation model

As s_τ varies, the EM power limits change as well, referring to (4.27), as shown in Figure 4.11. Note that the EM power limits also consider the effect of the CVT ($E_c(\gamma_v, s_\gamma)$). Regarding the EM power limits, as can be seen from Figure 4.9, they mainly relate to two parts, i.e., one before the base speed and the other after the base speed ($\omega_{m,b}$). Hence, the speed information is important. As speed information is mostly conveyed by E_c, it is identified as one of the key parameters. As a result, factors that influence the EM power limits could be, e.g., s_τ and $E_c(\gamma_v, s_\gamma)$. Based on these parameters, possible models that preserve convexity are developed, which are fitted to represent the EM power limitation. Based on fitting accuracy, the convex

EM power limitation model including motoring and generating modes is identified as follows:

$$\overline{P}_{\mathrm{m}} = \min\{(c^{+}_{\mathrm{m},0}\ E_{\mathrm{c}}(k) + c^{+}_{\mathrm{m},1}\ \sqrt{s_\tau\ E_{\mathrm{c}}(k)} + c^{+}_{\mathrm{m},2}\ s_\tau + c^{+}_{\mathrm{m},3}), s_\tau\ \overline{P}_{\mathrm{m}}\}, \tag{4.30}$$

$$\underline{P}_{\mathrm{m}} = \max\{(c^{-}_{\mathrm{m},0}\ E_{\mathrm{c}}(k) + c^{-}_{\mathrm{m},1}\ \sqrt{s_\tau\ E_{\mathrm{c}}(k)} + c^{-}_{\mathrm{m},2}\ s_\tau + c^{-}_{\mathrm{m},3}), s_\tau\ \underline{P}_{\mathrm{m}}\}, \tag{4.31}$$

where $c^{+}_{\mathrm{m},0}$, $c^{+}_{\mathrm{m},1}$, $c^{+}_{\mathrm{m},2}$, $c^{+}_{\mathrm{m},3}$, $c^{-}_{\mathrm{m},0}$, $c^{-}_{\mathrm{m},1}$, $c^{-}_{\mathrm{m},2}$, and $c^{-}_{\mathrm{m},3}$ are the coefficients identified, which are shown in Table G.1. The plus sign (+) represents the motoring mode and the minus sign (-) the generating mode. This model has a fitting accuracy of around 99% based on (4.8). The terms $\overline{P}_{\mathrm{m}}$ and $\underline{P}_{\mathrm{m}}$ represent the maximum and minimum power of the original EM, respectively, which can be obtained from Figure 4.9a. An example of this model for $s_\tau = 1$ in motoring mode ($\overline{P}_{\mathrm{m}}$) is depicted in Figure 4.12, which can be mirrored for generating mode ($\underline{P}_{\mathrm{m}}$). Note that while the approximated convex model appears as straight lines in Figure 4.12 for $s_\tau = 1$, they may not be for other scaling factors, depending on (4.30) and (4.31). Note that this model is mainly used in Section 4.5.3.

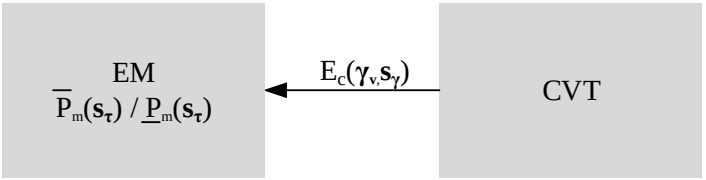

Figure 4.11: Convex modeling of the EM power limits.

4.3.7 Thermal EM-CVT model

The heat (power losses) generated by the CVT ($P^{\mathrm{s}}_{\mathrm{c,loss}}$ in (4.22)) and EM ($P_{\mathrm{m,loss}}$ in (4.29)) is removed by a TMS, as demonstrated in Figure 4.13. The main difference between Figure 4.13 and Figure C.4 is that there is an extra small off-the-shelf heat exchanger in Figure 4.13, which enables heat exchange between the CVT cooling medium and the EM cooling medium. The EM and the CVT are physically attached. The heat from the CVT is removed directly by its cooling medium, which exchanges that with the EM cooling medium. Furthermore, the heat from the EM is taken away by its cooling medium driven by a pump, which is eventually removed by the radiator with a fan providing the required air-flow rate. The EM and CVT dissipate heat to the ambient air due to convection. The aim of the TMS is to find the desired air-flow rate (ϕ_{a}) that maintains the EM temperature (θ_{m}) below its prescribed thermal limit (65°C) dictated by the manufacturer. A lumped-parameter approach is utilized to describe the thermal behavior of the EM and CVT. Based on first principles of thermodynamics, referring to Section C.4, the thermal EM-CVT model is given by

$$\begin{aligned} c_{\mathrm{m}}\ m_{\mathrm{m}}\ \dot{\theta}_{\mathrm{m}}(k) =& P_{\mathrm{m,loss}}(k) - h_{\mathrm{m}}\ A_{\mathrm{m}}\ (\theta_{\mathrm{m}}(k) - \theta_{\mathrm{o}}(k)) - k_{\mathrm{m}}\ (\theta_{\mathrm{m}}(k) - \theta_{\mathrm{c}}(k)) \\ & - h_{\mathrm{a}}\ A_{\mathrm{a}}\ (\theta_{\mathrm{m}}(k) - \theta_{\mathrm{a}}), \end{aligned} \tag{4.32}$$

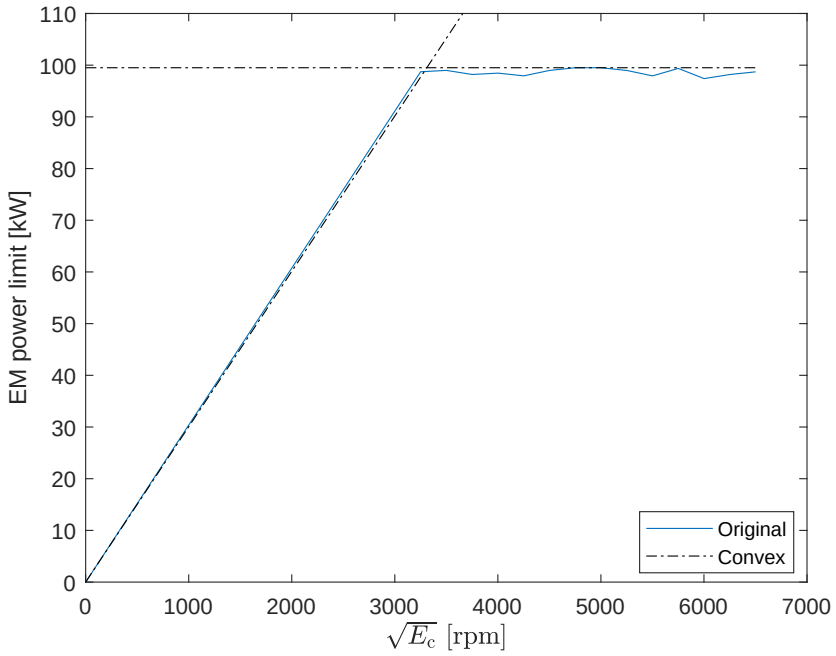

Figure 4.12: Convex EM power limitation model for $s_\tau = 1$ in motoring mode ($\overline{P}_\mathrm{m}$). The dash-dot lines represent the approximated convex model before and after the base speed. This model has a fitting accuracy of around 99%, i.e., ζ=99% (4.8).

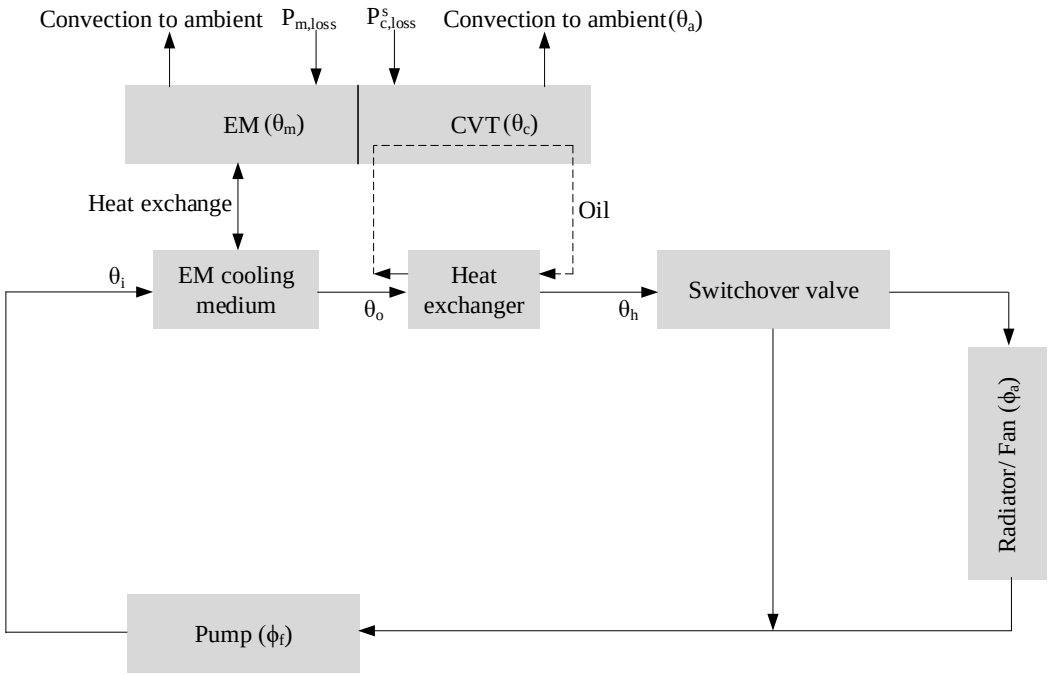

Figure 4.13: Thermal management configuration for the EM-CVT.

$$c_\mathrm{f}\ m_\mathrm{f}\ \dot{\theta}_\mathrm{o}(k) = h_\mathrm{m}\ A_\mathrm{m}\ (\theta_\mathrm{m}(k) - \theta_\mathrm{o}(k)) - \phi_\mathrm{f}\ c_\mathrm{f}\ (\theta_\mathrm{o}(k) - \theta_\mathrm{i}(k)), \tag{4.33}$$

$$c_\mathrm{f}\ m_\mathrm{f}\ \dot{\theta}_\mathrm{h}(k) = k_\mathrm{h}\ (\theta_\mathrm{c}(k) - \theta_\mathrm{h}(k)) - \phi_\mathrm{f}\ c_\mathrm{f}\ (\theta_\mathrm{h}(k) - \theta_\mathrm{o}(k)), \tag{4.34}$$

$$\begin{aligned} c_\mathrm{h}\ c_\mathrm{c}\ m_\mathrm{c}\ \dot{\theta}_\mathrm{c}(k) =& P^\mathrm{s}_{\mathrm{c,loss}}(k) + k_\mathrm{e}\ (\theta_\mathrm{m}(k) - \theta_\mathrm{c}(k)) - k_\mathrm{h}\ (\theta_\mathrm{c}(k) - \theta_\mathrm{h}(k)) \\ & - h_\mathrm{c}\ A_\mathrm{c}\ (\theta_\mathrm{c}(k) - \theta_\mathrm{a}), \end{aligned} \tag{4.35}$$

$$c_\mathrm{f}\ m_\mathrm{f}\ \dot{\theta}_\mathrm{i}(k) = \phi_\mathrm{c}\ c_\mathrm{f}\ (\theta_\mathrm{h}(k) - \theta_\mathrm{i}(k)) - \epsilon\ \phi_\mathrm{a}(k)\ c_\mathrm{a}\ (\theta_\mathrm{h}(k) - \theta_\mathrm{a}). \tag{4.36}$$

The thermal variables are restricted by

$$\theta_\mathrm{m}(k) \in [\underline{\theta}_\mathrm{m}, \overline{\theta}_\mathrm{m}], \tag{4.37}$$

$$\theta_\mathrm{o}(k) \in [\underline{\theta}_\mathrm{o}, \overline{\theta}_\mathrm{o}], \tag{4.38}$$

$$\theta_\mathrm{i}(k) \in [\underline{\theta}_\mathrm{i}, \overline{\theta}_\mathrm{i}]. \tag{4.39}$$

This model is validated against measurement data in terms of temperature, which is presented in Appendix C.4. Note that since detailed pump and fan signals are not available in the measurement data, validation of cooling power consumption is not performed. Hence, the cooling power consumption is not added to the overall energy consumption, which does not influence the purpose of this study, focusing on evaluation of thermal performance (Section 4.5.4).

4.3.8 Convex battery model

The electric power of the EM is provided by the battery. The battery model is based on lithium-ion (nickel manganese cobalt oxide) technology with identical cells. The required battery power is given by

$$\begin{aligned} P_\mathrm{b}(k) =& P_\mathrm{el}(k) + P_\mathrm{b,loss}(k) \\ =& P_\mathrm{m}(k) + P_\mathrm{m,loss}(k) + P_\mathrm{b,loss}(k), \end{aligned} \tag{4.40}$$

where $P_\mathrm{b,loss}$ represents the battery losses, which is calculated by

$$\begin{aligned} P_\mathrm{b,loss}(k) =& s_\mathrm{b}\ N_0\ I_\mathrm{c}^2(k)\ R_\mathrm{c} \\ =& \frac{P_\mathrm{b}^2(k) R_\mathrm{c}}{s_\mathrm{b}\ N_0\ V_\mathrm{c}^2(k)}, \end{aligned} \tag{4.41}$$

where I_c is the cell current and R_c its resistance. The battery sizing is performed based on the scaling factor s_b for scaling the battery cells, which linearly influences the battery energy, weight and cost. N_0 is the original number of battery cells when $s_\mathrm{b} = 1$. To preserve convexity for the co-design problem, the open circuit voltage of a battery cell (V_c) is approximated as a linear function of the state-of-charge of the battery (ξ), as shown in Figure 4.14, given by

$$V_\mathrm{c}(k) = \frac{Q_\mathrm{c}}{F_\mathrm{c}}\ \xi(k) + V_0, \tag{4.42}$$

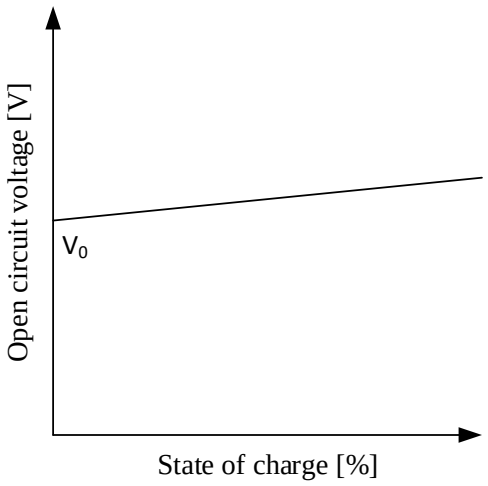

Figure 4.14: Open circuit voltage of a battery cell.

where Q_{c} is the cell capacity and F_{c} the capacitance. The battery energy can then be calculated by

$$\begin{aligned} E_{\mathrm{b}}(k) =& s_{\mathrm{b}}\ N_0\ \int_0^{\xi} V_{\mathrm{c}}(k)\ Q_{\mathrm{c}} \mathrm{d}\xi \\ =& \frac{F_{\mathrm{c}}}{2}\ s_{\mathrm{b}}\ N_0\ (V_{\mathrm{c}}^2(k) - V_0^2). \end{aligned} \tag{4.43}$$

Taking the derivative of E_{b} yields

$$\dot{E}_{\mathrm{b}}(k) = -P_{\mathrm{b}}(k). \tag{4.44}$$

In order to model the battery on a pack level instead of a cell level, which does not require information of series-parallel connection, the cell voltage V_{c} is replaced by a new variable U_{b}, by applying a change of variables, given by

$$U_{\mathrm{b}}(k) = s_{\mathrm{b}}\ N_0\ V_{\mathrm{c}}^2(k) = \frac{2}{F_{\mathrm{c}}}\ E_{\mathrm{b}}(k) + s_{\mathrm{b}}\ N_0\ V_0^2. \tag{4.45}$$

The battery power losses can then be expressed as

$$\begin{aligned} P_{\mathrm{b,loss}}(k) =& \frac{P_{\mathrm{b}}^2(k)\ R_{\mathrm{c}}}{U_{\mathrm{b}}(k)} \\ =& \frac{P_{\mathrm{b}}^2(k)\ R_{\mathrm{c}}\ F_{\mathrm{c}}}{2\ E_{\mathrm{b}}(k) + s_{\mathrm{b}}\ N_0\ F_{\mathrm{c}}\ V_0^2}. \end{aligned} \tag{4.46}$$

The battery energy and power are constrained by

$$E_{\mathrm{b}}(k) \in [\frac{F_{\mathrm{b}}}{2}\ s_{\mathrm{b}}\ N_0\ (\underline{V}_{\mathrm{c}}^2 - V_0^2), \frac{F_{\mathrm{b}}}{2}\ s_{\mathrm{b}}\ N_0\ (\overline{V}_{\mathrm{c}}^2 - V_0^2)], \tag{4.47}$$

$$P_{\mathrm{b}}(k) \in [\underline{I}_{\mathrm{c}}\ V_{\mathrm{b}}(k), \overline{I}_{\mathrm{c}}\ V_{\mathrm{b}}(k)], \tag{4.48}$$

where V_b is given by

$$\begin{aligned} V_\mathrm{b}(k) =& s_\mathrm{b}\ N_0\ V_\mathrm{c}(k) \\ =& \sqrt{s_\mathrm{b}\ N_0\ U_\mathrm{b}(k)}. \end{aligned} \tag{4.49}$$

Note that the effect of the battery temperature is not considered, as the battery power losses are low in this case.

4.3.9 Convex mass and cost models

Apart from powertrain and thermal models, mass and cost models are required for the implementation of the co-design method. This section describes convex mass and cost models associated with CVT and EM sizes. The CVT mass includes the mass of the variator and final drive. The EM mass includes the mass of the EM and inverter.

For a generic CVT, its weight can be approximated as a function of its torque capacity $\overline{\tau}_\mathrm{c}$ based on existing CVTs [201]. As shown in Figure 4.15, the CVT weight m_c is modeled by

$$m_\mathrm{c} = 0.28\ \overline{\tau}_\mathrm{c} + 23.21. \tag{4.50}$$

The original production CVT with a full ratio range of [0.38, 2.63], implying a ratio coverage of around 7, has a torque capacity of 250 Nm. On the basis of this CVT, assume the ratio affects the torque capacity proportionally. For each torque capacity (ratio coverage), the corresponding weight can be computed based on (4.50). Specifically for the CVT in this study, a one-on-one mapping between the weight m_c and ratio coverage s_γ can thus be expressed as

$$m_\mathrm{c} = 1.19\ s_\gamma^2 + 39.12. \tag{4.51}$$

Therefore, given the specific cost of CVT [7] (a_c in Table G.1), the CVT cost C_c (in €) is given by

$$C_\mathrm{c} = a_\mathrm{c}\ (1.19\ s_\gamma^2 + 39.12). \tag{4.52}$$

The prediction (4.52) is valid on the basis of this CVT, since the ratio coverage is scaled down.

The EM weight is estimated as a function of its scaling factor [202], i.e.,

$$m_\mathrm{m} = s_\tau\ \overline{m}_\mathrm{m}, \tag{4.53}$$

where $\overline{m}_\mathrm{m}$ is the original EM mass when $s_\tau = 1$, which is provided in Table 4.1.

The EM cost C_m (in €) is estimated as a function of its scaling factor [203, 204], giving

$$C_\mathrm{m} = b_\mathrm{m}\ s_\tau. \tag{4.54}$$

The battery weight is described as a function of its scaling factor, given by

$$m_\mathrm{b} = s_\mathrm{b}\ \overline{m}_\mathrm{b}, \tag{4.55}$$

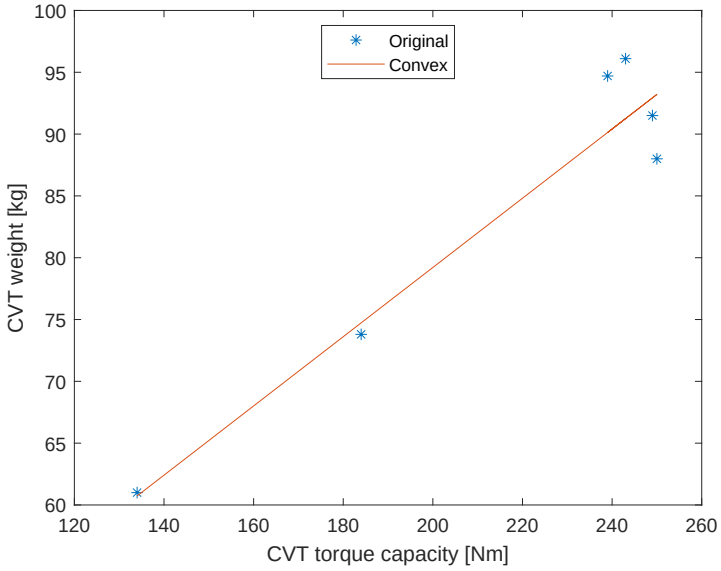

Figure 4.15: CVT weight as a function of its torque capacity.

where $\overline{m}_{\mathrm{b}}$ is the original battery mass when $s_{\mathrm{b}} = 1$, which is provided in Table 4.1. The battery cost C_{b} (in €) is approximated by [204, 205]

$$C_{\mathrm{b}} = s_{\mathrm{b}}\ c_{\mathrm{b}}\ \overline{E}_{\mathrm{b}}. \tag{4.56}$$

Note that, the price of CVT could be lowered, as some parts of the CVT for conventional applications are not needed in EVs, such as torque converter and DNR (drive, neutral and reverse). However, since part of this information is taken into account in (4.51) and the exact weight is not known before optimization, it is not further addressed. Moreover, currently, there is no consensus on the component price. The numbers used in this study are only indicative figures (e.g., b_{m}, $c_{\mathrm{b}}\ \overline{E}_{\mathrm{b}}$), which have no direct relation to possible market prices. They do not affect the comparison, as the same scale is employed in all the systems (S_1, S_2 and S_3).

Additionally, notice that the component specifications appear large in this case. The components are scaled down, which means that, for example, $s_\tau > 1$ and $\gamma_{\mathrm{v}} > 2.63$, are not necessary. The models are always valid within their feasible ranges based on the measurement data. The right combination of the speed ratio of the CVT over time γ_{v}, air-flow rate of the cooling system ϕ_{a}, ratio coverage s_γ, the scaling factor for the EM s_τ and the scaling factor for the battery s_{b} will be determined simultaneously by the optimization algorithm, which is discussed in the next section.

This section presents a convex EV model and its associated cost models for the co-design optimization problem. A data-driven approach is used to derive the convex CVT and EM models. In particular, the coupling between the EM and CVT from design and control perspectives is described in detail. Compared to the original model based on measurements, the convex CVT power loss model is developed with a correlation accuracy of 98%. The convex EM power loss and power limitation

models are developed with correlation accuracies of 95% and 99%, respectively. An experimentally validated thermal EM-CVT model is subsequently presented. Finally, convex mass and cost models that are size-dependent for the CVT and EM are created. The overall system has a large number of states, and there is strong coupling between the CVT and EM. By applying CP, not only will it find an optimal solution but also it will find the solution in a computationally efficient manner, allowing for extensive parameter variation studies and evaluation of diverse design aspects on system and component level, which will be discussed in the next section.

4.4 Numerical optimization

On the basis of the convex models developed in the last chapter, the objective of the co-design optimization strategy is to minimize the TCO. It aims at generating an optimal control trajectory of the speed ratio of the CVT (γ_v) and finding the desired air-flow rate of the cooling system (ϕ_a). Furthermore, it aims to identify the optimal sizes of the CVT (s_γ), EM (s_τ) and battery (s_b). Based on (4.1), the overall co-design optimization problem in S_3 can be formulated as follows:

$$\begin{aligned}\min \sum_{k=1}^{N} \rho_\mathrm{e}\ & P_\mathrm{b}(s_\gamma, s_\tau, s_\mathrm{b}, E_\mathrm{b}(k), \theta_\mathrm{m}(k), \theta_\mathrm{c}(k), \theta_\mathrm{o}(k), \theta_\mathrm{i}(k), \phi_\mathrm{a}(k), \gamma_\mathrm{v}(k) \mid v_\mathrm{v}(k), \\ & a_\mathrm{v}(k))\ \Delta t + \frac{S_\mathrm{d}}{S_\mathrm{v}}\ (C_\mathrm{c}(s_\gamma) + C_\mathrm{m}(s_\tau) + C_\mathrm{b}(s_\mathrm{b})), \qquad (4.57)\end{aligned}$$

$$\text{s.t.} \quad (4.9) - (4.54). \qquad (4.57a)$$

The final time is fixed, as the drive cycle is given. The final state of the battery energy is not constrained, considering the battery capacity and the power demand of the drive cycle. The overall optimization problem is convex, including convex cost function, models and constraints. Basic convex functions, e.g., linear, quadratic, quadratic-over-linear and opposite of geometric mean functions, and operations that preserve convexity, e.g., nonnegative weighted sums and pointwise maximum, are used to verify model convexity. For example, the battery mass model (4.55) is linear and the CVT cost model (4.52) is quadratic. A quadratic-over-linear term is used in the EM loss model (4.29). This optimization problem is solved by using SDPT3 [206]. Implementation of the co-design optimization method is provided in Appendix F.

4.5 Optimization results and discussion

4.5.1 Control and design freedom

The co-design optimization method tends to obtain a globally optimal solution by simultaneously optimizing the design and control variables to minimize the TCO. As

illustrated in Figure 4.16, the EM operation in S_1 is relatively fixed, which has no control freedom because of the fixed gear ratio. The EM has to operate according to the driving conditions, which can hardly be efficient in consideration of real-world dynamic behavior. In contrast, the EM in S_2 has relatively more freedom to adjust operating points to reduce the power dissipation, by changing the speed ratio of the CVT, depending on the loading conditions. Yet, implementing the standard CVT controllers developed for conventional vehicles (with internal combustion engine) would reduce only the EM power losses (Section 4.2), regardless of the CVT efficiency. While the EM operation in S_2 is efficient, which follows its OOL, the system (combined EM and CVT) is not able to operate efficiently over a dynamic cycle (WLTC). The combined EM and transmission losses are thus higher in S_2 than that in S_1, as shown in Figure 4.17. The co-design optimization strategy, however, takes full advantage of control freedom (continuous ratio adjustment depending on the driving conditions) provided by the CVT. Specifically, apart from the EM power dissipation, the CVT power losses are also monitored in S_3. The CVT speed ratio over time γ_v (4.17) is selected to improve the overall system efficiency. Ratio variation that results in a higher loss is penalized. Smooth ratio change improves efficiency, drivability and reduced ELOP power losses. This effect can be seen in Figure 4.17, where the CVT power dissipation in S_3 is significantly lower than that in S_2 and the system efficiency is higher. The EM efficiency is also high in S_3, as demonstrated in Figure 4.16.

Additionally, the control freedom offered by the CVT creates design flexibility, which is not explored by S_2, as the component sizes are fixed. The design space is larger in S_3, with different combinations of CVT (4.19) and EM (4.28) sizes, which bring opportunities of optimizing the system from design perspective. The optimal component sizes, namely the right combination of the scaling factor for the battery (s_b^o), scaling factor for the EM (s_τ^o) and the ratio coverage of the CVT (s_γ^o), are eventually determined by the co-design optimization method based on the coupling between the EM and CVT, cost function, and the drive cycle.

As shown in Table 4.1, the maximum EM torque is reduced from $s_\tau = 1$ in S_1 and S_2 to $s_\tau = 0.79$ in S_3. Reduced EM torque and increased base speed decrease the EM losses (Figure 4.16). The optimal battery size is found and the number of battery cells is reduced because of improved efficiency. The EM in S_3 has the same maximum power as the other systems. Because the same EM from the SST-based EV on the market (S_1) is utilized in S_2, which is not optimized for the CVT application. Even if the EM is made smaller in S_2, the overall system efficiency is not necessarily always be higher, see Figure 4.9 about the OOL, as the CVT efficiency is not considered.

This reduced EM size is achieved due to a variable ratio coverage. The right ratio coverage of the CVT can also thus be determined in combination with the EM size in terms of torque and power. It is reduced from [0.7,2.63] with a ratio coverage of 3.76 before optimization to [0.7,2.34] with a ratio coverage of 3.34 after optimization. In S_2, the CVT is oversized considering the WLTC. First, the CVT used in S_2 is based on an off-the-shelf component, which is not optimized. Second, the CVT is controlled only to reduce the EM power dissipation, regardless of the CVT size. The system

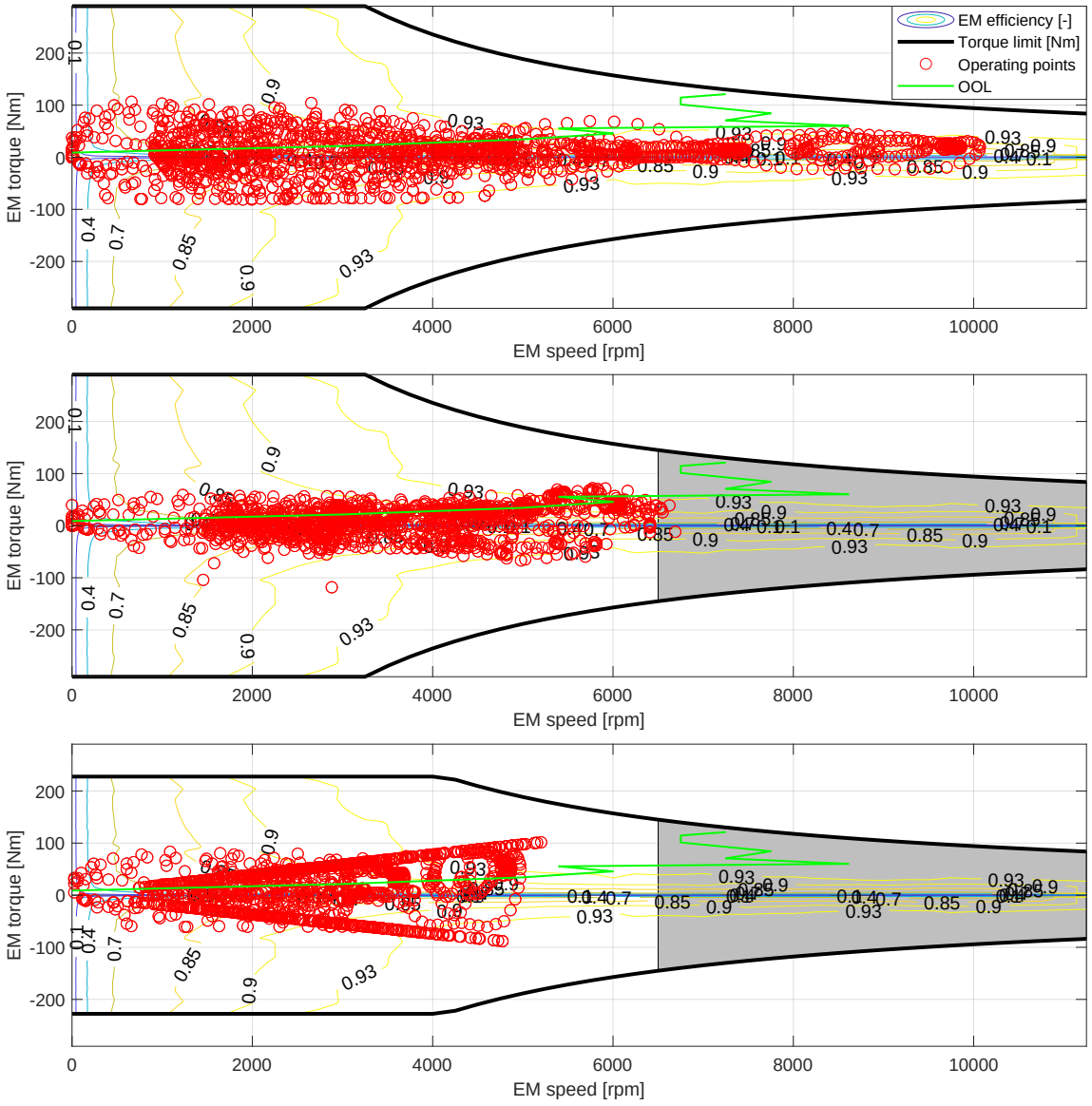

Figure 4.16: EM operating points on the WLTC. (**Top** to **bottom**) S_1, S_2, and S_3.

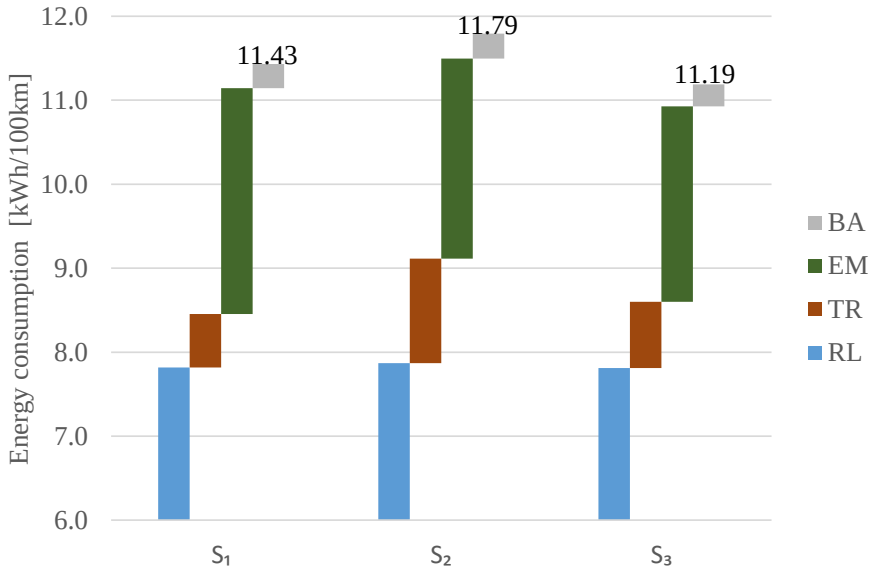

Figure 4.17: Comparison of energy consumption between S_1 (with a total vehicle mass of 1670 kg), S_2 (with a total vehicle mass of 1700 kg) and S_3 (with a total vehicle mass of 1666 kg) on the WLTC, where RL represents road load. The transmission (TR) losses include the ELOP power dissipation, which is zero in S_1. The EM power losses include the effect of the DC-AC inverter.

mass (Table 4.1) is thus reduced in S_3 due to the reduced component sizes, resulting in a decrease in power demand (Figure 4.17).

Table 4.1: Comparison of component parameters between S_1, S_2 and S_3.

Parameter	Unit	S_1	S_2	S_3
Transmission ratio	-	9.02	[4.47,16.8]	[3.5,11.68]
EM scaling factor	-	1	1	0.79
Battery cells	-	264	264	253
Maximum EM torque	Nm	290 ($\overline{\tau}_{\mathrm{m}}$)	290	228
EM base speed	rpm	3293 ($\omega_{\mathrm{m,b}}$)	3293	4188
Maximum EM power	kW	100 ($\overline{P}_{\mathrm{m}}$)	100	100
Curb weight	kg	1252 (m_{cw})	1252	1252
Transmission mass	kg	26 (m_{s})	56 ($\overline{m}_{\mathrm{c}}$)	52
EM mass	kg	74 ($\overline{m}_{\mathrm{m}}$)	74	58
Battery mass	kg	318 ($\overline{m}_{\mathrm{b}}$)	318	303
Driver mass	kg	90 (m_{d})	90	90

Owing to high CVT power losses in S_2, the energy consumption is reduced by around 3.1% in S_1. Compared with S_2, because of the reduction in the system power losses (Figure 4.17), the energy consumption is decreased by around 5.1% in S_3. The decrease in the CVT power dissipation contributes more to the energy saving. Given the component sizes, the component costs are calculated based on (4.52), (4.54) and (4.56). As shown in Figure 4.18, compared with S_1, the system cost is increased

by around 5.1% in S_2, as the CVT cost is higher than the SST price. Due to the reduction in the component sizes (Table 4.1), compared to S_1, the system cost is reduced by around 1.8% in S_3. Reduced EM torque decreases the EM mass and cost. The decrease in the battery and EM prices contributes more to the cost saving.

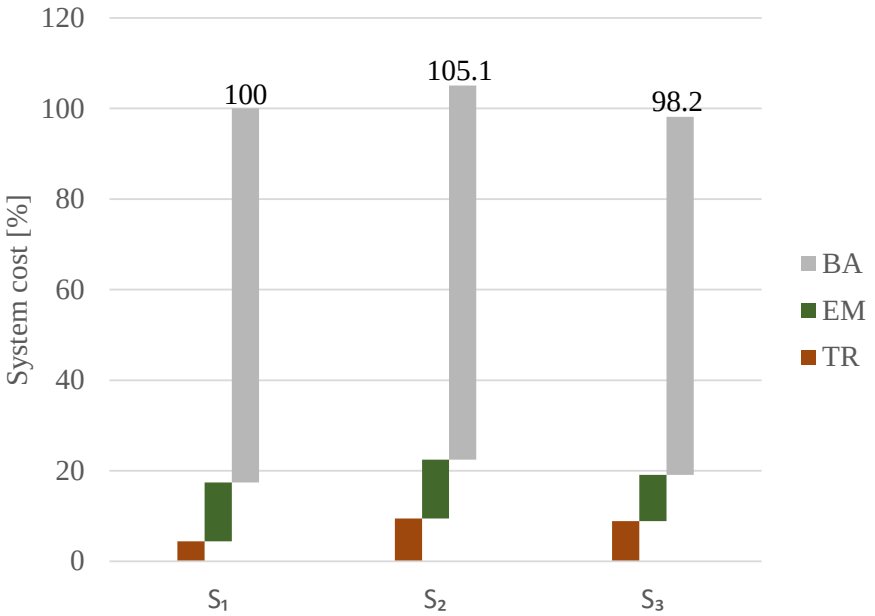

Figure 4.18: Comparison of normalized system cost between S_1, S_2 and S_3, where the EM cost includes the DC-AC inverter.

Overall, as shown in Figure 4.19, S_3 has the lowest TCO because of reduced energy consumption and system cost, which is around 2% lower than S_1. The optimization results demonstrate that the optimized EM-CVT system can be compact, lightweight, energy-efficient, and cost-effective, very different from its traditional image. Additionally, it can be suggested that automotive suppliers could greatly benefit from highly integrated components and systems to maximize their system efficiency and minimize cost targets. It can also be observed that for CVT-based EVs, reducing the maximum EM torque and increasing the base speed while having a higher slope of OOL compared with that of SST are beneficial. Most importantly, it shows the importance of cycle-driven (Section 4.3.2) and co-design (Section 4.4) in identifying the optimal control trajectories and component sizes. Specifically, it finds the trade-off between CVT power losses (4.22), CVT size (4.19), EM power losses (4.29), and EM size (4.28), based on the combined EM-CVT characteristics (Figure 4.8) and cost function (4.57).

4.5.2 Sequential design versus simultaneous design

The strength of co-design (simultaneous design in this case) lies in the fact that it finds the optimal design and control variables simultaneously to minimize the cost

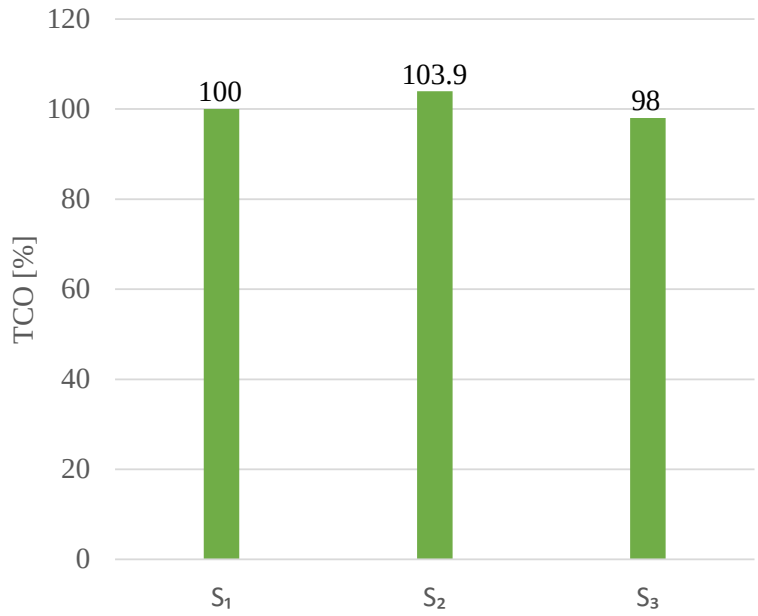

Figure 4.19: Comparison of normalized TCO between S_1, S_2 and S_3.

function for a strongly coupled problem, which is the case for the integration of the EM and CVT (Figure 4.1). The CVT speed ratio (control) influences the CVT and EM sizes (design/plant), and vice versa (e.g., (4.22) and (4.29)). The cost function, namely the minimization of the TCO (4.1), consists of the energy consumption (4.6) and system cost (4.7), and both are affected by the design and control variables. In order to demonstrate the effectiveness of the co-design approach in S_3, it is compared to a sequential design (SD) method. Background information on sequential approach can be found in Chapter 2. Note that for purposes of comparison, not all the plant parameters are predetermined. SD is defined as follows:

- SD: Based on S_3, assuming that the EM size is fixed (i.e., $s_\tau = 1$) in order to achieve the required performance (Section 4.1), the goal is to find the CVT speed ratio over time, CVT and battery size reducing the TCO.

Referring to (4.57), the corresponding cost function is given by

$$\min \sum_{k=1}^{N} \rho_{\mathrm{e}}\ P_{\mathrm{b}}(s_\gamma, s_{\mathrm{b}}, x(k), u(k) \mid s_\tau)\ \Delta t + \frac{S_{\mathrm{d}}}{S_{\mathrm{v}}}\ (C_{\mathrm{c}}(s_\gamma) + C_{\mathrm{m}} + C_{\mathrm{b}}(s_{\mathrm{b}})), \tag{4.58}$$

where C_{m} is a constant because of the fixed EM size. Other constraints remain the same, which can be found in Table F.1. The comparison between SD and S_3 is shown in Figure 4.20.

It can be seen from Figure 4.20 that the energy consumption and system cost are reduced in S_3 compared with SD. Overall, the TCO is decreased by around 3.4% in S_3. The primary reason is that the control and design freedom provided by the CVT cannot be fully exploited in SD because of the fixed EM size. Admittedly, the CVT is optimized in SD, especially the CVT cost because of a reduced ratio coverage of

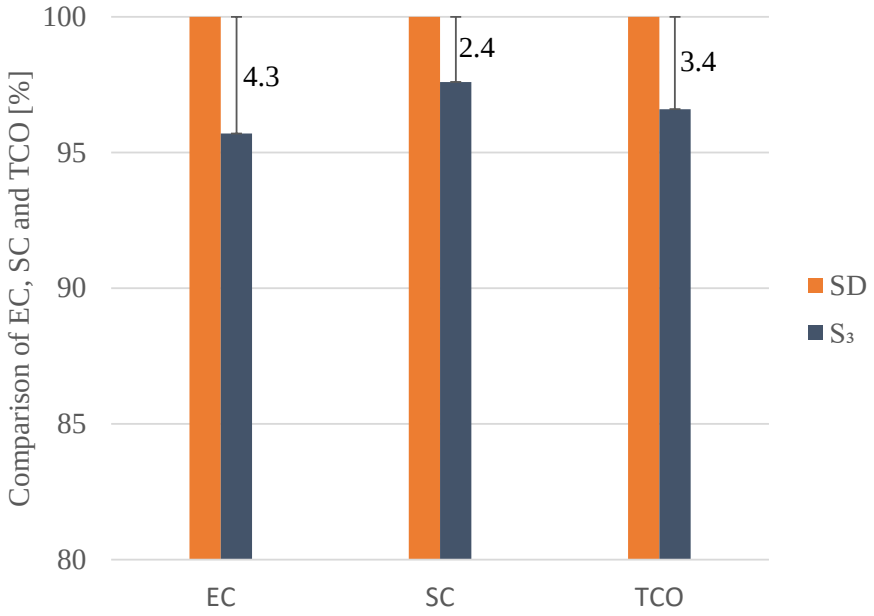

Figure 4.20: Comparison of normalized EC, SC and TCO between SD (with a total vehicle mass of 1677 kg) and S_3, where EC represents the energy consumption and SC the system cost.

around 2, which is significantly lower than that of 3.34 in S_3. Nevertheless, the EM and battery optimization are not taken into account, leading to a higher system cost. The control trajectory identified may not be efficient for the overall system. In SD, the problem is decoupled and the interconnections between the CVT (4.22), EM (4.29) and battery (4.40) are not considered, resulting in a higher TCO. For an inherently coupled problem (i.e., the integration of the EM and CVT), SD creates a separation and cannot guarantee an optimal solution. This issue is tackled by the co-design approach (S_3), where the right combination of the control policy and component sizes reducing the TCO is identified considering the coupling between the components from design and control perspectives.

4.5.3 Towards a low-power application

As illustrated in Figure 4.16, the usage of the available EM torque is low considering WLTC. It implies that powertrain components are typically oversized (considering WLTC) to meet certain vehicle performance requirements. The selection of electric powertrain components (e.g., EM) for future EV applications is still an ongoing question. Current selection criteria are largely based on performance requirements, such as top speed, acceleration time and gradability (Section 4.1), which usually lead to oversized components, considering drive cycles used for efficiency indicators. Therefore, even with the co-design approach, the downsizing potential is limited (Section 4.5.1). High performance, however, may not be required in urban driving. In order to see the downsizing potential, a low-power (LP) design is utilized as an example. Note that

for purposes of comparison, the EM design is not restricted by (4.27). LP is defined as follows:

- LP: Based on S_3, assuming that there are no performance requirements (Section 4.1), the aim is to find the optimal design and control variables reducing the TCO while satisfying drive cycle requirements.

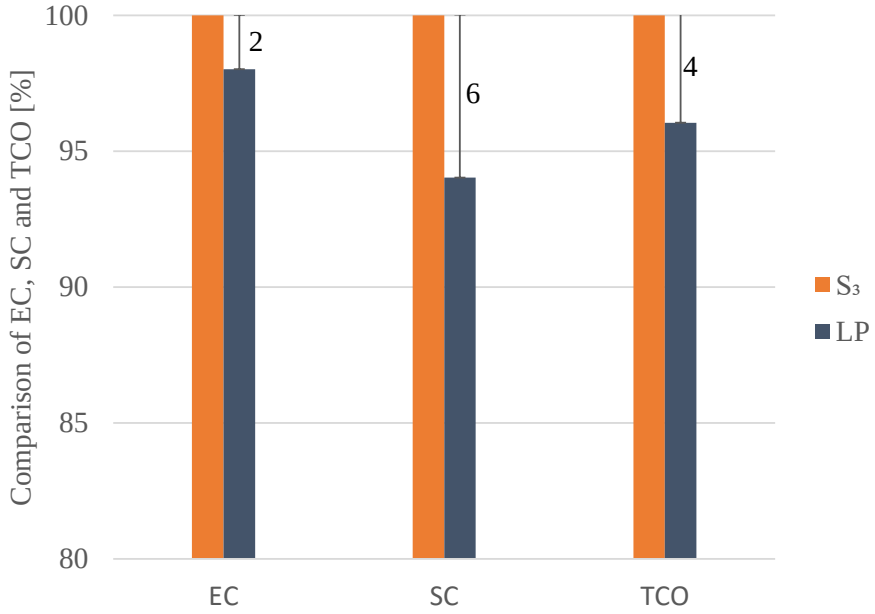

Figure 4.21: Comparison of normalized EC, SC and TCO between LP (with a total vehicle mass of 1635 kg) and S_3, where EC represents the energy consumption and SC the system cost.

The objective function in this case is similar to (4.57). The comparison between LP and S_3 is shown in Figure 4.21. It can be observed from Figure 4.20 that compared with LP, the energy consumption and system cost are decreased in S_3. Overall, in S_3, the TCO is reduced by around 4%. The main reason is that LP takes full advantage of the control and design freedom provided by the CVT without performance constraints. Compared to S_3, all the parameters as presented in Table 4.1, Figure 4.17 and Figure 4.18 are reduced in LP, e.g., the maximum EM power is reduced from 100 kW in S_3 to 54 kW in LP with a CVT ratio coverage of around 2.06. The battery size is decreased in LP as well. The minimum required component size is found in LP. For a specific use case (WLTC) and a given EM-CVT system (combined EM-CVT characteristics), there is a lower bound for the system (i.e., the CVT, EM and battery) so as to complete the driving mission. The result also demonstrates the importance of co-design optimization in determining the system size for a representative use case, considering the coupling between the EM and CVT (combined EM-CVT characteristics). Although reduction of peak power has a negative effect on vehicle performance (e.g., the 0-50 km/h and 0-100 km/h acceleration times of LP are around 6 s and 18 s, respectively), LP is energy-efficient and cost-effective, which can be used for urban driving that does not require high performance.

4.5.4 Thermal performance

The EM is a power source. It is also a heat source, and so does the transmission. They generate heat during operation, which needs to be taken away efficiently by a cooling system. For purposes of comparison, S_1, S_2 and S_3 have the same control target, maintaining the EM temperature below its thermal limit 65°C dictated by the manufacturer at the end of the drive cycle. All the other conditions are the same, including the coolant flow rate. For simplicity, the problem is translated to finding a constant air-flow rate for each system over the WLTC. Assume the air-flow rate is proportional to the cooling power consumption. They are compared in terms of cooling power consumption and temperature profile.

It is found that $\phi_{\mathrm{a}}(S_2) = 0.89\ \phi_{\mathrm{a}}(S_1)$, which means that compared to S_1, the cooling power consumption is reduced in S_2, as shown in Figure 4.22. Recall that the system losses are higher in S_2 (Figure 4.17). The EM power dissipation in S_2 is less than that in S_1 but the transmission power dissipation is much higher. In this case, the EM is more dominant in determining the level of the cooling power consumption. Another reason is that the thermal mass (EM and CVT) is higher in S_2 (Table 4.1). Moreover, because of topology difference, the extra small off-the-shelf heat exchanger in S_2 enables heat exchange between the EM and CVT and changes the overall thermal behavior of the cooling system. It is also calculated that $\phi_{\mathrm{a}}(S_3) = 0.78\ \phi_{\mathrm{a}}(S_2)$, which implies that compared to S_2, the cooling power consumption is decreased in S_3. They have the same topology. The primary reason is that the power losses are less in S_3, which requires less cooling power to remove the heat, although the system mass is reduced in S_3. The corresponding temperature profiles are illustrated in Figure 4.23.

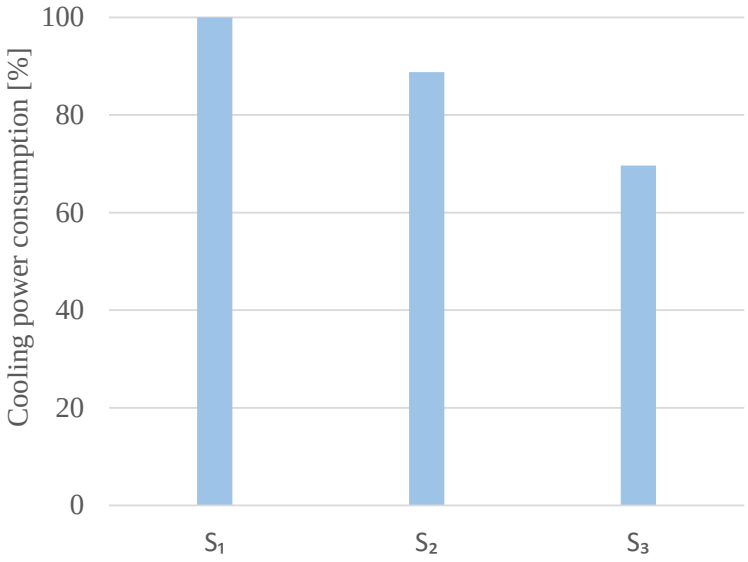

Figure 4.22: Comparison of normalized cooling power consumption between S_1, S_2 and S_3.

Additionally, an important finding from Figure 4.23 is that due to extra heat exchange between the EM and the CVT, provided by a small heat exchanger, the EM temperature

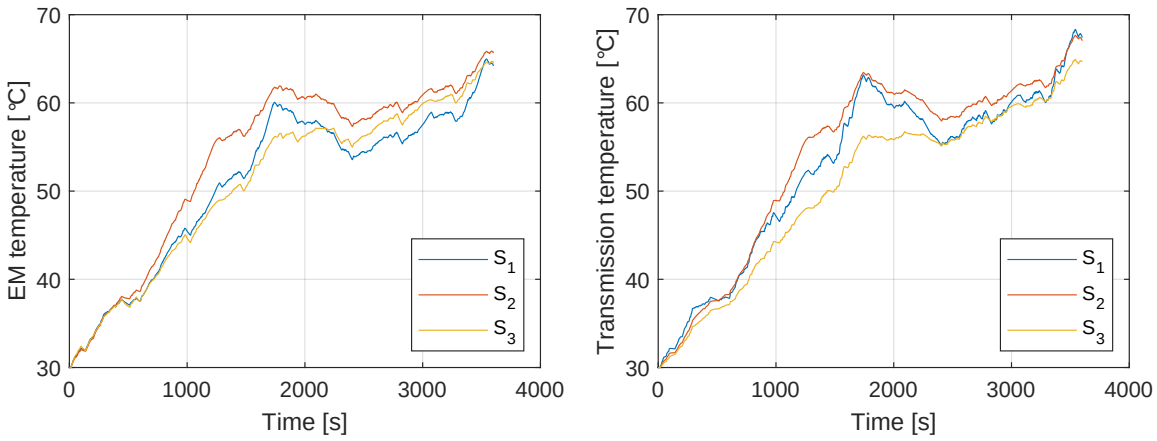

Figure 4.23: Comparison of temperature profile between S_1, S_2 and S_3.

and the CVT temperature are very similar in S_3. It is a crucial step towards a thermally integrated EM and CVT, for example, using a combined cooling loop with a dedicated cooling medium, taking into account such as corrosion, viscosity and conductivity [160–162]. It would make the system even more compact and efficient.

Note that as the systems overall are efficient, this amount of reduction will not significantly influence the total energy consumption, although depending on the use case. Furthermore, the exact value of cooling power is not provided, because detailed pump and fan signals are not available in the controller area network (CAN) data, as mentioned in Section 4.3.7. However, based on physics and model validation (Appendix C.4), the result is representative. Previously, it is shown that there is a strong coupling between the EM and CVT, and the combined system can be lightweight, efficient and low-cost. Now, it is demonstrated that they can also be integrated thermally, and a further reduction in weight, energy usage and cost can be expected. In the future, a highly integrated EM-CVT system can be anticipated for EV applications.

4.6 Conclusions

A co-design optimization method based on CP is proposed for a CVT-based EV to minimize the TCO, focusing on the integration of the EM and CVT. The co-design optimization method finds the optimal CVT speed ratio, air-flow rate of the cooling system, CVT size, EM size and battery size simultaneously, by taking full advantage of the control and design freedom provided by the CVT. The optimized system with the co-design approach decreases the TCO by around 2% compared with an SST-based EV with reference to a series production vehicle and by around 5.9% compared with a non-optimized CVT-based EV (based on off-the-shelf components). The advantages of the co-design approach are also highlighted by comparing to a sequential method. Moreover, for urban driving, insights into the design of a low-power EV are given based on the co-design approach, which finds the minimum required component size.

It can be concluded that although the current EV market is dominated by SSTs, multi-speed transmissions, e.g., CVTs, are competitive alternatives for EVs in terms of TCO, due to continuous ratio adjustment depending on driving conditions and the resulting design freedom. For EV applications, a highly and thermally integrated EM-CVT system, which is low-cost, efficient, and lightweight, can be anticipated.

Chapter 5

Conclusions and recommendations

This chapter presents the main conclusions of the thesis and gives recommendations for future developments.

5.1 Conclusions

This thesis has investigated design and control optimization methods for electrified powertrains considering both the energy and thermal domains. In Chapter 2, an extensive overview of design and control optimization layers and the related coordination schemes for electrified powertrains is provided. On the basis of the findings from Chapter 2, as electrified powertrains comprise hybrid electric vehicles (HEVs) and electric vehicles (EVs), two case studies are then carried out to show the effectiveness of the integrated design approach. In Chapter 3, from a control point of view, integrated energy and thermal management of a continuously variable transmission (CVT)-based plug-in HEV (PHEV) is explored, from which design considerations are also derived. In Chapter 4, from optimal design and control perspective, combined optimal design and control optimization of a CVT-based EV is investigated, which is extended by an integrated energy and thermal management design. In the introduction, three research questions have been posed. The answers to the research questions are given below.

5.1.1 Review of design and control of electrified vehicles

In the introduction, the first set of research questions of the thesis regarding the integrated design approach for electrified vehicles ($\boldsymbol{R}_{1a}$ and $\boldsymbol{R}_{1b}$) has been posed as follows:

- $\boldsymbol{R}_{1a}$: *What are the interconnections between the various optimization layers (i.e., topology, component size, and control), considering both the energy and thermal domains; and,*

- $\boldsymbol{R}_{1b}$: *How do they influence the optimality of an electrified vehicle design?*

The answer to the first set of research questions is summarized as follows: in Chapter 2, a comprehensive overview of design (topology and size) and control optimization layers and coordination schemes for electrified powertrains is presented. Both the energy and thermal domains are taken into account. The general problem of combined topology, size and control optimization is summarized mathematically. The relationships between different optimization levels are revealed. Energy saving and cost reduction can be achieved, by integrating these optimization layers. For optimality, nested and simultaneous approaches deliver superior performance to sequential and iterative ones, depending on the coupling and how sensitive the solution is to uncertainties in the design parameters. Nested coordination methods are often computationally heavy, whereas simultaneous schemes usually require convexification of the original problem. From control perspective, current energy and thermal management systems are classified into separate energy and thermal management systems (SETMSs) and combined energy and thermal management systems (CETMSs). In CETMSs, control decisions are made only once at the supervisory level, which outperform SETMSs with respect to energy efficiency improvement. These improvements are investigated in detail with examples. It is found that there is a trade-off between optimality, complexity, computation time, and causality. To reduce the total-cost-of-ownership (TCO) further, opportunities for future research are identified, such as utilizing waste heat recovery (WHR) systems, upgrading mechanical actuators, exchanging heat between powertrain components, and developing integrated plant and controller optimization methods.

5.1.2 Control of hybrid electric vehicles

In the introduction, the second research question of this thesis with respect to integrated energy and thermal management of HEVs ($\boldsymbol{R}_2$) has been posed as follows:

- $\boldsymbol{R}_2$: *What is the fuel efficiency improvement of using a DSWHR system comprising an EGWHR sub-system and an EPWHR sub-system in a CVT-based PHEV with cabin heating and cold-start conditions?*

The answer to this research question is given as follows: in Chapter 3, an integrated energy and thermal management system (IETMS) is proposed to quantify the impact of cold-start conditions on the fuel-saving potential and the benefit of employing WHR technologies on the ultimate fuel savings of a CVT-based PHEV with cabin heating. In cold-start conditions, the engine has to bring its thermal energy to the desired thermal energy level, leading to excess fuel consumption. The dual-source

waste heat recovery (DSWHR) system recovers waste heat from the engine exhaust gases and the electric path, which increases the battery energy content and decreases the battery load, resulting in additional fuel savings. The optimal solution is identified by using dynamic programming (DP). On the basis of validated component models, it is shown that a cold-start increases the fuel consumption significantly, up to around 7.1%, depending on the initial engine temperature. The DSWHR system improves the fuel economy remarkably, up to around 13.1%, which provides insights into the design of WHR technologies and the dimensioning of electrified powertrain components. During electric driving, waste heat from the electric path can be used to heat the engine to reduce the impact of a cold-start on the fuel consumption. Utilizing a small exhaust gas waste heat recovery (EGWHR) sub-system and a small electric path waste heat recovery (EPWHR) sub-system can obtain the same fuel economy as the ideal warm-start condition. The battery size can be reduced due to the recovered power from the DSWHR system. The cold impact and recovered power also depend on the driving conditions. The fuel saving of using the DSWHR system is even higher on a more aggressive drive cycle.

5.1.3 Co-design of electric vehicles

In the introduction, the third set of research questions of the thesis regarding integrated design and control of CVT-based EVs ($\boldsymbol{R}_{3a}$ and $\boldsymbol{R}_{3b}$) has been posed as follows:

- $\boldsymbol{R}_{3a}$: *What are the interconnections between the CVT and EM in an EV including the thermal domain; and,*

- $\boldsymbol{R}_{3b}$: *How can they be efficiently and optimally designed and controlled in order to minimize the TCO?*

The answer to the third set of research questions is summarized as follows: in Chapter 4, a convex programming (CP)-based co-design optimization approach is proposed for a CVT-based EV, concentrating on the integration of the electric machine (EM) and CVT. A single-speed transmission (SST)-based EV model in reference to a series production vehicle is firstly built, which is experimentally validated. A CVT-based EV model is then created on the basis of the SST-based EV model, where only the SST is replaced by a CVT (based on off-the-shelf component, which is not optimized). The CVT-based EV model is subsequently optimized with the co-design optimization method. Convexification procedures, especially the dependencies between the EM and CVT from design and control perspectives, are presented in detail. Although convex modeling introduces approximation error, it is small in this case due to the small discrepancy between the convex and original models based on measurements. The optimized system with the co-design method reduces the TCO by around 5.9% compared to the non-optimized CVT-based EV (based on off-the-shelf component) and by around 2% compared to the SST-based EV. The co-design optimization strategy identifies the optimal CVT speed ratio and air-flow rate of the cooling system to

reduce the TCO, by taking full advantage of the control and design freedom provided by the CVT. It simultaneously finds the optimal sizes of the battery, EM and CVT.

Moreover, the strengths of the co-design method are highlighted, by comparing with a sequential approach. For urban driving, insights into the design of a low-power EV are provided as well, which is energy-efficient and cost-effective. The results show that even though SSTs currently dominate the EV market, multi-speed transmissions, for example, CVTs, are suitable for EVs. A CVT can be a competitive alternative in terms of TCO, thanks to the continuous ratio adjustment functionality depending on the driving conditions and the resulting design freedom. The strong coupling between the EM and CVT recommends that these two components should be designed together by automotive suppliers. A highly and thermally integrated EM-CVT system that is efficient, affordable, and lightweight can thus be anticipated for EV applications.

5.2 Recommendations

This thesis has addressed various topics in optimal design and control of electrified powertrains. To further fulfill the potential of an electrified vehicle and reduce the TCO, the design and control optimization as presented in this thesis can be extended, by taking into account extra relevant aspects. Several research directions are identified below.

5.2.1 Design and control optimization

Based on the review in Chapter 2, it is found that integrated design and control of a complete electrified powertrain taking into account both the energy and thermal domains to reduce the TCO has yet to be addressed, while satisfying performance, driving comfort, passenger thermal comfort, and reliability requirements. In order to formulate this optimization problem, an integrated powertrain and thermal management configuration based on the latest technologies is required. There are many variants of this architecture. For example, different powertrain topologies would require distinct thermal management architectures. There are also many ways of exchanging heat between the powertrain components. An interesting extension to this thesis is to develop a tool, which automatically generates all possible and feasible powertrain and thermal management configurations for different applications. In order to select the best topology that results in the lowest TCO, the generated feasible powertrain and thermal management architectures should be evaluated. The objective is to find the trade-off between the energy consumption, system cost, passenger thermal comfort, reliability, vehicle performance, and driving comfort. It can provide insights into the design and control of electrified powertrains in an optimal manner.

5.2.2 Control optimization

In Chapter 3, the aim is to gain qualitative insights into the order of fuel savings that could be achieved on system level. Hence, detailed EGWHR and EPWHR models are not developed. A black-box approach is adopted instead, where lumped efficiencies are used. Furthermore, the cabin heating power is assumed to be a constant. Developing detailed WHR and cabin models is recommended for future work. Including the dynamics and constraints of the WHR and cabin systems in the optimization problem may change the control decision of the energy and thermal controller, resulting in different fuel savings. A cost-benefit analysis would also be required for the DSWHR system.

Moreover, a framework for designing complete energy consumption minimization strategy (CECMS) is created in Appendix B, which aims at minimizing the overall energy consumption, including WHR, transient, and steady-state thermal behavior. This strategy obtains a close-to-optimal solution and it is online implementable. But it is necessary to implement the CECMS with a case study to verify its optimality, by using DP as a baseline. A sensitivity analysis of the co-states should also be conducted in the presence of driving condition uncertainties.

5.2.3 Design optimization

In Chapter 4, for the purpose of this study, decreasing the maximum EM torque and increasing the EM base speed are taken into account. To better represent the EM dynamics depending on the size in reality, an extension to the current study is to investigate other scaling techniques for the EM, for example, axial scaling, radial scaling, and rewinding. This would influence the control and design. Moreover, implementing a combined EM-CVT cooling circuit with a dedicated cooling medium is recommend to identify its energy-saving potential compared with current thermal management topologies. Additionally, electric oil pump (ELOP) sizing can also be included in the optimization problem and finding the right size for an application would further increase the overall driveline efficiency.

Appendix A

Dynamic programming

Given a system, dynamic programming (DP) can be employed to find the optimal control input by minimizing a cost function. The main ingredients of a DP problem are summarized here, and interested readers are referred to [10, 58], where a rigorous treatment of this subject is given. Considering a discrete-time dynamic system:

$$x_{k+1} = f_k(x_k, u_k, w_k), k = 0, 1, ..., N-1, \tag{A.1}$$

where k represents discrete time, $x_k \in X_k$ the state of the system, $u_k \in U_k$ the control input, w_k the disturbance, N the control horizon, and f_k the system update.

Let the initial condition be x_0. The cost of using a specific control policy $\pi = \{\mu_0, \mu_1, \mu_2..., \mu_{N-1}\}$ on the system is written as

$$J_\pi(x_0) = g_N(x_N) + \sum_{k=0}^{N-1} g_k(x_k, \mu_k, w_k). \tag{A.2}$$

The optimal sequence π^o is the one that minimizes J_π:

$$J^o(x_0) = \min_{\pi \in \Pi} J_\pi(x_0), \tag{A.3}$$

where Π represents all admissible sequences.

Next, suppose a given state x_i occurs at time i. The cost-to-go from time i to time N can be expressed as

$$J_\pi(x_i) = E\left\{ g_N(x_N) + \sum_{k=i}^{N-1} g_k(x_k, \mu_k(x_k), w_k) \right\}. \tag{A.4}$$

The truncated policy $\pi^o(x_i) = \{\mu_i^o, \mu_{i+1}^o, \mu_{i+2}^o, ...\mu_{N-1}^o\}$ is the optimal solution for this sub-problem. This is Bellman's principle of optimality.

Assume w_k is known in advance, referring to deterministic dynamic programming (DDP). For every x_0, $J^o(x_0)$ is equal to $J_0(x_0)$, which is given by the last step of the

algorithm described below. Proceeding backwards, the terminal cost is calculated by

$$J_N(x_N) = g_N(x_N). \tag{A.5}$$

Then, the intermediate step is computed by

$$J_k(x_k) = \min_{u_k \in U_k(x_k)} g_k(x_k, u_k) + J_{k+1}(f_k(x_k, u_k)). \tag{A.6}$$

Moreover, if $u_k^{\mathrm{o}} = \mu_k^{\mathrm{o}}(x_k)$, which minimizes (A.6) for each x_k and k, the control sequence $\pi^{\mathrm{o}} = \{\mu_0^{\mathrm{o}}, \mu_1^{\mathrm{o}}, ..., \mu_{N-1}^{\mathrm{o}}\}$ is optimal.

Appendix B

Towards an online implementable strategy

It is known that the computation time of dynamic programming (DP) increases exponentially with the number of states (e.g., thermal states), the so-called curse of dimensionality [58]. Furthermore, DP demands that the driving profile is known a priori, which is not implementable. In real situations, driving conditions are not available in advance, which requires the control strategy to calculate the solution online. Therefore, it is important to devise an online implementable strategy that preserves optimality, taking into consideration both energy and thermal aspects. This is realized by establishing relationships between DP, Pontryagin's minimum principle (PMP), and equivalent consumption minimization strategy (ECMS).

B.1 Dynamic programming

DP offers sufficient conditions for the global optimality and provides insights into the design of an online energy and thermal management system. In DP, the optimal control policy is found using an exhaustive search by evaluating the following value function, referring to (3.53), in which the dynamic states are embedded,

$$\begin{aligned} \min_{u(k)\in\mathcal{U}}: \quad J(x(k),k) = \Bigg\{ & G(x(k_n),k_n) \\ & + \sum_{k_0}^{k_{n-1}} (1 + c_{\mathrm{e},1}\ (\overline{\theta}_{\mathrm{e}} - \theta_e(k))\ e^{c_{\mathrm{e},2}\ (\overline{\theta}_{\mathrm{e}} - \theta_{\mathrm{e}}(k))})\ \Delta m_{\mathrm{f}}(k)\ \Delta t\ H_{\mathrm{l}} \Bigg\}, \end{aligned} \tag{B.1}$$

where $\mathcal{U}$ represents the admissible controls and $G(x(k_n), k_n)$ represents the terminal cost. The intermediate cost can be calculated by

$$J(x(k),k) = \min_{u(k)\in\mathcal{U}} \Big\{ J(x(k+1),k+1) + (1 + c_{\mathrm{e},1}\ (\overline{\theta}_{\mathrm{e}} - \theta_{\mathrm{e}}(k))\ e^{c_{\mathrm{e},2}\ (\overline{\theta}_{\mathrm{e}} - \theta_{\mathrm{e}}(k))})\ \Delta m_{\mathrm{f}}(k)\ H_{\mathrm{l}} \Big\}. \tag{B.2}$$

B.2 Pontryagin's minimum principle

Mathematically, DP, which is a numerical representation of the Hamilton–Jacobi–Bellman (HJB) equation, has a close relation with PMP, which originates from the Calculus of Variations [88]. The computing time is reduced significantly, as PMP evaluates second-order differential equations. Note that PMP yields necessary conditions that the optimal solution must satisfy. Using convex models (which can be derived from the nonlinear models described in Section 3.3) and a convex cost formulation the existence of sufficient conditions for global optimality can be proved. Moreover, in the context of energy management problems, the solution computed is very close to the DP outcome, as made evident by [88]. The optimal control law minimizes the Hamiltonian function at each instant,

$$H(x(k),\lambda(k),u(k),k) \geq H(x(k),\lambda(k),u^{\mathrm{o}}(k),k), \tag{B.3}$$

where λ represents the co-state vector. Traditionally, the Hamiltonian comprises a cost criterion (e.g., the fuel power (B.1)), and the battery dynamics (3.51), which strikes the balance between the fuel consumption and the battery electricity. In the presence of the engine thermodynamics (3.35) corresponding to cold-start conditions, the engine heating cost is added to the Hamiltonian. The extended PMP can be formulated as

$$\begin{aligned} H =& (1 + c_{\mathrm{e},1}\ (\overline{\theta}_{\mathrm{e}} - \theta_{\mathrm{e}}(k))\ e^{c_{\mathrm{e},2}\ (\overline{\theta}_{\mathrm{e}} - \theta_{\mathrm{e}}(k))})\ \Delta m_{\mathrm{f}}(k)\ H_{\mathrm{l}} \\ &+ \lambda_{\xi}(k)\ \dot{\xi}(k) + \lambda_{\theta_{\mathrm{e}}}(k)\ \dot{\theta}_{\mathrm{e}}(k), \end{aligned} \tag{B.4}$$

where the co-state λ_{ξ} can be interpreted as the weight of the battery electricity. In this case, the price of using the battery is reduced, due to the DSWHR system. Normally, necessary conditions for solution optimality reduce the original optimization problem to a boundary value problem, which is then solved by a shooting algorithm [207]. The initial values of the co-states, thus, play a crucial role in obtaining the optimal solution. In charge sustenance mode, the battery operates in a very narrow range, which implies that the open circuit voltage and the internal resistance are almost constants [139]. Hence, the state-of-charge (SOC) dynamics $\dot{\xi}$ does not depend on the SOC itself, giving

$$\frac{\mathrm{d}\lambda_{\xi}}{\mathrm{d}k} = -\frac{\partial H}{\partial \xi} = 0. \tag{B.5}$$

Therefore, λ_{ξ} is a constant, which is equal to the initial value (i.e., $\lambda_{\xi}(k) = \lambda_{\xi}(k_0)$). Similar to the approach used in [208, 209], the initial co-state can be obtained from

the DP results, which can be computed by

$$\lambda_{\xi}(k) = -\frac{1}{V_{\mathrm{b}}\ Q_{\mathrm{b}}}\ \frac{\partial J(\xi, \theta_{\mathrm{e}}, k)}{\partial \xi}\bigg|_{\xi^{\mathrm{o}}(k), \theta_{\mathrm{e}}^{\mathrm{o}}(k), k}. \tag{B.6}$$

Equation (B.6) generates the trace of the SOC, which is expected to fluctuate around a constant, and this reference value can be calculated in a least-squares sense. While λ_{ξ} is typically a constant, the co-state of the engine temperature changes over time. For instance, as the engine temperature increases, the heating cost decreases. The engine temperature trajectory can also be attained from the DP algorithm; that is,

$$\lambda_{\theta_{\mathrm{e}}}(k) = -\frac{1}{c_{\mathrm{h}}\ c_{\mathrm{e}}\ m_{\mathrm{e}}}\ \frac{\partial J(\xi, \theta_{\mathrm{e}}, k)}{\partial \theta_{\mathrm{e}}(k)}\bigg|_{\xi^{\mathrm{o}}(k), \theta_{\mathrm{e}}^{\mathrm{o}}(k), k}. \tag{B.7}$$

Denote the heating interval as $[k_0, k_w]$ and the warm interval as $[k_w, k_n]$. The engine temperature is represented by $\theta_{\mathrm{e,w}}$ during the warm interval and k_w represents the time instant when the engine temperature reaches its operating temperature for the first time. As the engine temperature increases and reaches its operating temperature, the cold impact vanishes and the corresponding co-state value approaches zero; that is

$$\lambda_{\theta_{\mathrm{e}}}(k_{\mathrm{w}}) = 0. \tag{B.8}$$

The relationship between the co-state $\lambda_{\theta_{\mathrm{e}}}$ and the engine temperature can be identified through post-analysis (referring to Section 3.5.2) by utilizing polynomial functions:

$$\lambda_{\theta_{\mathrm{e}}} = a_{\mathrm{n}}\ \theta_{\mathrm{e}}^{n} + a_{\mathrm{n}-1}\ \theta_{\mathrm{e}}^{n-1} + ... + a_0, \tag{B.9}$$

where a_{n}, $a_{\mathrm{n}-1}$, and a_0 are the fitting coefficients. The co-state values of the engine temperature can be pre-calculated and stored.

B.3 Complete energy consumption minimization strategy

It should be noted that PMP still demands the future drive cycle to be given beforehand. To deal with driving condition uncertainties, ECMS, which is essentially derived from PMP, is often used; in which, the battery electricity is translated into its equivalent fuel cost [70]. ECMS and PMP share almost the same structure, with the equivalence factors being the co-states [210]. Admittedly, it is difficult to use ECMS as an online strategy to replicate the optimal solution obtained from PMP. Nevertheless, a close-to-optimal solution can be expected. Using results from DP and PMP, this study proposes a complete energy consumption minimization strategy (CECMS) framework, including both energy and thermal aspects. As the driving condition is not known in advance, the equivalence factor λ_{ξ} changes over time; furthermore, λ_{ξ} can be regulated with a PI controller [211], by tracking a reference,

$$\lambda_{\xi}(k) = \lambda_{\xi}(k_0) - k_{\xi,\mathrm{p}}\ (\xi(k) - \xi_{\mathrm{r}}) - k_{\xi,\mathrm{i}}\ \int_{k_0}^{k_n} (\xi(\lambda_{\xi}) - \xi_{\mathrm{r}})\ \mathrm{d}\lambda_{\xi}, \tag{B.10}$$

where $k_{\xi,\mathrm{p}}$ and $k_{\xi,\mathrm{i}}$ are the proportional and integral gains of λ_ξ, respectively. The reference value can be chosen as the final SOC, which is equal to the initial SOC. More advanced adaptation methods can be found in [212, 213]. The co-state of the engine temperature can be retrieved from the pre-stored tables, as mentioned above. Note that, so far, only the transient behavior of the engine—namely, the cold interval—has been taken into consideration. For the warm interval, it is assumed that $\theta_{\mathrm{e,w}} = 80$ °C for $[k_w, k_n]$. In practice, however, the engine temperature often fluctuates around the operating temperature, and the temperature variation corresponds to the energy consumption of the cooling system. The power request is non-negligible and should be determined at the supervisory level. In contrast, conventional control strategies treat them separately, where the energy management system and the engine cooling system are not combined. The goal of the integrated controller is to keep the engine temperature as close as possible to the operating temperature with minimum power consumption. The equivalence factor of the warm interval is different from that of the cold period, which can be updated by

$$\lambda_{\theta_{\mathrm{e,w}}}(k) = \theta_{\mathrm{e}}(k_{\mathrm{w}}) - k_{\mathrm{e,p}}\ (\theta_{\mathrm{e,w}}(k) - \theta_{\mathrm{e,r}}) - k_{\mathrm{e,i}}\ \int_{k_w}^{k_n} (\theta_{\mathrm{e,w}}(\lambda_{\theta_{\mathrm{e,w}}}) - \theta_{\mathrm{e,r}})\ \mathrm{d}\lambda_{\theta_{\mathrm{e,w}}}, \quad \text{(B.11)}$$

where $k_{\mathrm{e,p}}$ and $k_{\mathrm{e,i}}$ are the proportional and integral gains of $\lambda_{\theta_{\mathrm{e,w}}}$, respectively. Initially, when the engine temperature is lower than the desired temperature $\overline{\theta}_{\mathrm{e}}$, it follows the temperature dynamics of (3.35). Once the operating temperature is reached, assume that its dynamics are subject to $\dot{\theta}_{\mathrm{e,w}}$, where the cooling power is considered. Moreover, a new control input is added to the control vector, which controls the actuator of the cooling system, associated with the cooling power consumption [138]. The optimization problem during the warm interval is formulated as

$$H(\xi, \theta_{\mathrm{e,w}}, \lambda_\xi, \lambda_{\mathrm{e,w}}, u, k) = \Delta m_{\mathrm{f}}(k)\ H_{\mathrm{l}} + \lambda_\xi\ \dot{\xi} + \lambda_{\theta_{\mathrm{e,w}}}\ \dot{\theta}_{\mathrm{e,w}}, \quad \text{(B.12)}$$

where $\dot{\theta}_{\mathrm{e,w}}$ represents the corresponding cooling power consumption. Therefore, in reality, in order to achieve optimal performance, the CECMS is defined as

$$H = \begin{cases} (1 + c_{\mathrm{e},1}\ (\overline{\theta}_{\mathrm{e}} - \theta_{\mathrm{e}}(k))\ e^{c_{\mathrm{e},2}\ (\overline{\theta}_{\mathrm{e}} - \theta_{\mathrm{e}}(k))})\ \Delta m_{\mathrm{f}}(k)\ H_{\mathrm{l}} \\ \quad + \lambda_\xi\ \dot{\xi} + \lambda_{\theta_{\mathrm{e}}}\ \dot{\theta}_{\mathrm{e}}, \text{if } k \in [k_0, k_w], \\ \Delta m_{\mathrm{f}}(k)\ H_{\mathrm{l}} + \lambda_\xi\ \dot{\xi} + \lambda_{\theta_{\mathrm{e,w}}}\ \dot{\theta}_{\mathrm{e,w}}, \text{if } k \in [k_w, k_n]. \end{cases} \quad \text{(B.13)}$$

The control variable is decided by

$$u(k) \in arg\min_{u \in \mathcal{U}^{\mathrm{ad}}} H(\xi, \theta_{\mathrm{e}}, \theta_{\mathrm{e,w}}, \lambda_\xi, \lambda_{\theta_{\mathrm{e}}}, \lambda_{\theta_{\mathrm{e,w}}}, u, k). \quad \text{(B.14)}$$

Since the optimal solution is found offline in Section 3.5, to preserve optimality and enable online implementation, a CECMS framework considering both energy and thermal domains is proposed, by establishing relationships between DP, PMP, and ECMS. The real-time implementable CECMS make decisions (e.g., on the power split and heating/cooling power) only once at the supervisory level to minimize the overall energy consumption, which can also be extended to consider multiple thermal systems.

Appendix C

SST-based EV model

The single-speed transmission (SST)-based EV model (S_1) is validated by measurement data obtained from a series production vehicle driven on a real-world drive cycle, namely intercity drive cycle (ICDC). The measurement data are extracted from the controller area network (CAN) signals of the vehicle control unit (VCU) in the series production vehicle driven on the ICDC. The sampling time is 0.01 s. The vehicle specification is provided in Table G.1.

C.1 Longitudinal dynamics

The drive cycle introduced in Section 4.3.2 is also used in S_1. Given the drive cycle represented by vehicle velocity v_v and acceleration a_v and taking into account aerodynamic drag force, rolling resistance, and inertia force, the demanded wheel torque τ_w and speed w_w can be calculated by

$$\tau_\mathrm{w}(k) = \left(\frac{1}{2}\ \rho_\mathrm{a}\ c_\mathrm{d}\ A_\mathrm{f}\ v_\mathrm{v}^2(k) + c_\mathrm{r}\ m_\mathrm{v}\ g\ \mathrm{sign}(v_\mathrm{v}(k)) + \left(m_\mathrm{v} + 4\ \frac{J_\mathrm{w}}{r_\mathrm{w}^2}\right)\ a_\mathrm{v}(k)\right)\ r_\mathrm{w}, \quad \text{(C.1)}$$

$$\omega_\mathrm{w}(k) = \frac{v_\mathrm{v}(k)}{r_\mathrm{w}}, \quad \text{(C.2)}$$

where the total vehicle mass m_v is given by

$$m_\mathrm{v} = m_\mathrm{cw} + m_\mathrm{s} + \overline{m}_\mathrm{m} + \overline{m}_\mathrm{b} + m_\mathrm{d}, \quad \text{(C.3)}$$

where m_s is the SST mass (Table 4.1).

C.2 Single-speed transmission

The SST including the final drive provides a fixed speed ratio γ_s between the EM and the wheel. To meet the torque and speed at the wheels given by (C.1) and (C.2), the required torque and speed of the SST are obtained by

$$\tau_\mathrm{s}(k) = \begin{cases} \frac{\tau_\mathrm{w}(k)}{\eta_\mathrm{s}\ \gamma_\mathrm{s}}, & \text{if } \tau_\mathrm{w}(k) > 0, \\ \frac{\eta_\mathrm{s}\ \tau_\mathrm{w}(k)}{\gamma_\mathrm{s}}, & \text{if } \tau_\mathrm{w}(k) \leq 0, \end{cases} \tag{C.4}$$

$$\omega_\mathrm{s}(k) = \gamma_\mathrm{s}\ \omega_\mathrm{w}(k), \tag{C.5}$$

where η_s is the combined efficiency of the fixed gear η_g and the final drive η_f.

C.3 Electric machine

The electric machine (EM) is a permanent magnet synchronous machine (PMSM), featuring motoring and generating modes. Its specification is provided in Table 4.1. The torque and speed of the EM are computed by

$$\tau_\mathrm{m}(k) = \tau_\mathrm{c}(k), \tag{C.6}$$

$$\omega_\mathrm{m}(k) = \omega_\mathrm{p}(k). \tag{C.7}$$

Given the same inputs (vehicle speed and acceleration) from the ICDC on which the series production vehicle is driven, the outputs of the EM from the developed model (simulation), namely the EM torque and speed, are compared with the corresponding CAN signals regarding EM torque and speed (measurement), as shown in Figure C.1 and Figure C.2, respectively. It should be noted that the measurement data are presented as they are in this study. In consideration of noise, driving environment, data recording, and effect of CAN signals, the simulation and measurement resemble well.

The mechanical power of the EM is then given by

$$P_\mathrm{m}(k) = \tau_\mathrm{m}(k)\ \omega_\mathrm{m}(k). \tag{C.8}$$

An efficiency map as shown in Figure C.3 is used to calculate the power losses of the EM, i.e.,

$$P_\mathrm{m,loss}(k) = P_\mathrm{m,loss}(\tau_\mathrm{m}(k), \omega_\mathrm{m}(k)). \tag{C.9}$$

Therefore, the electrical power supplied to/by the EM is expressed as

$$P_\mathrm{m,el}(k) = P_\mathrm{m}(k) + P_\mathrm{m,loss}(k). \tag{C.10}$$

The EM torque and speed are bounded by

$$\tau_\mathrm{m}(k) \in [\underline{\tau}_\mathrm{m}(\omega_\mathrm{m}(k)), \overline{\tau}_\mathrm{m}(\omega_\mathrm{m}(k))], \tag{C.11}$$

$$\omega_\mathrm{m}(k) \in [\underline{\omega}_\mathrm{m}, \overline{\omega}_\mathrm{m}]. \tag{C.12}$$

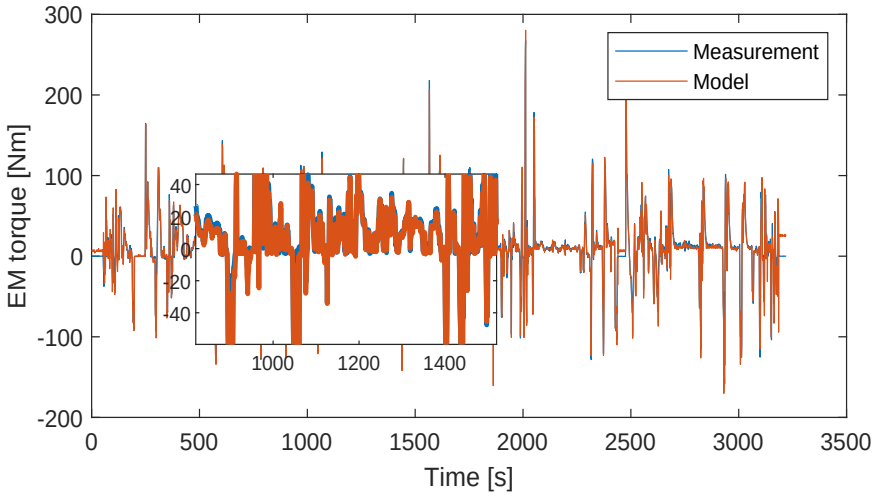

Figure C.1: Validation of the EM torque for the ICDC.

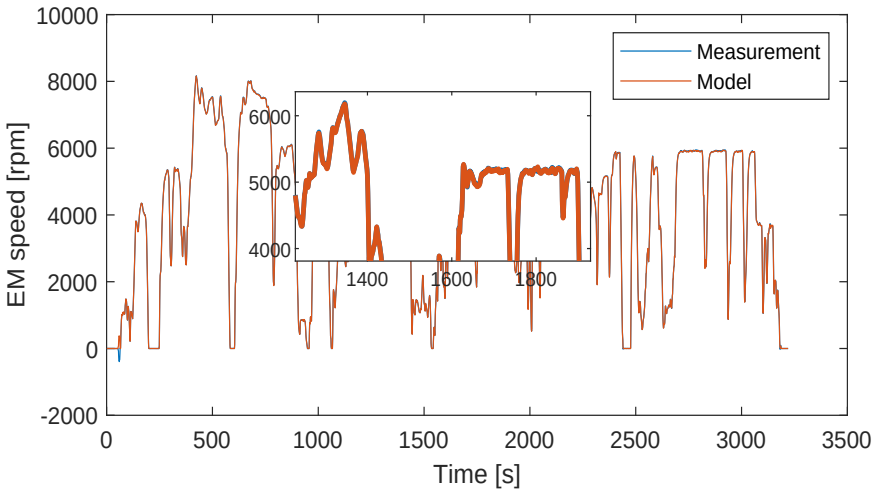

Figure C.2: Validation of the EM speed for the ICDC.

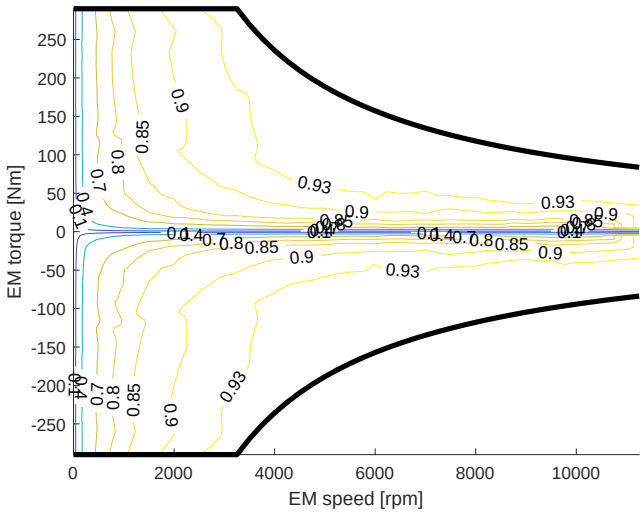

Figure C.3: Efficiency map of the EM including the DC-AC inverter.

C.4 Thermal EM-SST model

The SST ($P_{\mathrm{s,loss}}$) and EM ($P_{\mathrm{m,loss}}$) power losses appear as heat, which is removed by a thermal management system (TMS), as demonstrated in Figure C.4. The EM and the SST are physically attached, and the SST is cooled based on oil splashing, where its heat is taken away by the EM cooling medium indirectly and the ambient air directly due to convection. The EM dissipates heat to the ambient air. Moreover, the cooling medium driven by a pump removes heat from the EM. When the EM temperature is higher than a predefined threshold, the EM is cooled down with a radiator. The goal of the TMS is to maintain the EM temperature below its prescribed thermal limit. A lumped-parameter method is used to capture the thermal behavior of the EM and SST. On the basis of first principles, the thermal EM-SST model is described by

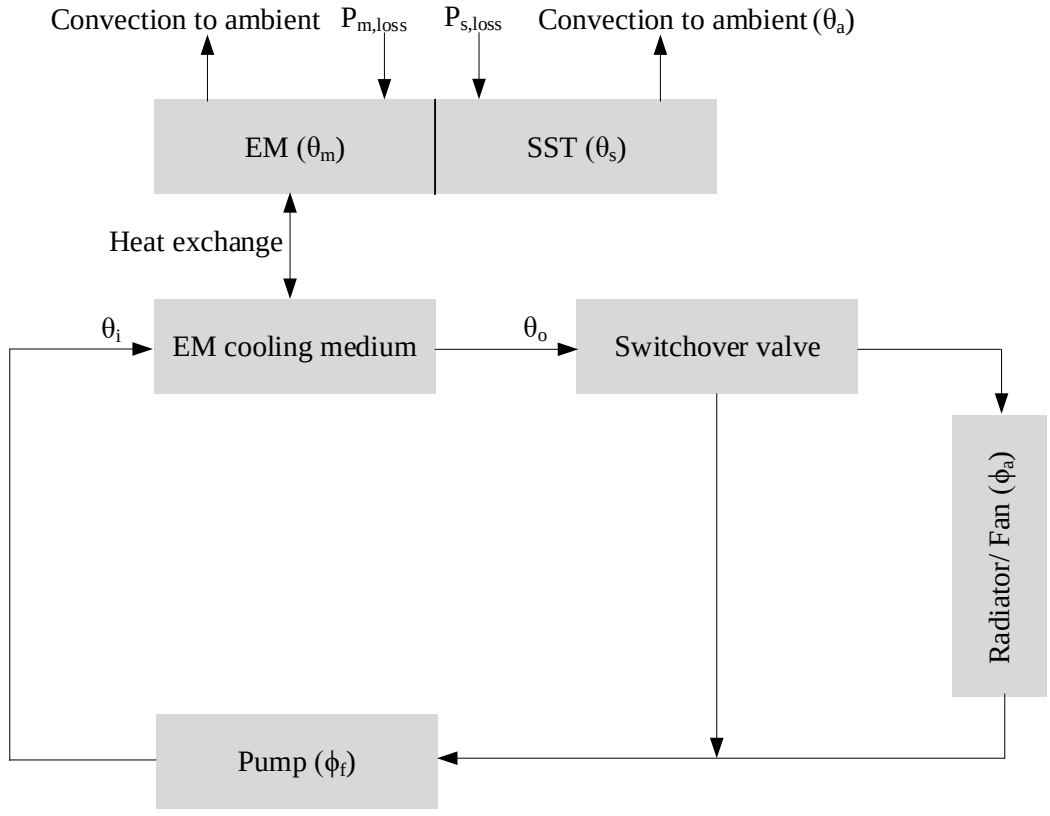

Figure C.4: Thermal management architecture for the EM-SST.

$$\begin{aligned} c_{\mathrm{m}}\ m_{\mathrm{m}}\ \dot{\theta}_{\mathrm{m}}(k) =& P_{\mathrm{m,loss}}(k) - h_{\mathrm{m}}\ A_{\mathrm{m}}\ (\theta_{\mathrm{m}}(k) - \theta_{\mathrm{o}}(k)) - k_{\mathrm{m}}\ (\theta_{\mathrm{m}}(k) - \theta_{\mathrm{s}}(k)) \\ & - h_{\mathrm{a}}\ A_{\mathrm{a}}\ (\theta_{\mathrm{m}}(k) - \theta_{\mathrm{a}}), \end{aligned} \tag{C.13}$$

$$c_{\mathrm{f}}\ m_{\mathrm{f}}\ \dot{\theta}_{\mathrm{o}}(k) = h_{\mathrm{m}}\ A_{\mathrm{m}}\ (\theta_{\mathrm{m}}(k) - \theta_{\mathrm{o}}(k)) - \phi_{\mathrm{f}}\ c_{\mathrm{f}}\ (\theta_{\mathrm{o}}(k) - \theta_{\mathrm{i}}(k)), \tag{C.14}$$

$$c_{\mathrm{h}}\ c_{\mathrm{s}}\ m_{\mathrm{s}}\ \dot{\theta}_{\mathrm{s}}(k) = P_{\mathrm{s,loss}}(k) + k_{\mathrm{m}}\ (\theta_{\mathrm{m}}(k) - \theta_{\mathrm{s}}(k)) - h_{\mathrm{c}}\ A_{\mathrm{c}}\ (\theta_{\mathrm{s}}(k) - \theta_{\mathrm{a}}), \tag{C.15}$$

$$c_{\mathrm{f}}\ m_{\mathrm{f}}\ \dot{\theta}_{\mathrm{i}}(k) = \phi_{\mathrm{f}}\ c_{\mathrm{f}}\ (\theta_{\mathrm{o}}(k) - \theta_{\mathrm{i}}(k)) - \epsilon\ \phi_{\mathrm{a}}(k)\ c_{\mathrm{a}}\ (\theta_{\mathrm{o}}(k) - \theta_{\mathrm{a}}). \tag{C.16}$$

The thermal EM-SST model is validated by measurement data. Since the SST temperature is not available in the CAN data, the EM temperature is used for validation. The measurement data are extracted from the CAN signal regarding the EM temperature of the VCU in the series production vehicle driven on the ICDC, as described in Appendix C. The estimated thermal parameters are provided in Table G.1. As shown in Figure C.5, a good resemblance can be seen between the model and measurement.

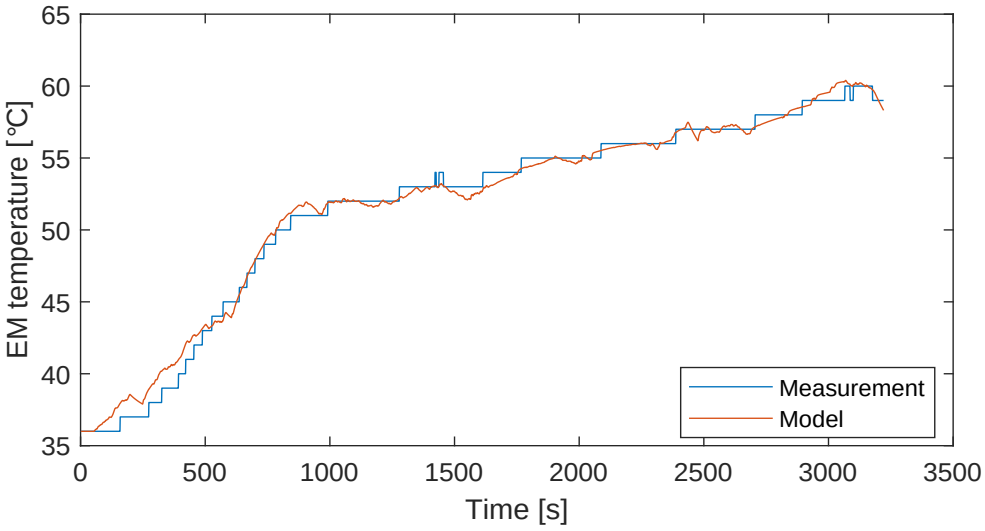

Figure C.5: Validation of the EM temperature for the ICDC.

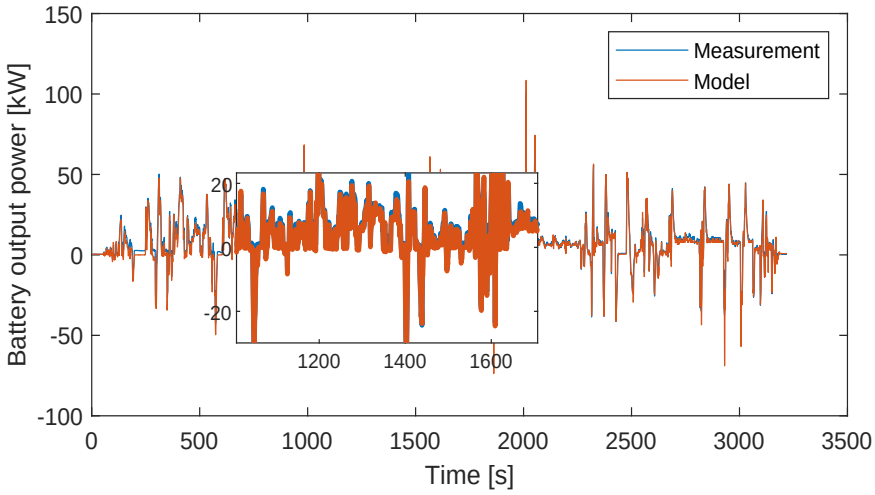

Figure C.6: Validation of the battery output power for the ICDC.

C.5 Battery

The battery provides the power required by the EM, i.e.,

$$P_{\mathrm{b}}(k) = P_{\mathrm{m,el}}(k), \tag{C.17}$$

$$\dot{E}_{\mathrm{b}}(k) = -P_{\mathrm{b}}(k). \tag{C.18}$$

For the same inputs from the ICDC on which the series production vehicle is driven, the battery output power from the model is compared to the corresponding CAN signal regarding the battery output power in terms of voltage and current (measurement). The comparison can be seen in Figure C.6, where the model and measurement resemble well.

Appendix D

CVT-based EV model

As presented in Section 4.1, a continuously variable transmission (CVT)-based EV model (S_2) is created based on S_1 (Appendix C). The main difference is that the SST model as described in Section C.2 is replaced by a CVT model and its associated electric oil pump (ELOP) model. The SST mass in (C.1) is replaced by $\overline{m}_{\mathrm{c}}$ (Table 4.1). The thermal model is the same as that in Section 4.3.7. All the other component models remain the same as S_1.

D.1 Continuously variable transmission

In this context, the variator of the pushbelt CVT has two pulleys, a primary pulley (subscript "p") and a secondary pulley (subscript "s"), which are connected by a pushbelt. The CVT provides a continuous variable speed ratio γ_{v} between the primary pulley and the secondary pulley, which permits the EM speed to be independent of the wheel speed to optimize its operating point. Given the required torque τ_{w} (C.1) and speed ω_{w} (C.2) at the wheels, the torque and speed of the primary pulley are obtained by

$$\tau_{\mathrm{p}}(k) = \begin{cases} \frac{\tau_{\mathrm{w}}(k)}{\eta_{\mathrm{f}}\ \gamma_{\mathrm{v}}(k)}, & \text{if } \tau_{\mathrm{w}}(k) > 0, \\ \frac{\eta_{\mathrm{f}}\ \tau_{\mathrm{w}}(k)}{\gamma_{\mathrm{v}}(k)}, & \text{if } \tau_{\mathrm{w}}(k) \leq 0, \end{cases} \tag{D.1}$$

$$\omega_{\mathrm{p}}(k) = \gamma_{\mathrm{v}}(k)\ \omega_{\mathrm{w}}(k), \tag{D.2}$$

The total torque input to the CVT is thus given by

$$\tau_{\mathrm{c}}(k) = \tau_{\mathrm{p}}(k) + \tau_{\mathrm{c,loss}}(k), \tag{D.3}$$

where $\tau_{\mathrm{c,loss}}$ represents the torque loss in the CVT, which is described by a lookup table, as shown in Figure D.1, i.e.,

$$\tau_{\mathrm{c,loss}}(k) = \tau_{\mathrm{c,loss}}(\tau_{\mathrm{p}}(k), \omega_{\mathrm{p}}(k), \gamma_{\mathrm{v}}(k)). \tag{D.4}$$

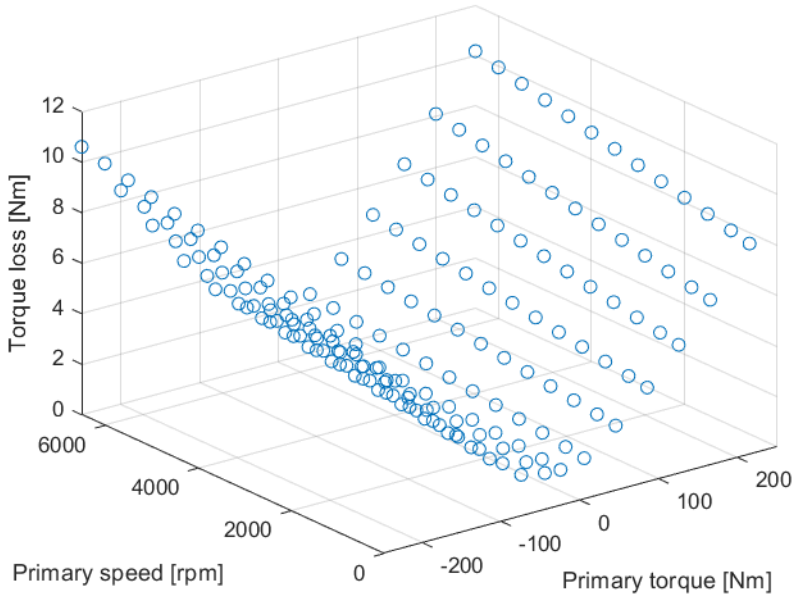

Figure D.1: CVT torque loss at $\gamma_v = 0.7$.

The power losses of the CVT can thus be calculated by

$$P_{\mathrm{c,loss}}(k) = \tau_{\mathrm{c,loss}}(\tau_{\mathrm{p}}(k), \omega_{\mathrm{p}}(k), \gamma_{\mathrm{v}}(k))\ \omega_{\mathrm{p}}(k). \tag{D.5}$$

The primary torque and speed ratio are constrained by

$$\tau_{\mathrm{p}}(k) \in [\underline{\tau}_{\mathrm{p}}, \overline{\tau}_{\mathrm{p}}], \tag{D.6}$$

$$\gamma_{\mathrm{v}}(k) \in [\underline{\gamma}_{\mathrm{v}}, \overline{\gamma}_{\mathrm{v}}], \tag{D.7}$$

where $\underline{\gamma}_{\mathrm{v}}$ is the overdrive ratio and $\overline{\gamma}_{\mathrm{v}}$ the underdrive ratio. Bounds on the primary speed will be implicitly taken into consideration in the constraints on the EM speed.

D.2 Electric oil pump

Hydraulic actuation power is needed from the ELOP to vary the CVT speed ratio γ_{v}. A general schematic of an actuation system can be found in [214]. Given a CVT speed ratio γ_{v}, the running radii of the primary pulley, secondary pulley, secondary pulley at overdrive ratio and secondary pulley at underdrive ratio can be obtained by

$$R_{\mathrm{p}}(k) = \frac{2\ (L_{\mathrm{b}} - 2\ S_{\mathrm{c}})}{\pi\ (\gamma_{\mathrm{v}}(k) + 1) + \sqrt{\pi^2\ (\gamma_{\mathrm{v}}(k) + 1)^2 + 4\ (\gamma_{\mathrm{v}}(k) - 1)^2\ \left(\frac{L_{\mathrm{b}}}{S_{\mathrm{c}}} - 2\right)}}, \tag{D.8}$$

$$R_{\mathrm{s}}(k) = \gamma_{\mathrm{v}}(k)\ R_{\mathrm{p}}(k), \tag{D.9}$$

$$\underline{R}_{\mathrm{s}} = \frac{2\ (L_{\mathrm{b}} - 2\ S_{\mathrm{c}})}{\pi\ (\underline{\gamma}_{\mathrm{v}} + 1) + \sqrt{\pi^2\ (\underline{\gamma}_{\mathrm{v}} + 1)^2 + 4\ (\underline{\gamma}_{\mathrm{v}} - 1)^2\ \left(\frac{L_{\mathrm{b}}}{S_{\mathrm{c}}} - 2\right)}}, \tag{D.10}$$

$$\overline{R}_{\mathrm{s}} = \frac{2\ (L_{\mathrm{b}} - 2\ S_{\mathrm{c}})}{\pi\ (\overline{\gamma}_{\mathrm{v}} + 1) + \sqrt{\pi^2\ (\overline{\gamma}_{\mathrm{v}} + 1)^2 + 4\ (\overline{\gamma}_{\mathrm{v}} - 1)^2\ \left(\frac{L_{\mathrm{b}}}{S_{\mathrm{c}}} - 2\right)}}, \tag{D.11}$$

where the belt length is given by

$$L_{\mathrm{b}} = (D_{\mathrm{b}} - 2\ S_{\mathrm{r}})\ \pi. \tag{D.12}$$

The sheave position of the secondary pulley can then be calculated by

$$S_{\mathrm{s}}(k) = 2\ \tan(\alpha_{\mathrm{p}})\ (R_{\mathrm{s}}(k) - \underline{R}_{\mathrm{s}}), \tag{D.13}$$

$$\overline{S}_{\mathrm{s}} = 2\ \tan(\alpha_{\mathrm{p}})\ (\overline{R}_{\mathrm{s}} - \underline{R}_{\mathrm{s}}). \tag{D.14}$$

To maintain the CVT speed ratio, the secondary clamping force including spring and centrifugal forces, the primary clamping force including centrifugal force, the spring force of the secondary pulley, and the centrifugal forces of the primary pulley and secondary pulley can be computed by

$$F_{\mathrm{s,c}}(k) = \frac{\max(|\tau_{\mathrm{p}}(k)|, \tau_{\mathrm{c}})\ \cos(\alpha_{\mathrm{p}})\ f}{2\ \mu_{\mathrm{b}}\ R_{\mathrm{p}}(k)}, \tag{D.15}$$

$$F_{\mathrm{p,c}}(k) = kpks(k)\ F_{\mathrm{s,c}}(k), \tag{D.16}$$

$$F_{\mathrm{s,s}}(k) = k_{\mathrm{s}}\ (\overline{S}_{\mathrm{s}} - S_{\mathrm{s}}(k)) + F_{\mathrm{s,p}}, \tag{D.17}$$

$$F_{\mathrm{p,ce}}(k) = \mu_{\mathrm{p}}\ \left(\frac{3\ \omega_{\mathrm{p}}(k)}{100\pi}\right)^2, \tag{D.18}$$

$$F_{\mathrm{s,ce}}(k) = \mu_{\mathrm{s}}\ \left(\frac{3\ \omega_{\mathrm{p}}(k)}{100\ \pi\ \gamma_{\mathrm{v}}(k)}\right)^2, \tag{D.19}$$

where $kpks$ is described by a lookup table, assuming a constant safety factor, i.e.,

$$kpks(k) = kpks\left(\tau_{\mathrm{p}}(k), \frac{30\ \omega_{\mathrm{p}}(k)}{\pi}, \gamma_{\mathrm{v}}(k)\right). \tag{D.20}$$

The clamping forces resulting from applied pressure for both pulleys can thus be obtained by

$$F_{\mathrm{p}}(k) = F_{\mathrm{p,c}}(k) - F_{\mathrm{p,ce}}(k), \tag{D.21}$$

$$F_{\mathrm{s}}(k) = \max(F_{\mathrm{s,c}}(k), F_{\mathrm{s,s}}(k)) - F_{\mathrm{s,s}}(k) - F_{\mathrm{s,ce}}(k). \tag{D.22}$$

Therefore, the required ELOP pressure can be calculated by

$$p_{\mathrm{e}}(k) = \max\left(\max\left(\frac{F_{\mathrm{p}}(k)}{10^5\ A_{\mathrm{p}}}, \frac{F_{\mathrm{s}}(k)}{10^5\ A_{\mathrm{s}}}\right), \underline{p}_{\mathrm{e}}\right). \tag{D.23}$$

Moreover, given the ratio change, the primary pulley flow and secondary pulley flow can be computed by

$$k_{\mathrm{p}}(k) = 60\ c_{\mathrm{p}}(k)\ \frac{\mathrm{d}R_{\mathrm{p}}(k)}{\mathrm{d}\gamma_{\mathrm{v}}(k)}, \tag{D.24}$$

$$k_{\mathrm{s}}(k) = 60\ c_{\mathrm{s}}(k)\ \frac{\mathrm{d}R_{\mathrm{s}}(k)}{\mathrm{d}\gamma_{\mathrm{v}}(k)}, \tag{D.25}$$

where the flow coefficients for both pulleys are given by

$$c_{\mathrm{p}}(k) = -2000\ A_{\mathrm{p}}\ \tan(\alpha_{\mathrm{p}}), \tag{D.26}$$

$$c_{\mathrm{s}}(k) = -2000\ A_{\mathrm{s}}\ \tan(\alpha_{\mathrm{p}}). \tag{D.27}$$

Hence, in consideration of leakage and lubrication q_{l}, the demanded ELOP flow rate can be obtained by

$$q_{\mathrm{e}}(k) = \max(-k_{\mathrm{p}}(k)\ \Delta\gamma_{\mathrm{v}}(k), -k_{\mathrm{s}}(k)\ \Delta\gamma_{\mathrm{v}}(k)) + q_{\mathrm{l}}. \tag{D.28}$$

The ELOP hydraulic actuation power is then computed by

$$P_{\mathrm{e}}(k) = p_{\mathrm{e}}(k)\ q_{\mathrm{e}}(k). \tag{D.29}$$

Consequently, the ELOP power dissipation is calculated, by using an efficiency map, i.e.,

$$P_{\mathrm{e,loss}}(k) = P_{\mathrm{e,loss}}(p_{\mathrm{e}}(k), q_{\mathrm{e}}(k)). \tag{D.30}$$

Appendix E

Convex programming

Convex programming (CP) demands all the models to be convex. A brief introduction to CP is given here, and interested readers are referred to [199] for a rigorous treatment. A convex optimization problem can be formulated as follows:

$$\begin{aligned} \min \quad & f_0(x), \\ \text{s.t.} \quad & f_{\mathrm{i}}(x) \leq 0, \quad i = 1, ..., m, \\ & h_{\mathrm{j}}(x) = A_{\mathrm{j}}^T(x) - B_{\mathrm{j}} = 0, \quad j = 1, ..., n, \end{aligned} \tag{E.1}$$

where $f_{\mathrm{i}}(x)$ are convex functions and $h_{\mathrm{j}}(x)$ are affine functions. The feasible set of this optimization problem is convex with m convex sublevel sets and n hyperplanes. A convex function can be described as

$$f(\beta\ x_1 + (1-\beta)\ x_2) \leq \beta\ f(x_1) + (1-\beta)\ f(x_2), \tag{E.2}$$

where $\beta \in [0, 1]$, and it means that the line segment between any two points lies above the graph, as illustrated in Figure E.1. Models that are originally non-convex

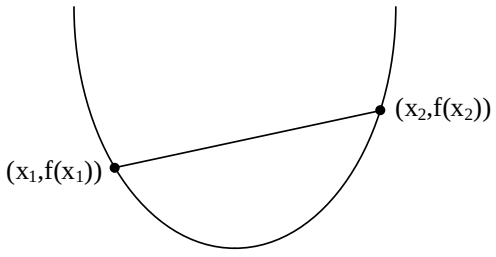

Figure E.1: A typical convex function.

can be reformulated based on approximations, relaxations, and change of variables. Model convexity can be verified, by using basic convex functions, e.g., linear functions, quadratic functions, quadratic-over-linear functions, and opposite of geometric mean functions, and operations that preserve convexity, such as nonnegative weighted sums and pointwise maximum. A product of two variables is generally not a convex function.

Appendix F

Implementation of co-design optimization method

As described in Section 4.4, the overall co-design optimization problem is solved by employing SDPT3. A general and high-level representation of the optimization method

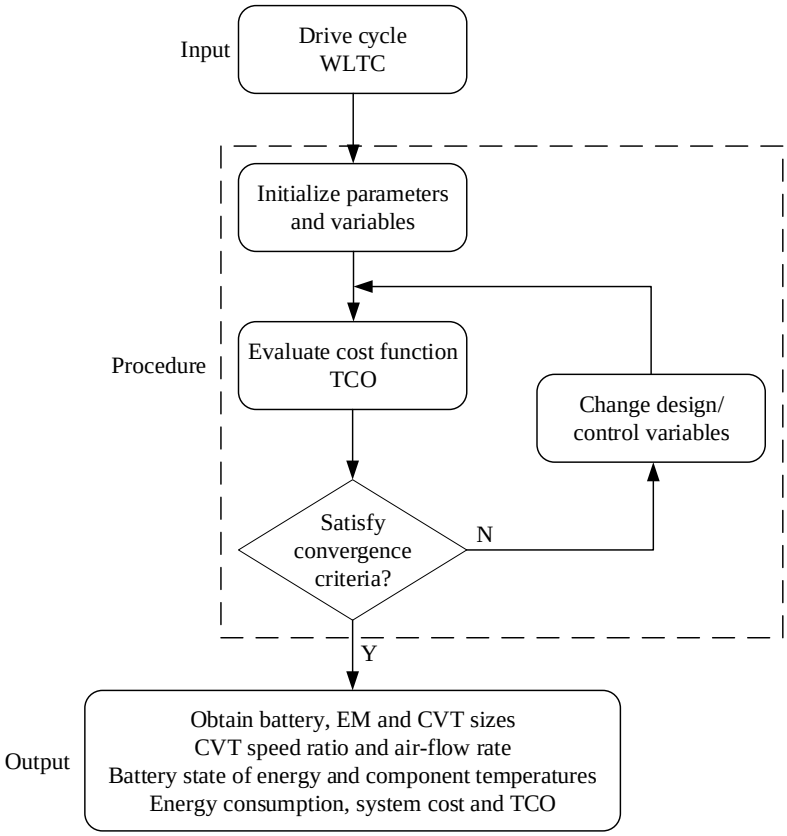

Figure F.1: Flowchart of the co-design optimization method, where TCO is the total-cost-of-ownership, EM the electric machine, and CVT the continuously variable transmission.

consisting of input, procedure and output associated with the co-design problem can be seen in Figure F.1.

The main procedure is shown in Table F.1. The problem can be recognized as a semidefinite program, which is translated automatically by a tool CVX into a form required by SDPT3 [206], permitting the problem to be written in a natural and readable form, e.g., using expressions/symbols to hold operations over variables. It solves the dual problem with 161906 variables and 68119 constraints for improved computation efficiency (see [199] for duality). It is solved in around 95 s.

Table F.1: Co-design optimization method.

cvx_precision high	
cvx_solver sdpt3	
cvx_quiet false	
cvx_begin	
Optimization variables	s_τ, s_γ, s_b, γ_v, E_c, P_d, $P^\mathrm{s}_\mathrm{c,loss}$, $P_\mathrm{m,loss}$, P_m, $\overline{P}_\mathrm{m}$, $\underline{P}_\mathrm{m}$, P_b, E_b, ϕ_a, θ_m, θ_c, θ_o, θ_i
minimize	$J_\mathrm{e}(s_\mathrm{b}, s_\tau, s_\gamma, \gamma_\mathrm{v}(k), \phi_\mathrm{a}(k)) + J_\mathrm{s}(s_\mathrm{b}, s_\tau, s_\gamma)$
subject to	$P_\mathrm{d}(k) = \left(\frac{1}{2}\rho_\mathrm{a} c_\mathrm{d} A_\mathrm{f} v_\mathrm{v}^2(k) + c_\mathrm{r} m_\mathrm{v} g \mathrm{sign}(v_\mathrm{v}(k)) + \left(m_\mathrm{v} + 4\frac{J_\mathrm{w}}{r_\mathrm{w}^2}\right) a_\mathrm{v}(k)\right) v_\mathrm{v}(k)$
	$P^\mathrm{s}_\mathrm{c,loss}(k) = c_0 \left(\frac{P_\mathrm{d}(k)}{w_\mathrm{w}(k)}\right)^2 + c_1 E_\mathrm{c}(k) + c_2 \lvert P_\mathrm{d}(k)\rvert + c_3 s_\tau w_\mathrm{w}(k) + c_4 s_\tau + c_5$
	$P_\mathrm{m}(k) = P_\mathrm{d}(k) + P^\mathrm{s}_\mathrm{c,loss}(k)$
	$P_\mathrm{m,loss}(k) = e_0 \frac{P_\mathrm{m}^2(k)}{E_\mathrm{c}(k)} + e_1 E_\mathrm{c}(k) + e_2 \lvert P_\mathrm{m}(k)\rvert + e_3 s_\tau + e_4$
	$\overline{P}_\mathrm{m} = \min\{(m_0 E_\mathrm{c}(k) + m_1 \sqrt{s_\tau E_\mathrm{c}(k)} + m_2 s_\tau + m_3), s_\tau \overline{P}_\mathrm{m}\}$
	$\underline{P}_\mathrm{m} = \max\{(g_0 E_\mathrm{c}(k) + g_1 \sqrt{s_\tau E_\mathrm{c}(k)} + g_2 s_\tau + g_3), s_\tau \underline{P}_\mathrm{m}\}$
	$c_\mathrm{m} m_\mathrm{m} \dot{\theta}_\mathrm{m}(k) = P_\mathrm{m,loss}(k) - h_\mathrm{m} A_\mathrm{m}(\theta_\mathrm{m}(k) - \theta_\mathrm{o}(k)) - k_\mathrm{e}(\theta_\mathrm{m}(k) - \theta_\mathrm{c}(k)) - h_\mathrm{a} A_\mathrm{a}(\theta_\mathrm{m}(k) - \theta_\mathrm{a})$
	$c_\mathrm{f} m_\mathrm{f} \dot{\theta}_\mathrm{o}(k) = h_\mathrm{m} A_\mathrm{m}(\theta_\mathrm{m}(k) - \theta_\mathrm{o}(k)) - \phi_\mathrm{f} c_\mathrm{f}(\theta_\mathrm{o}(k) - \theta_\mathrm{i}(k))$
	$c_\mathrm{h} c_\mathrm{c} m_\mathrm{c} \dot{\theta}_\mathrm{c}(k) = P^\mathrm{s}_\mathrm{c,loss}(k) + k_\mathrm{e}(\theta_\mathrm{m}(k) - \theta_\mathrm{c}(k)) - h_\mathrm{c} A_\mathrm{c}(\theta_\mathrm{c}(k) - \theta_\mathrm{a})$
	$c_\mathrm{f} m_\mathrm{f} \dot{\theta}_\mathrm{i}(k) = \phi_\mathrm{c} c_\mathrm{f}(\theta_\mathrm{o}(k) - \theta_\mathrm{i}(k)) - \epsilon_\mathrm{r} \phi_\mathrm{a}(k) c_\mathrm{a}(\theta_\mathrm{o}(k) - \theta_\mathrm{a})$
	$P_\mathrm{b}(k) = P_\mathrm{m}(k) + P_\mathrm{m,loss}(k) + + P_\mathrm{b,loss}(k)$
	$P_\mathrm{b,loss}(k) = \frac{P_\mathrm{b}^2(k) R_\mathrm{c} F_\mathrm{c}}{2E_\mathrm{b}(k) + s_\mathrm{b} N_0 F_\mathrm{c} V_0^2}$
	$\dot{E}_\mathrm{b}(k) = -P_\mathrm{b}(k)$
	$m_\mathrm{c} = 1.19 s_\gamma^2 + 39.12$
	$m_\mathrm{m} = s_\tau \overline{m}_\mathrm{m}$
	$m_\mathrm{b} = s_\mathrm{b} \overline{m}_\mathrm{b}$
	$C_\mathrm{c} = a_\mathrm{c} m_\mathrm{c}$
	$C_\mathrm{m} = b_\mathrm{m} s_\tau$
	$C_\mathrm{b} = s_\mathrm{b} c_\mathrm{b} \overline{E}_\mathrm{b}$
	$\gamma_\mathrm{v}(k) \in [\underline{\gamma}_\mathrm{v}, s_\gamma \underline{\gamma}_\mathrm{v}]$
	$E_\mathrm{c}(k) \in [\underline{\gamma}_\mathrm{v}^2 \omega_\mathrm{w}^2(k), s_\gamma^2 \underline{\gamma}_\mathrm{v}^2 \omega_\mathrm{w}^2(k)]$
	$E_\mathrm{b}(k) \in [\frac{F_\mathrm{b}}{2} s_\mathrm{b} N_0 (\underline{V}_\mathrm{c}^2 - V_0^2), \frac{F_\mathrm{b}}{2} s_\mathrm{b} N_0 (\overline{V}_\mathrm{c}^2 - V_0^2)]$
	$s_\gamma^2 \in [\underline{s}_\gamma^2, \overline{s}_\gamma^2]$
	$s_\tau \in [\underline{s}_\tau, \overline{s}_\tau]$
	$s_\mathrm{b} \in [\underline{s}_\mathrm{b}, \overline{s}_\mathrm{b}]$
	$\theta_\mathrm{m}(k) \in [\underline{\theta}_\mathrm{m}, \overline{\theta}_\mathrm{m}]$
	$\theta_\mathrm{o}(k) \in [\underline{\theta}_\mathrm{o}, \overline{\theta}_\mathrm{o}]$
	$\theta_\mathrm{i}(k) \in [\underline{\theta}_\mathrm{i}, \overline{\theta}_\mathrm{i}]$
cvx_end	

Appendix G

Main parameters of EV model

The main EV model parameters are provided in the following table.

Table G.1: Main parameters of EV model.

Parameter	Value	Unit	Description
ρ_a	1.18	kg/m^3	Density of air
c_d	0.27	-	Aerodynamic drag coefficient
A_f	2.21	m^2	Frontal area
c_r	0.00724	-	Rolling resistance coefficient
J_w	1	kgm^2	Wheel inertia
r_w	0.312	m	Wheel radius
η_g	0.98	-	Fixed gear efficiency
η_f	0.985	-	Final drive efficiency
$\overline{\gamma}_v$	2.63	-	Underdrive ratio
$\underline{\gamma}_v$	0.7	-	Overdrive ratio
D_b	0.2294	m	Pushbelt inner diameter
S_r	0.001	m	Pushbelt element rocking edge-saddle distance
S_c	0.1715	m	Variator centre distance
f	1.3	-	Safety factor
α_p	11	$^\circ$	Pulley sheave angle
τ_c	28	Nm	Minimum torque for safety calculation
μ_b	0.1	-	Friction coefficient between belt and pulley
k_s	20000	N/m	Spring stiffness of secondary pulley
$F_{s,p}$	500	N	Spring preload of secondary pulley
μ_p	312.93	N/1000rpm^2	Centrifugal force coefficient of primary pulley
μ_s	30.06	N/1000rpm^2	Centrifugal force coefficient of secondary pulley
A_p	0.01833	m^2	Plunger area of primary pulley
A_s	0.009541	m^2	Plunger area of secondary pulley
$\underline{p}_e$	5	bar	Minimum pump pressure for solenoid feed
q_l	2	lpm	Miscellaneous ELOP flow rate
$\overline{p}_e$	20	bar	Maximum ELOP pressure
$\overline{q}_e$	25	lpm	Maximum ELOP flow rate
V_e	12	V	ELOP voltage
I_e	65	A	ELOP current
$c_{c,0}$	0.000061	W/Nm^2	Fitting coefficient of convex CVT model

$c_{c,1}$	0.0034	W/rpm^2	Fitting coefficient of convex CVT model
$c_{c,2}$	0.045	-	Fitting coefficient of convex CVT model
$c_{c,3}$	-7.13	Nm	Fitting coefficient of convex CVT model
$c_{c,4}$	479.6	W	Fitting coefficient of convex CVT model
$c_{c,5}$	-365.65	W	Fitting coefficient of convex CVT model
$c_{m,0}$	0.067	W/Nm^2	Fitting coefficient of convex EM model
$c_{m,1}$	0.000016	W/rpm^2	Fitting coefficient of convex EM model
$c_{m,2}$	0.028	-	Fitting coefficient of convex EM model
$c_{m,3}$	583.89	W	Fitting coefficient of convex EM model
$c_{m,4}$	447.4	W	Fitting coefficient of convex EM model
$c^{+}_{m,0}$	-0.049	W/rpm^2	Fitting coefficient of convex EM power limitation model
$c^{+}_{m,1}$	231.45	Nm	Fitting coefficient of convex EM power limitation model
$c^{+}_{m,2}$	21258.88	W	Fitting coefficient of convex EM power limitation model
$c^{+}_{m,3}$	-11711.25	W	Fitting coefficient of convex EM power limitation model
$c^{-}_{m,0}$	0.049	W/rpm^2	Fitting coefficient of convex EM power limitation model
$c^{-}_{m,1}$	-231.45	Nm	Fitting coefficient of convex EM power limitation model
$c^{-}_{m,2}$	-21258.88	W	Fitting coefficient of convex EM power limitation model
$c^{-}_{m,3}$	11711.25	W	Fitting coefficient of convex EM power limitation model
c_m	430 [186]	J/kgK	Specific heat capacity of EM
c_c	630 [7]	J/kgK	Specific heat capacity of CVT
c_s	630 [7]	J/kgK	Specific heat capacity of SST
c_f	4090	J/kgK	Specific heat capacity of EM cooling medium
c_a	1000	J/kgK	Specific heat capacity of air
c_h	0.62 [7]	-	CVT heating coefficient
h_m	2000	W/m^{2}K	Heat transfer coefficient between EM and its cooling medium
h_a	10	W/m^{2}K	Heat transfer coefficient between EM and ambient air
h_c	10	W/m^{2}K	Heat transfer coefficient between CVT and ambient air
k_m	111	W/K	Heat transfer coefficient between EM and CVT
k_h	125	W/K	Heat transfer coefficient between EM cooling medium and CVT oil
A_m	0.2	m^2	Heat exchange area between EM and its cooling medium
A_a	0.32	m^2	Heat exchange area between EM and ambient air
A_c	0.17	m^2	Heat exchange area between CVT and ambient air
m_f	1.5	kg	Cooling medium mass
ϕ_f	0.35	kg/s	Coolant flow rate
ϵ	0.6 [115]	-	Radiator effectiveness
$\overline{\theta}_m$	65	°C	Maximum EM temperature
$\overline{\theta}_o$	65	°C	Maximum cooling medium temperature at EM outlet
$\overline{\theta}_i$	65	°C	Maximum cooling medium temperature at EM inlet
S_d	46.532	km	Two repeated WLTC length
S_v	300000	km	Traveled distance of vehicle in its lifetime
ρ_e	0.23	€/kWh	Price of electricity
a_c	13 [7]	€/kg	Specific cost of CVT
b_m	1000	€	Specific cost of EM
c_b	250	€/kWh	Specific cost of battery
$\overline{E}_b$	25.4	kWh	Battery energy
N_0	264	-	Battery cells

Bibliography

[1] F. van der Sluis. "CVT4EV Design and Validation". *TMC*. 2020.

[2] *Electric Surge: Carmakers' Electric Car Plans across Europe 2019-2025*. Technical Report. Belgium: European Federation for Transport and Environment, 2019.

[3] Reuters. *Subaru Sets Mid-2030s Target to Sell Only Electric Vehicles*. 2020. URL: https://www.reuters.com/article/us-subaru-ev/subaru-sets-mid-2030s-target-to-sell-only-electric-vehicles-idUSKBN1ZJ0BU.

[4] T. I. Times. *Nissan to Phase Out Diesel Cars in Europe*. 2018. URL: https://www.irishtimes.com/life-and-style/motors/nissan-to-phase-out-diesel-cars-in-europe-1.3487800.

[5] F. van der Sluis. "The Pushbelt designed for Change". *3rd International VDI Conference: CVT in Automotive Applications*. Baden-Baden, Germany, Mar. 2019.

[6] D. V. Ngo. "Gear Shift Strategies for Automotive Transmissions". PhD thesis. Eindhoven University of Technology, 2012.

[7] K. van Berkel. "Control of a Mechanical Hybrid Powertrain". PhD thesis. Eindhoven University of Technology, 2013.

[8] *Bosch push belt for CVT*. URL: https://www.bosch-presse.de/pressportal/de/en/bosch-push-belt-for-cvt-34781.html.

[9] T. C. Moore. "HEV Control Strategy: Implications of Performance Criteria, System Configuration and Design, and Component Selection". *1997 American Control Conference*. Albuquerque, NM, USA, June 1997.

[10] L. Guzzella and A. Sciarretta. *Vehicle Propulsion Systems: Introduction to Modeling and Optimization*. 2nd ed. Berlin, Germany: Springer-Verlag, 2010.

[11] E. Silvas, T. Hofman, N. Murgovski, L. F. P. Etman, and M. Steinbuch. "Review of Optimization Strategies for System-Level Design in Hybrid Electric Vehicles". *IEEE Trans. Veh. Technol.* Vol. 66 (2017), pp. 57–70.

[12] S. J. Moura, D. S. Callaway, H. K. Fathy, and J. L. Stein. "Tradeoffs between Battery Energy Capacity and Stochastic Optimal Power Management in Plug-in Hybrid Electric Vehicles". *J. Power Sources* vol. 195 (2010), pp. 2979–2988.

[13] C. Lin, H. Peng, J. Grizzle, and J. Kang. "Power Management Strategy for a Parallel Hybrid Electric Truck". *IEEE Trans. Control Syst. Technol.* Vol. 11 (2003), pp. 839–849.

[14] A. Sciarretta, M. Back, and L. Guzzella. "Optimal Control of Parallel Hybrid Electric Vehicles". *IEEE Trans. Control Syst. Technol.* Vol. 12 (2004), pp. 352–363.

[15] O. Sundström, L. Guzzella, and P. Soltic. "Optimal Hybridization in Two Parallel Hybrid Electric Vehicles using Dynamic Programming". *17th IFAC World Congress*. Seoul, Korea, July 2008.

[16] D. Bianchi, L. Rolando, L. Serrao, S. Onori, G. Rizzoni, N. Al-Khayat, T.-M. Hsieh, and P. Kang. "A Rule-based Strategy for a Series/Parallel Hybrid Electric Vehicle: An Approach based on Dynamic Programming". *ASME 2010 Dynamic Systems and Control Conference*. Cambridge, MA, USA, Sept. 2010.

[17] T. Pham. "Integrated Energy and Battery Life Management for Hybrid Vehicles". PhD thesis. Eindhoven University of Technology, 2015.

[18] T. C. J. Romijn, M. C. F. Donkers, J. T. B. A. Kessels, and S. Weiland. "A Distributed Optimization Approach for Complete Vehicle Energy Management". *IEEE Trans. Control Syst. Technol.* Vol. 27 (2019), pp. 964–980.

[19] B. Sakhdari and N. Azad. "An Optimal Energy Management System for Battery Electric Vehicles". *4th IFAC Workshop on Engine and Powertrain Control, Simulation and Modeling E-COSM 2015*. Columbus, OH, USA, Aug. 2015.

[20] W. Zhuang, X. Zhang, H. Peng, and L. Wang. "Simultaneous Optimization of Topology and Component Sizes for Double Planetary Gear Hybrid Powertrains". *Energies* vol. 9 (2016), pp. 1–17.

[21] S. Park and D. Jung. "Numerical Modeling and Simulation of the Vehicle Cooling System for a Heavy Duty Series Hybrid Electric Vehicle". *SAE Technical Paper 2008-01-2421* (2008).

[22] J. Liu and H. Peng. "A Systematic Design Approach for Two Planetary Gear Split Hybrid Vehicles". *Veh. Syst. Dyn.* Vol. 48 (2010), pp. 1395–1412.

[23] X. Zhang, A. Ivanco, X. Tao, J. Wagner, and Z. Filipi. "Optimization of the Series-HEV Control with Consideration of the Impact of Battery Cooling Auxiliary Losses". *SAE Int. J. Alt. Power* vol. 3 (2014), pp. 234–243.

[24] S. Ebbesen. "Optimal Sizing and Control of Hybrid Electric Vehicles". PhD thesis. ETH Zurich, 2012.

[25] E. Vinot. "Comparison of Different Power-Split Architectures Using a Global Optimisation Design Method". *Int. J. Electr. Hybrid Veh.* Vol. 8 (2016), pp. 225–241.

[26] L. Guzzella and A. Sciarretta. "Control of Hybrid Electric Vehicles". *IEEE Control Syst. Mag.* Vol. 27 (2007), pp. 60–70.

[27] C. Musardo, G. Rizzoni, Y. Guezennec, and B. Staccia. "A-ECMS: An Adaptive Algorithm for Hybrid Electric Vehicle Energy Management". *Eur. J. Control* vol. 11 (2005), pp. 509–524.

[28] V. van Reeven, T. Hofman, F. Willems, R. Huisman, and M. Steinbuch. "Optimal Control of Engine Warmup in Hybrid Vehicles". *Oil Gas Sci. Technol.* Vol. 71 (2016).

[29] C. Wei, T. Hofman, E. Ilhan Caarls, and R. van Iperen. "Integrated Energy and Thermal Management for Electrified Powertrains". *Energies* vol. 12 (2019).

[30] M. Kadota and K. Yamamoto. "Advanced Transient Simulation on Hybrid Vehicle Using Rankine Cycle System". *SAE Int. J. Engines* vol. 1 (2009), pp. 240–247.

[31] T. Wang, Y. Zhang, Z. Peng, and G. Shu. "A Review of Researches on Thermal Exhaust Heat Recovery with Rankine Cycle". *Renew. Sustain. Energy Rev.* Vol. 15 (2011), pp. 2862–2871.

[32] H. Teng, J. Klaver, T. Park, G. Hunter, and B. van der Velde. "A Rankine Cycle System for Recovering Waste Heat from HD Diesel Engines—Experimental Results". *SAE 2011 World Congress & Exhibition*. Detroit, MI, USA, Apr. 2011.

[33] G. Latz. "Waste Heat Recovery from Combustion Engines based on the Rankine Cycle". PhD thesis. Chalmers University of Technology, 2016.

[34] F. Merz, A. Sciarretta, J.-C. Dabadie, and L. Serrao. "On the Optimal Thermal Management of Hybrid-electric Vehicles with Heat Recovery Systems". *Oil Gas Sci. Technol.* Vol. 67 (2012), pp. 601–612.

[35] T. A. Horst, H.-S. Rottengruber, M. Seifert, and J. Ringler. "Dynamic Heat Exchanger Model for Performance Prediction and Control System Design of Automotive Waste Heat Recovery Systems". *Appl. Energy* vol. 105 (2013), pp. 293–303.

[36] J. Peralez, P. Tona, M. Nadri, P. Dufour, and A. Sciarretta. "Optimal Control for an Organic Rankine Cycle on Board a Diesel-Electric Railcar". *J. Process Control* vol. 33 (2015), pp. 1–13.

[37] J. Ringler, M. Seifert, V. Guyotot, and W. Hübner. "Rankine Cycle for Waste Heat Recovery of IC Engines". *SAE Int. J. Engines* vol. 2 (2009), pp. 67–76.

[38] Z. Qi. "Advances on Air Conditioning and Heat Pump System in Electric Vehicles—A Review". *Renew. Sustain. Energy Rev.* Vol. 38 (2014), pp. 754–764.

[39] Q. Peng and Q. Du. "Progress in Heat Pump Air Conditioning Systems for Electric Vehicles—A Review". *Energies* vol. 9 (2016).

[40] Y. Higuchi, H. Kobayashi, Z. Shan, M. Kuwahara, Y. Endo, and Y. Nakajima. "Efficient Heat Pump System for PHEV/BEV". *SAE Technical Paper 2017-01-0188* (2017).

[41] J. Ahn, H. Kang, H. Lee, H. Jung, C. Baek, and Y. Kim. "Heating Performance Characteristics of a Dual Source Heat Pump Using Air and Waste Heat in Electric Vehicles". *Appl. Energy* vol. 119 (2014), pp. 1–9.

[42] D. Lee. "Experimental Study on the Heat Pump System Using R134a Refrigerant for Zero-Emission Vehicles". *Int. J. Autom. Technol.* Vol. 16 (2015), pp. 923–928.

[43] H. Fathy, J. A. Reyer, P. Papalambros, and A. G. Ulsog. "On the Coupling between the Plant and Controller Optimization Problems". *2001 American Control Conference*. Arlington, VA, USA, June 2001.

[44] J. Ruan, P. Walker, and N. Zhang. "A Comparative Study Energy Consumption and Costs of Battery Electric Vehicle Transmissions". *Appl. Energy* vol. 165 (2016), pp. 119–134.

[45] F. van der Sluis, L. Römers, G. van Spijk, and I. Hupkes. "CVT, Promising Solutions for Electrification". *SAE Technical Paper 2019-01-0359* (2019).

[46] M. S. Rahimi Mousavi and B. Boulet. "Modeling, Simulation and Control of a Seamless Two-Speed Automated Transmission for Electric Vehicles". *2014 American Control Conference*. Portland, OR, USA, June 2014.

[47] M. Roozegar and J. Angeles. "The Optimal Gear-Shifting for a Multi-Speed Transmission System for Electric Vehicles". *Mech. Mach. Theory* vol. 116 (2017), pp. 1–13.

[48] T. Hofman and N. H. J. Janssen. "Integrated Design Optimization of the Transmission System and Vehicle Control for Electric Vehicles". *20th IFAC World Congress*. Toulouse, France, July 2017.

[49] M. Roozegar, Y. D. Setiawan, and J. Angeles. "Design, Modelling and Estimation of a Novel Modular Multi-speed Transmission System for Electric Vehicles". *Mechatronics* vol. 45 (2017), pp. 119–129.

[50] Porsche. *The Powertrain: Pure Performance*. 2020. URL: `https://newsroom.porsche.com/en/products/taycan/powertrain-18555.html`.

[51] ZF. *Paradigm Shift for Electromobility: ZF Presents New Electric 2-Speed Drive for Passenger Cars*. 2019. URL: `https://press.zf.com/press/en/releases/release_10181.html`.

[52] T. Hofman and M. Salazar. "Transmission Ratio Design for Electric Vehicles via Analytical Modeling and Optimization". *2020 IEEE Vehicle Power and Propulsion Conference*. Gijón, Spain, Oct. 2020.

[53] I. Hupkes. "Variable Drive EV: Comfort Solution for Full Electric Vehicles". *3rd International VDI Conference: CVT in Automotive Applications*. Baden-Baden, Germany, Mar. 2019.

[54] D. Gunji and H. Fujimoto. "Efficiency Analysis of Powertrain with Toroidal Continuously Variable Transmission for Electric Vehicles". *IECON 2013 - 39th Annual Conference of the IEEE Industrial Electronics Society*. Vienna, Austria, Nov. 2013.

[55] J. Hellgren and B. Jacobson. "A Systematic Way of Choosing Driveline Configuration and Sizing Components in Hybrid Vehicles". *SAE Technical Paper 2000-01-3098* (2001).

[56] V. Galdi, L. Ippolito, A. Piccolo, and A. Vaccaro. "A Genetic-based Methodology for Hybrid Electric Vehicles Sizing". *Soft Comput.* Vol. 5 (2001), pp. 451–457.

[57] O. Sundström, L. Guzzella, and L. P. Soltic. "Torque-Assist Hybrid Electric Powertrain Sizing: From Optimal Control towards a Sizing Law". *IEEE Trans. Control Syst. Technol.* Vol. 18 (2010), pp. 837–849.

[58] D. Bertsekas. *Dynamic Programming and Optimal Control*. 3rd ed. Belmont, MA, USA: Athena Scientific, 2005.

[59] M. Pourabdollah, N. Murgovski, A. Grauers, and B. Egardt. "Optimal Sizing of a Parallel PHEV Powertrain". *IEEE Trans. Veh. Technol.* Vol. 62 (2013), pp. 2469–2480.

[60] C. Wei, T. Hofman, E. Ilhan Caarls, and R. van Iperen. "Evolution and Classification of Energy and Thermal Management Systems in Electrified Powertrains". *2019 IEEE Vehicle Power and Propulsion Conference*. Hanoi, Vietnam, Oct. 2019.

[61] C. Wei, T. Hofman, E. Ilhan Caarls, and R. van Iperen. "A Review of the Integrated Design and Control of Electrified Vehicles". *Energies* vol. 13 (2020).

[62] C. Wei, T. Hofman, E. Ilhan Caarls, and R. van Iperen. "Optimal Control of an Integrated Energy and Thermal Management System for Electrified Powertrains". *2019 American Control Conference*. Philadelphia, PA, USA, July 2019.

[63] C. Wei, T. Hofman, E. Ilhan Caarls, and R. van Iperen. "Co-design of CVT-based Electric Vehicles". *submitted as journal article, currently under review.*

[64] C. Wei, T. Hofman, E. Ilhan Caarls, and R. van Iperen. "Design and Analysis of CVT-based Electric Vehicles". *submitted as journal article, currently under review.*

[65] K. Bennion and M. Thornton. *Integrated Vehicle Thermal Management for Advanced Vehicle Propulsion Technologies*. Technical Report. USA: National Renewable Energy Laboratory, 2010.

[66] S. Park. "A Comprehensive Thermal Management System Model for Hybrid Electric Vehicles". PhD thesis. University of Michigan, 2011.

[67] X. Tao. "Modeling and Control of a Thermal Management System for Hybrid Electric Vehicles". PhD thesis. Clemson University, 2016.

[68] S. Shojaei, A. McGordon, S. Robinson, J. Marco, and P. Jennings. "Developing a Model for Analysis of the Cooling Loads of a Hybrid Electric Vehicle by Using Co-simulations of Verified Submodels". *Proc. IMechE D, J. Autom. Eng.* Vol. 232 (2018), pp. 766–784.

[69] G. De Nunzio, A. Sciarretta, A. Steiner, and A. Mladek. "Thermal Management Optimization of a Heat-Pump-Based HVAC System for Cabin Conditioning in Electric Vehicles". *Thirteenth International Conference on Ecological Vehicles and Renewable Energies (EVER)*. Monte-Carlo, Monaco, Apr. 2018.

[70] G. Paganelli, S. Delprat, T. Guerra, J. Rimaux, and J. J. Santin. "Equivalent Consumption Minimization Strategy for Parallel Hybrid Powertrains". *55th Vehicular Technology Conference*. Birmingham, AL, USA, May 2002.

[71] X. Tao and J. Wagner. "Cooling Air Temperature and Mass Flow Rate Control for Hybrid Electric Vehicle Battery Thermal Management". *ASME 2014 Dynamic Systems and Control Conference*. San Antonio, Texas, USA, Oct. 2014.

[72] E. Vinot, R. Trigui, B. Jeanneret, J. Scordia, and F. Badin. "HEVs Comparison and Components Sizing Using Dynamic Programming". *2007 IEEE Vehicle Power and Propulsion Conference*. Arlington, TX, USA, Sept. 2007.

[73] A. Emadi, K. Rajashekara, S. Williamson, and S. Lukic. "Topological Overview of Hybrid Electric and Fuel Cell Vehicular Power System Architectures and Configurations". *IEEE Trans. Veh. Technol.* Vol. 54 (2005), pp. 763–770.

[74] D. Gao, C. Mi, and A. Emadi. "Modeling and Simulation of Electric and Hybrid Vehicles". *Proc. IEEE* vol. 95 (2007), pp. 729–745.

[75] C. C. Chan, A. Bouscayrol, and K. Chen. "Electric, Hybrid, and Fuel-Cell Vehicles: Architectures and Modeling". *IEEE Trans. Veh. Technol.* Vol. 59 (2010), pp. 589–598.

[76] E. Silvas, T. Hofman, A. Serebrenik, and M. Steinbuch. "Functional and Cost-based Automatic Generator for Hybrid Vehicles Topologies". *IEEE/ASME Trans. Mechatronics* vol. 20 (2015), pp. 1561–1572.

[77] X. Zhang, C.-T. Li, D. Kum, and H. Peng. "Prius$^+$ and Volt$^-$: Configuration Analysis of Power-Split Hybrid Vehicles with a Single Planetary Gear". *IEEE Trans. Veh. Technol.* Vol. 61 (2012), pp. 3544–3552.

[78] A. E. Bayrak, N. Kang, and P. Papalambros. "Decomposition-based Design Optimization of Hybrid Electric Powertrain Arhitectures: Simultaneous Configuration and Sizing Design". *J. Mech. Des.* Vol. 138 (2016).

[79] X. Zhang, H. Peng, J. Sun, and S. Li. "Automated Modeling and Mode Screening for Exhaustive Search of Double-Planetary-Gear Power Split Hybrid Powetrain". *ASME 2014 Dynamic Systems and Control Conference*. San Antonio, TX, USA, Oct. 2014.

[80] X. Zhang, S. Eben Li, H. Peng, and J. Sun. "Efficient Exhaustive Search of Power-Split Hybrid Powertrains with Multiple Planetary Gears and Clutches". *J. Dyn. Sys., Meas., Control* vol. 137 (2015).

[81] O. H. Dagci, H. Peng, and J. W. Grizzle. "Hybrid Electric Powertrain Design Methodology with Planetary Gear Sets for Performance and Fuel Economy". *IEEE Access* vol. 6 (2018), pp. 9585–9602.

[82] X. Xu, H. Sun, Y. Liu, and P. Dong. "Automatic Enumeration of Feasible Configuration for the Dedicated Hybrid Transmission with Multi-Degree-of-Freedom and Multiplanetary Gear Set". *J. Mech. Des.* Vol. 141 (2019).

[83] R. Johri and Z. Filipi. "Optimal Energy Management of a Series Hybrid Vehicle with Combined Fuel Economy and Low-Emission Objectives". *Proc. IMechE D, J. Autom. Eng.* Vol. 228 (2014), pp. 1424–1439.

[84] J. P. F. Trovão and P. J. G. Pereirinha. "Control Scheme for Hybridised Electric Vehicles with an Online Power Follower Management Strategy". *IET Electr. Syst. Transp.* Vol. 5 (2015), pp. 12–23.

[85] N. Schouten, M. Salman, and N. Kheir. "Energy Management Strategies for Parallel Hybrid Vehicles using Fuzzy Logic". *Control Eng. Pract.* Vol. 11 (2003), pp. 171–177.

[86] N. Jalil, N. A. Kheir, and M. Salman. "A Rule-based Energy Management Strategy for a Series Hybrid Vehicle". *1997 American Control Conference*. Albuquerque, NM, USA, June 1997.

[87] M. Ehsani, Y. Gao, and A. Emadi. *Modern Electric, Hybrid Electric, and Fuel Cell Vehicles: Fundamentals, Theory, and Design*. 2nd ed. Boca Raton, FL, USA: CRC, 2010.

[88] N. Kim, S. Cha, and H. Peng. "Optimal Control of Hybrid Electric Vehicles based on Pontryagin's Minimum Principle". *IEEE Trans. Control Syst. Technol.* Vol. 19 (2011), pp. 1279–1287.

[89] S. Azad, M. Behtash, A. Houshmand, and M. J. Alexander-Ramos. "PHEV Powertrain Co-design with Vehicle Performance Considerations using MDSDO". *Struct. Multidiscip. Optim.* Vol. 60 (2019), pp. 1155–1169.

[90] J. Liu and H. Peng. "Modeling and Control of a Power-Split Hybrid Vehicle". *IEEE Trans. Control Syst. Technol.* Vol. 16 (2008), pp. 1242–1251.

[91] H. Borhan, A. Vahidi, A. M. Phillips, M. L. Kuang, I. V. Kolmanovsky, and S. Di Cairano. "MPC-based Energy Management of a Power-Split Hybrid Electric Vehicle". *IEEE Trans. Control Syst. Technol.* Vol. 20 (2012), pp. 593–603.

[92] A. Panday and H. O. Bansal. "A Review of Optimal Energy Management Strategies for Hybrid Electric Vehicle". *Int. J. Veh. Technol.* Vol. 2014 (2014).

[93] M. F. M. Sabri, K. A. Danapalasingam, and M. F. Rahmat. "A Review on Hybrid Electric Vehicles Architecture and Energy Management Strategies". *Renew. Sustain. Energy Rev.* Vol. 53 (2016), pp. 1433–1442.

[94] E. Silvas, E. Bergshoeff, T. Hofman, and M. Steinbuch. "Comparison of Bi-Level Optimization Frameworks for Sizing and Control of a Hybrid Electric Vehicle". *2014 IEEE Vehicle Power and Propulsion Conference*. Coimbra, Portugal, Oct. 2014.

[95] T. Hofman, M. Steinbuch, R. van Druten, and A. Serrarens. "Rule-based Energy Management Strategies for Hybrid Vehicles". *Int. J. Electr. Hybrid Veh.* Vol. 1 (2007), pp. 71–94.

[96] V. Ngo, T. Hofman, M. Steinbuch, and A. Serrarens. "Optimal Control of the Gearshift Command for Hybrid Electric Vehicles". *IEEE Trans. Veh. Technol.* Vol. 61 (2012), pp. 3531–3543.

[97] T. Nüesch, P. Elbert, M. Flankl, C. Onder, and L. Guzzella. "Convex Optimization for the Energy Management of Hybrid Electric Vehicles Considering Engine Start and Gearshift Costs". *Energies* vol. 7 (2014), pp. 834–856.

[98] R. A. Weinstock, P. T. Krein, and R. A. White. "Optimal Sizing and Selection of Hybrid Electric Vehicle Components". *IEEE Power Electronics Specialist Conference - PESC '93*. Seattle, WA, USA, June 1993.

[99] D. Sinoquet, G. Rousseau, and Y. Milhau. "Design Optimization and Optimal Control for Hybrid Vehicles". *Optim. Eng.* Vol. 12 (2011), pp. 199–213.

[100] F. Colzi, M. de Nigris, A. Corti, and S. M. Savaresi. "Extended Range Electric Vehicles Components Preliminary Sizing based on Real Mission Profiles". *2013 World Electric Vehicle Symposium and Exhibition*. Barcelona, Spain, Nov. 2013.

[101] C. Ma, S. Y. Ko, K. Y. Jeong, and H. S. Kim. "Design Methodology of Component Design Environment for PHEV". *Int. J. Automot. Technol.* Vol. 14 (2013), pp. 785–795.

[102] W. Gao and S. K. Porandla. "Design Optimization of a Parallel Hybrid Electric Powertrain". *2005 IEEE Vehicle Power and Propulsion Conference*. Chicago, IL, USA, Sept. 2005.

[103] A. Shojaei, D. Strickland, D. Scott, M. Tucker, G. Kirkpatrick, B. Price, S. Luke, and J. Richmond. "Powertrain Optimisation in a Hybrid Electric Bus". *2012 IEEE Vehicle Power and Propulsion Conference*. Seoul, South Korea, Oct. 2012.

[104] C. Desai and S. S. Williamson. "Optimal Design of a Parallel Hybrid Electric Vehicle Using Multi-Objective Genetic Algorithms". *2009 IEEE Vehicle Power and Propulsion Conference*. Dearborn, MI, USA, Sept. 2009.

[105] D. Assanis et al. "Optimization Approach to Hybrid Electric Propulsion System Design". *Mech. Struct. Mach.* Vol. 27 (1999), pp. 393–421.

[106] M. Pourabdollah, N. Murgovski, A. Grauers, and B. Egardt. "An Iterative Dynamic Programming/Convex Optimization Procedure for Optimal Sizing and Energy Management of PHEVs". *19th IFAC World Congress*. Cape Town, South Africa, Aug. 2014.

[107] P. Tulpule, V. Marano, and G. Rizzoni. "Energy Management for Plug-in Hybrid Electric Vehicles Using Equivalent Consumption Minimisation Strategy". *Int. J. Electric and Hybrid Vehicles* vol. 2 (2010), pp. 329–350.

[108] D. Bianchi, L. Rolando, L. Serrao, S. Onori, G. Rizzoni, N. Al-Khayat, T.-M. Hsieh, and P. Kang. "Layered Control Strategies for Hybrid Electric Vehicles based on Optimal Control". *Int. J. Electr. Hybrid Veh.* Vol. 3 (2011), pp. 191–217.

[109] T. Hofman, S. Ebbesen, and L. Guzzella. "Topology Optimization for Hybrid Electric Vehicles with Automated Transmissions". *IEEE Trans. Veh. Technol.* Vol. 6 (2012), pp. 2442–2451.

[110] T. Nüesch, T. Ott, S. Ebbesen, and L. Guzzella. "Cost and Fuel-Optimal Selection of HEV Topologies using Particle Swarm Optimization and Dynamic Programming". *2012 American Control Conference*. Montreal, QC, Canada, June 2012.

[111] B. Wang, M. Xu, and L. Yang. "Study on the Economic and Environmental Benefits of Different EV Powertrain Topologies". *Energy Convers. Manage.* Vol. 86 (2014), pp. 916–926.

[112] K. Ramakrishnan, G. Mastinu, and M. Gobbi. "Multidisciplinary Design of Electric Vehicles based on Hierarchical Multi-Objective Optimization". *J. Mech. Des.* Vol. 141 (2019).

[113] C. Wei, T. Hofman, E. Ilhan Caarls, and R. van Iperen. "Zone Model Predictive Control for Battery Thermal Management Including Battery Aging and Brake Energy Recovery in Electrified Powertrains". *9th IFAC Symposium Advances in Automotive Control*. Orléans, France, June 2019.

[114] Y.-H. Hung, Y.-F. Lue, and H.-J. Gu. "Development of a Thermal Management System for Energy Sources of an Electric Vehicle". *IEEE/ASME Trans. Mechatronics* vol. 21 (2016), pp. 402–411.

[115] M. Salah. "Nonlinear Control Strategies for Advanced Vehicle Thermal Management Systems". PhD thesis. Clemson University, 2007.

[116] N. Staunton, V. Pickert, and R. Maughan. "Assessment of Advanced Thermal Management Systems for Micro-Hybrid Trucks and Heavy Duty Diesel Vehicles". *2008 IEEE Vehicle Power and Propulsion Conference*. Harbin, China, Sept. 2008.

[117] T. Wang, A. Jagarwal, J. R. Wagner, and G. Fadel. "Optimization of an Automotive Radiator Fan Array Operation to Reduce Power Consumption". *IEEE/ASME Trans. Mechatronics* vol. 20 (2015), pp. 2359–2369.

[118] J. Lopez-Sanz, C. Ocampo-Martinez, J. Álvarez-Flórez, M. Moreno-Eguilaz, R. Ruiz-Mansilla, J. Kalmus, M. Gräeber, and G. Lux. "Thermal Management in Plug-in Hybrid Electric Vehicles: A Real-Time Nonlinear Model Predictive Control Implementation". *IEEE Trans. Veh. Technol.* Vol. 66 (2017), pp. 7751–7760.

[119] J. Saha, H. Chen, and S. Rahman. "Model based Design and Optimization of Vehicle Thermal Management System". *SAE Technical Paper 2016-01-0283* (2016).

[120] C. Hughes and M. Wiseman. "Feasibility of Intelligent Control Strategies to Reduce Cooling System Size". *SAE Technical Paper 2001-01-1759* (2001).

[121] R. W. Johnson, J. L. Evans, P. Jacobsen, J. R. Thompson, and M. Christopher. "The Changing Automotive Environment: High-Temperature Electronics". *IEEE Trans. Electron. Packag. Manuf.* Vol. 27 (2004), pp. 164–176.

[122] H. Cho, D. Jung, Z. Filipi, D. N. Assanis, J. Vanderslice, and W. Bryzik. "Application of Controllable Electric Coolant Pump for Fuel Economy and Cooling Performance Improvement". *J. Eng. Gas Turbines Power* vol. 129 (2007), pp. 239–244.

[123] S. Park, M. Kokkolaras, A. Malikopoulos, B. AbdulNour, J. Sedarous, and D. Jung. "Thermal Management System Modeling and Optimization for Heavy Hybrid Electric Military Vehicles". *2010 NDIA Ground Vehicle Systems Engineering and Technology Symposium*. Dearborn, MI, USA, Aug. 2010.

[124] X. Tao and J. Wagner. "Optimization of a Military Ground Vehicle Engine Cooling System Heat Exchanger - Modeling and Size Scaling". *SAE Technical Paper 2017-01-0259* (2017).

[125] S. Park and D. Jung. "Design of Vehicle Cooling System Architecture for a Heavy Duty Series-Hybrid Electric Vehicle Using Numerical System Simulations". *J. Eng. Gas Turbines Power.* Vol. 132 (2010).

[126] M. Stellato, L. Bergianti, and J. Batteh. "Powertrain and Thermal System Simulation Models of a High Performance Electric Road Vehicle". *12th International Modelica Conference*. Prague, Czech Republic, May 2017.

[127] Z. Rao and S. Wang. "A Review of Power Battery Thermal Energy Management". *Renew. Sustain. Energy Rev.* Vol. 15 (2011), pp. 4554–4571.

[128] P. Ponomarev, M. Polikarpova, and J. Pyrhönen. "Thermal Modeling of Directly-Oil-Cooled Permanent Magnet Synchronous Machine". *2012 XXth International Conference on Electrical Machines*. Marseille, France, Sept. 2012.

[129] M. Li, Y. Liu, X. Wang, and J. Zhang. "Modeling and Optimization of an Enhanced Battery Thermal Management System in Electric Vehicles". *Front. Mech. Eng.* Vol. 14 (2019), pp. 65–75.

[130] Y. Gai, M. Kimiabeigi, Y. C. Chong, J. D. Widmer, X. Deng, M. Popescu, J. Goss, D. A. Staton, and A. Steven. "Cooling of Automotive Traction Motors: Schemes, Examples, and Computation Methods". *IEEE Trans. Ind. Electron.* Vol. 66 (2019), pp. 1681–1692.

[131] J. Huang, S. S. Naini, R. Miller, D. Rizzo, K. Sebeck, S. Shurin, and J. Wagner. "A Hybrid Electric Vehicle Motor Cooling System—Design, Model, and Control". *IEEE Trans. Veh. Technol.* Vol. 68 (2019), pp. 4467–4478.

[132] G. J. Marshall, C. P. Mahony, M. J. Rhodes, S. R. Daniewicz, N. Tsolas, and S. M. Thompson. "Thermal Management of Vehicle Cabins, External Surfaces, and Onboard Electronics: An Overview". *Engineering* vol. 5 (2019), pp. 954–969.

[133] H. H. Pang and C. J. Brace. "Review of Engine Cooling Technologies for Modern Engines". *Proc. IMechE D, J. Autom. Eng.* Vol. 218 (2004), pp. 1209–1215.

[134] W. Lin and B. Sunden. "Vehicle Cooling Systems for Reducing Fuel Consumption and Carbon Dioxide: Literature Survey". *SAE Technical Paper 2010-01-1509* (2010).

[135] Q. Wang, B. Jiang, B. Li, and Y. Yan. "A Critical Review of Thermal Management Models and Solutions of Lithium-Ion Batteries for the Development of Pure Electric Vehicles". *Renew. Sustain. Energy Rev.* Vol. 64 (2016), pp. 106–128.

[136] X. Zhang. "Supervisory Control Optimization for a Series Hybrid Electric Vehicle with Consideration of Battery Thermal Management and Aging". PhD thesis. Clemson University, 2016.

[137] F. J. Jiménez-Espadafor, D. P. Guerrero, E. C. Trujillo, M. T. García, and J. Wideberg. "Fully Optimized Energy Management for Propulsion, Thermal Cooling and Auxiliaries of a Serial Hybrid Electric Vehicle". *Appl. Therm. Eng.* Vol. 91 (2015), pp. 694–705.

[138] T. Pham, J. Kessels, P. van den Bosch, R. Huisman, and R. Nevels. "On-Line Energy and Battery Thermal Management for Hybrid Electric Heavy-Duty Truck". *2013 American Control Conference*. Washington, DC, USA, June 2013.

[139] L. Serrao. "A Comparative Analysis of Energy Management Strategies for Hybrid Electric Vehicles". PhD thesis. Ohio State University, 2009.

[140] N. Murgovski. "Optimal Powertrain Dimensioning and Potential Assessment of Hybrid Electric Vehicles". PhD thesis. Chalmers University of Technology, 2012.

[141] T. J. Böhme and B. Frank. *Hybrid Systems, Optimal control and Hybrid Vehicles: Theory, Methods and Applications*. 1st ed. Cham, Switzerland: Springer, 2017.

[142] E. D. Tate, J. W. Grizzle, and H. Peng. "SP-SDP for Fuel Consumption and Tailpipe Emissions Minimization in an EVT Hybrid". *IEEE Trans. Control Syst. Technol.* Vol. 18 (2010), pp. 673–687.

[143] L. Serrao, S. Onori, A. Sciarretta, Y. Guezennec, and G. Rizzoni. "Optimal Energy Management of Hybrid Electric Vehicles Including Battery Aging". *2011 American Control Conference*. San Francisco, CA, USA, June 2011.

[144] P. Pisu, K. Koprubasi, and G. Rizzoni. "Energy Management and Drivability Control Problems for Hybrid Electric Vehicles". *44th IEEE Conference on Decision and Control*. Seville, Spain, Dec. 2005.

[145] O. Barbarisi, E. R. Westervelt, F. Vasca, and G. Rizzoni. "Power Management Decoupling Control for a Hybrid Electric Vehicle". *44th IEEE Conference on Decision and Control*. Seville, Spain, Dec. 2005.

[146] M. H. Salah, T. H. Mitchell, J. R. Wagner, and D. M. Dawson. "Nonlinear-Control Strategy for Advanced Vehicle Thermal-Management Systems". *IEEE Trans. Veh. Technol.* Vol. 57 (2008), pp. 127–137.

[147] M. H. Salah, T. H. Mitchell, J. R. Wagner, and D. M. Dawson. "A Smart Multiple-Loop Automotive Cooling System—Model, Control, and Experimental Study". *IEEE/ASME Trans. Mechatronics* vol. 15 (2010), pp. 117–124.

[148] A. Choukroun and M. Chanfreau. "Automatic Control of Electric Actuators for an Optimized Engine Cooling Thermal Management". *SAE Technical Paper 2001-01-1758* (2001).

[149] R. Cipollone and C. Villante. "Vehicle Thermal Management: A Model-based Approach". *ASME 2004 Internal Combustion Engine Division Fall Technical Conference*. Long Beach, CA, USA, Oct. 2004.

[150] J. Chastain, J. Wagner, and J. Eberth. "Advanced Engine Cooling – Components, Testing and Observations". *6th IFAC Symposium Advances in Automotive Control*. Munich, Germany, July 2010.

[151] T. Wang and J. Wagner. "A Smart Engine Cooling System - Experimental Study of Integrated Actuator Transient Behavior". *SAE Technical Paper 2015-01-1604* (2015).

[152] X. Tao, K. Zhou, A. Ivanco, J. Wagner, H. Hofmann, and Z. Filipi. "A Hybrid Electric Vehicle Thermal Management System - Nonlinear Controller Design". *SAE Technical Paper 2015-01-1710* (2015).

[153] D. Crane, G. Jackson, and D. Holloway. "Towards Optimization of Automotive Waste Heat Recovery Using Thermoelectrics". *SAE 2001 World Congress*. Detroit, MI, USA, Mar. 2001.

[154] Q. Hussain, D. Brigham, and C. Maranville. "Thermoelectric Exhaust Heat Recovery for Hybrid Vehicles". *SAE Int. J. Engines* vol. 2 (2009), pp. 1132–1142.

[155] J. Martins, L. Goncalves, J. Antunes, and F. Brito. "Thermoelectric Exhaust Energy Recovery with Temperature Control through Heat Pipes". *SAE 2011 World Congress & Exhibition*. Detroit, MI, USA, Apr. 2011.

[156] C. Baker and L. Shi. "Experimental and Modeling Study of a Heat Exchanger Concept for Thermoelectric Waste Heat Recovery from Diesel Exhaust". *SAE 2012 World Congress & Exhibition*. Detroit, MI, USA, Apr. 2012.

[157] S. Kumar, S. Heister, X. Xu, J. Salvador, and G. Meisner. "Thermoelectric Generators for Automotive Waste Heat Recovery Systems Part I: Numerical Modeling and Baseline Model Analysis". *J. Electron. Mater.* Vol. 42 (2013), pp. 665–674.

[158] B. Orr, A. Akbarzadeh, M. Mochizuki, and R. Singh. "A Review of Car Waste Heat Recovery Systems Utilising Thermoelectric Generators and Heat Pipes". *Appl. Therm. Eng.* Vol. 101 (2016), pp. 490–495.

[159] P. Skarke, S. Midlam-Mohler, and M. Canova. "Waste Heat Recovery from Internal Combustion Engines: Feasibility Study on an Organic Rankine Cycle with Application to the Ohio State EcoCAR PHEV". *ASME 2012 Internal Combustion Engine Division Fall Technical Conference*. Vancouver, BC, Canada, Sept. 2012.

[160] T. Tang, M. Devlin, N. Mathur, T. Henly, and L. Saathoff. "Lubricants for (Hybrid) Electric Transmissions". *SAE Int. J. Fuels Lubr.* Vol. 6 (2013), pp. 289–294.

[161] C. McFadden, K. Hughes, L. Raser, and T. Newcomb. "Electrical Conductivity of New and Used Automatic Transmission Fluids". *SAE Int. J. Fuels Lubr.* Vol. 9 (2016), pp. 519–526.

[162] K. Bennion and G. Moreno. "Convective Heat Transfer Coefficients of Automatic Transmission Fluid Jets with Implications for Electric Machine Thermal Management". *ASME 2015 International Technical Conference and Exhibition on Packaging and Integration of Electronic and Photonic Microsystems InterPACK2015*. San Francisco, CA, USA, July 2015.

[163] R. Dubouil, J. Hetet, and A. Maiboom. "Modelling of the Warm-Up of a Spark Ignition Engine: Application to Hybrid Vehicles". *SAE International Powertrains, Fuels and Lubricants Meeting*. Kyoto, Japan, Aug. 2011.

[164] G. Titov and J. Lustbader. "Modeling Control Strategies and Range Impacts for Electric Vehicle Integrated Thermal Management Systems with MATLAB/Simulink". *SAE Technical Paper 2017-01-0191* (2017).

[165] R. Staunton, C. Ayers, L. Marlino, C. Chiasson, and T. Burress. *Evaluation of 2004 Toyota Prius Hybrid Electric Drive System*. Technical Report. USA: Oak Ridge National Laboratory, 2006.

[166] K. Muta, M. Yamazaki, and J. Tokieda. "Development of New-Generation Hybrid System THS II - Drastic Improvement of Power Performance and Fuel Economy". *SAE Technical Paper 2004-01-0064* (2004).

[167] A. Pesaran, A. Vlahinos, and T. Stuart. "Cooling and Preheating of Batteries in Hybrid Electric Vehicles". *6th ASME-JSME Thermal Engineering Conference*. Hawaii Island, HI, USA, Mar. 2003.

[168] R. Semel. "Fuel Economy Improvements through Improved Automatic Transmission Warmup - Stand Alone Oil to Air (OTA) Transmission Cooling Strategy with Thermostatic Cold Flow Bypass Valve". *SAE Technical Paper 2001-01-1760* (2001).

[169] K. Laboe and M. Canova. "Powertrain Waste Heat Recovery: A Systems Approach to Maximize Drivetrain Efficiency". *ASME 2012 Internal Combustion Engine Division Spring Technical Conference*. Torino, Italy, May 2012.

[170] C. Wei, T. Hofman, E. Ilhan Caarls, and R. van Iperen. "Energy-Efficiency Improvement Potential of Electric Vehicles Considering Transmission Temperature". *8th IFAC Symposium on Mechatronic Systems*. Vienna, Austria, Sept. 2019.

[171] S. F. Tie and C. W. Tan. "A Review of Energy Sources and Energy Management System in Electric Vehicles". *Renew. Sustain. Energy Rev.* Vol. 20 (2013), pp. 82–102.

[172] G. Wu, X. Zhang, and Z. Dong. "Powertrain Architectures of Electrified Vehicles: Review, Classification and Comparison". *J. Franklin Inst.* Vol. 352 (2015), pp. 425–448.

[173] Q. Ren, D. A. Crolla, and A. Morris. "Effect of Transmission Design on Electric Vehicle (EV) Performance". *2009 IEEE Vehicle Power and Propulsion Conference*. Dearborn, MI, USA, Sept. 2009.

[174] F. Di Nicola, A. Sorniotti, T. Holdstock, F. Viotto, and S. Bertolotto. "Optimization of a Multiple-Speed Transmission for Downsizing the Motor of a Fully Electric Vehicle". *SAE Int. J. Alt. Power*. Vol. 1 (2012), pp. 134–143.

[175] H. Laitinen, A. Lajunen, and K. Tammi. "Improving Electric Vehicle Energy Efficiency with Two-Speed Gearbox". *2017 IEEE Vehicle Power and Propulsion Conference*. Belfort, France, Dec. 2017.

[176] P. Spanoudakis, N. C. Tsourveloudis, L. Doitsidis, and E. S. Karapidakis. "Experimental Research of Transmissions on Electric Vehicles' Energy Consumption". *Energies* vol. 12 (2019).

[177] W. Gao and C. Mi. "Hybrid Vehicle Design using Global Optimisation Algorithms". *Int. J. Electric and Hybrid Vehicles* vol. 1 (2007), pp. 57–70.

[178] M. Scholl, K. Minnerup, C. Reiter, B. Bernhardt, E. Weisbrodt, and S. Newiger. "Optimization of a Thermal Management System for Battery Electric Vehicles". *Fourteenth International Conference on Ecological Vehicles and Renewable Energies (EVER)*. Monte-Carlo, Monaco, May 2019.

[179] M. Pourabdollah, E. Silvas, N. Murgovski, M. Steinbuch, and B. Egardt. "Optimal Sizing of a Series PHEV: Comparison between Convex Optimization and Particle Swarm Optimization". *4th IFAC Workshop on Engine and Powertrain Control, Simulation and Modeling E-COSM 2015*. Columbus, OH, USA, Aug. 2015.

[180] P. Mock, J. Kühlwein, U. Tietge, V. Franco, A. Bandivadekar, and J. German. *The WLTP: How a New Test Procedure for Cars Will Affect Fuel Consumption Values in the EU*. Technical Report. Germany: International Council on Clean Transportation, 2014.

[181] C. Samhaber, A. Wimmer, and E. Loibner. "Modeling of Engine Warm-Up with Integration of Vehicle and Engine Cycle Simulation". *SAE Technical Paper 2001-01-1697* (2001).

[182] J. Lescot, A. Sciarretta, Y. Chamaillard, and A. Charlet. "On the Integration of Optimal Energy Management and Thermal Management of Hybrid Electric Vehicles". *2010 IEEE Vehicle Power and Propulsion Conference*. Lille, France, Sept. 2010.

[183] J.-S. Won, R. Langari, and M. Ehsani. "An Energy Management and Charge Sustaining Strategy for a Parallel Hybrid Vehicle with CVT". *IEEE Trans. Control Syst. Technol.* Vol. 13 (2005), pp. 313–320.

[184] G. van Spijk. "CVT Pushing Hybrid Technology to New Heights". *2nd International VDI Conference: CVT in Automotive Applications*. Eindhoven, The Netherlands, Oct. 2017.

[185] L. Jarrier, J. C. Champoussin, R. Yu, and D. Gentile. "Warm-Up of a D.I. Diesel Engine: Experiment and Modeling". *SAE 2000 World Congress*. Detroit, MI, USA, Mar. 2000.

[186] T. Markel, A. Brooker, T. Hendricks, V. Johnson, K. Kelly, B. Kramer, M. O'Keefe, S. Sprik, and K. Wipke. "Advisor: A Systems Analysis Tool for Advanced Vehicle Modeling". *J. Power Sources* vol. 110 (2002), pp. 255–266.

[187] I. Arsie, A. Cricchio, C. Pianese, and V. Ricciardi. "Modeling and Optimization of Organic Rankine Cycle for Waste Heat Recovery in Automotive Engines". *SAE Technical Paper 2016-01-0207* (2016).

[188] K. Smith and T. M. "Feasibility of Thermoelectrics for Waste Heat Recovery in Hybrid Vehicles". *23rd International Electric Vehicle Symposium*. Anaheim, CA, USA, Dec. 2007.

[189] K. Upendra and A. Grauers. *Synergy and Conflicts between Waste Heat Recovery System and Hybrid Electric Vehicle*. Technical Report. Sweden: Chalmers University of Technology, 2015.

[190] C. Cho, H. Lee, J. Won, and M. Lee. "Measurement and Evaluation of Heating Performance of Heat Pump Systems Using Wasted Heat from Electric Devices for an Electric Bus". *Energies* vol. 5 (2012), pp. 658–669.

[191] O. Sundström and L. Guzzella. "A Generic Dynamic Programming Matlab Function". *2009 IEEE Control Applications, (CCA) Intelligent Control, (ISIC)*. Saint Petersburg, Russia, July 2009.

[192] T. Hofman and C. Dai. "Energy Efficiency Analysis and Comparison of Transmission Technologies for an Electric Vehicle". *2010 IEEE Vehicle Power and Propulsion Conference*. Lille, France, Sept. 2010.

[193] F. Bottiglione, S. De Pinto, G. Mantriota, and A. Sorniotti. "Energy Consumption of a Battery Electric Vehicle with Infinitely Variable Transmission". *Energies* vol. 7 (2014), pp. 8317–8337.

[194] W. Dib, A. Chasse, P. Moulin, A. Sciarretta, and G. Corde. "Optimal Energy Management for an Electric Vehicle in Eco-driving Applications". *Control Eng. Pract.* Vol. 29 (2014), pp. 299–307.

[195] B. Luin, S. Petelin, and F. Al-Mansour. "Microsimulation of Electric Vehicle Energy Consumption". *Energy* vol. 174 (2019), pp. 24–32.

[196] J. Felipe, J. C. Amarillo, J. E. Naranjo, F. Serradilla, and A. Díaz. "Energy Consumption Estimation in Electric Vehicles Considering Driving Style". *2015 IEEE 18th International Conference on Intelligent Transportation Systems*. Las Palmas, Spain, Sept. 2015.

[197] C. De Cauwer, J. Van Mierlo, and T. Coosemans. "Energy Consumption Prediction for Electric Vehicles based on Real-World Data". *Energies* vol. 8 (2015), pp. 8573–8593.

[198] N. Murgovski, L. Johannesson, and J. Sjöberg. "Convex Modeling of Energy Buffers in Power Control Applications". *3rd IFAC Workshop on Engine and Powertrain Control, Simulation and Modeling*. Rueil-Malmaison, France, Oct. 2012.

[199] S. Boyd and L. Vandenberghe. *Convex Optimization*. Cambridge, UK: Cambridge University Press, 2009.

[200] C. A. Fahdzyana and T. Hofman. "Integrated Design for a CVT: Dynamical Optimization of Actuation and Control". *9th IFAC Symposium Advances in Automotive Control*. Orléans, France, June 2019.

[201] F. van der Sluis, S. Yildiz, A. Brandsma, P. Veltmans, and M. Kunze. "The CVT Pushbelt reinvented for Future Compact and Efficient Powertrains". *2017 JSAE Annual Congress*. Yokohama, Japan, May 2017.

[202] M. Pourabdollah. "Optimization of Plug-in Hybrid Electric Vehicles". PhD thesis. Chalmers University of Technology, 2015.

[203] *Electrical and Electronics Technical Team Roadmap*. Technical Report. USA: U.S. DRIVE, 2017.

[204] N. Lutsey and M. Nicholas. *Update on Electric Vehicle Costs in the United States through 2030*. Technical Report. USA: International Council on Clean Transportation, 2019.

[205] G. Berckmans, M. Messagie, J. Smekens, N. Omar, L. Vanhaverbeke, and J. Van Mierlo. "Cost Projection of State of the Art Lithium-Ion Batteries for Electric Vehicles Up to 2030". *Energies* vol. 10 (2017).

[206] *Software for Disciplined Convex Programming*. URL: `http://cvxr.com/`.

[207] S. Delprat, T. Hofman, and S. Paganelli. "Hybrid Vehicle Energy Management: Singular Optimal Control". *IEEE Trans. Veh. Technol.* Vol. 66 (2017), pp. 9654–9666.

[208] D. Kirk. *Optimal Control Theory: An Introduction*. Mineola, NY, USA: Dover Publications, 2004.

[209] A. Sciarretta, D. di Domenico, P. Pognant-Gros, and G. Zito. "Optimal Energy Management of Automotive Battery Systems Including Thermal Dynamics and Aging". *Optimization and Optimal Control in Automotive Systems*. Ed. by H. Waschl, I. Kolmanovsky, M. Steinbuch, and L. del Re. Vol. 455. Cham, Switzerland: Springer, 2014, pp. 219–236.

[210] L. Serrao, S. Onori, and G. Rizzoni. "ECMS as a Realization of Pontryagin's Minimum Principle for HEV Control". *2009 American Control Conference*. St. Louis, MO, USA, June 2009.

[211] J. Kessels, M. Koot, P. van den Bosch, and D. Kok. "Online Energy Management for Hybrid Electric Vehicles". *IEEE Trans. Veh. Technol.* Vol. 57 (2008), pp. 3428–3440.

[212] S. Onori, L. Serrao, and G. Rizzoni. "Adaptive Equivalent Consumption Minimization Strategy for Hybrid Electric Vehicles". *ASME 2010 Dynamic Systems and Control Conference*. Cambridge, MA, USA, Sept. 2010.

[213] M. Sivertsson and L. Eriksson. "Design and Evaluation of Energy Management Using Map-based ECMS for the PHEV Benchmark". *Oil Gas Sci. Technol.* Vol. 70 (2014), pp. 195–211.

[214] F. van der Sluis, T. van Dongen, G. van Spijk, A. van der Velde, and A. van Heeswijk. "Fuel Consumption Potential of the Pushbelt CVT". *FISITA 2006 World Automotive Congress*. Yokohama, Japan, Oct. 2006.